STEEL AND CONCRETE COMPOSITE DIAPHRAGMS

A Thesis submitted for

the Degree of

DOCTOR OF PHILOSOPHY

by

JEFFREY FISHER

Department of Civil Engineering

University of Salford

December 1981

C O N T E N T S

LIST OF ILLUSTRATIONS

LIST OF TABLES

DECLARATION

None of the material contained in this thesis has been submitted in support of an application for another degress or qualification of this or any other university or institution of learning.

Jeffrey Fisher

December 1981

ABSTRACT

Stressed skin design has now been developed into an important tool for designing buildings. In developing stressed skin theory, it has been shown that the inherent inplane stiffness of the materials considered is of predominate importance in the distribution of lateral forces within a structure. The materials that have been incorporated in the theory so far are profiled steel and aluminium sheeting.

Lately, work on multi-storey buildings has shown the advantage of using infill panels in the vertical plane to control the sway deflection of the building. No account, however, has been taken of the horizontal floors acting as diaphragms. Incorporating the floor into the sway analysis would clearly model the building more realistically. A typical floor construction commonly adopted in steel framed buildings is the composite slab. This consists of trapezoidally profiled steel sheeting fastened to the structure and overlain by concrete. Design formulae are derived for the shear strength and flexibility of the above floor construction and verified by experimental work.

In the basic stressed skin concept the shear distortional flexibility of profiled sheeting has been shown to be dependent on the overall dimensions of the diaphragm, the shape of the profile and the fastener arrangement. At present the analysis considers a typical corrugation to lie within a large "field or corrugations" and so edge effects are neglected. A Finite Strip program has been written to analyses these fields of corrugations under the action of a shear flow and to investigate the effect of edge members on the shear flexibility.

The large end distortions of the profiled sheeting, that arise as a result of the action of the shear flow on the profile, can cause failure of the sheeting and fasteners in this region. A study has been undertaken to investigate the possible failure modes, as a result of which three modes have been identified, namely, failure of the sheet / purlin fasteners, buckling of the profile web and a sideways collapse of the profile. Numerical expressions are developed for these failures and compared with experimental results.

ACKNOWLEDGEMENTS

I would like to thank my supervisor, Professor J. M. Davies, for his valuable advise and encouragement throughout the period of study, and to Professor E. R. Bryan for introducing me to this subject and his interest throughout the project.

I also would like to express my thanks to

- the Structure and Concrete Laboratory staff and inparticular Mr W. Deakin
- Mr C. Tivey for his preparation of the photographs
- Miss K. Edwards for typing the manuscript
- and to my parents for their continued support.

I acknowledge with thanks Holorib and H. H. Robertsons who supplied the sheeting for the composite diaphragm tests.

NOTATION

a	-	width of diaphragm
b	-	length of diaphragm
$b_{\angle}, b_{\tau}, b_s$	-	profile dimensions
b_p	-	width of purlin
$c_{1.1}, c_{1.2} - c_3$	-	flexibility factors
d	-	pitch of corrugations
E	-	elastic modules
F_s, F_p, F_{sc}	-	failure load of fastener
F_{sc}	-	longitudinal shear force
F_T	-	tension force
$F_{\frac{nf-1}{2}}$	-	transerve shear force
G	-	modulus of rigidity
g_1, g_2	-	force distribution coefficients
h	-	height of profile
$I_1 - I_5$	-	product integrals for bending strip
I_y	-	2nd moment of areas about the neutral axis for a single corrugation
$\overline{K}, K_B$	-	shear distortion factors
k, k_1, k_2	-	propping force factors
$L_1 - L_8$	-	product integrals for plain stress strip
ℓ_{eff}	-	effective length (buckling of web)
m	-	plastic moments
nsc	-	number of sheet/shear connectors
np	-	number of purlins
nsh	-	number of sub panels
nf	-	number of fasteners per purlin

ns	-	number of seam fasteners
p	-	plastic load constant
pa	-	spacing of fasteners in the "a" direction
pb	-	spacing of fasteners in the "b" direction
p	-	propping force
Q	-	diaphragm load
Q_p	-	plastic load
q	-	shear flow
Sp	-	slip of sheet/purlin fasteners
Ssc	-	slip of sheet/shear connectors
Ss	-	slip of seam fasteners
t	-	thickness of sheeting
β, β^*, β'	-	force coefficients for composite slab
Δ	-	shear deflections
σ	-	yield stress
σ_{crit}	-	critical stress
σ_{eff}	-	effective stress
ν	-	poissons ratio
ν_s	-	poissons ratio for steel
ν_c	-	poissons ratio for concrete
τ_{xy}	-	shear stress
ε	-	strain

1. Introduction

Until recently, the stiffening effect of a building's cladding on its framework could not always be incorporated in the design. In the past full-scale tests carried out on complete buildings showed that actual deflections and stresses had a value significantly less than the design values [1], and designers therefore appreciated that the cladding could be sufficiently stiff against inplane forces to reduce the design deflections and stresses. However, this additional strength could not be incorporated into a design as no guidance could be formulated to determine the effect of the cladding on a building.

With the advent of the modern computer, the mathematical problem of analysing structures with a high degree of indeterminacy could be undertaken with greater ease, and new techniques for solving structures rapidly developed. Consequently, new design philosophies followed.

One of these design philosophies was the concept known as "Stressed Skin Design". The basis of this philosophy is that the material or cladding of the building will resist lateral forces applied in the plane of the cladding. The force resisted by the cladding is then redistributed to rigid end gables as shown in Fig. 1.1. The concept of stressed skin design, applied to this particular structural element, is likened to the analogy of a deep plate girder. The sheeting of the element, usually trapezoidally profiled sheeting, acting as the web of the plate girders in resisting the shear forces, and the axial tensile and compressive forces in the flanges of the beam are carried by the framing member of the building.

Over the past thirty years research has been carried out to determine the inplane strength of trapezoidal sheeting fastened with adequately stiff connections to the framing members, such as with welded or mechanical fasteners. The first tests on diaphragms were carried out by Johnson [2] in California in 1947, and they consisted of applying forces laterally with cables on a full-scale building. This was followed shortly afterwards by a second programme of tests by S. B. Barnes using cellular type panels.

This concept developed rapidly following the work of Nilson [3] at Cornell University who undertook a systematic testing programme with a wide range of profiles. In this programme a standard test was developed, that of the cantilever test rig, which is now associated with all testing of profiled steel diaphragms.

Clearly, the testing of full-scale diaphragms is expensive and only economical when a "system" type of building is under consideration, as was the case on the CLASP and SEAC building systems [4]. Therefore a theoretical means of predicting the diaphragms strength and flexibility had to be found. This was the first undertaken by Bryan [5] and his team of researchers at Manchester University. They separated the diaphragm into its structural components and determined the overall strength and flexibility from the strength and flexibility of each of the components. Bryan's expressions for both strength and flexibility have recently been modified by Davies [6] and Lawson [7,8] to accommodate certain irregularities in the theory.

A third method of analysing profiled steel diaphragms has been developed in Australia [9] and North America [10] using finite element techniques. The approach in this case has been to

incorporate discrete elements for each of the structural components. This method however has been found to be unsuitable for design purposes although it has given much useful information into the force distribution in the fasteners.

Initially, the work in stressed skin design concentrated on profiled steel diaphragms. However, as the theory developed, new applications have been considered, namely the use of internal diaphragms to restrict the lateral sway in multi-storey buildings and in frameless structures. The development of this concept in structural design has now opened the field to a wider range of materials, such as concrete, steel / concrete composite slabs, brickwork and blockwork. Recently, a large amount of work has been carried out to obtain design recommendations for the inclusion of the effect of cladding in the analysis of multi-storey buildings[11] . Most of the work has been concerned with plane frames, but clearly, buildings do not act as plane frames and each frame should be considered to act as an integral part of the overall structure. In fact very few structures designed on a plane frame basis will behave in the manner designed.

The floor construction is the prime distributor between the frames, but there can be many variations in floor construction. The work given in this thesis is concerned with just one type, that of composite slabs, which are a recent development in the European market. One notable example todate of this floor construction is the National Westminster Tower in London. The composite floor construction has one advantage over other floors in multi-storey construction, in that no temporary formwork need be considered.

Part of the work given in this thesis has been concerned

with the diaphragm action of this floor construction, and which has recently been published [12] . A copy of this publication is given in Appendix 5.

Certain limitations were found with Bryan's original theory, inparticular the prime component of flexibility, that of shear distortion of the profile. Recently much theoretical and experimental work on this subject, by Davies and Lawson [7,8] and Libove [13] , have shown the factors that influence this component. However, these analyses have been based on the idealisation that the sheeting between fasteners has a similar effect on the overall sheeting and no account of edge effects has been considered. With this in view a Finite Strip program has been written to analyse large diaphragms and to consider edge effects. Also all previous analyses lack generality in that only simple trapezoidal or arc and tangent profiles were considered; the Finite Strip solution gives a more general approach and can readily incorporate irregular profiles.

A third area of study has been concerned with the modes of failure of profiled steel diaphragms in the region of the sheet / purlin fasteners. The failures have for this study been termed as "End Failures". Design expressions are given for the three failure modes identified, namely failure of the sheet / purlin fasteners, the profile web buckling at outermost purlin and the lateral sway of the profile.

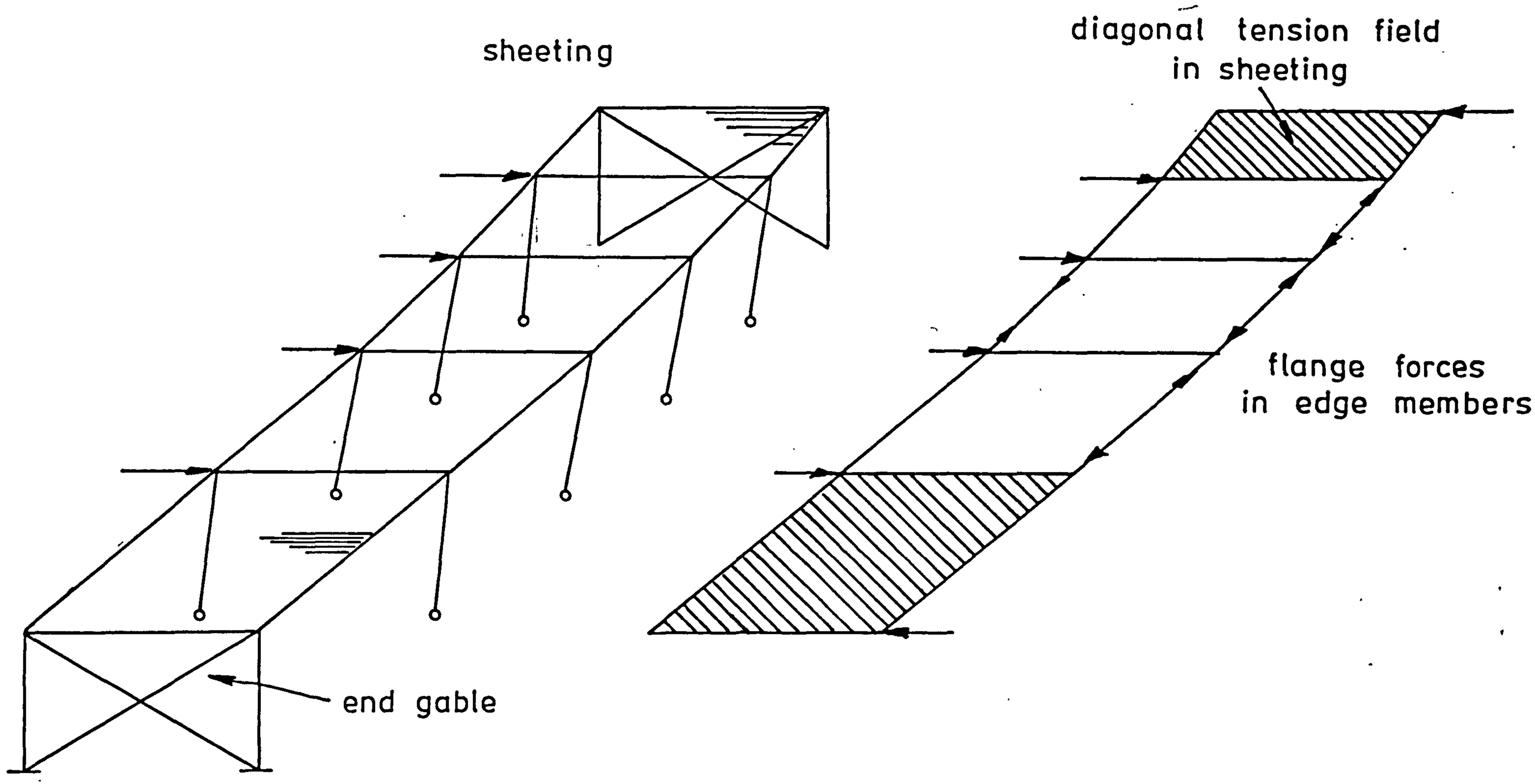

Fig 1.1 Stressed Skin Action in Rect. Frame Structure Under Side Loading

2. Composite Diaphragms

2.1 Introduction

Composite floors, consisting of profiled steel sheeting acting in conjunction with an insitu concrete topping have been popular in the United States of America for many years. With more overlapping of American and European design philosophies, the spread of technology between the two continents has brought the use of composite floors into the European market. Recently this trend has been extended by the preparation of a new European design procedure for composite floors (14).

The primary purpose of spanning between the supporting beams under the action of vertical load is efficiently undertaken by the composite floors. Together with the efficient bending action, the composite floors or roofs have a very high inplane stiffness and strength and, as with all diaphragms, it is obvious that they distribute lateral loads between the frames of the primary structure. As in the more familiar use of stressed skin principles in the prediction of the stiffening effect of light gauge steel cladding, the diaphragm action of the composite floors can be likened to the action of a deep beam. A consequence of the proportions of the beam, the influence of shear is likely to be more important than that of bending. Scant attention has been paid to the performance of composite decks acting as diaphragms and it is with this aspect that the present work is concerned.

As a consequence of this study, two basic types of composite diaphragms have been identified, namely :-

A. diaphragms in which the profiled steel sheeting is fastened to the supporting structure by mechanical fasteners or welds in such a way that there is no direct attachment of the concrete to the supporting structure.

B. diaphragms incorporating shear connectors. These typically take the form of studs welded through the sheeting to the supporting steelwork thereby fastening the sheeting to the steelwork and, at the same time providing a direct shear connection to the concrete. Such diaphragms are likely to be significantly more efficient in resisting shear loads than those without direct connections.

There are many different profiles used in composite construction and a selection is shown in Fig. 2.1 (a). These profiles can be divided into two distinct types, as shown in Fig. 2.1 (b). The profiles are termed "re-entrant" profiles and "trapezoidal" profiles and as there are certain significant differences in their behaviour under diaphragm shear loads it is necessary to distinguish between the two types of profile.

In this study, both types of profile are considered but attention is confined to the first type of composite diaphragms only, namely, diaphragms with no direct attachment of the concrete to the supporting structure. At the present time there seems to be little work on the second type of diaphragm with shear connectors through to the concrete infill. One reason for this absence of work is that the high failure loads required of such diaphragms require much more expensive test facilities.

2.2 Composite Slabs in Bending

Over the last fifty years labour and material costs for

construction have been increasing rapidly. To minimise these costs, designers have turned to new building techniques in the hope that they would provide a means of reducing costs. Composite slabs were developed for this purpose, by eliminating the cost of floor formwork in multi-storey construction. The composite slab floor is supported by the steel sheeting until the "green" concrete has attained sufficient strength. The sheeting then acts as steel reinforcement as in a normal reinforced concrete slab.

The primary purpose of the slab is to carry the floor loads acting on the slab, to the supporting frame. Most of the work to-date has been concerned with this bending action. Current design methods for this form of construction, however, were not advanced sufficiently to allow for both the strength of the steel and concrete to be fully utilised together in the design. This lack of knowledge has been rectified over the last decade and a number of design approaches have been formulated. The three most important are :-

A. the European Recommendatuons for the Design of Composite Floors with Profiled Steel Sheeting (14).

B. the Tentative Criteria for the Design and Construction of Composite Steel Deck Slabs (15).

and

C. the French "Bond Stress" Method (16).

The European Recommendations are based on test slab results only and no extension of the test results to different slab dimensions are allowed. From the research carried out, two failure modes were identified, namely the "Shear / Bond" failure and the normal flexural failure of reinforced concrete slabs.

The "Shear / Bond" failure is caused by inadequate shear resistance between the concrete and steel sheeting, causing a loss of bond. This loss of bond can be reduced by manufacturing embossments into the profile, see Fig. 2.1 (b), or by welding shear studs through the sheeting to the frames of the building.

The main purpose of the recommendations though has been to formulate a standard testing method so that the results from the different countries can be collectively studied.

The American Code [15] also distinguishes between the two previously mentioned failure modes, but allows for the results to be extrapolated for other slab dimensions. The "Shear / Bond Regression Analysis" was developed by Schuster [17] for this extrapolation and is based on a number of test slabs. From the results, which must include variations of both span and thickness a graph is constructed using the plot of

$$\frac{V_e \cdot S}{b_1 \; d' \sqrt{f_c'}} \quad \text{v} \quad \frac{\rho \cdot d'}{L' \sqrt{f_c'}}$$

where
- $V_e = P_e / 2 \cdot b_d$
- P_e = Ultimate experimental load
- b_d = Test span width
- b_1 = Unit width (12 ins.)
- d' = Effective depth of slab
- ρ = Steel ratio = $A_s / (b_d \cdot d)$
- L' = Shear span
- f_c' = Characteristic concrete strength
- S = Spacing of embossments

A regression analysis is then undertaken and an equation obtained of the form

$$y = mx + k \qquad (2.1)$$

From this equation, an expression for the shear bond capacity Vu is given by

$$Vu = \frac{m \cdot \rho \cdot (d^1)^2 \cdot b_1}{s \cdot L^1} + \frac{k \cdot b_1 \cdot d \cdot \sqrt{fc^1}}{S} \quad \ldots . (2.2)$$

Expressions are also given for the flexural capacity taking into account both the over-reinforced and under-reinforced conditions.

The Shear / Bond failure is a result of the failure of the bond between the concrete and steel sheeting. Although it has been difficult to quantify the actual bond stress at failure, the French Bond Stress Method [16] developed by Fulop and Moum, is based on this failure stress. One of the main assumptions of the method is that the slip between the concrete and the steel is zero, which in most cases is doubtful. However, the analysis does give an estimate of the actual bond stress, which is discussed in a later section.

From the work carried out for the method, the "mean bond stress" τ_m was calculated for varying spans and thicknesses,

where

$$\tau_m = \frac{Fr}{l_x \cdot b} \qquad (2.3)$$

where Fr = critical interaction force = $\alpha_1 M / \alpha_2$

l_x = shear span

b = width

α_1 and α_2 are coefficients depending on the properties of the slab

and Mr = bending moment at the section.

Roberts [18] extended the bond stress approach into a regression analysis incorporating the steel ratio $\rho = As / b_1 d$, finding that the results compared more favourably than the method suggested by Fulop and Moum. Roberts method can quite easily be considered as a combined approach of the French Bond Stress Method and the American criteria for the shear / bond failure.

2.3 Previous Tests on Composite Diaphragms

The first reported shear tests on composite diaphragms were carried out by S. B. Barnes and Associates [19]. They were only three in number and of these one used lightweight vermiculite fill and one was fabricated using a two skin box-section steel

deck, so that only one test is directly relevant to the work carried out in this study. The diaphragms were of the type where there is no direct attachment of the concrete to the supporting structure and the connections consisted of puddle welds, as is usual in the United States practice.

Each of the three tested diaphragms appears to have failed by cracking of the concrete topping. The directly relevant test was carried out on a trapezoidal profile steel deck of 76.2mm deep with a concrete topping of depth 63.5mm, which at the time of testing had obtained a strength of 16.1 N/mm^2. Tension cracking commenced at a shear load / unit width of 31 kN / m and continued to increase until failure took place at a shear load of 86.4 kN / m, due to direct shear of the concrete over the crest of the profile. From the tests there was no indication of any slippage in the button-punched seams between adjacent sheets despite the fact that such seams are considerably more flexible than those seams with mechanical fasteners, such as blind rivets or self-tapping screws.

The only other test series carried out on composite diaphragms, known to the author were undertaken by Luttrell [20]. A total of nine diaphragms were tested, incorporating trapezoidal profiled steel sheeting of depth varying from 9.5mm to 34.9mm. The fill was made of lightweight concrete of depth 63.5mm or 76.2mm and having a mean strength of 1.01 N/mm^2. He compared the stiffness and ultimate load of composite diaphragms with those of similar steel diaphragms. A considerable increase in both stiffness and strength was reported, though the failure modes were not identified. As the concrete topping was very weak Luttrell's tests are not of direct help in this study.

2.4 Test Programme on Composite Slabs

The tests so far described have only identified some of the primary failure modes of composite diaphragms. The work on profiled steel diaphragm behaviour was developed more recently and so further tests were instigated to relate composite slabs into the stressed skin theory [22]. A test rig was therefore constructed so that cantilever diaphragms of size 3.5m X 3.5m could be subjected to shear loads up to 150 kN. A cantilever diaphragm was eventually constructed instead of a simply supported diaphragm as the recent work in the stressed skin theory showed that the characteristics of the two forms of diaphragm were similar, but that the cantilever was more cost effective. A general arrangement of the diaphragm is shown in Fig. 2.2 and 2.3. The connections between the edge member and the main beams were pinned so that the stiffness of the test frame was then negligible.

The steel decking was either of Type A or B as shown in Fig. 2.1 (b) and was fastened to the supporting structure on four sides using 6mm diameter Teks self-drilling, self-tapping screws. In all the tests the seams between the sheeting was fastened with 4.8mm diameter Monel Pop rivets at 152mm centres. Four tests were carried out in the programme, the fastener spacings etc., are shown in Table 2.1

TEST No.	SHEETING TYPE	SLAB THICKNESS (mm)	TOPPING THICKNESS (mm)	NOMINAL PICTH OF FASTENERS	
				MAIN BEAM	EDGE BEAM
1	A	100	50	300	304
2	B	150	70	585	608
3	A	100	50	500	304
4	A	100	50	700	456

Table 2.1 Details of Tests

With the exception of test 4, the procedure for each test was to first attach the sheeting to the frame, then to obtain the stiffness of the steel diaphragm by applying the load in the elastic range. The extent of the elastic range was dependent on the buckling load of the diaphragm. In order to predict this limit, Easley's formula [21] for buckling of corrugated sheeting was used, where

$$V_{crit} = \frac{36 \cdot Dx^{\frac{1}{4}} \cdot Dy^{\frac{3}{4}}}{b} \qquad (2.4)$$

where $Dx = \dfrac{E \cdot t^3 \cdot d}{12(1 - \nu^2)\, u}$

$$Dy = \frac{E \cdot Iy}{d}$$

b = length of diaphragm

u = perimeter length of a single corrugation

Iy = 2nd moment of area about the neutral axis for a single corrugation.

Having obtained the stiffness of the steel sheeting the concrete topping was then placed. In all of the tests the

concrete used 9.5mm aggregate and was designed to have a strength of 25 N/mm^2 at 28 days. A typical diaphragm, ready for testing is shown in Fig. 2.5.

The composite slab was then tested by loading in increments up to failure. In the case of three of the four tested diaphragms at a load of between one half and three quarters of the expected failure load, the diaphragms were unloaded and subsequently reloaded before continuing the test to failure. The load-deflection curves for each diaphragm are given in Fig. 2.6 - 2.9.

The shear deflection (Δ) plotted was in each case obtained from the reading of the four dial gauges shown in Fig. 2.4 as

$$\Delta = \delta_1 - \delta_2 - \frac{b}{a}\left(\delta_3 + \delta_4\right) \qquad (2.5)$$

In the "Barnes" series of tests, failure occured by tension cracks and a loss of bond between the steel and concrete. To determine the concrete strains and slip between the steel and concrete "Demec" gauges and dial gauges were attached to Diaphragm 1. At no time though during the test did the measured strains approach the tensile strain capacity of the concrete, nor was there any measurable slip between the steel deck and concrete topping. For these reasons the above measurements were

discontinued for subsequent tests.

For Diaphragm Test 4, the tested Diaphragm 3 was re-instated by carefully breaking away the perimeter concrete to a width of about 150mm in order to expose the failed fasteners. They were then removed and the diaphragm re-fixed with fresh fasteners at the required pitch, shown in Table 2.1. The concrete slab was then made good by replacing the concrete that had been removed.

This procedure was adopted not only for reasons of economy but also to investigate the shape of the load deflection curve as will be discussed later.

Table 2.2 shows the concrete properties for each of the diaphragms tested.

TEST No.	CUBE STRENGTH N/mm^2	TENSILE STRENGTH N/mm^2	"E" VALUE N/mm^2
1	25.5	4.82	21.5
2	24.3	4.57	24.2
3	27.7		26.2
4	28.0		26.5

Table 2.2 Characteristics of Concrete

2.5 Ultimate Load of Composite Diaphragms

2.5.1 Failure Mechanisms

In the analysis of composite diaphragms the work of Barnes and Luttrell were not influenced by the more recent work in the field of light gauge steel diaphragms. Luttrell[20], in fact, offers a simple empirical treatment, which is only applicable to the diaphragms that he tested. No suggestions on any overall failure mechanisms are given. Barnes does give a more comprehensive theoretical treatment which is an extension of his work on light gauge steel diaphragms. However, his expressions are complex and include empirical constants derived for welded diaphragms only. Therefore none of the previous work can be applied to obtain practical failure mechanisms of the slabs.

From the tests carried out by the author three failure mechanisms were identified, namely :-

1. failure of the fasteners only, Fig. 2.10. At failure a parallelogram like movement of the frame below the comparatively rigid slab resulting in a failure of the fasteners about the centre line, as shown in Fig. 2.12. This mode was only associated with the re-entrant profiles, Type A.
2. failure of the fasteners again, but with a rotation of the slab relative to the frame, as shown in Fig. 2.13 No actual failure occurred of this failure mechanism.
3. The final mode of failure was a result of a combined failure of the profile sheeting and of the fasteners. The slab and frame rotating relative to each other causing the fasteners to fail on two sides and the profile to collapse on the third side as in Fig. 2.14.

2.5.2. Analysis of Mechanism 1

As stated previously, failure occurred in the self-drilling self-tapping perimeter fasteners, the actual deformations being very much as shown in Fig. 2.12. In the analyses that follows a number of alternative assumptions for the fastener forces are made, namely

1. the main beam perimeter fasteners all reach their ultimate load, further load applied to the diaphragm is distributed to the edge member fasteners.

and 2. a distribution of the force in the fasteners along the edge member. Three specific cases are considered and will be termed the fully plastic, quadratic and linear. The actual force distribution is difficult to obtain experimentally as it is dependant on a number of factors, chiefly the bending of the edge member.

Considering the internal and external work done in Fig. 2.12 and assuming that all the fasteners fail simultaneously, that is to say the "fully plastic" condition. Then the deflection Δ_i of a typical fastener i is given by

$$\Delta_i = \frac{\Delta . i}{n_a} \qquad (2.6)$$

where $n_a = \frac{a}{p_a}$

The above expression is only concerned with the distribution

of fasteners that include a fastener on the centre line of the edge member.

Including the corner fastener with the edge fasteners, the work equation for the complete diaphragm at failure is therefore given by

$$P.\Delta = 2(n_b - 1)F\frac{\Delta}{2} + 4\sum_{i=1}^{n_a/2}\left(\frac{i}{n_a}\right)\Delta . F$$

$$\text{so} \quad P = (n_b - 1)F + \frac{(n_a + 2)}{2}F$$

$$= \left(n_b + \frac{n_a}{2}\right)F \qquad (2.7)$$

Similarly if the total number of fasteners along the edge member is even, so that there is no fastener on the centre line, then

$$P = \left(n_b + \frac{n_a}{2} + \frac{1}{2\,n_a}\right)F \qquad (2.8)$$

which gives very similar results to the previous equation, unless n_a is small.

The fully plastic distribution of the edge fastener forces does not truly represent the actual failure condition of the diaphragm. Edge beam fasteners that are away from the region of the main beam would in practice not obtain the ultimate load of the fastener before failure of the diaphragm has occurred. So that a realistic estimate of the failure load can be obtained alternative linear and quadratic distribution of fastener forces are now considered.

Considering a linear distribution of the fastener forces, then the force in the i^{th} fastener is

$$Fi = \frac{2.\ i.\ F}{n_a} \qquad (2.9)$$

and the work equation is given by

$$P.\Delta = 2\,(n_b - 1)\ F\ \frac{\Delta}{2} + 4 \sum_{i=1}^{n_a/2} \left(\frac{i}{n_a}\right)\Delta \left(\frac{2i}{n_a}\right)\ F$$

. . . . . (2.10)

eliminating Δ we obtain

$$P = (n_b + \beta)\ F \qquad \ldots\ldots (2.11)$$

where $$\beta = 8 \sum_{i=1}^{n/2} \left(\frac{i}{n_a}\right)^2 - 1$$

Similarily the analysis for an even number of fasteners in the edge member lead to

$$\beta = 8 \sum_{i=1}^{\frac{n_a + 1}{2}} \left(\frac{i - \frac{1}{2}}{n_a}\right)^2 - 1 \qquad \ldots\ldots (2.12)$$

For the quadratic distribution of the fastener forces, the force in the i^{th} fastener is

$$Fi = \left\{1 - \left(1 - \frac{2i}{na}\right)^2\right\} F \qquad \ldots\ldots (2.13)$$

this leads to

$$P = (n_b + \beta)\, F \qquad (2.14)$$

where $$\beta = 4 \sum_{i=1}^{n/2} \left(\frac{i}{n_a}\right)\left[1 - \left(1 - \frac{2i}{n_a}\right)^2\right]^{-1} \qquad (2.15)$$

for an odd number of edge member fasteners

and $$\beta = 2 \sum_{i=1}^{\frac{n_a+1}{2}} \left(\frac{2i-1}{n_a}\right)\left\{1 - \left[1 - \frac{(2i-1)}{n_a}\right]^2\right\}^{-1} \qquad (2.16)$$

for an even number of edge member fasteners.

The values of β for the three distributions are given in Table 2.3.

n	B		
	Plastic	Quadratic	Linear
2	1.0	1.0	1.0
3	1.67	1.37	1.22
4	2.0	1.75	1.5
5	2.6	2.15	1.8
6	3.0	2.56	2.11
7	3.57	2.97	2.43
8	4.0	3.38	2.75
9	4.56	3.78	3.07
10	5.0	4.2	3.4
11	5.55	4.61	3.73

Table 2.3 Values of B in expressions for failure load

2.5.3 Analysis of Mechanism 2

For an isolated cantilever diaphragm, as tested, there is an alternative failure mode. This involves bodily rotation of the concrete slab as well as parallelogram-like deformation of the supporting structure leading to fastener failure on all four sides. The deformed failure mode is shown in Fig. 2.13.

In contrast to the previous analysis, it is assumed that the edge fasteners, instead of the main beam fasteners, reach

ultimate load then distribute further load to the main beam fasteners.

Comparing the Mechanisms 1 and 2, the work equations are found to be similar, so that for a linear distribution of the fastener forces

$$P.\Delta = 2(n_a - 1)\frac{F.\Delta^1}{2} + 4\sum_{i=1}^{n_b/2}\left(\frac{i}{n_b}\right)\Delta^1\left(\frac{2i}{n_b}\right)F \qquad \ldots\ldots (2.17)$$

where $\Delta^1 = \dfrac{\Delta . b}{a}$

giving $$P = \frac{b}{a}(n_a + B)F \qquad (2.18)$$

Equations 2.14 and 2.18 are similar except that β is now dependent on the number of fasteners n_b to the main beam.

2.5.4 Analysis of Mechanism 3

In Diaphragm Test 2, failure again took place with relative movement between the slab and the supporting frame with no noticeable deformation of the concrete. However, the relative movement took place partly by failure of the fasteners, as in the previous mechanism, and partly by the collapse of the profile

adjacent to the fixed rafter, as shown in Fig. 2.14. For the collapse of the profile to occur at failure compatibility of movement between the edge beam fasteners and the deflections of the profile at B in Fig. 2.14 must occur, so for compatibility

$$b.\theta = \text{failure slip of the edge beam fasteners} \quad (2.19)$$

where b = diaphragm width

θ = rotation of the diaphragm

For this mechanism, the entire slab rotated about the line of the edge beam fasteners leading to the displacement pattern shown in Fig. 2.14. This mechanism will be termed Mode 3.

Considering the collapse of the profile at a distance x along the profile the deformation is as shown in Fig. 2.16. Assuming that this deformation arises as a result of plastic hinges at P and Q and, neglecting the small amount of twisting implied, the work done in a short length δx is

$$\frac{t^2 \sigma_y . \theta . x . \delta x}{2h} \quad (2.20)$$

and the total work done along the complete corrugation is ,

$$\int_0^b \frac{t^2 \cdot \sigma_y \cdot \theta_{.x} \cdot \ dx}{2h}$$

$$= \frac{t^2 \ b^2 \ \sigma_y \ \theta}{4h} \qquad (2.21)$$

In the analysis only the fully plastic and linear force distributions will be considered for the main beam fasteners. Incorporating equation 2.21 and the fully plastic force distribution the work equation is

$$P.\ a.\ \theta_{.} = n_a .\ F.\ b. + \sum_{i=1}^{n_b-1} \left(\frac{i}{n_b}\right) F.\ b.\theta_{.} +$$

$$\frac{t^2 \ b^2 \ \sigma_y \ \theta}{4h}$$

$$\text{giving} \quad P = \frac{b}{a}\left[n_a F + \sum_{i=1}^{n_{b-1}} \left(\frac{i}{n_b}\right) F + \frac{t^2\, b\, \sigma_y}{4h} \right] \qquad \ldots\ldots (2.22)$$

$$\text{and if } \beta^1 = \sum_{i=1}^{n_{b-1}} \frac{i}{n_b}$$

$$\text{then} \quad P = \frac{b}{a}\left[\left(n_a + \beta^1\right) F + \frac{t^2 \cdot b \cdot \sigma_y}{4.h} \right] \ldots\ldots (2.23)$$

Comparing the values of β^1 and β for the fully plastic condition, it can be shown that

$$\beta^1 = \beta - \tfrac{1}{2} \qquad (2.24)$$

Similarly the linear force distribution gives

$$P = \frac{b}{a}\left[\left(na + \beta^* \right) F + \frac{t^2\, b\, \sigma_y}{4h} \right] \qquad (2.25)$$

where $\beta^* = \sum_{i=1}^{n_{b-1}} \left(\frac{i}{n_b}\right)^2$

The above expressions are conservative in that the work done for the collapse of the profile shown in Fig. 2.16 requires the weight of concrete topping to be lifted a small distance and the resistance due to the head of the fastener being embedded in the concrete to be removed.

2.5.5 Modified Analysis of Mechanism 3

The previous analysis takes no account of the possibility that the point of rotation occurs at some other position than the top right hand corner in Fig. 2.14. In practice, because other small relative movements are possible, the composite slab probably rotates about some other point between A and B, resulting in a lower failure load.

In the analysis that follows, in order to determine the variations of the ultimate load as the centre of rotation moves towards B, two cases of fastener positions have to be considered, namely

a) No fasteners between the centre of rotation and the corner A.

and b) Fasteners between the centre of rotation and corner A.

As the centre of rotation moves towards B the concrete has the effect of restraining the profile between A and the

point of rotation. This reduces the length in which plastic moments can form.

Considering the fully plastic force distribution for the main beam fasteners and no fasteners between the hinge and position A, then the fastener deformations are as shown in Fig. 2.15 (a).

The work done by the collapse of the profile is reduced to

$$\frac{t^2 (b - j \cdot p_a)^2 \sigma_y}{4h} \qquad (2.26)$$

and so the work equation for the slab is given by

$$P. a. \theta . = (b - j. p_a) \theta . n_a . F + j p_a . \theta . n_a . F +$$

$$\sum_{i=1}^{n_{b-1}} \Delta_i . F + \frac{t^2 (b - j p_a)^2 \sigma_y . \theta}{4h}$$

where $\Delta i = \frac{b}{n_b} (i - j)$

So that

$$P = \frac{b}{a}\left[n_a F + \sum_{i=1}^{n_{b-1}} \left(\frac{i-j}{n_b}\right) F + \frac{t^2 b \left(1 - \frac{j}{n_b}\right)^2 \sigma_y}{4h} \right]$$

.....(2.27)

For the linear force distribution of the main beam fasteners the force diagram is shown in Fig. 2.15 (b) and the force in the i^{th} fastener is

$$F_i = \frac{(i-j)\,F}{n_b} \qquad (2.28)$$

The expression for the failure load P is then given by

$$P = \frac{b}{a}\left[n_a F + \sum_{i=1}^{n_{b-1}} \left(\frac{i-j}{n_b}\right)^2 F + \frac{t^2 b \left(1 - \frac{j}{n_b}\right)^2 \sigma_y}{4h} \right]$$

..... (2.29)

The analysis is now extended to consider case (b) for fasteners between the hinge line and position A. From Fig. 2.17 the expressions for deformations and forces, for the linear distribution are given by

$$\left.\begin{aligned} \Delta_k &= \frac{b}{n_b}\ (j - i) \\ F_k &= \frac{(j - i)}{n_b}\ F \end{aligned}\right\} \qquad \ldots\ldots\ldots\ (2.30)$$

Expressions 2.27 and 2.29 are now modified to take account of the additional work, so

$$P = \frac{b}{a}\left[n_a .\ F + \sum_{i=1}^{j} \left(\frac{j - i}{n_b}\right) F + \sum_{i=n_j+1}^{n_b-1} \left(\frac{i - j}{n_b}\right) F + \frac{t^2\ b\ (1 - {}^{j}/_{n_b})^2\ \sigma_y}{4h} \right] \qquad (2.31)$$

for the fully plastic force distribution

where n_j is the truncated value of j

$$P = \frac{b}{a}\left[n_a F + \sum_{i=1}^{n_{b-1}} \left(\frac{i-j}{n_b}\right)^2 F + \frac{t^2 b (1 - j/n_b)^2 \sigma_y}{4h}\right] \quad \ldots\ldots(2.32)$$

for the linear distribution.

A plot of the variation of the ultimate load P for varying values of j are shown in Fig. 2.18, the two curves show the variation for the fully plastic and linear force distributions. The results show that a change in position of the centre of rotation can cause a considerable reduction in the predicted failure load.

2.6. Flexibility of Composite Diaphragms

The flexibility of a corrugated sheet diaphragm was first shown by Bryan [22] to be the sum of the individual flexibilities of the components of the diaphragm, namely

$C_{1.1}$ = flexibility due to distortion of profiled sheeting

$C_{1.2}$ = flexibility due to shear strain in the sheeting

$C_{2.1}$ = flexibility due to slip in sheet to purlin fasteners

$C_{2.2}$ = flexibility due to slip in seam fasteners

$C_{2.3}$ = flexibility due to slip in connection to rafters

C_3 = flexibility due to axial strain in purlins

Some of the expressions used in the evaluation of the above components have subsequently been modified (6.7), but the basic principle remains valid and will be dealt in more depth in Chapter 4.

For the analysis of composite diaphragms the above approach may readily be extended, if the following reasonable assumptions are made :-

a) the confining effect of the concrete eliminates distortion of the steel profile, so that $C_{1.1}$ may be ignored.

b) at seams between adjacent steel sheets, the concrete carries almost all of the shear force and $C_{2.2}$ may be ignored.

c) the expressions for $C_{2.1}$, $C_{2.3}$ and C_3 are unchanged

and d) the shear force is shared between the steel and concrete according to the requirements for strain compatibility and $C_{1.2}$ requires modification.

In order to derive the modified expression for $C_{1.2}$, the shear strain of the composite slab, the notation of Fig. 2.19 will be used.

Considering a single corrugation subject to a unit shear load and a shear deflection $C_{1.2}$, let the load carried by the steel be Ps and the load carried by the concrete Pc.

Then $$Ps + Pc = 1 \qquad (2.33)$$

From the accepted expression (9) for shear strain in the steel

$$C_{1.2} = \frac{2\,(1+\nu s)\,(d+2h)\,Ps}{Es.ts.b} \qquad \ldots\ldots (2.34)$$

where νs and Es are Poisson's Ratio and the Elastic Modulus respectively for steel.

For shear strain in the concrete, and assuming an equivalent thickness of concrete, tc

$$Gc = \frac{Pc.\ d}{b.\ tc.\ C_{1.2}}$$

so $$C_{1.2} = \frac{2\,(1+\nu c)\ d.\ Pc}{Ec.\ tc.\ b} \qquad (2.35)$$

where Gc, Ec and νc are the Shear Modulus, Elastic Modulus and Poisson's ratio for concrete.

Substituting equations 2.33, 2.34 and 2.35 we obtain

$$1 = \frac{C_{1.2} \cdot Es.\ ts.\ d}{2(1+\nu s)\ (d+2h)} + \frac{C_{1.2} \cdot Ec.\ tc.\ b}{2\,(1+\nu c)\ d}$$

where d is the pitch of the profile

and h is the height of the profile

Rearranging

$$C_{1.2} = \frac{2\,(1+\nu s)\;(1+\nu c)\;(d+2h)\,d}{\left[Es.\,ts\,(1+\nu c)\,d + Ec.\,tc\,(1+\nu s)\;(d+2h)\right]b}$$

For the overall diaphragm, then

$$C_{1.2} = \frac{2\,(1+\nu s)\;(1+\nu c)\;(d+2h)\,a}{\left[Es.\,ts\,(1+\nu c)\;d + Ec.\,tc\;(1+\nu s)\;(d+2h)\right]\;b} \qquad \ldots\ldots\ldots (2.36)$$

The theoretical value of "C" of a composite diaphragm is then calculated as

$$C = C_{1.2} + C_{2.1} + C_{2.3} + C_3 \qquad (2.37)$$

where $C_{2.1} = \dfrac{2a.\,Sp.\,p}{b^2}$

$$C_{2.3} = \frac{2.\,Ssc}{\eta_{sc}}$$

and $$C_3 = \frac{n^2\;a^3}{6\;E\;A\;b^2}$$

Values for Sp and Ssc, the slip of the fasteners, are obtained by actual load / slip test results.

2.7 Discussion of Theoretical and Experimental Results

Before the results of the theoretical and experimental work could be compared shear tests on the actual fasteners and sheeting used were undertaken. The tests were carried out in accordance with the European Recommendations [23] using the standard shear test comprising of a single lap joint with two fasteners per lap. Values for the average ultimate load and flexibility are shown in Table 2.4.

Fastener	Sheeting (mm)	No. of Tests	Ultimate Load (kN)	Flexibility (mm/kN)
6mm Tek	Holorib (0.9)	3	6.15	0.017
6mm Tek	Robertson (1.5)	4	10.38	0.058

Table 2.4 Average Experimental Fastener Characteristics

The above values were then used in the failure expressions, previously developed, to give a comparison between the theoretical and experimental ultimate load, details of which are given in Table 2.5.

From the table, the fully plastic force distribution for

TEST	Na	Nb	Experimental failure load kN	Predicted failure load kN			Predicted failure mode	Failure load per unit length kN/m
				Plastic	Quad	Linear		
1	11	12	100	104.6	98.6	92.6	2	28.6
2	6	6	74	93.4	88.9	84.2	1, 2 or 3	21.1
3	11	7	75	77.2	71.1	66.0	1	21.4
4	8	6	52	61.5	57.7	53.0	2	15.0

Table 2.5 Comparison of Theoretical and Experimental Failure Loads

the failure of the fasteners in Tests 1, 3 and 4 are found to be unsafe and therefore must be rejected. The actual distribution appears to lie between the quadratic and linear cases, though it would seem to lie closer to the linear condition. For practical diaphragms a linear distribution would therefore be the most suitable.

For Test 2, in which failure is in a mode including profile collapse, even the linear case is unconservative. This is probably inherent in the assumption of the centre of rotation and as developed in the modified analysis shows that movement of the hinge line causes a reduction in the theoretical failure load. Fig. 2.18 considers both the linear and fully plastic force distributions, with the linear case giving a reasonable result. The value of j, for the linear condition, equal to the actual failure load is 1.075, which is a hinge line position of 629mm from position A.

This mode of failure does require further investigation, though it must be admitted that both failure modes 2 and 3 are of a limited relevance to practical diaphragms. The main reason for this is that the slab has to rotate in the failure mechanism. For most practical panels the structural actions is that of a simply supported beam and not of a cantilever. In such circumstances, rotation of the composite slab is prevented by the adjacent slabs and, of the modes investigated, only mode 1 is possible.

Barnes [19] reported failure in the concrete topping whereas in the present tests no distress of the topping was observed. However, the highest shear per unit length in the present tests were 28.6 kN/m, whereas in the Barnes tests

cracking did not commence until a load of 31.0 kN/m had been reached and failure was delayed until the load carried was 86.4 kN/m. The difference in behaviour is clearly a consequence of the relatively high strength of welded connections to the perimeter structure.

The behaviour of the slabs prior to failure is described in the load / deflection curves, Fig. 2.6 - 2.9. In each case the predicted stiffness is shown as a broken line both through the origin and also alongside the relevant part of the load / deflection curve.

In the initial stages of loading in Tests 1, 2 and 3 the response is dominated by a large non-linear movement. The movement, though does not appear on unloading and re-loading. This is probably due to initial freedom of movement between the steel and concrete before full composite action takes place. Shrinkage of the concrete is the most likely cause of the initial movement. Roberts [18] has recorded that the shrinkage occurs away from the ribs so reducing the bond between the steel and concrete, Fig. 2.20. This separation causes the concrete and steel to "jam" against each other after some load has been applied, so producing the non-linear movement.

Test 4 shows that the initial non-linear movement has been eliminated and is confirmation of the shrinkage cause of the movement. As described previously the construction of Test 4 was different to the other tests to minimise this initial movement, as the concrete would have already "jammed" against the steel sheeting during Test 3.

2.8 A further note on composite slabs

In the test programme there were no cases of loss of bond between the steel and concrete. Barnes [19] does state that a failure due to the loss of bond was possible. This could be critical in combination with a shear / bond failure due to the bending action. The combined failure would occur in the region of the main beam fasteners where the transfer of the shear force, due to the diaphragm action, from the concrete to the fasteners interacts with the bond stress from the shear / bond failure.

A check would be the mose convenient means of avoiding this failure in the region of the first corrugation, so that

$$F_{bsc} = F_{bsb} + F_{bss} \qquad \ldots\ldots (2.38)$$

where F_{bsc} = combined bond stress

F_{bsb} = bond stress due to bending action

F_{bss} = bond stress due to diaphragm action

At the present time, though, some doubt occurs over the validity of the bond stress due to bending action. Here the French Bond Stress method could be a means of evaluating this stress. However, the other methods do not give any means for determining the bond stress due to the bending action.

2.9 Composite Slabs acting as Horizontal Diaphragms

In the previous sections of this chapter, expressions

for the strength and flexibility of composite slabs in shear have been developed and verified experimentally. It would now seem appropriate to investigate the characteristics of the slabs acting as floors in multi-storey buildings. At present a number of methods of analysis are available [24] [25] but these consider rigid floor movement or do not investigate the effect of the distribution of the shear force in the floors. In practice there are a number of simplified design approaches depending on the size and layout of the buildings, a survey of the methods has been undertaken by Davies [11]. For all the design methods the floor slabs are assumed to be of infinite stiffness. The test results, presented previously, have been shown that this assumption to be invalid. In order to investigate the effect of non-rigid slabs a full three dimensional building has been analysed.

For this analysis a simple means of analysing the structure was sort. Davies [26] has suggested a possible method for determining the lateral and vertical loading distribution in complex multi-bay industrial buildings, which is easily adopted to multi-storey buildings. The method consists of using a standard two dimensional plane frame computer program with each frame assumed to be moved coincidence with each other frame. Elastic springs in the same plane connect the frames to each other, to idealise the corrugated sheeting as shown in Fig. 2.21. Davies developed an expression for the area of the springs from the flexibility as

$$\text{Area of spring} = \frac{L}{C \cdot E} \qquad (2.39)$$

where L = Length of the sheeting

E = Elastic constant of the sheeting

C = Flexibility of the sheeting

The structure analysed in the study was designed by Bates [27] in 1963. Modifications to the structure are only required to the floor construction, where precast concrete floor units are replaced by the composite floors under consideration.

A typical floor level is illustrated in Fig. 2.22. The building consists of a central tower block 21.3m wide by 41.8m long, 11 storeys in height and at the base of the tower the floor width is increased to 39.58m for the two lower floors. At each end of the building there are lift shafts and stairs that act as shear walls. A layout of the building is shown in Fig. 2.23.

A plane frame computer program developed by Dr. J. M. Davies has been modified to analyse the structure. As the storage requirements of the three dimensional structure is large the program adopts the "partitioning" technique for solving the stiffness matrix.

In the study three different configurations were analysed, namely

(a) a plane frame analysis of the single frame.

(b) the three dimensional structure without the shear walls.

and (c) the three dimensional structure with the shear walls included.

For configurations (b) and (c) the composite slabs were assumed to be of similar construction depth to that of Diaphragm Test 2.

The deflection profiles at frame 8 are given in Fig. 2.24, through the deflections for configuration (c) are small compared with the other configerations.

From the results, analysing a three dimensional structure without shear walls produces a reduction of 13% in the maximum deflection compared with the plane frame structure. This is explained by the fact that the end frames are only loaded by half the internal frame loads. For this case the effect of the composite slab is of limited value.

Inclusion of the shear walls causes the maximum deflection to be reduced to 1.3mm, a considerable reduction on 133mm for the bare frame. In this configuration the composite slab distributes a large proportion of the lateral load to the shear walls. So, as one would expect, the composite slab is acting as a deep beam and the relatively flexible frames are taking none of the lateral load.

The value of "C", the shear flexibility, for the composite slab has been obtained from only the linear portion of the load deflection curve. Some small additional movement could be accounted for if a non-linear analysis was undertaken, but at the present time this facility is not included in the program.

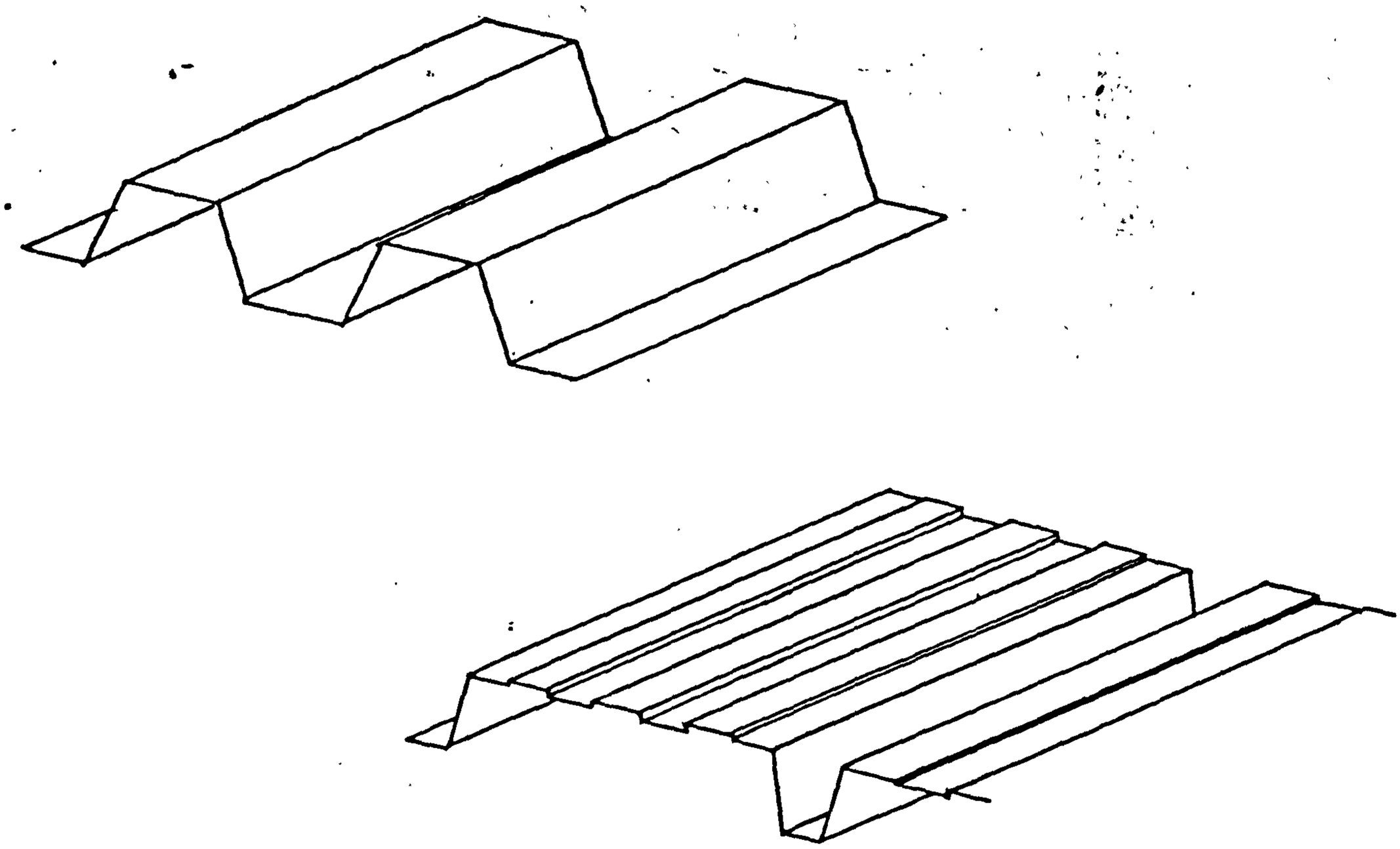

Fig 2.1(a) Typical Sections

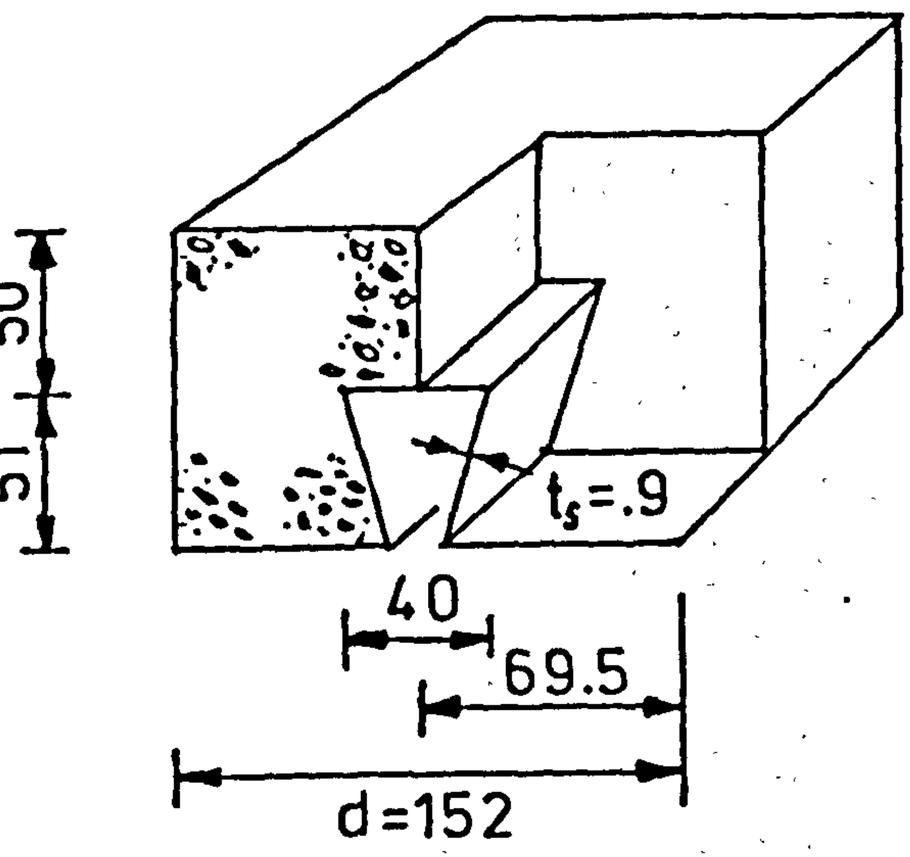

Type A - Re-entrant

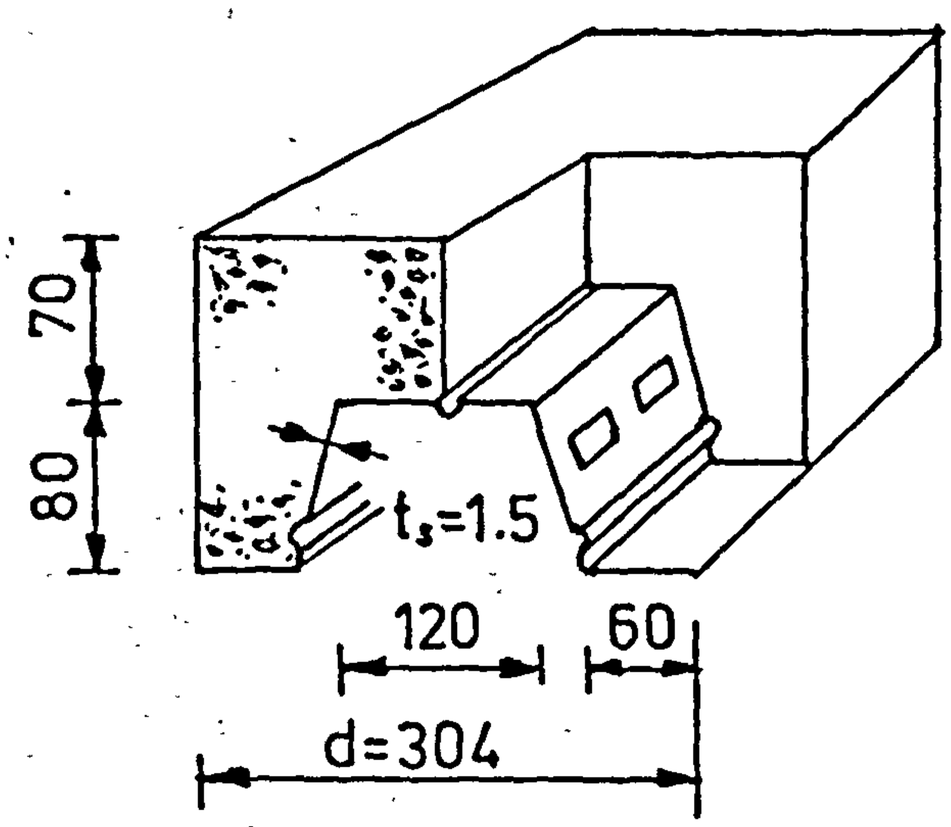

Type B - Trapezoidal

Fig 2.1 (b) Decking Profile Type

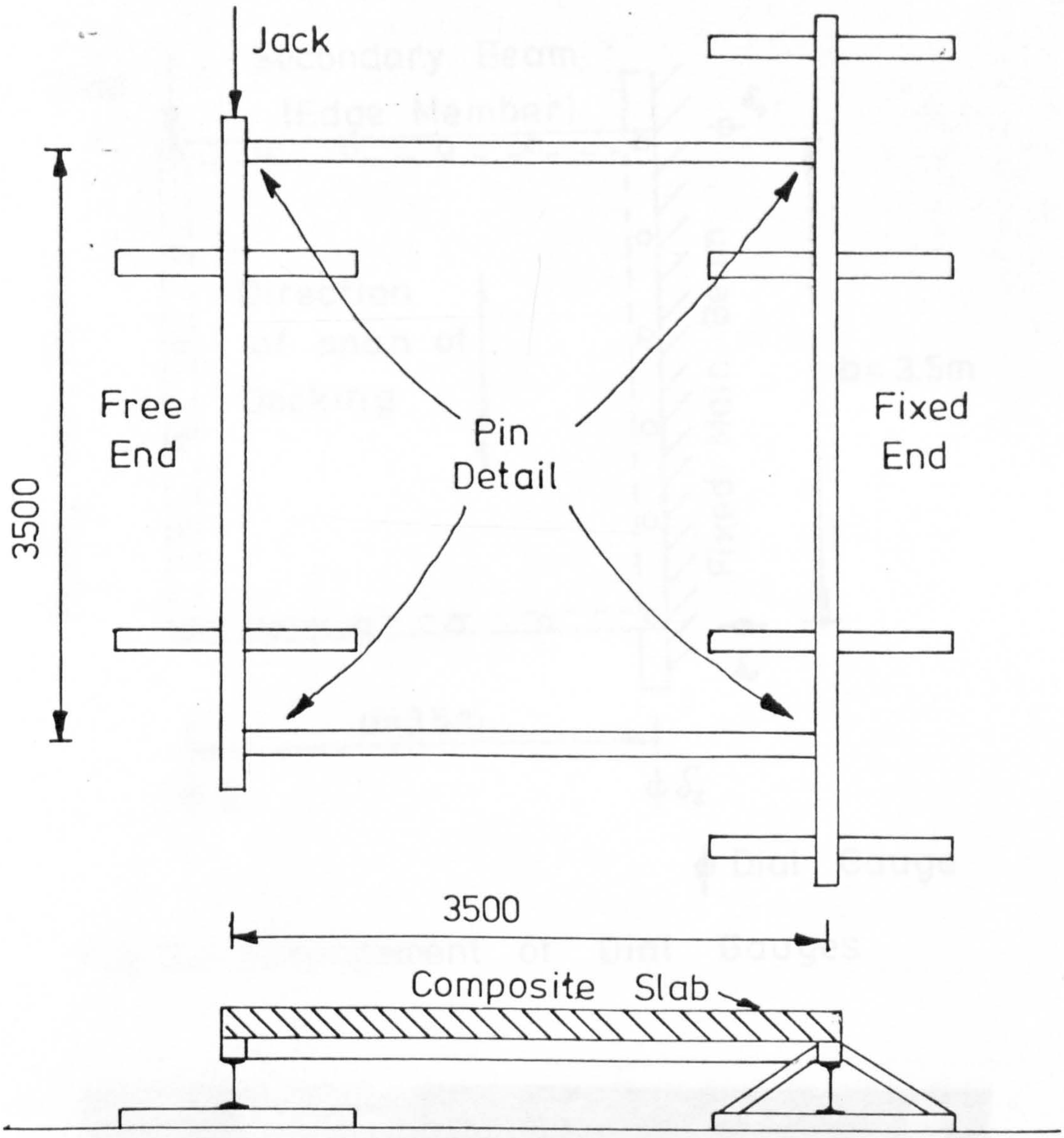

Fig 2.2 Layout of Test Frame

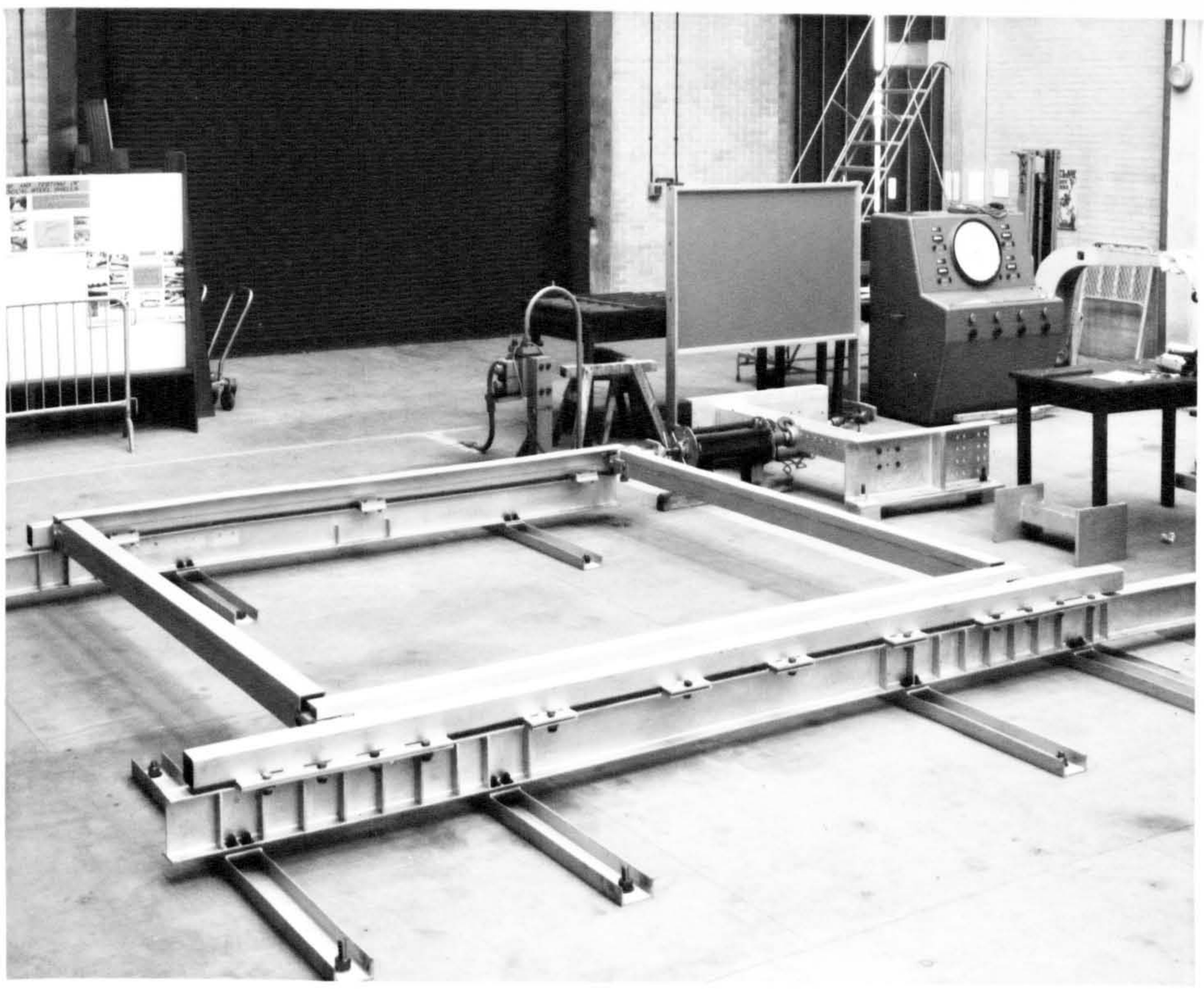

Fig 2.3 Test Frame

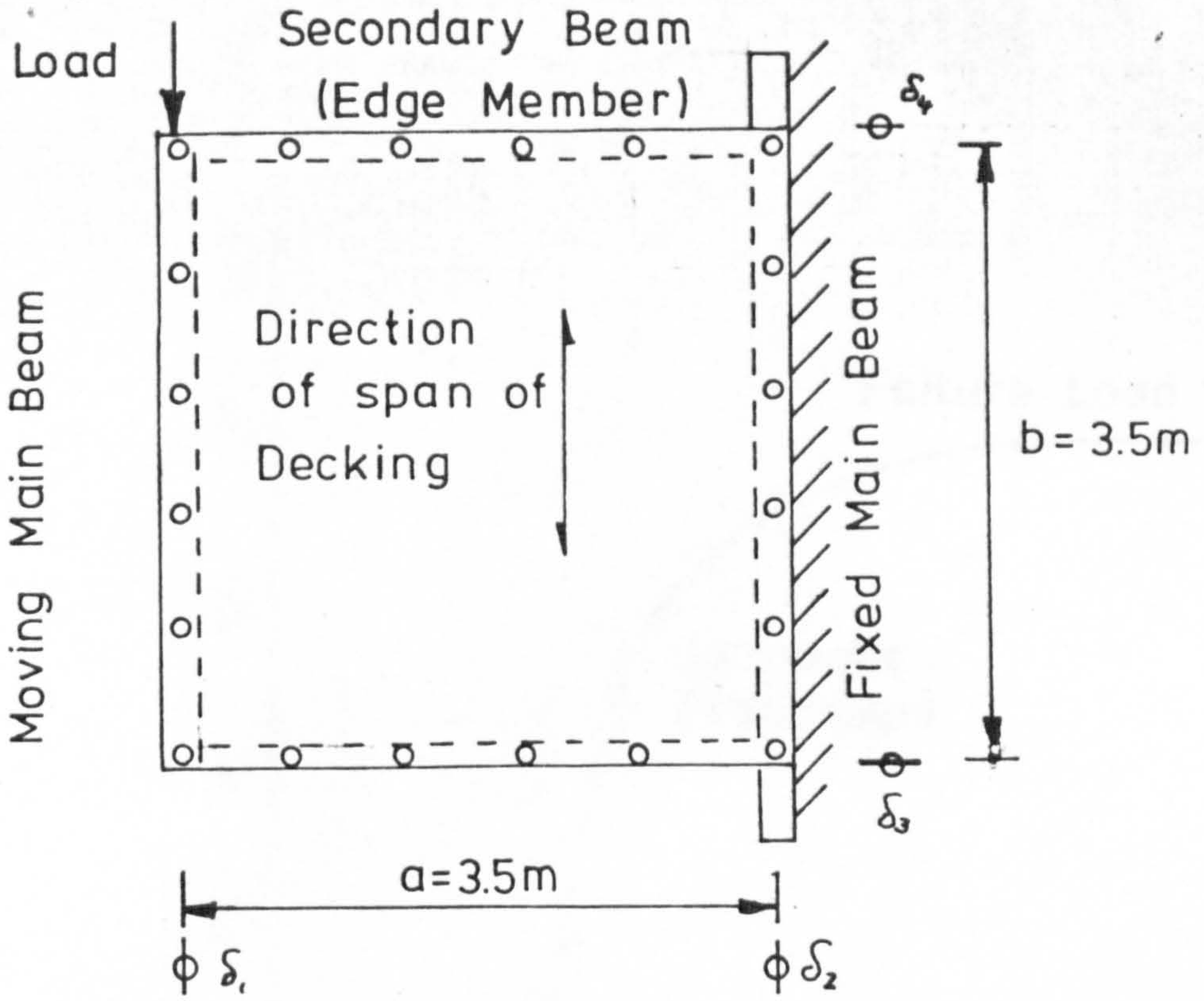

Fig 2.4 Arrangement of Dial Gauges

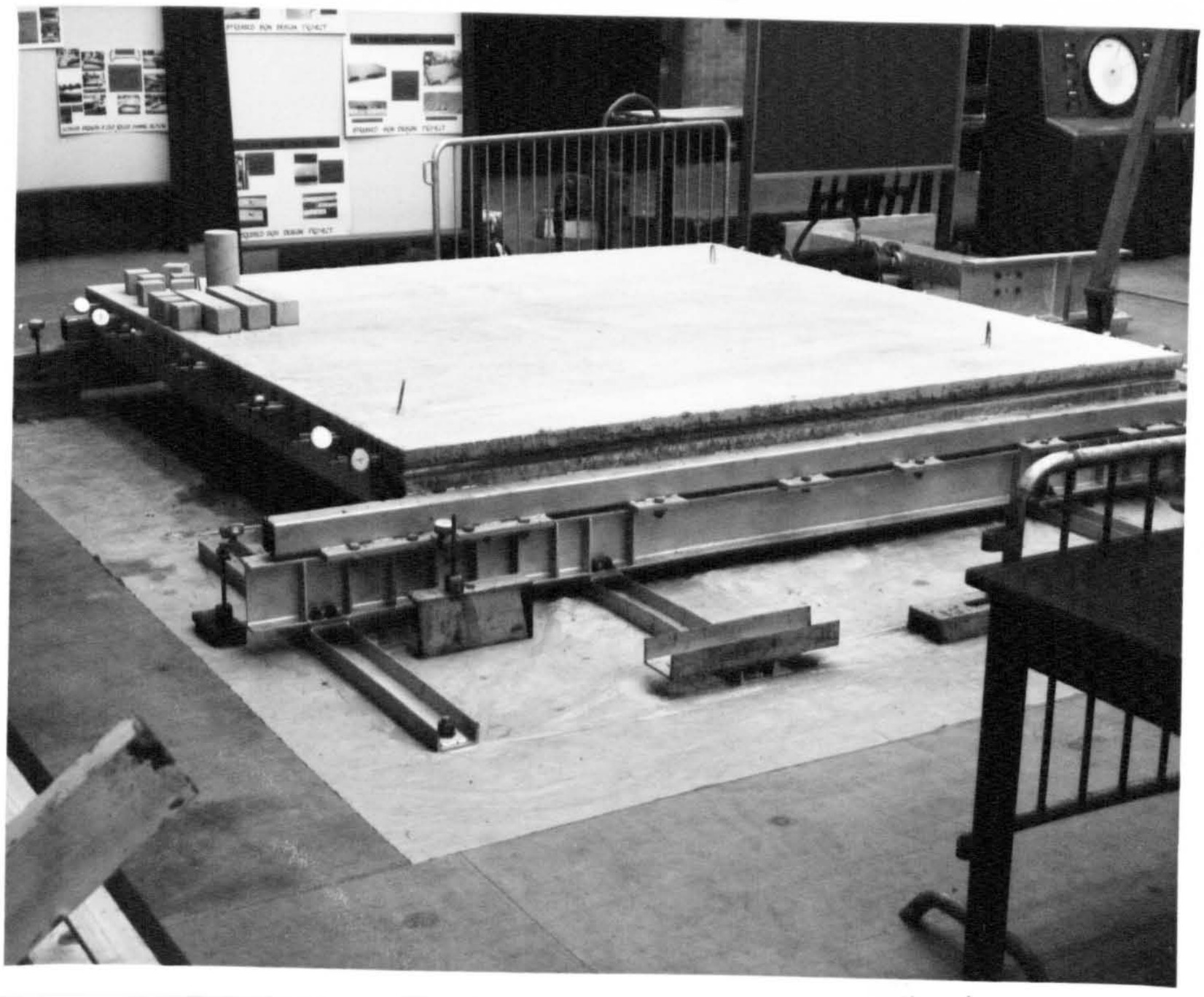

Fig 2.5 Diaphragm Prepared for Test

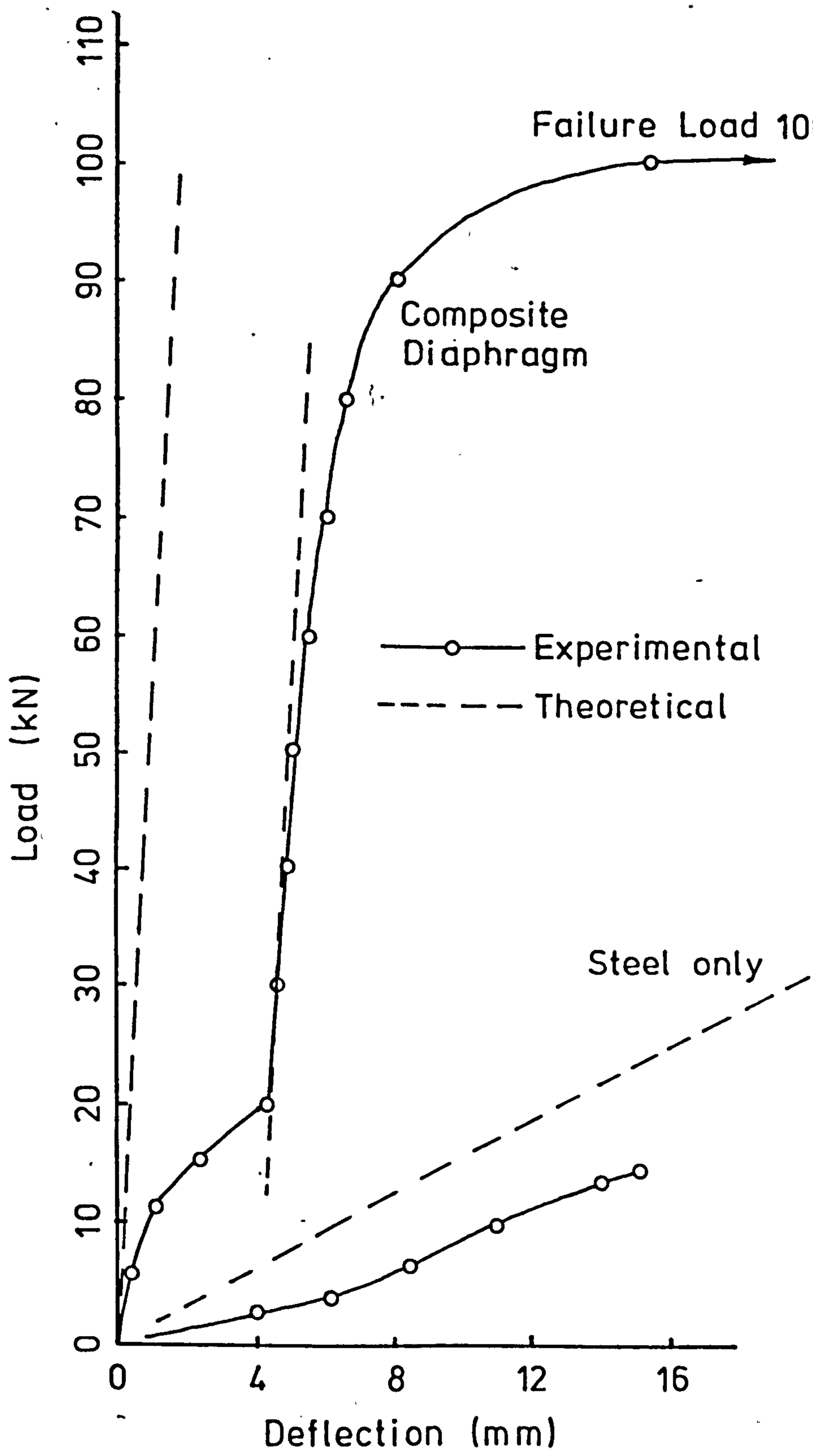

Fig 2.6 Diaphragm Test 1

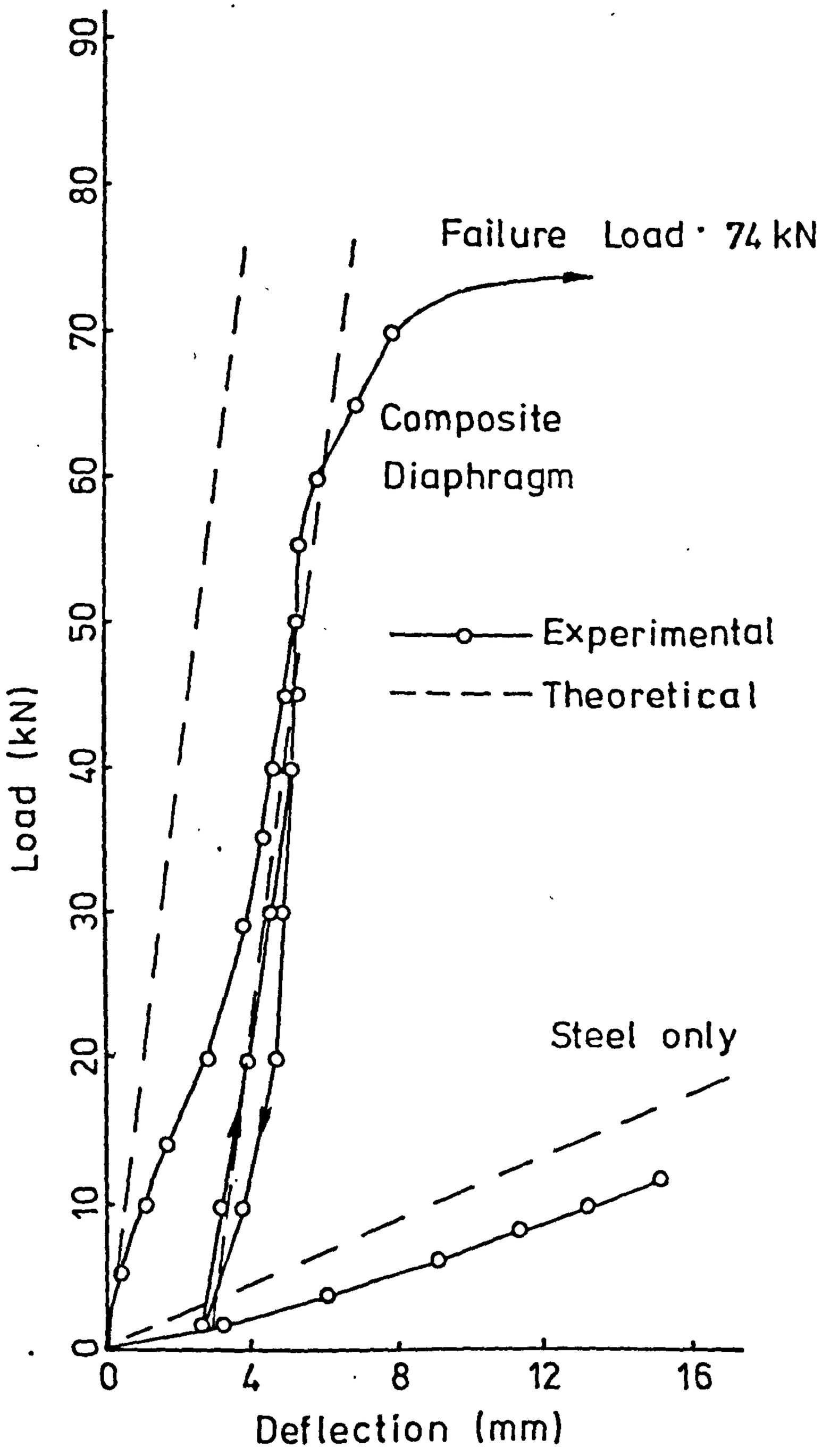

Fig 2.7 Diaphragm Test 2

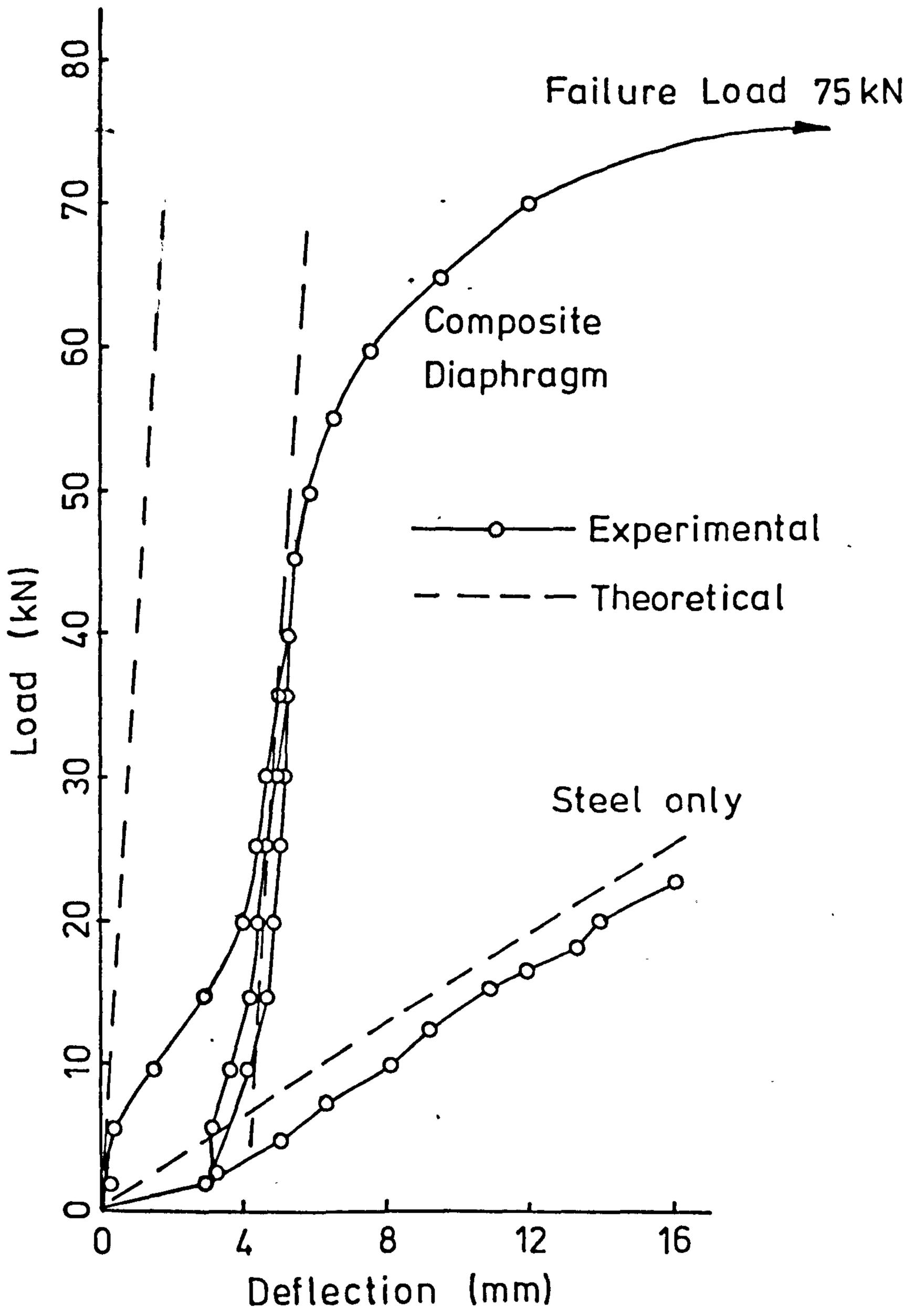

Fig 2.8 Diaphragm Test 3

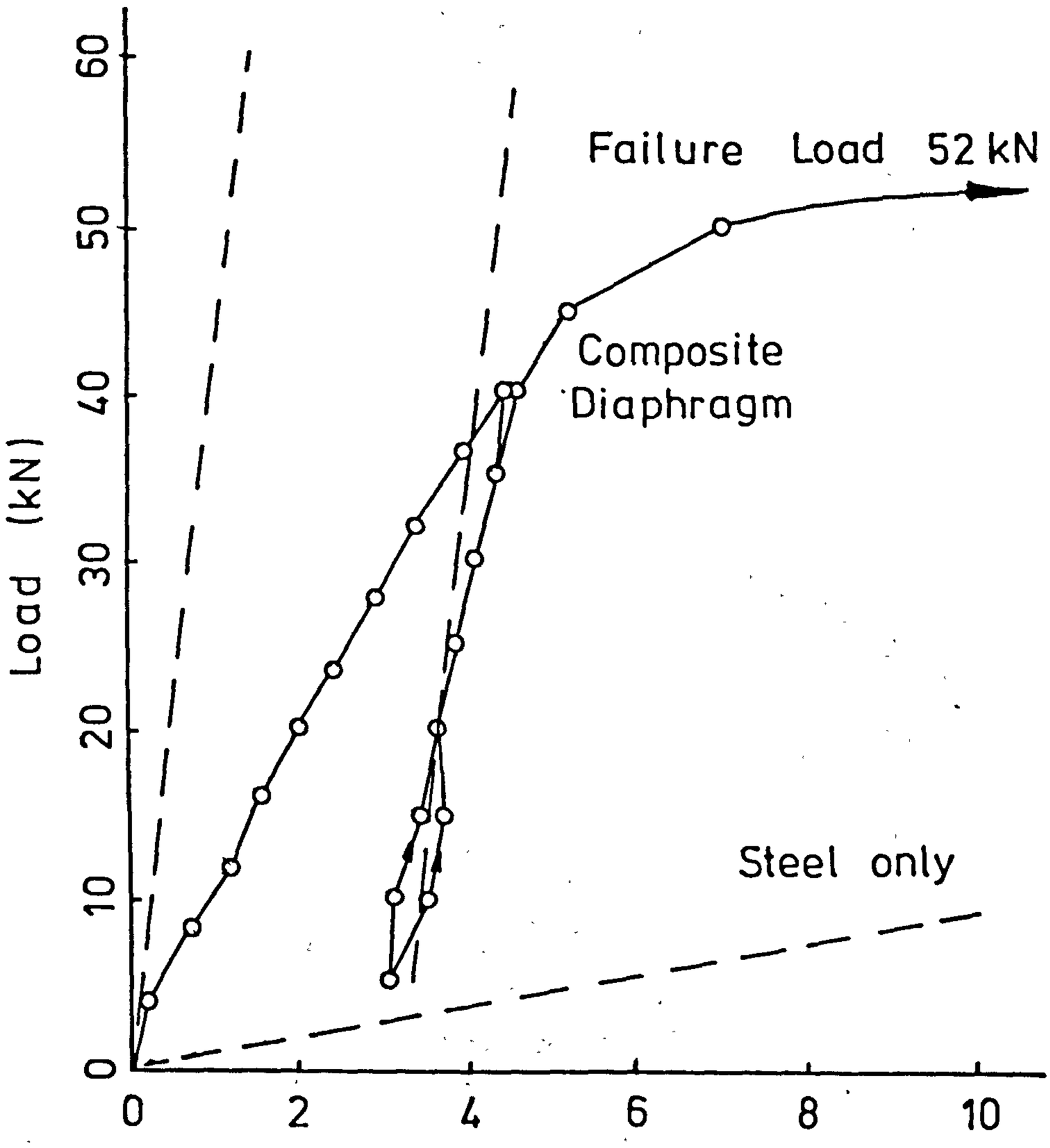

Fig 2.9 Diaphragm Test 4

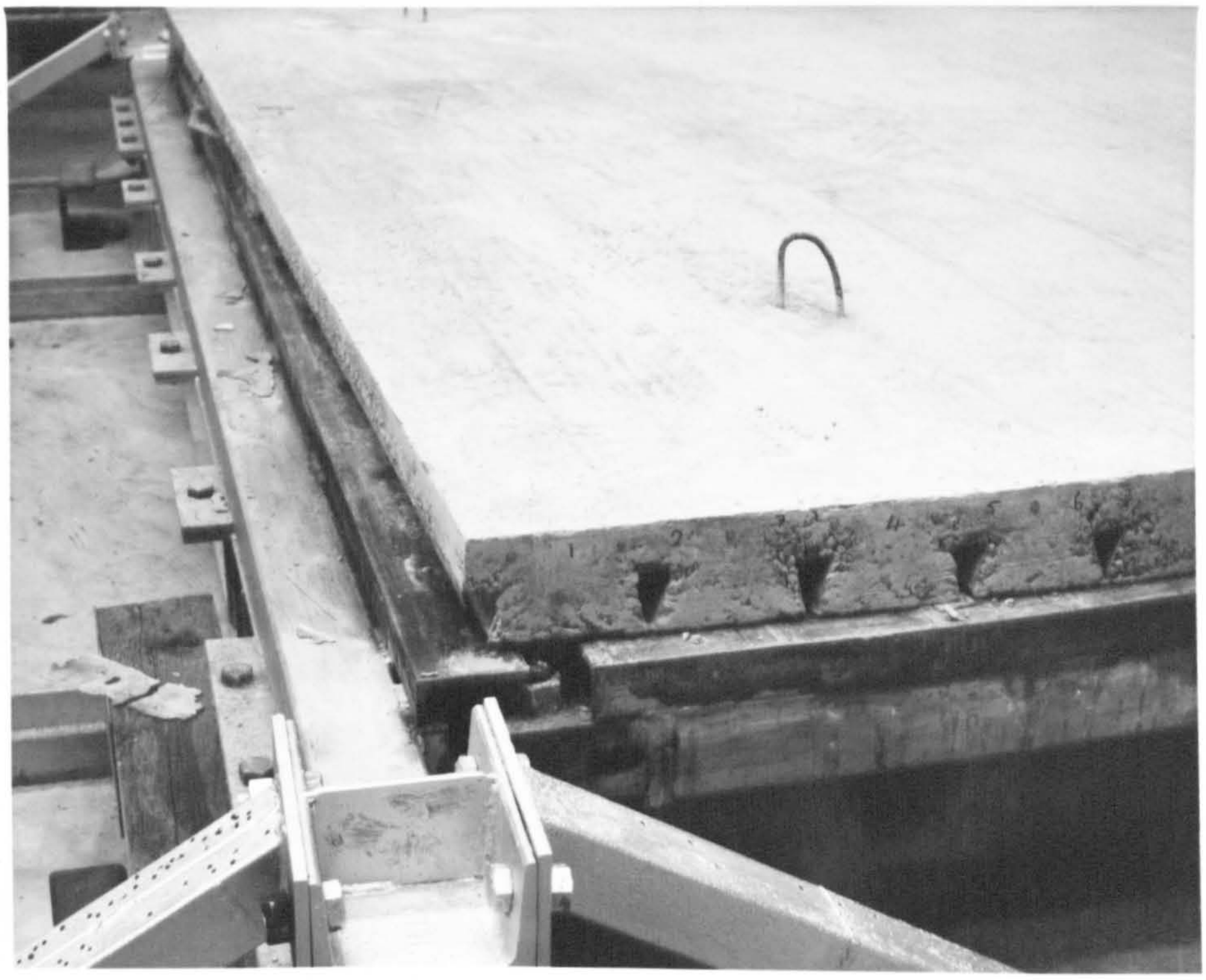

Fig 2.10 Failure of Mechanism 1

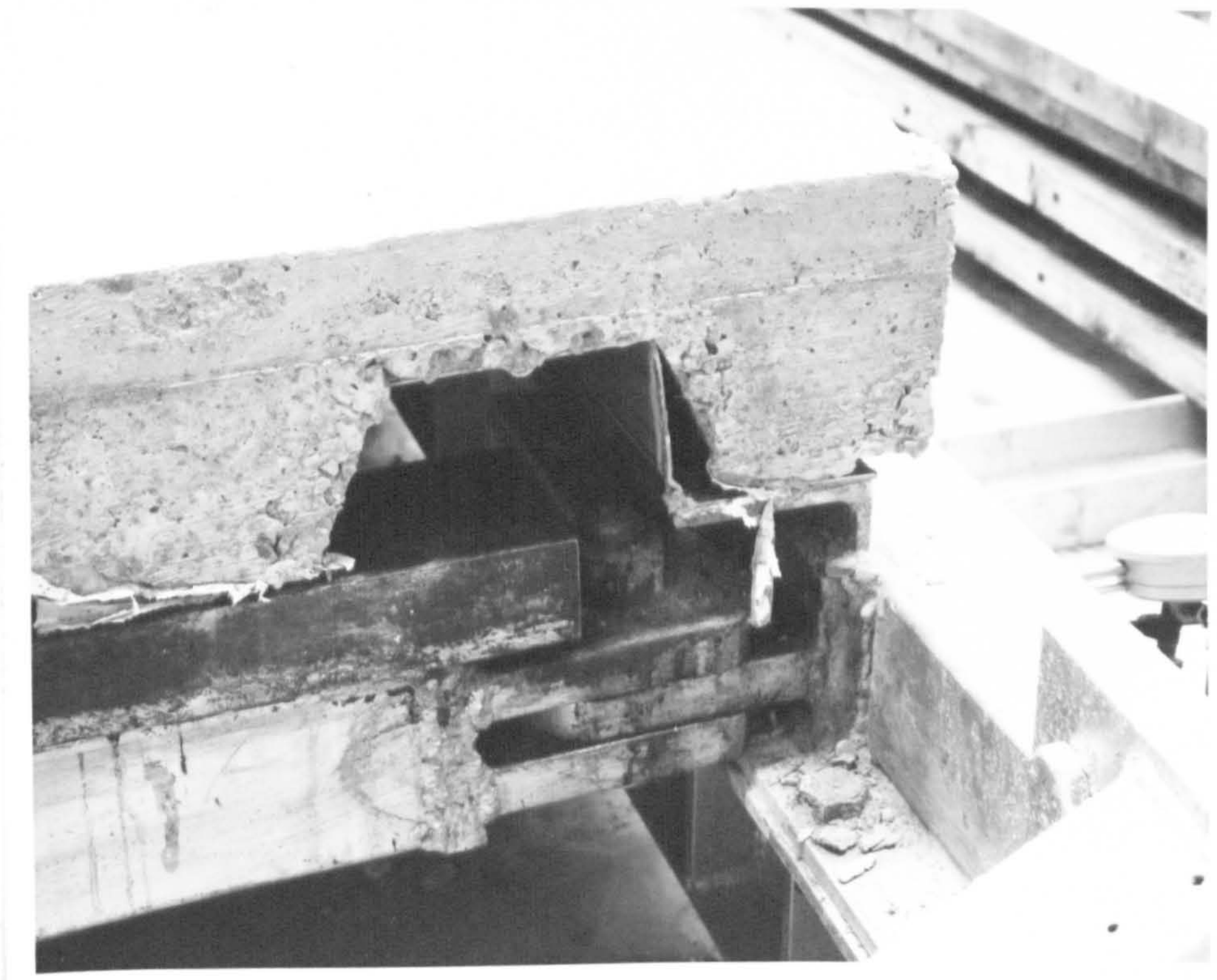

Fig 2.11 Failure of Mechanism 3

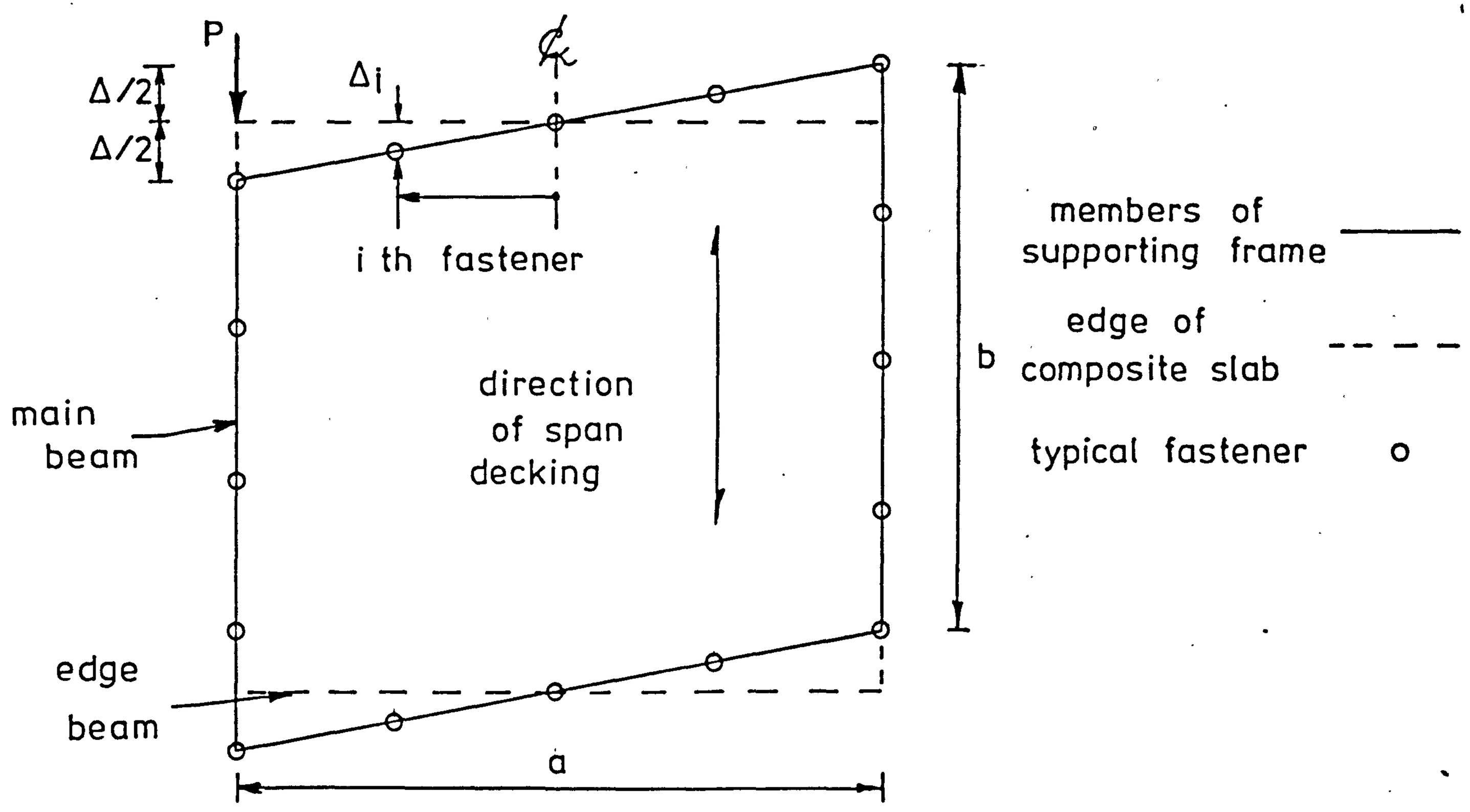

Fig 2.12 Analysis of Mechanism 1

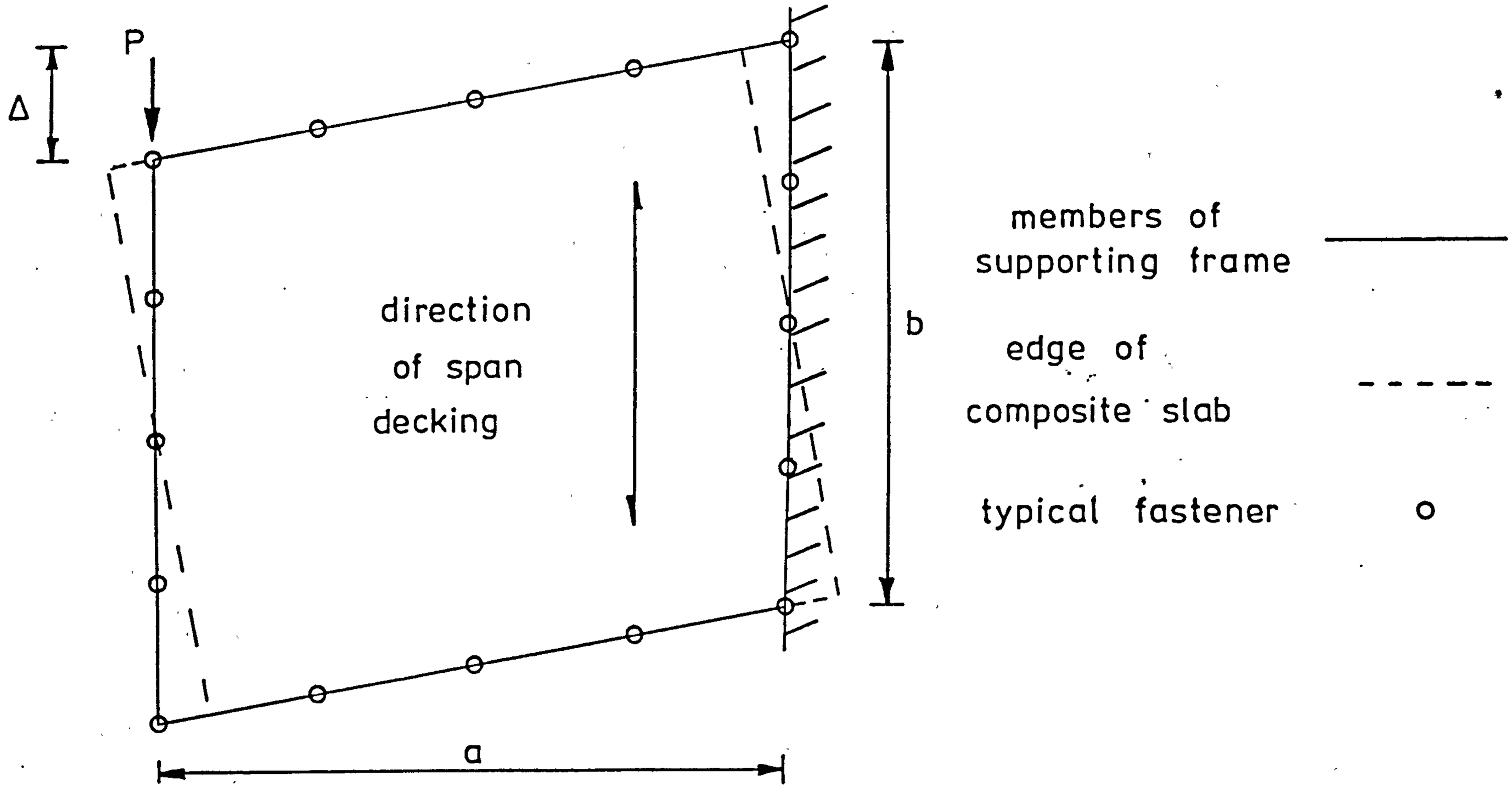

Fig 2.13 Analysis of Mechanism 2

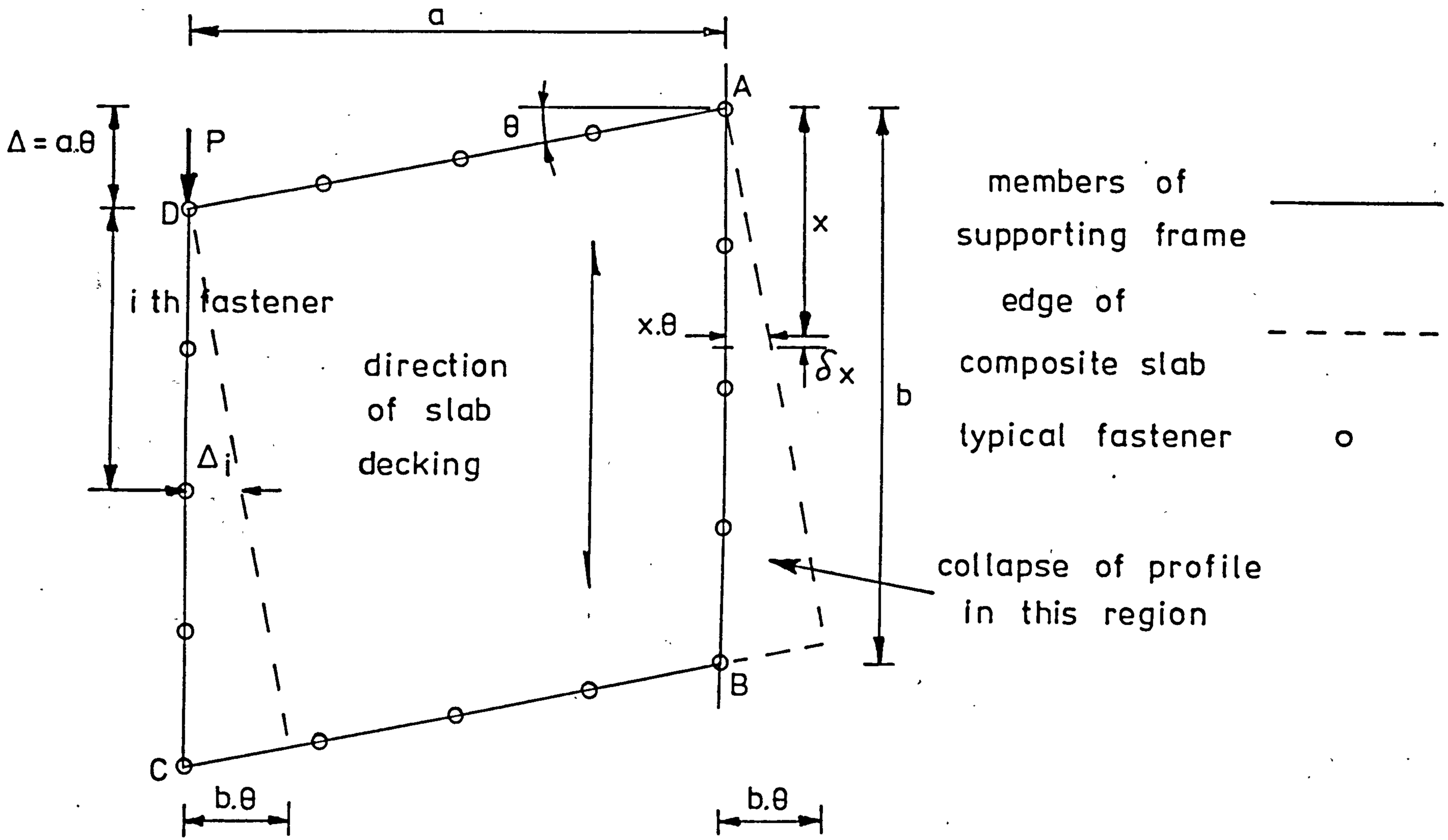

Fig 2.14 Analysis of Mechanism 3

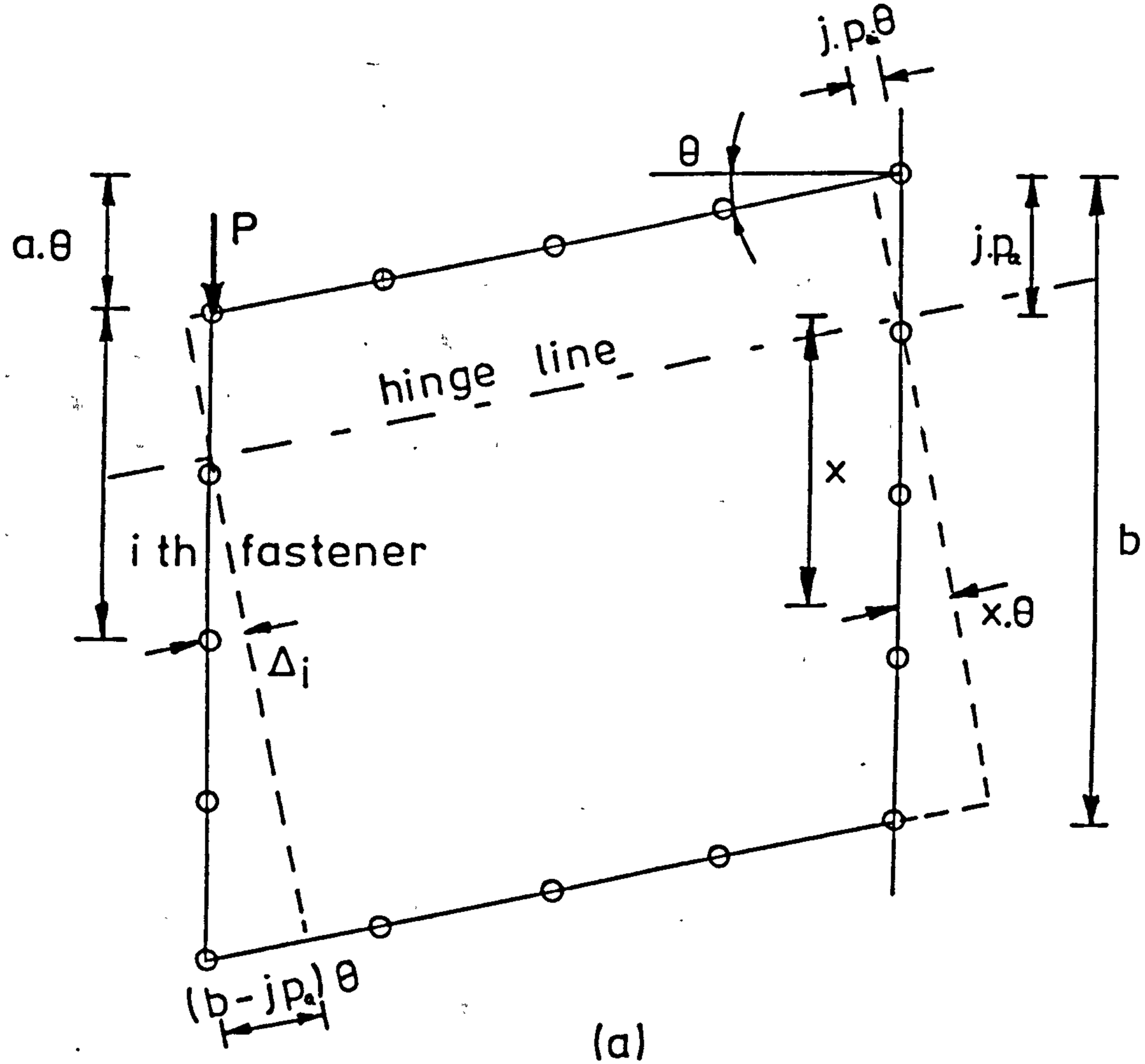

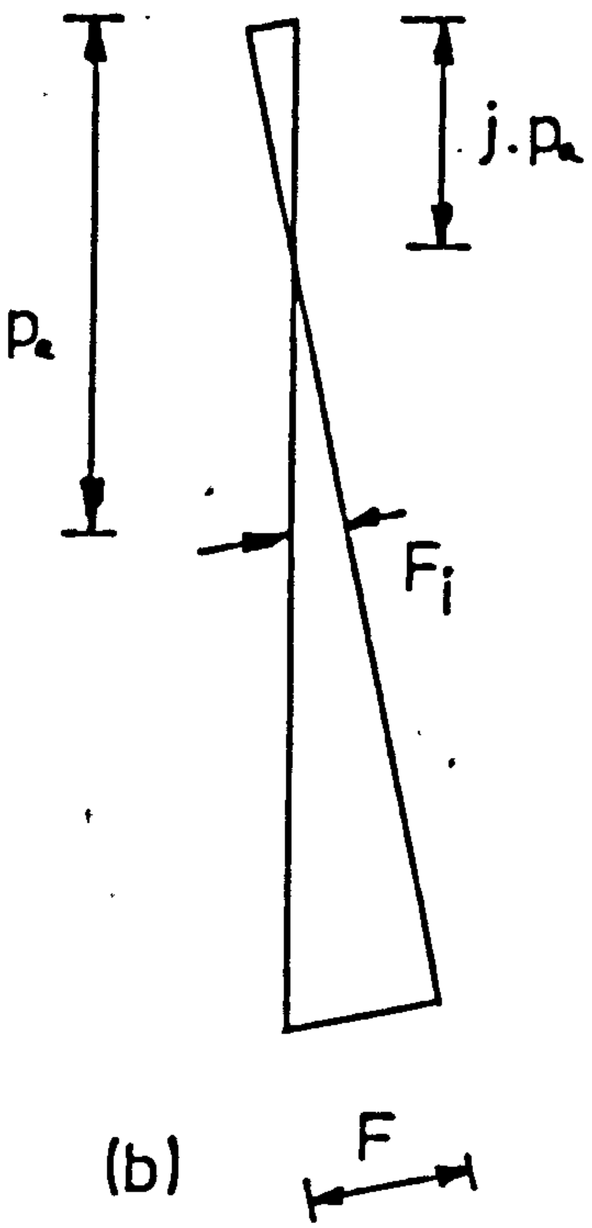

Fig 2.15 Modified Analysis of Mechanism 3

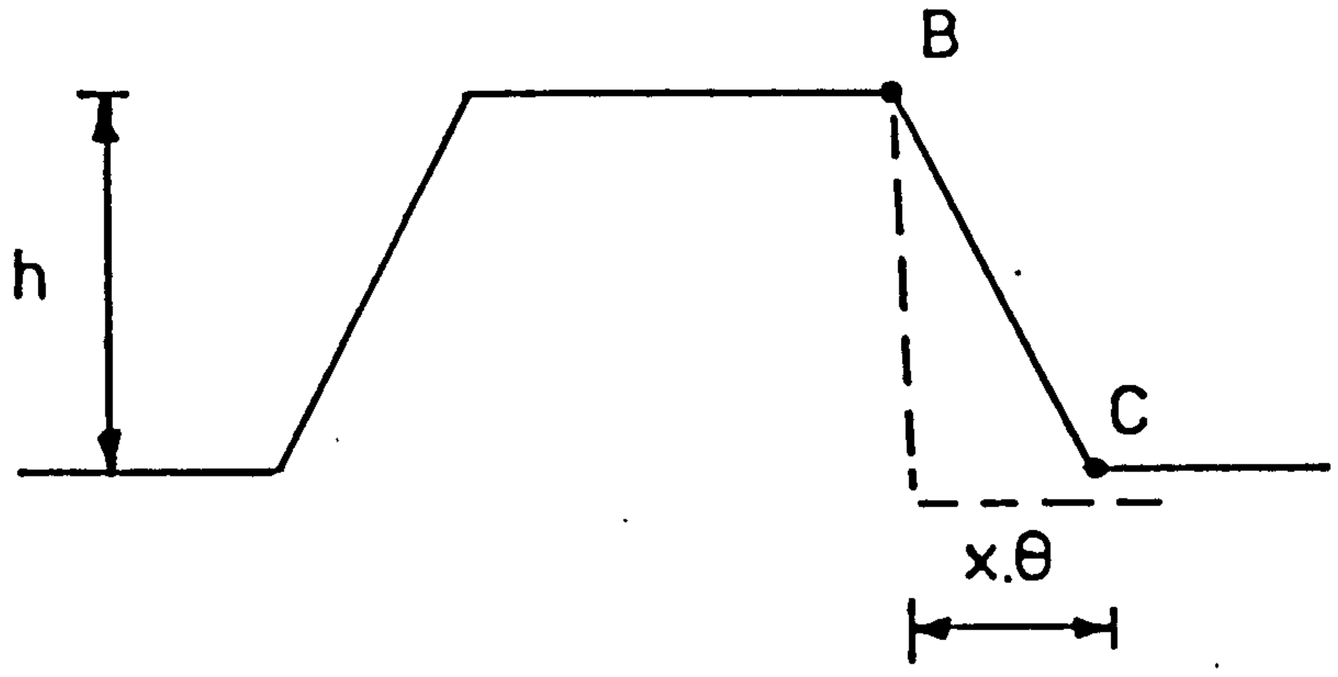

Fig 2.16 Movements at section X in collapsing profile

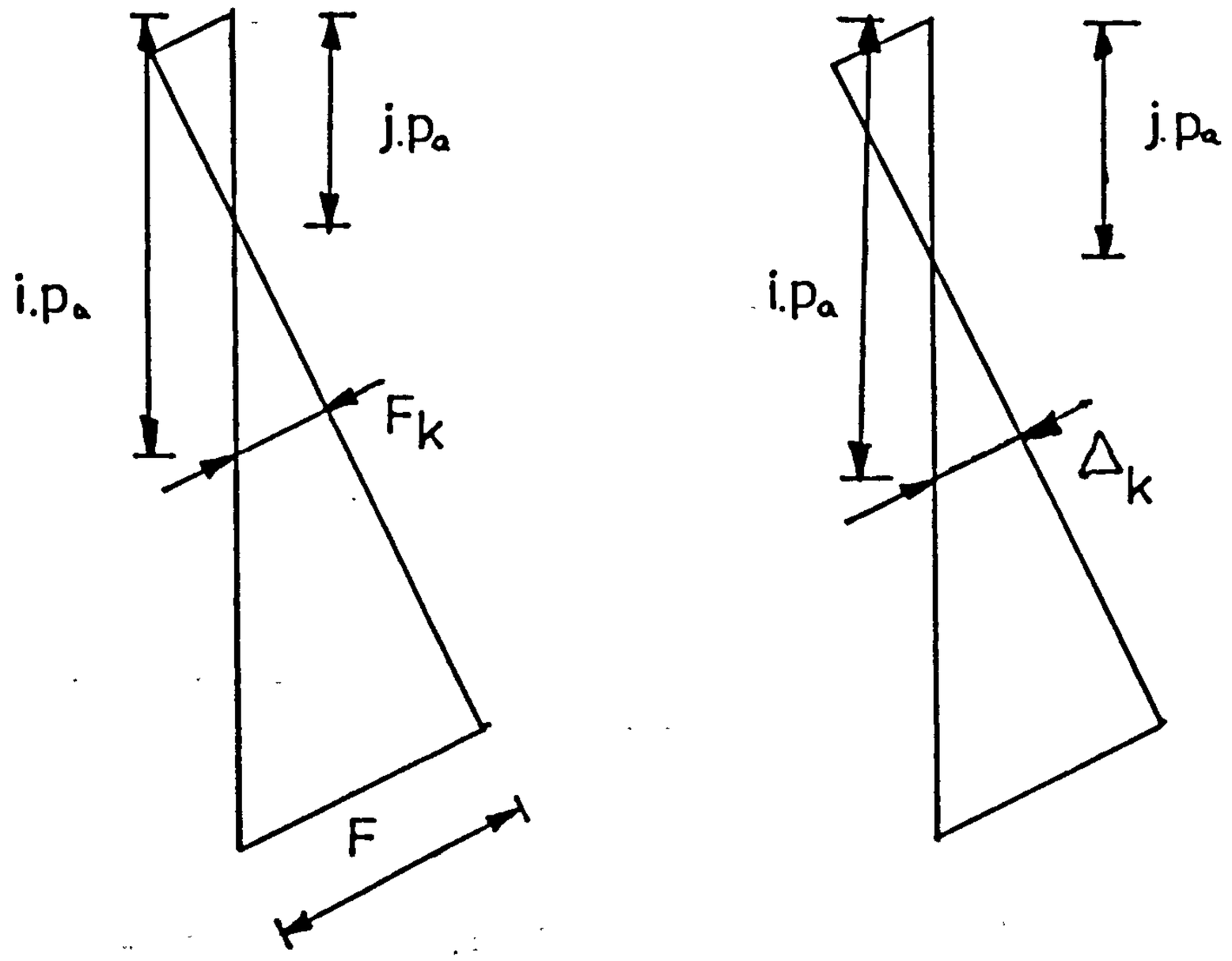

Fig 2.17 Force and Displacement diagrams for Modified Analysis 3

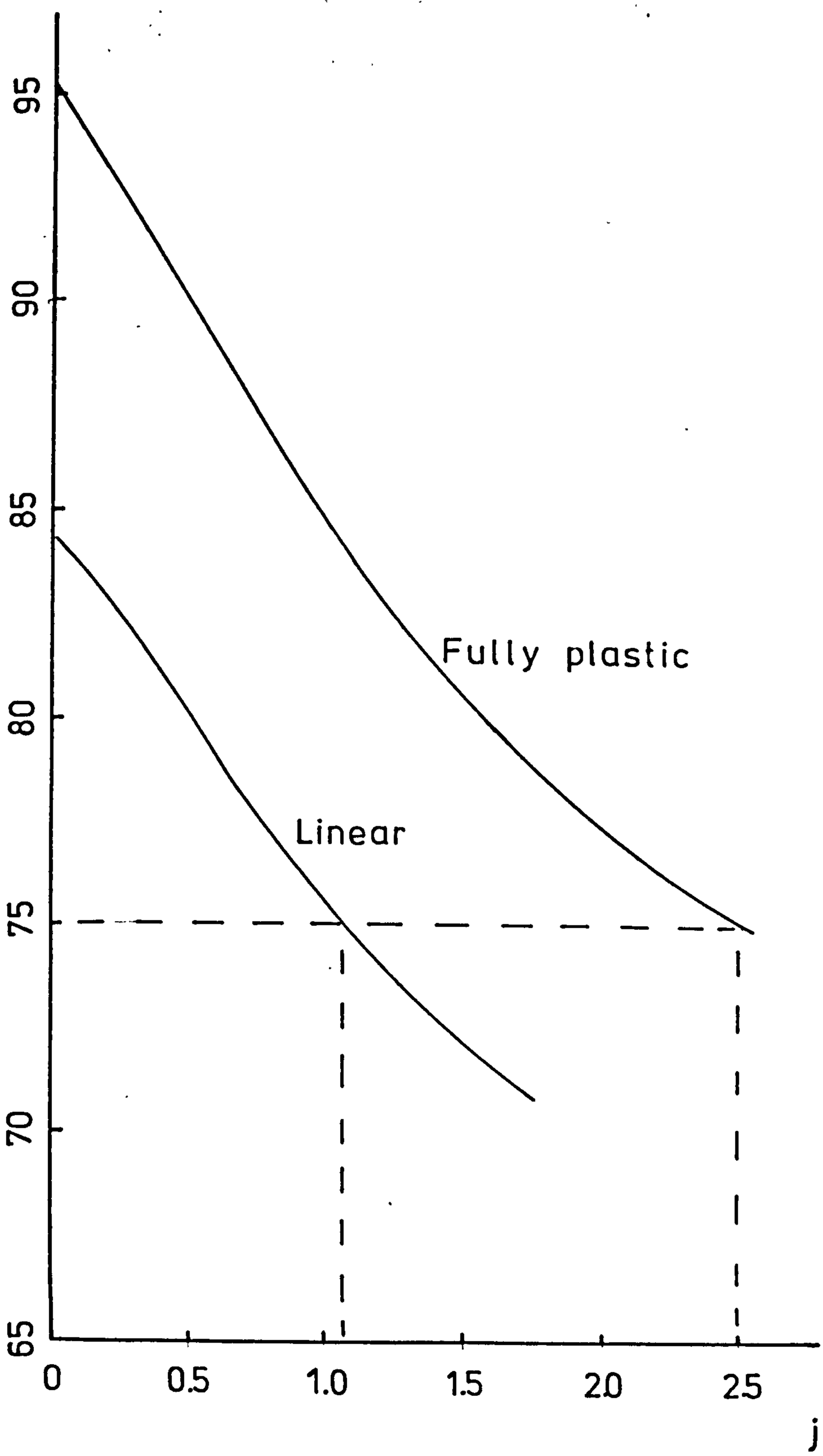

Fig 2.18 Variation of Ultimate Load with Hinge Line

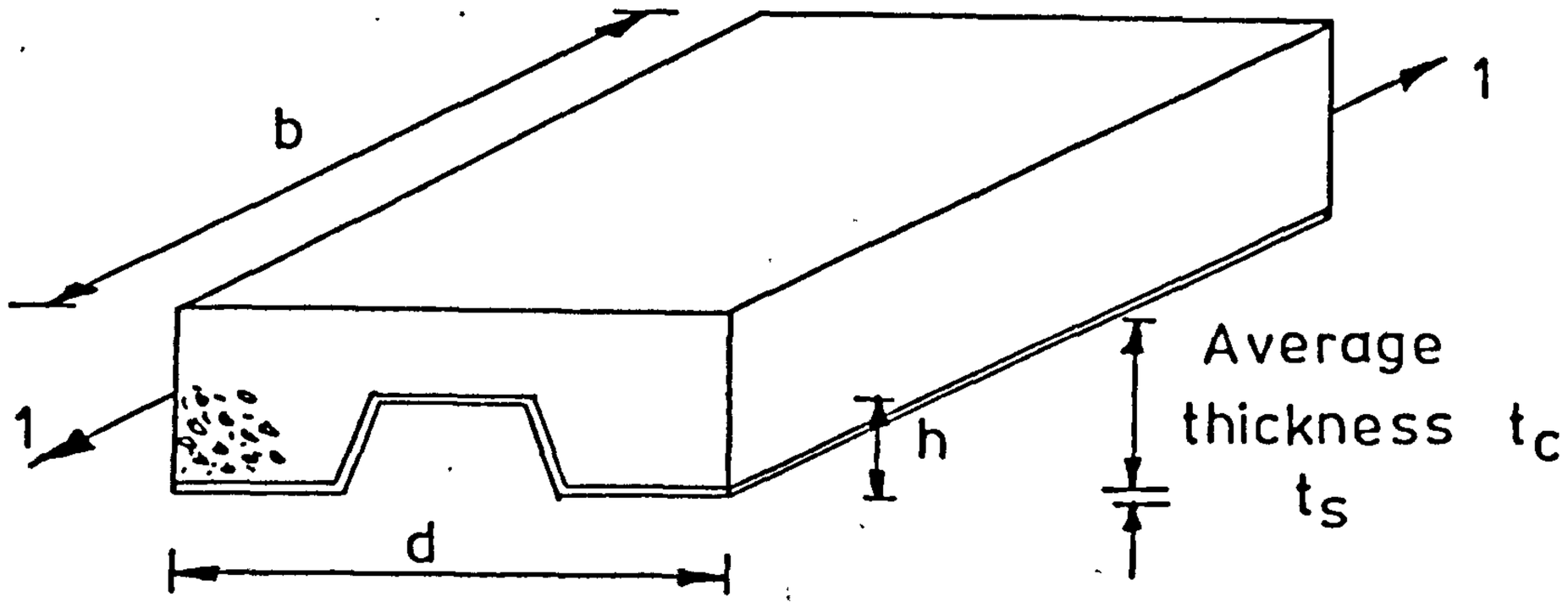

Fig 2.19 Notation for flexibility calculation

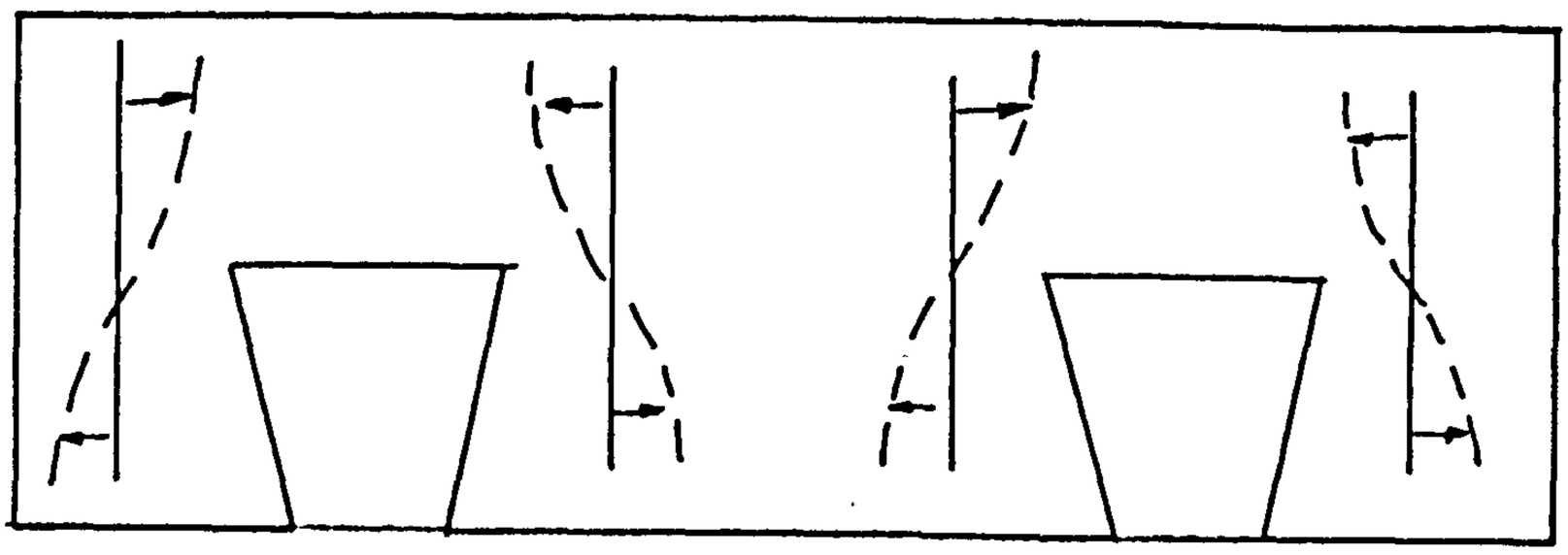

Fig 2.20 Shrinkage Movements (after Roberts)

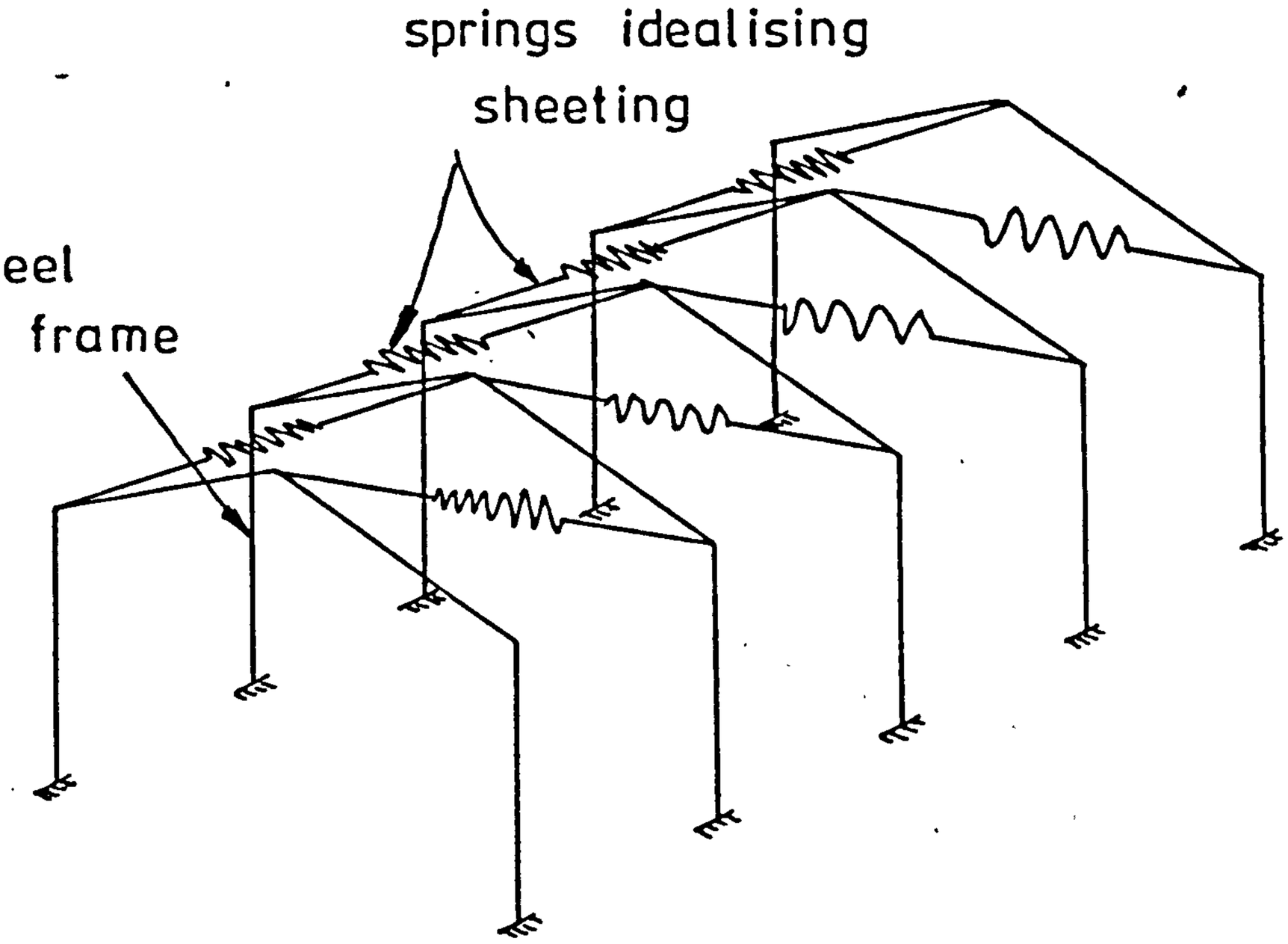

Fig 2.21 Idealised 3-Dimension Structure

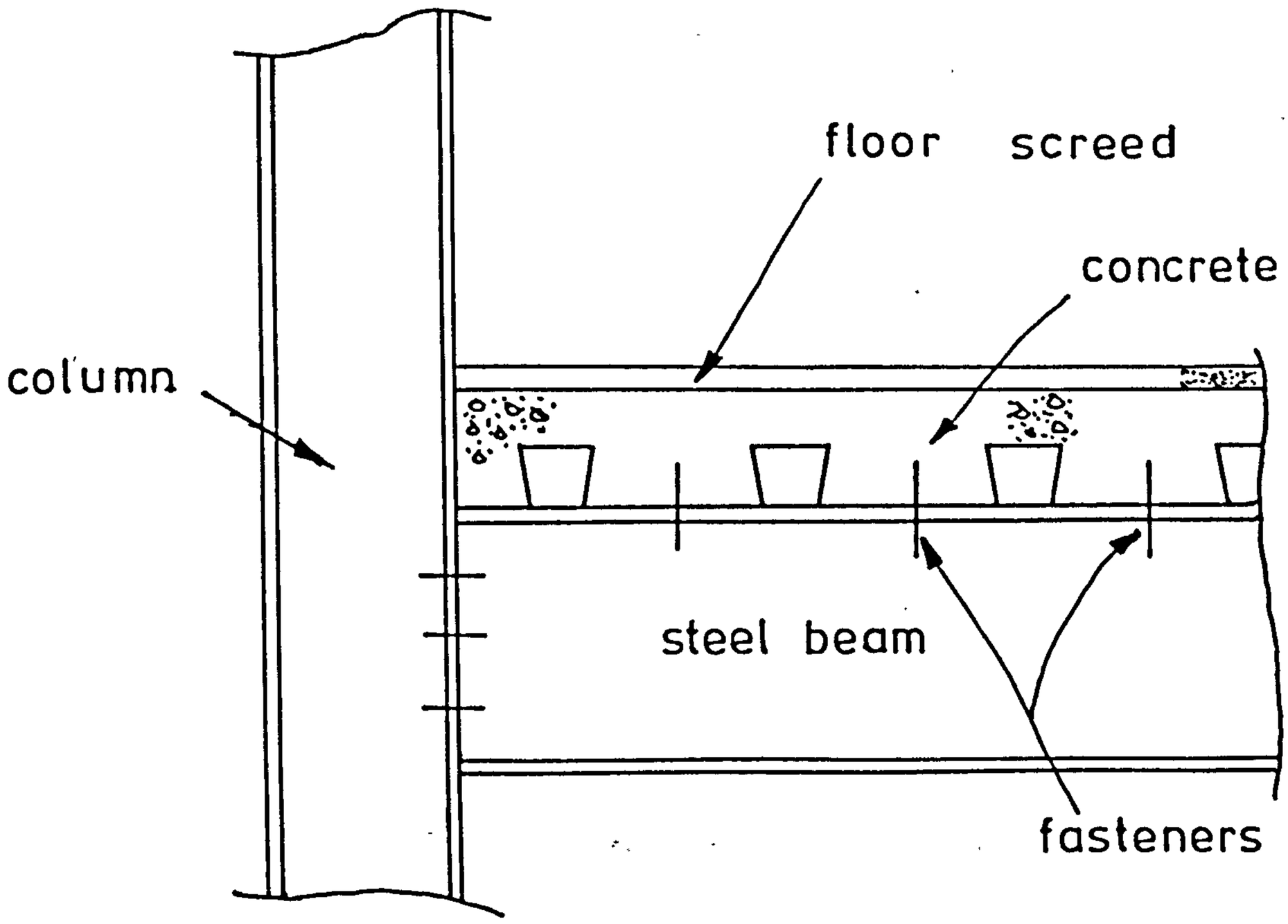

Fig 2.22 Typical Section thro' Floor

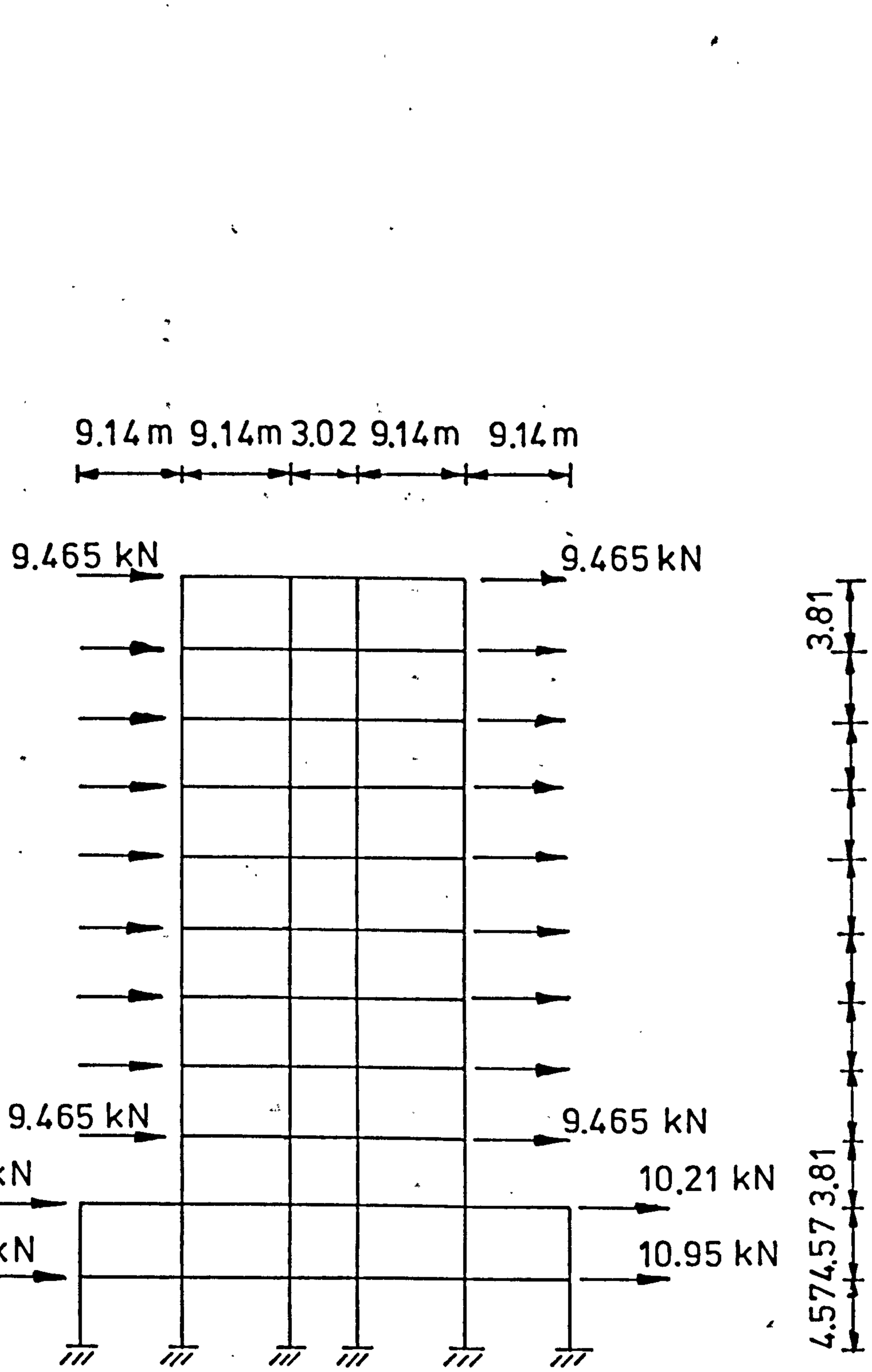

Fig 2.23 (a) Side Elevation of Structure

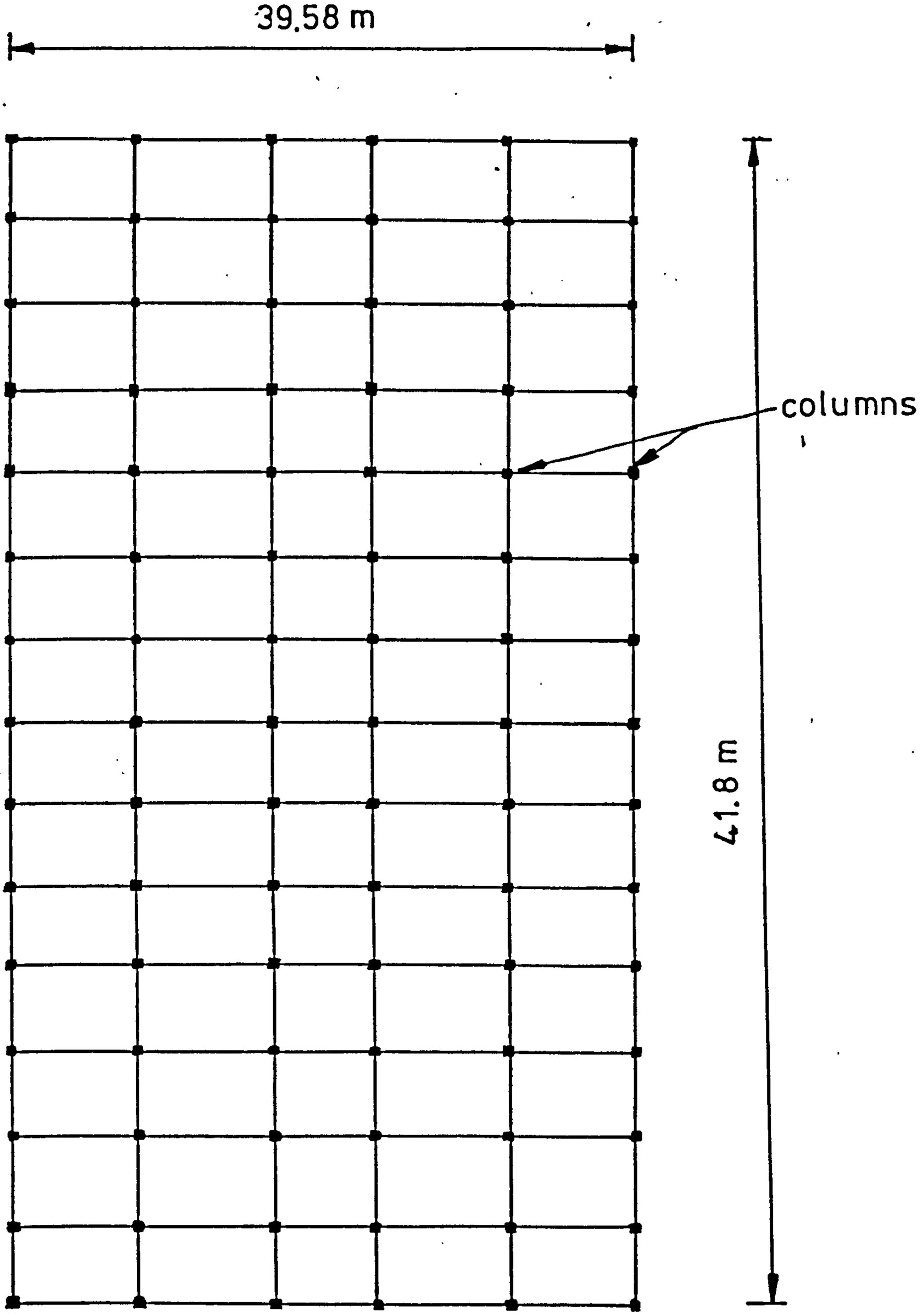

Fig 2 23 (b) Plan of Structure

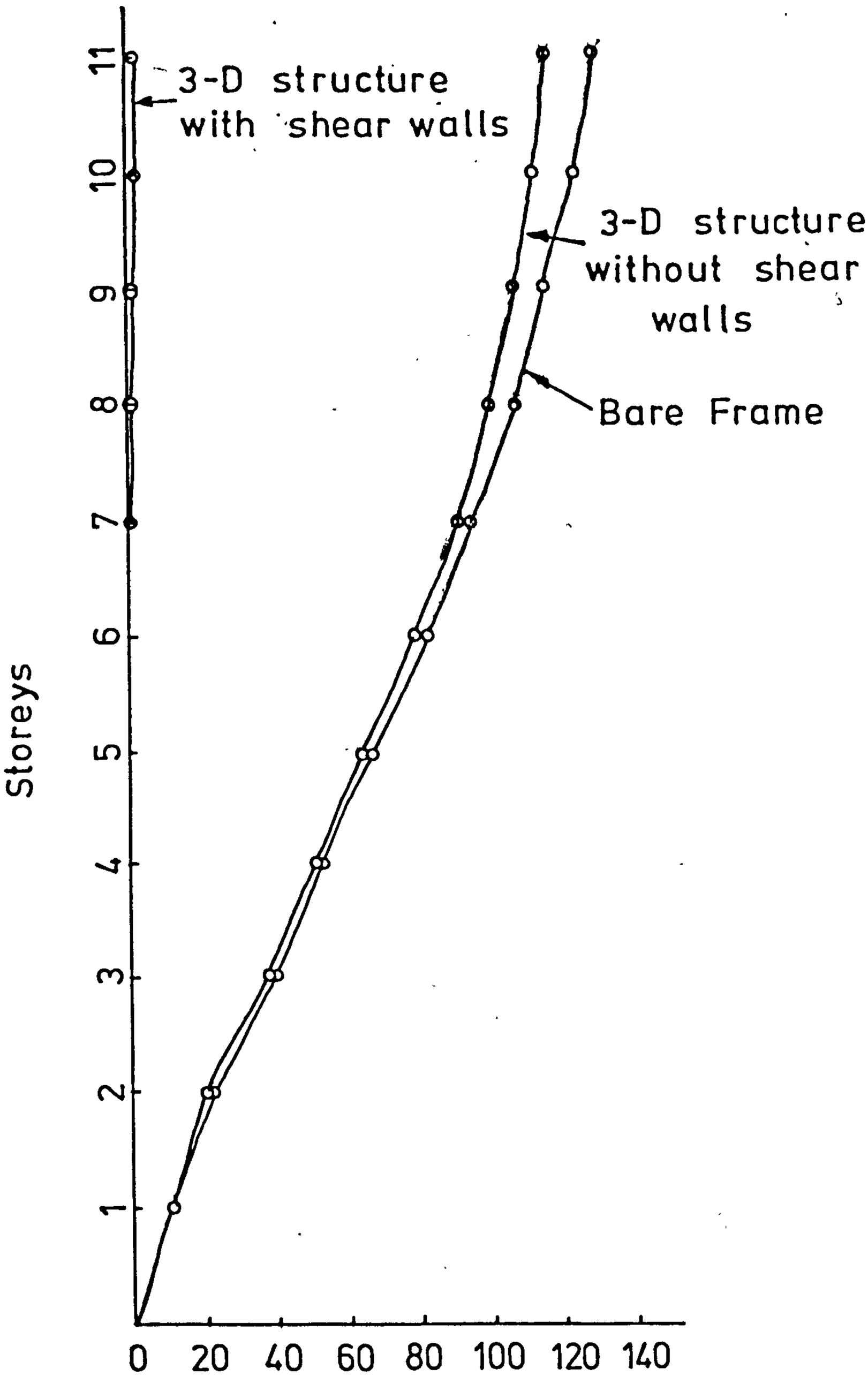

Fig 2.24 Deflection curves for multi-storey building

3. Finite Strip Analysis of Structures

3.1 Introduction

The Finite Element Method[28] is a powerful tool for the researcher and designer in the analysis of structural problems. However, the method can be time consuming, in both the preparation of the data and the running of the program. Where structures have regular geometry, material properties and simple boundary conditions the Finite Strip Method is a more suitable tool. For these types of structures, such as bridge decks,using the Finite Element Method the size of the stiffness matrix may be too large for a particular computer or the analysis too expensive, whereas with the Finite Strip Method the size of the stiffness matrix is reduced and so the problem is more economically solvable.

The Finite Strip Method was developed from the Finite Element Method by Cheung[29] as the cost of solutions to problems with two or more dimensions increased. Cheung's method was to simplify a three-dimensional problem into a two-dimensional problem by analysing a number of two dimensional problems. A simple example is the case of a prismatic bar, shown in Fig. 3.1. The problem is three-dimensional and three components of displacement U, V and W are considered. The bar is restrained at $Z = 0$ and $Z = b$ such that the displacements in the $x - y$ plane are restrained, but displacement in the $Z -$ direction is unrestrained.

Dividing the $x - y$ plane into triangles, for the particular case, the m^{th} displacement function in the $x -$ direction is given by

$$\left\{U\right\}_z^m = \left[N_1, \; N_2, \; N_3 \qquad\qquad \right] \left\{Y\right\}_z^m \left\{U\right\}^m \qquad (3.1)$$

Similarly in the y - direction

$$\left\{V\right\}_z^m = \left[N_1, \; N_2, \; N_3 \qquad\qquad \right] \left\{Y\right\}_z^m \left\{V\right\}^m \qquad (3.2)$$

where N_1, N_2, N_3 etc., are the shape functions for the element considered, which in this case are triangles and Y_z^m is given by

$$\text{Sin } \frac{m\pi z}{b}$$

From the above functions the stresses and strains can be related to the nodal displacements. Applying the principle of minimum potential energy the parameters U_m and V_m can be determined for an applied load. The actual displacements are then obtained by the theory of superposition from the summation of all terms in U or V at the position z along the axis, so

$$U = \sum_{m=1}^{r} \left\{U\right\}_m Y_z^m \qquad (3.3)$$

$$V = \sum_{m=1}^{r} \left\{V\right\}_m Y_z^m \qquad (3.4)$$

The development of the analysis of the total potential energy, as will be described later, shows that the terms in the stiffness matrix are uncoupled so that the individual strip stiffness matrices can be generated and solved separately. This, of course, reduces the working core necessary for the analysis.

3.2 Philosophy of the Finite Strip Method

3.2.1 Original Theory

Cheung[29] developed the Finite Strip Method to reduce the numerical computations in the computer by analysing a number of similar structures simultaneously. Unlike the Finite Element Method, which has polynomial displacement functions in all directions, the Finite Strip Method's displacement function is the product of two displacement functions; a simple polynomial function in one direction and a continuous differentiable smooth series function in the other direction, Fig. 3.2. The smooth series function must satisfy the specific boundary conditions at the ends of the strip.

The first strip element developed by Cheung[29] was the simply supported bending strip, shown in Fig. 3.2 (b). Considering each harmonic individually, there are four degrees of freedom, namely

$$\{\delta\}_m = \begin{Bmatrix} w_i^m \\ \theta_i^m \\ w_j^m \\ \theta_j \end{Bmatrix} \qquad (3.5)$$

The shape functions for the strip were derived so that there was compatibility between adjacent strips of displacement and slope, Loo [30] later developed a similar strip but included an additional compatibility of curvature between the strips. Cheung's displacement function is given as

$$W = \sum_{m=1}^{r} \left[\left(1 - \frac{3x^3}{a^2} + \frac{2x^3}{a^3}\right) W_i^m + \left(x - \frac{2x^2}{a} + \frac{x^3}{a^2}\right)\theta_i^m \right.$$

$$\left. + \left(\frac{3x^2}{a^2} - \frac{2x^3}{a^3}\right) W_j^m + \left(\frac{x^3}{a^2} - \frac{x^2}{a}\right) \theta_j^m \right] \operatorname{Sin} \frac{m\pi y}{b} \quad \ldots\ldots (3.6)$$

Applying the "Principle of Minimum Potential Energy" to the stress and strain matrices, which can be derived from equation (3.6), a stiffness matrix is formed from the integral.

$$\int_0^b \int_0^a [B]^T [D][B] \, dx \, dy \qquad (3.7)$$

where $[B]$ is the strain matrix

and $[D]$ is the property matrix

The bending stiffness matrix derived by Cheung [31] is given in Appendix 1. From the integration five product integrals are obtained, namely

$$I_1 = \int_o^b Ym \; Yn \; dy \qquad I_2 = \int_o^b Ym^{11} \; Yn \; dy$$

$$I_3 = \int_o^b Ym \; Yn^{11} \; dy \qquad I_4 = \int_o^b Ym^{11} \; Yn^{11} \; dy$$

$$I_5 = \int_o^b Ym^{1} \; Yn^{1} \; dy$$

where Ym and Yn are the displacement functions in the y- direction and for the simply supported strip are $\text{Sin} \frac{m \pi y}{b}$

Ym^{11}, n Yn^{1}, n are the derivates for the displacement function.

Convergence of the harmonics, for a particular solution, was found by Cheung to be within the first five harmonics of the function, $\text{Sin} \frac{m \pi y}{b}$. These solutions included simply supported beams and plates of various boundary conditions.

Two methods were available for increasing the accuracy of

the problems. The simplest is by increasing the number of strips in the problem. Another method was to develop higher order strips. The incorporation of curvature compatibility between the strips was one method that was successfully adopted. A second group of higher order strips were again developed by Loo[30] in which an internal node was introduced into the rectangular strip. This is an extension of the developments in the Finite Element Method, where internal nodes were introduced to increase the accuracy of the elements.

At present, only strips which are simply supported at the ends have been considered. For varying end conditions the beam differential equation was used to derive further displacement functions. The beam differential equation is

$$Y^{1111} = \left(\frac{\mu^4}{b^4}\right) Y \qquad (3.8)$$

where b is the length of the strip

μ is a parameter (in this case the harmonic considered)

Y is the basic form of the displacement function

and Y^{1111} is the fourth derivative of Y.

The displacement function of Y in the above equation, for the possible end conditions, have been derived in the literature[32].

A later development was the simply supported plane stress matrix[31] which was combined with the simply supported bending matrix assuming small displacement theory, to form a folded plate stiffness matrix. The displacement function for the plane stress matrix was developed with only a compatability of displacement between the adjacent strips. The displacement functions for a typical strip shown in Fig. 3.3. are

$$\begin{Bmatrix} u \\ v \end{Bmatrix} = \sum_{m=1}^{r} \begin{bmatrix} (1-\bar{x})\ Ym & 0 & \bar{x}\ Ym & 0 \\ 0 & (1-\bar{x})\ \frac{b}{\mu m}\ Y_m^1 & 0 & \frac{\bar{x}\ b}{\mu m} Y_m^1 \end{bmatrix} \begin{Bmatrix} U_1 \\ V_1 \\ U_2 \\ V_2 \end{Bmatrix}_m$$

$$\text{where } \bar{x} = x/a \tag{3.9}$$

For both the plane stress and bending strips so far developed the member coordinate and the global coordinates are coincident with the mid-surface of the strip. However, for the folded plate strip the member coordinates have to be transformed to the global coordinate system so that the equilibrium of the nodal forces and compatibility of the displacements can be achieved. The notation for the two coordinate axes is given in Fig. 3.4. From the diagram, it can be seen that the y and y' axes are coincident with each other, whereas the other axes have to be transformed.

The transformation of the forces and displacements between the two sets of coordinate systems are given by

$$\{F\}_m = [R]\{F'\}_m \tag{3.10}$$

and $$\{\delta'\}_m = [R]^T \{\delta\}_m \qquad (3.11)$$

in which the transformation matrix $[R]^T$ is given by an 8 X 8 matrix

$$[R] = \begin{bmatrix} [r] & [o] \\ [o] & [r] \end{bmatrix}$$

and where

$$[r] = \begin{bmatrix} c & o & -s & o \\ o & 1 & o & o \\ s & o & c & o \\ o & o & o & 1 \end{bmatrix}$$

$[o]$ = null matrix

c = cos (Beta)

s = sin (Beta)

Beta = angle between x and x' axes (clockwise tve)

So applying equations (3.10) and (3.11) to the member force / deflection equation we can obtain the global stiffness matrix $[S\ S]$ in the terms of the member stiffness matrix $[SS']$ and the transformation matrix $[R]^T$ as

$$[S]_{mn} = [R]^T [S']_{mn} [R] \quad \ldots\ldots (3.12)$$

Analysis of profiled sheeting under the action of a shear flow requires that the folded plate is not simply supported at the ends. The actual distortion of a profile, fixed in every corrugation, from energy methods [7] and experimental work is shown in Fig. 3.5. This condition requires that a free end displacement function for a folded plate be developed. The definition of a free end being that the displacements u, v, w and θ are all assumed to be free to move at the ends of the strip and that the shear stress at the ends be zero. Whereas for the simply supported strip u, w and θ are all restrained at the ends. Cheung and Cheung [33] developed a function for a bending strip with both ends free, so that

$$W \neq 0 \quad \text{at} \quad y = 0 \quad \text{and} \quad y = b$$

This strip has been successfully applied to bending and vibrational problems. No free end plane stress displacement function has been possible with the functions so far developed, as the requirement of u and v not equal to zero and the shear stress τ_{xy} to be equal to zero at $y = 0$ and $y = b$ is difficult to obtain. The problem has been overcome by the work of Siddiqi and Girija Vallabham [34,35]. They extended

the simply supported displacement function to allow for the relative movement of the nodes.

3.2.2. Extended Theory

The extended theory was developed by Siddiqi [36] so that folded plates other than simply supported end conditions could be analysed. The method consists of separating the displacement function in the y- direction into two specific parts. The first part consists of movements of the longitudinal node lines and the second part of displacements of a simply supported strip, previously developed.

The displacement function for the plane stress strip are now written as

$$\begin{Bmatrix} u \\ v \end{Bmatrix} = \sum_{m=1}^{r} \begin{bmatrix} (1-\bar{x})\,Ym & 0 & \bar{x}\,Ym & 0 \\ 0 & (1-\bar{x})Xm & 0 & \bar{x}\,Xm \end{bmatrix} \begin{Bmatrix} u_1 \\ v_1 \\ u_2 \\ v_2 \end{Bmatrix}_m \quad \ldots\ldots(3.15)$$

in which Ym and Xm are the displacement function in the y-direction, Fig. 3.6. In numerical form

$$Ym = 1,\quad 1 - \frac{2y}{b},\ \mathrm{Sin}\ \frac{\pi y}{b},\ \mathrm{Sin}\ \frac{2\pi y}{b},\ \mathrm{Sin}\ \frac{(m-2)\pi}{b} y$$

with m = 3, 4, 5 etc.,

$$\text{and}\quad Xm = 1 - \frac{2y}{b},\ 1,\ \mathrm{Cos}\ \frac{\pi y}{b},\ \mathrm{Cos}\ \frac{2\pi y}{b},\ \mathrm{Cos}\ \frac{(m-2)\pi}{b} y$$

with m = 3, 4, 5 etc.

The bending action can also be separated into two parts, this displacement function is given by

$$W = \sum_{m=1}^{r} \left[\left(1 - 3\bar{x}^2 + 2\bar{x}^3\right) x \left(1 - 2\bar{x} + \bar{x}^2\right) \left(3\bar{x}^2 - 2\bar{x}^3\right) \right.$$

$$\left. x \left(\bar{x}^2 - \bar{x}\right) \right] Ym \begin{Bmatrix} W_i \\ \theta_i \\ W_j \\ \theta_j \end{Bmatrix}_m \quad \ldots\ldots (3.16)$$

The only change in this displacement function compared with (3.6) is in the form of Ym.

The first two terms of Ym and Xm represent the first part of the displacement, while the remaining terms represent the second part of the displacement. The series is no longer orthogonal and exhibits coupling between the first two terms and all the other terms in the stiffness matrix. This does reduce the efficiency of the Finite Strip Method in terms of working core in the computer; but does allow greater freedon of structures analysed.

Siddiqi and Girija Vallabham have not compared the

displacement functions of the extended Finite Strip Method to any theoretical or experimental results. Cheung [31] is also uncertain whether the criteria $\gamma_{xy} = 0$ at the ends of the strip can be satisfied. But as will be shown, a good comparison occurs between the Finite Element Energy Methods and the Finite Strip solutions of a corrugated profile, and it may be that the $\gamma_{xy} = 0$ criteria does not need to be adhered to as one would imagine.

3.3 Development of Stiffness Matrix

In the previous section the form of the extended Finite Strip displacement function have been enumerated. This function can be expressed in the form

$$\{f\} = \sum_{m=1}^{r} [N]_m \{\delta\}_m \qquad (3.17)$$

where $[N]_m$ is the displacement function for the m^{th} harmonic

and $\{\delta\}_m$ for the nodal displacement

Once the displacement function is formed the strains $\{\varepsilon\}$ can be related to the nodal displacements thus

$$\{\varepsilon\} = \sum_{m=1}^{r} [B]_m \{\delta\}_m \qquad (3.18)$$

where $[B]_m$ is termed the strain matrix for the m^{th} harmonic.

For the case of a bending strip the strains are

$$\{\varepsilon\} = \begin{Bmatrix} -\frac{\partial^2 w}{\partial x^2} \\ \frac{\partial^2 w}{\partial y^2} \\ 2\frac{\partial^2 w}{\partial x \partial y} \end{Bmatrix} \quad \ldots\ldots(3.19)$$

and the strains can be related to the displacements by the appropriate differentiations.

The plane stress strip can be related to the nodal displacement by the following differentiations

$$\{\varepsilon\} = \begin{Bmatrix} \varepsilon_x \\ \varepsilon_y \\ \gamma_{xy} \end{Bmatrix} = \begin{Bmatrix} \partial u/\partial x \\ \partial v/\partial y \\ \frac{\partial u}{\partial y} + \frac{\partial v}{\partial x} \end{Bmatrix} \quad \ldots\ldots(3.20)$$

By utilising the property matrix $[D]$ a relationship between the nodal displacements and the stresses may be obtained for each harmonic as

$$\{\sigma\} = [D]\ [B]_m\ \{\delta\}_m$$

where

$$[D] = \begin{bmatrix} D_x & D_1 & 0 \\ D_1 & D_y & 0 \\ 0 & 0 & Dxy \end{bmatrix}$$

and

$$Dx = \frac{E_x\ t^3}{12\ (1 - \nu^2)}$$

$$Dy = \frac{E_y\ t^3}{12\ (1 - \nu^2)}$$

$$D_1 = \nu . Dx$$

$$Dxy = \frac{G\ t^3}{12}$$

The strain matrix $[B]_m$ for the folded plate is given in Appendix 1.

Having obtained expressions for the strains and stresses in terms of the nodal displacements, the stiffness matrix can be obtained using the Principle of Minimization of Total Potential Energy. The principle states that :-

"the rate of change of the stored strain energy in the body and the potential energy of the loads is zero."

The strain energy of an elastic body is given by

$$Es = \frac{1}{2}\int \{\varepsilon\}^T \{\sigma\} \, d(vol) \qquad \ldots\ldots (3.22)$$

substituting expressions (3.18) and (3.21) into (3.22) we obtain

$$Es = \frac{1}{2}\int \{\delta\}^T [B]^T [D] [B] \{\delta\} \, d\,(vol) \ldots (3.23)$$

The potential energy of the external loads can be written as

$$Ep = -\int \{f\}^T \{q\} \; d\,(\text{area}) \quad \ldots\ldots (3.24)$$

where q is the external load matrix

substituting expression (3.17) into (3.24) we obtain

$$Ep = -\int \{\delta\}^T [N]^T \{q\} \; d\,(\text{area}) \quad (3.25)$$

The total potential energy $E_T p$ is then given by

$$E_T p = Ex + Ep$$

$$= \frac{1}{2}\int \{\delta\}^T [B]^T [D][B]\{\delta\} \; d\,(\text{vol}) - \int \{\delta\}[N]\{q\} \; d\,(\text{area}) \quad (3.26)$$

Applying the principle of minimum total potential energy to the expression we obtain

$$\frac{\partial E_{TP}}{\partial \{\delta\}} = \int [B]^T [D] [B] \{\delta\} \, d(\text{vol}) - \int [N]^T \{q\} \, d(\text{area}) = \{0\} \qquad (3.27)$$

or $$[S]\{\delta\} - \{F\} = \{0\} \qquad (3.28)$$

where $[S]$ is the stiffness matrix $\int [B]^T [D] [B] \, d(\text{vol})$

and $\{F\}$ is the force matrix $\int [N]^T \{q\} \, d(\text{area})$

In equation (3.27) there is a large amount of integration to be carried out over the strip. Applying this equation to both the bending and plane stress strips their respective matrices are obtained, which are given in Appendix 1. From the matrices a number of product integrals are formed, for the bending strips these have already been given, but for the plane stress strip the integrals are

$$L_1 = \int_0^b Ym\ Yn\ dy \qquad L_2 = \int_0^b Ym\ Xn'\ dy$$

$$L_3 = \int_0^b Ym'\ Xn\ dy \qquad L_4 = \int_0^b Ym'\ Yn'\ dy$$

$$L_5 = \int_0^b Xm'\ Yn\ dy \qquad L_6 = \int_0^b Xm\ Yn'\ dy$$

$$L_7 = \int_0^b Xm'\ Xn'\ dy \qquad L_8 = \int_0^b Xm\ Xn\ dy$$

An additional three product integrals are required compared with the bending strip as there are two displacement series in the y- direction, namely Ym and Xm.

The values of $I_1 \rightarrow I_5$ and $L_1 \rightarrow L_8$ have been determined explicitly in Appendix 2.

3.4 Computer Program

3.4.1 Formation of Global Stiffness Matrix

A computer program has been written using the matrices developed previously, an annotated listing of the program is given in Appendix 3. The program is written in Fortran, and associated flow chart given in Fig. 3.7

The program computes the individual stiffness matrix for each term of the displacement function, which is then transformed from its local coordinate system to the global system by the

transformation matrix (3.12). In the case of the folded plate stiffness matrix each term consists of an 8 * 8 stiffness matrix given in Appendix 1.

After transformation of the individual matrix it is then placed in the strip stiffness matrix, its position depending on the terms of the harmonic m and n . This is best shown in Fig. 3.8, where for a particular 8 * 8 matrix the position of the elements are given by

$$SS\ (\ NI,\ NJ\ )\ =\ BO\ \ (\ I,\ J\ )$$

where $$NI\ =\ 8\ *\ \ (\ M\ -\ 1\ )\ +\ I$$

$$NJ\ =\ 8\ *\ \ (\ N\ -\ 1\ )\ +\ J$$

When all the terms of the strip matrix have been fully developed the matrix is rearranged so that the displacement matrix $\{\delta\}$ are ordered in a nodal sequence and not as previously in a harmonic sequence. An example of the change in the sequence is shown below.

$$\{\delta\}^T = \{u_1\ v_1\ w_1\ \theta_1\ u_2\ v_2\ w_2\ \theta_2\ u_1^2\ v_1^2\ w_1^2\ \theta_1^2$$
$$u_2^2\ v_2^2\ w_2^2\ \theta_2^2\ u_1^3\ v_1^3\ w_1^3\ \theta_1^3\ u_2^3\ v_2^3\ w_2^3\ \theta_2^3\}$$

HARMONIC SEQUENCE

$$\{\delta\}^T = \{u_1\ v_1\ w_1\ \theta_1\ u_1^2\ v_1^2\ w_1^2\ \theta_1^2\ u_1^3\ v_1^3\ w_1^3\ \theta_1^3$$
$$u_2\ v_2\ w_2\ \theta_2\ u_2^2\ v_2^2\ w_2^2\ \theta_2^2\ u_2^3\ v_2^3\ w_2^3\ \theta_2^3\}$$

NODAL SEQUENCE

Having obtained the strip stiffness matrix the appropriate boundary conditions can now be introduced. Unlike the original Finite Strip displacement functions which formed a non-singular matrix the new displacement function form a singular matrix. Therefore boundary conditions must be applied before any solution of the equations can be undertaken. In the program this is carried out in the usual way by increasing the value of the leading diagonal term of the nodal displacement parameter to be restrained.

3.4.2 Solution of the Stiffness Matrix

The method of solution for the overall stiffness matrix is by use of the partitioning technique[37]. As each strip stiffness matrix is formed the previous node is eliminated from the preceding strip before the next matrix is formed. The method is best illustrated by reference to Fig. 3.9; which represents a problem with n - 1 numbers of strips.

The overall stiffness matrix can be written as

$$\begin{Bmatrix} P_1 \\ P_2 \\ P_3 \\ P_4 \\ \\ \\ P_{n-1} \\ P_n \end{Bmatrix} = \begin{bmatrix} K_{11} & K_{12} & 0 & 0 & & & & \\ K_{12}^T & K_{22} & K_{23} & 0 & & & & \\ 0 & K_{23}^T & K_{33} & K_{34} & \cdots & & & \\ & & & & & & & \\ & & \vdots & & & & & \\ & & & & & K_{n-1,n-2} & 0 & \\ & & & & & K_{n-1,n-1} & K_{n-1,n} & \\ & & & & 0 & K_{n-1,n}^T & K_{nn} & \end{bmatrix} \begin{Bmatrix} \delta_1 \\ \delta_2 \\ \delta_3 \\ \delta_4 \\ \\ \\ \delta_{n-1} \\ \delta_n \end{Bmatrix}$$

where $\bar{K}_{11}$, K_{12} etc., are the submatrices of the overall stiffness matrix.

The first two equations can be written as

$$P_1 = K_{11}\,\delta_1 + K_{12}\,\delta_2 \qquad (3.29)$$

$$P_2 = K_{12}^{T}\,\delta_1 + K_{22}\,\delta_2 + K_{23}\,\delta_3 \qquad (3.30)$$

On eliminating δ_1 in equation (3.30) we obtain

$$\bar{P}_2 = \bar{K}_{22}\,\delta_2 + K_{23}\,\delta_3 \qquad (3.31)$$

where $\bar{P}_2 = P_2 - K_{12}^{T}\,K_{11}^{-1}\,P_1$

and $\bar{K}_{22} = K_{22} - K_{12}^{T}\,K_{11}^{-1}\,K_{12}$

The procedure is repeated for each until the modified row becomes

$$\bar{P} = \bar{K}nn\,\delta_n \qquad (3.32)$$

from which δ_n can be obtained by direct inversion.

A back substitution is now carried out to obtain the unknown δ's.

The computer program's positioning routine stores the matrices $K_{\ell,\ell}$; $K_{\ell,\ell+1}$ etc., on magnetic tape for future use in the back substitution routine. This allows large problems of many strips to be handled by the computer, which would otherwise be impossible to consider.

3.5 Verification of Finite Strip Programe against Standard Solutions

3.5.1 Plane Stress Problems

A number of test problems were analysed to verify the matrices developed. For verification of the plane stress matrix two problems are given, the simply supported deep beam and the deep cantilever.

The simply supported deep beam shown in Fig. 3.10, consists of an isotropic beam supported at the ends to vertical movement. A uniform load is applied to the surface BC of intensity 175 N/mm. Verification of the results is undertaken by means of a flat rectangular finite element which was supplied to the author in a program written by Dr. J. M. Davies. The total number of elements in the example was sixty four. For the problem five strips were used with seven harmonics in the displacement function.

The results, given in Table 3.1, show that there is a good comparison between the results and further convergence could be achieved if more elements or strips were introduced.

The second problem deals with the analysis of an isotropic deep cantilever under the action of a uniform shear stress at the free end Fig. 3.11. The total value of the shear stress is unity. At the fixed end the cantilever is restrained along CD to movement in the x- and y- directions.

The problem exhibits a combination of inplane bending and shear distortion that is also found in the distortional analysis of corrugated profiles.

Three variations of strips were analysed, namely 6, 10 and 15 strips. The node lines are in the x- direction, so as

to allow the restraints to be consistent along each node line.

A solution for this problem is given by Timoshenki[39] and is

$$\Delta_x = \frac{12}{d^3}\left[\frac{x^3}{6} - \frac{\ell^2 x}{2} + \frac{\ell^3}{3} + 0.325\, d^2 (\ell - x)\right] \quad \ldots (3.33)$$

where ℓ = length of cantilever

d = depth of cantilever

and x = distance from free end

The deflection curves are given in Fig. 3.12 showing the Timoshenki solution and the three strip combinations.

Table 3.2 compares the deflection of the cantilever and the free end for the Timoshenki solution and the three strip combinations together with a number of Finite Element results undertaken by Young[39]. The results show that there is some agreement with the results though for the Finite Strip and Finite Element there is considerable agreement.

3.5.2 Cylindrical Shell

The cylindrical shell is loaded uniformily under its own self-weight in such a way that only symetrical displacements and stresses are obtained. This problem combines both bending and membrane stresses and has been used as a test case by many Finite Element investigators. The geometry and properties of the shell are given in Fig. 3.13. The straight edges of the shell are allowed to remain free to deform, while the curved edges are supported by rigid diaphragms. These diaphragms are assumed infinitely rigid in their plane and infinitely flexible, out of plane, in the V- direction. A solution has been given by Scordelis and Lo [40] and a Finite Element solution by Young [39] using flat rectangular elements.

The performance of an eight and sixteen strip arrangement was analysed using the Finite Strip program. The results are given in Fig. 3.14, for vertical displacements at the centre the inplane displacements at the support, the longitudinal bending moment My and the transverse bending moment Mx at the centre.

Figs. 3.14 (a) and (b), show that the deflections have good agreement with the previous work and that increasing the number of strips has not influenced the accuracy of the results. Whereas in the longitudinal bending moment the sixteen strip-arrangement has increased the accuracy and it would require durther strips to converge onto acceptable values.

3.5.3 Further Examples

Further examples of the verification of the matrices are given in the following chapter where the analysis of profiled sheeting by the Finite Strip Method is compared with Energy and Finite Element Solutions.

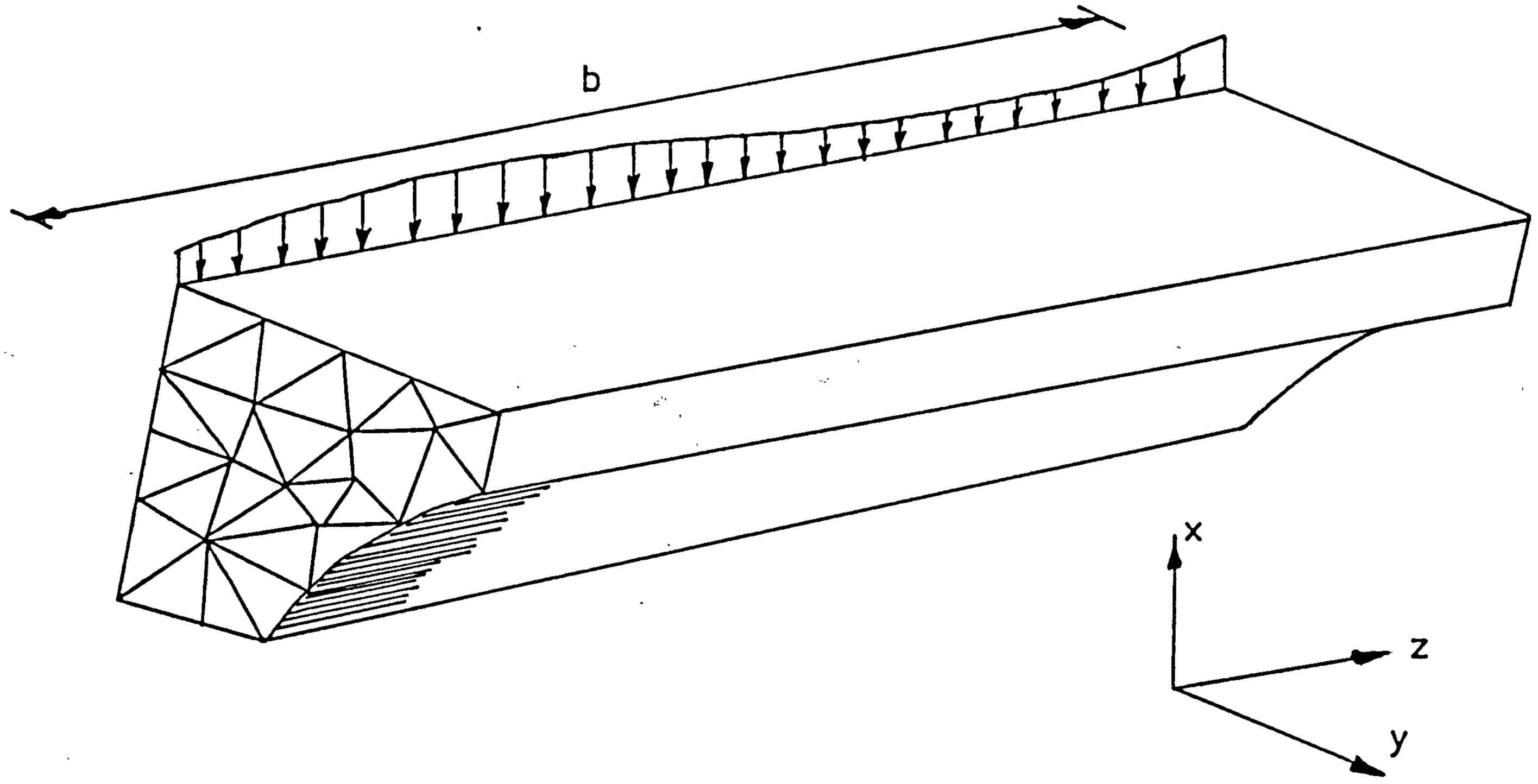

Fig 3.1 A Three Dimensional Structure Reduced to a Series of Two Dimensional Structures

Rect. Bending Element

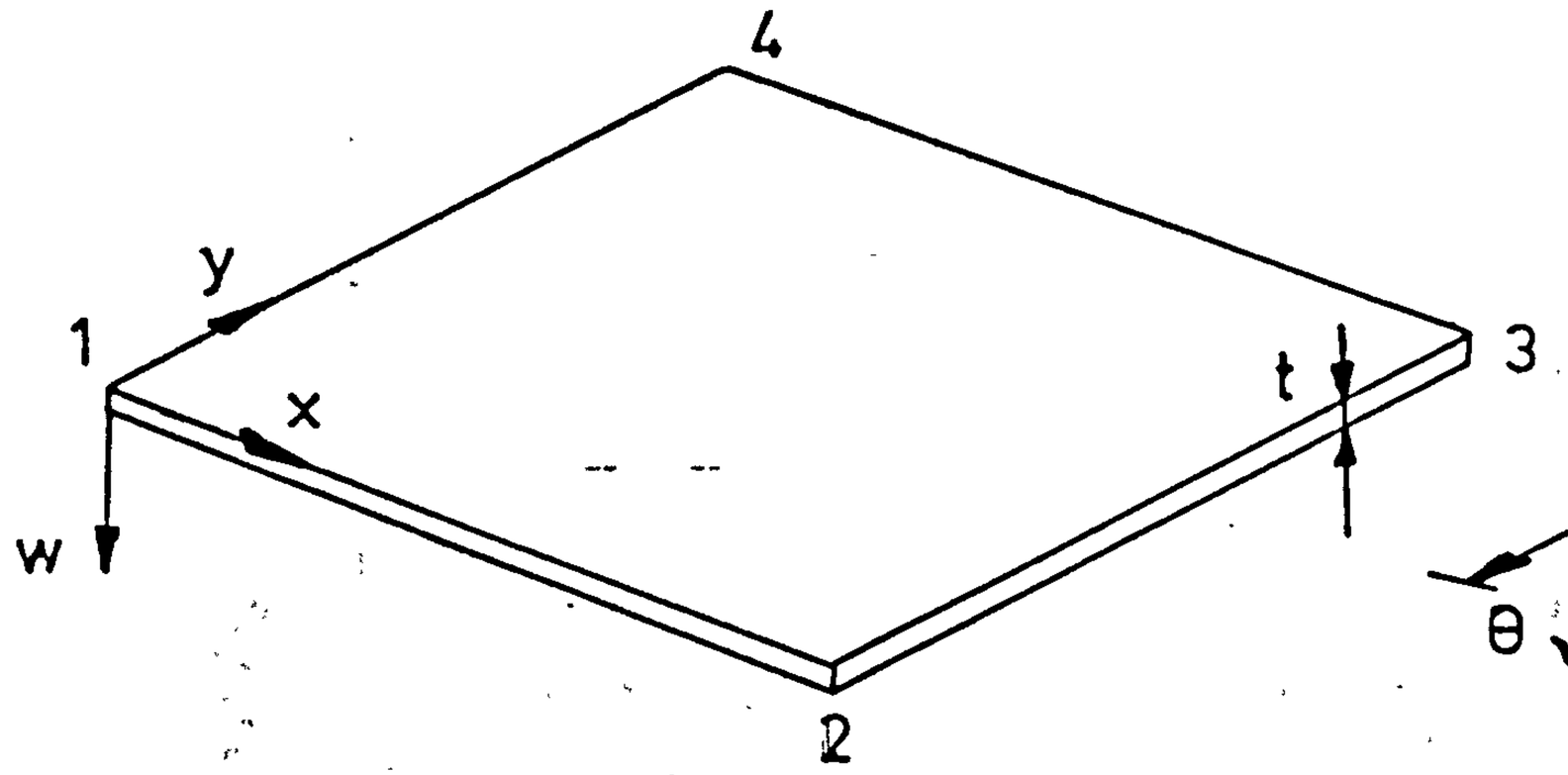

Rect. Bending Strip

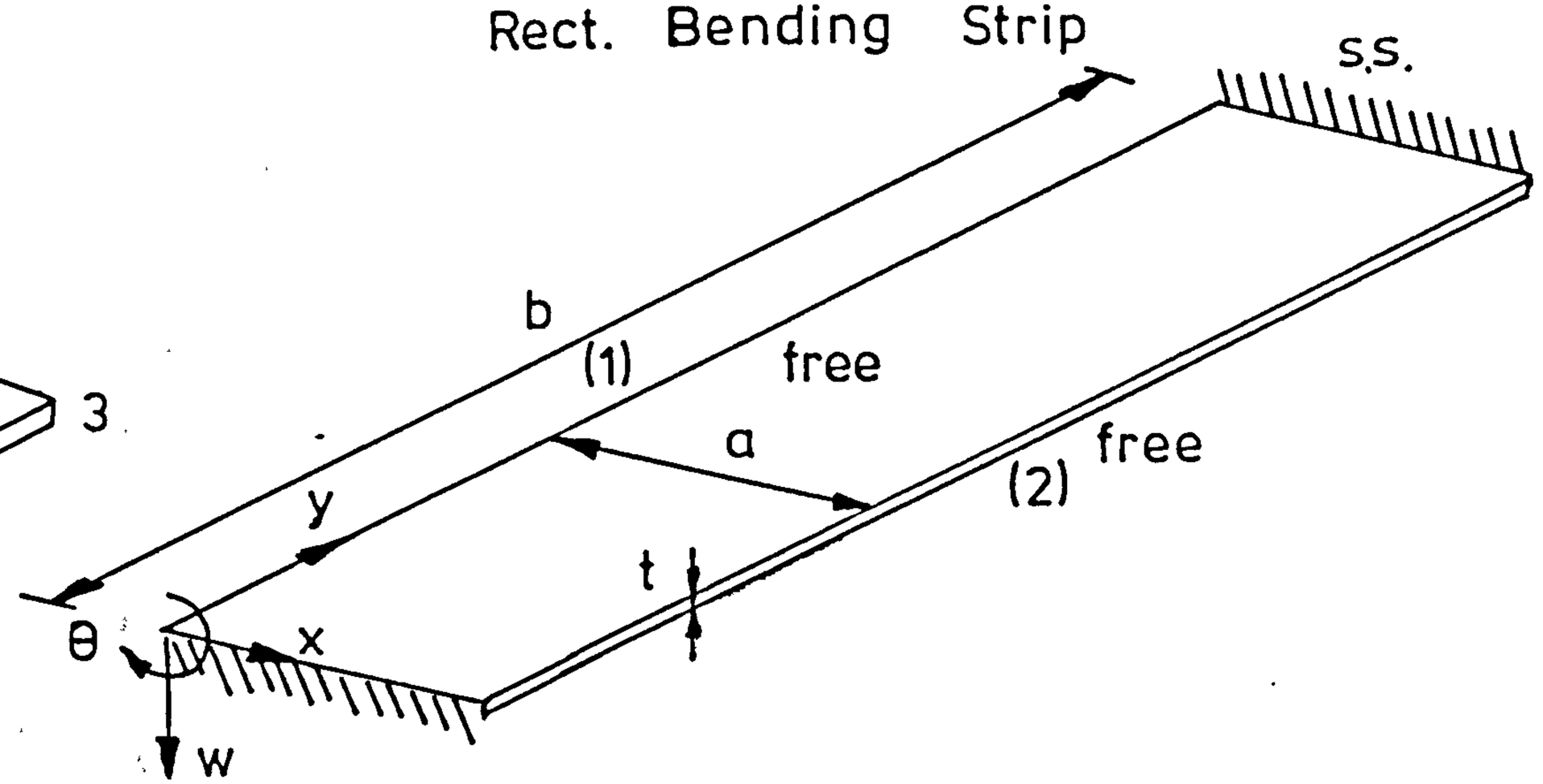

Displacement functions

$$w = \alpha_1 + \alpha_2 x + \alpha_3 y + \alpha_4 x^2 + \alpha_5 xy + \alpha_6 y^2 + \alpha_7 x^3 + \alpha_8 x^2 y + \alpha_9 x y^2 + \alpha_{10} y^3 + \alpha_{11} x^3 y + \alpha_{12} x y^3$$

where $\alpha_1 \rightarrow \alpha_{12}$ are coefficients depending on the boundary conditions

$$w = \sum_{m=1}^{r} f(x)_m \cdot Y_m \{\delta\}_m$$

where $f(x)$ is the shape function

$$Y_m = \sin\left(\frac{m\pi y}{b}\right)$$

m = harmonic

r = no. of harmonics.

Fig. 3.2 Displacement Functions for Finite Element and Strip for rectangular elements

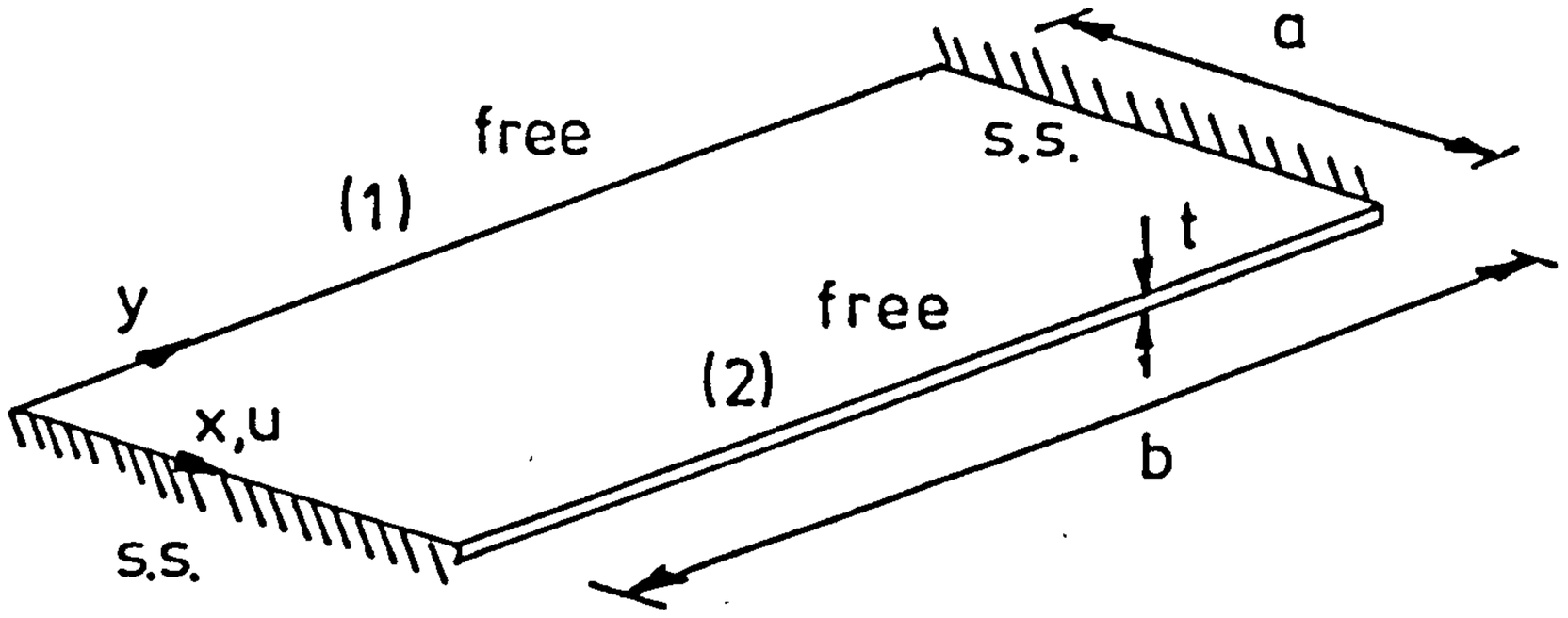

Fig. 3.3 Plane Stress Strip

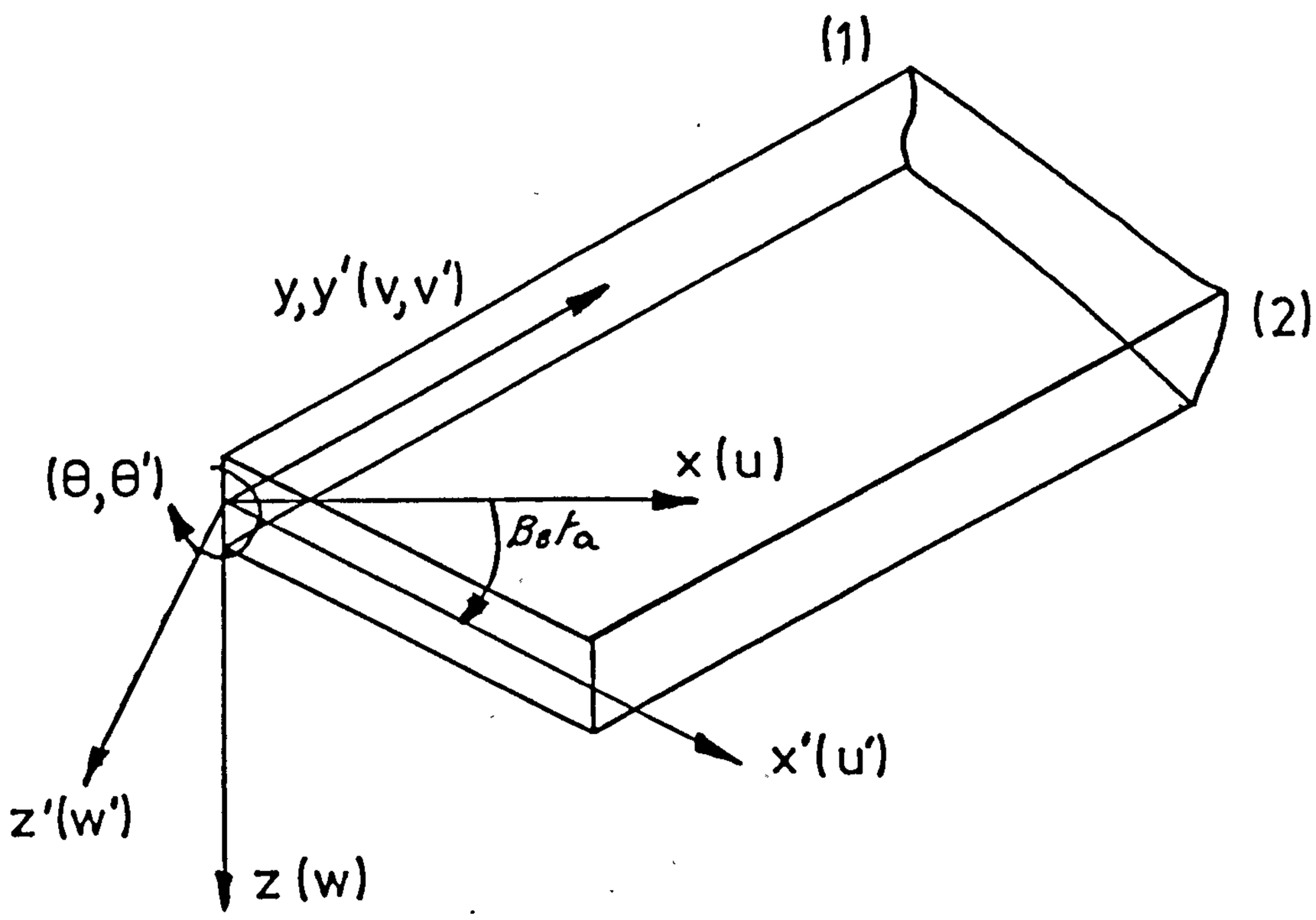

Member Coordinate System
x';y';z' (u';v';w';θ')

Global Coordinate System
x,y,z (u, v, w, θ)

Fig 3.4 Member and Global Coordinate System

m	Ym	Xm
1		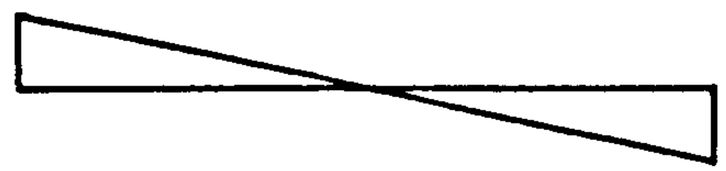
2		
3	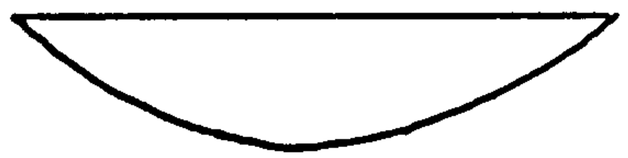	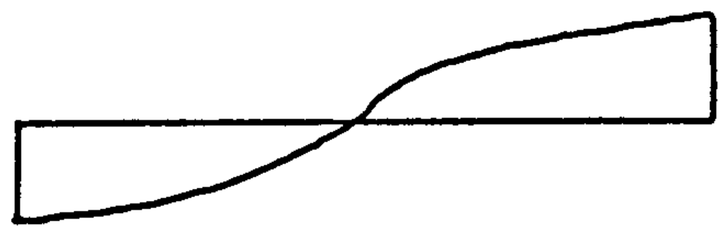
4	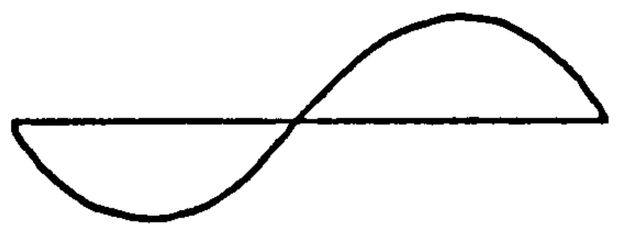	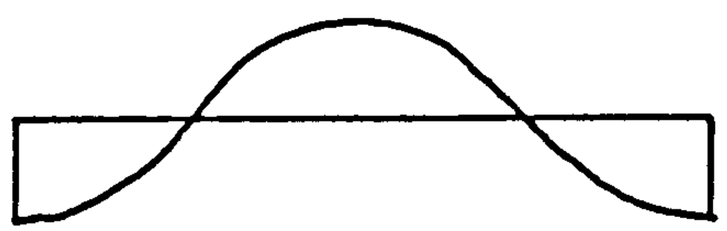
5	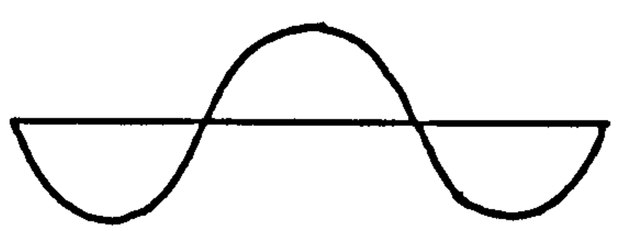	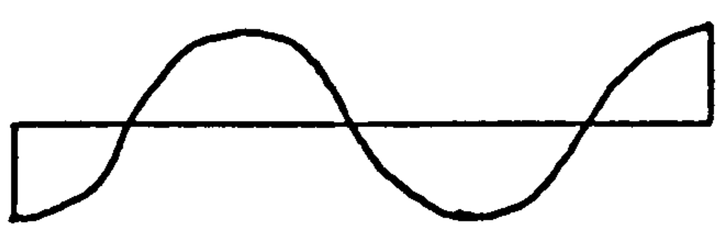

Fig 3.6 Extended Finite Strip Displacement Function

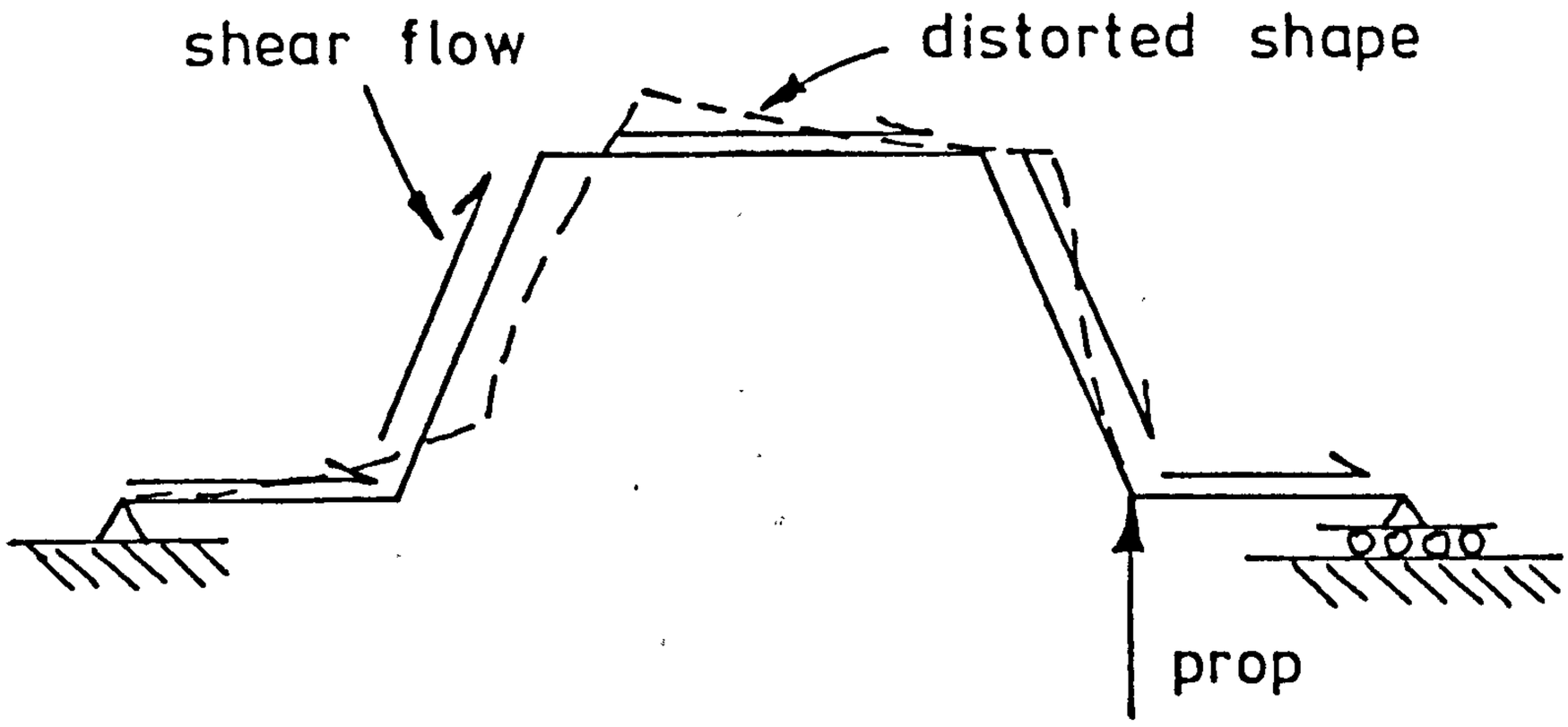

Fig 3.5 Distortion of a Profile

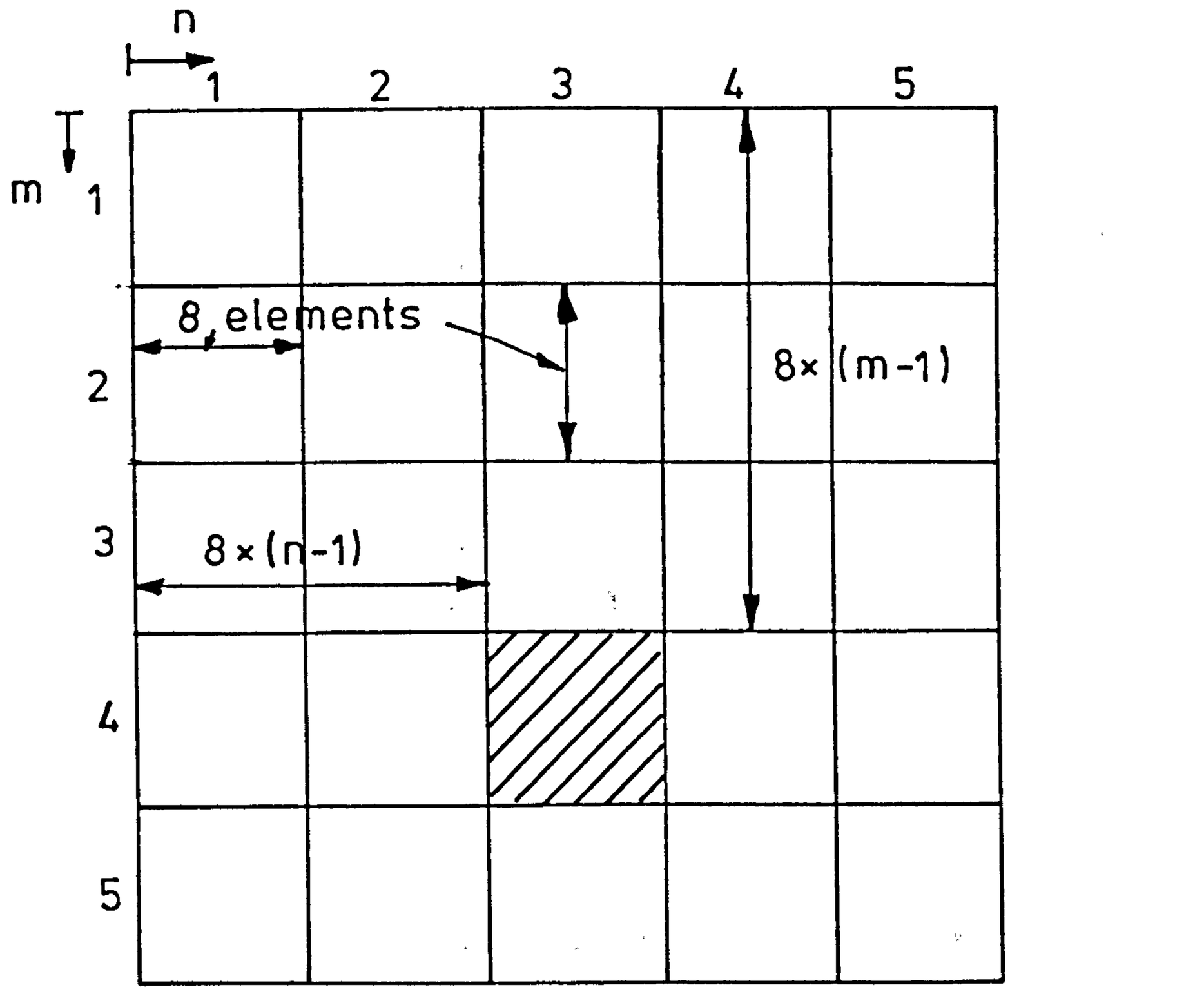

Fig 3.8 Position of 8×8 Matrix in Overall Stiffness Matrix

FLOW CHART FOR FINITE STRIP PROGRAMME

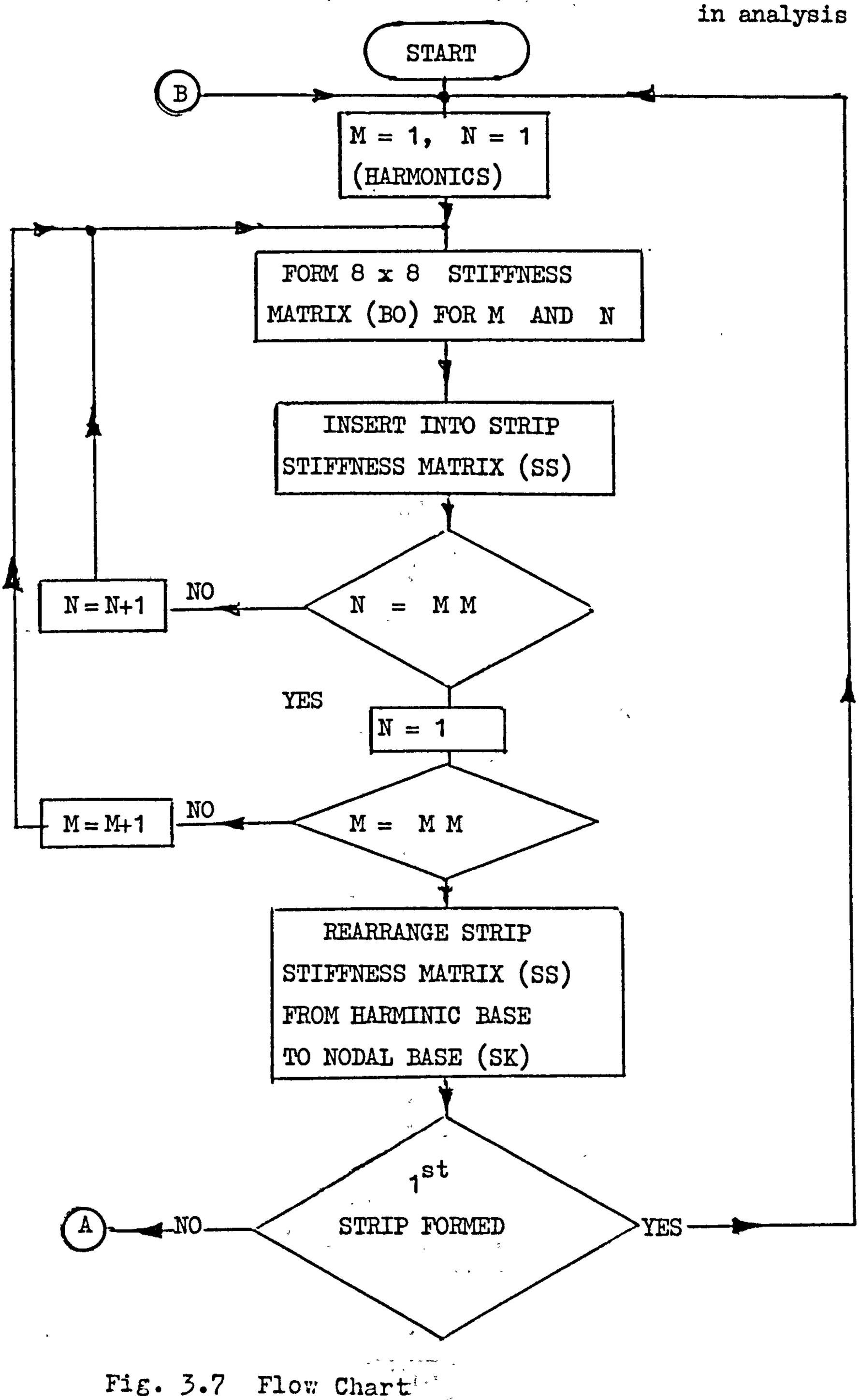

Fig. 3.7 Flow Chart

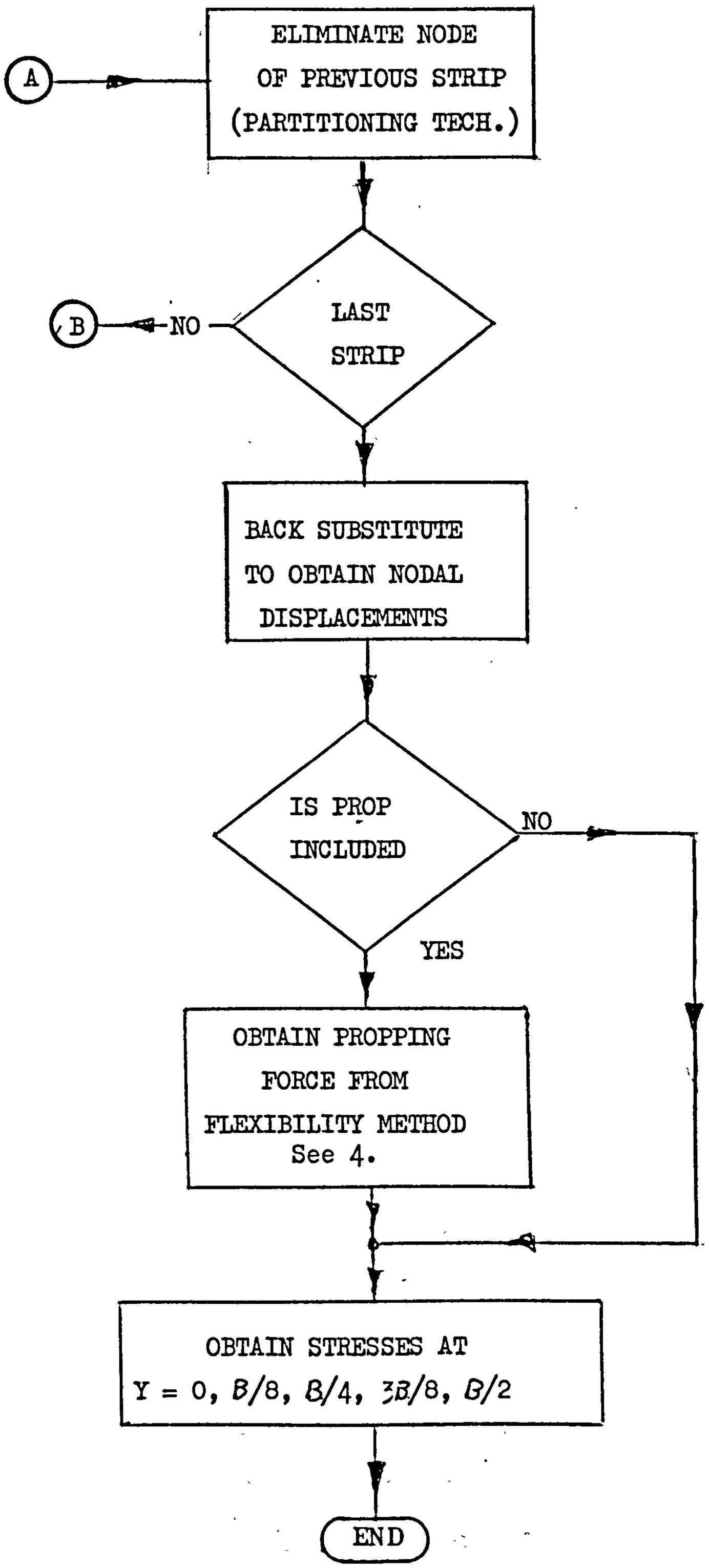
A
ELIMINATE NODE
OF PREVIOUS STRIP
(PARTITIONING TECH.)
B
NO
LAST
STRIP
BACK SUBSTITUTE
TO OBTAIN NODAL
DISPLACEMENTS
IS PROP
INCLUDED
NO
YES
OBTAIN PROPPING
FORCE FROM
FLEXIBILITY METHOD
See 4.
OBTAIN STRESSES AT
Y = 0, B/8, B/4, 3B/8, B/2
END

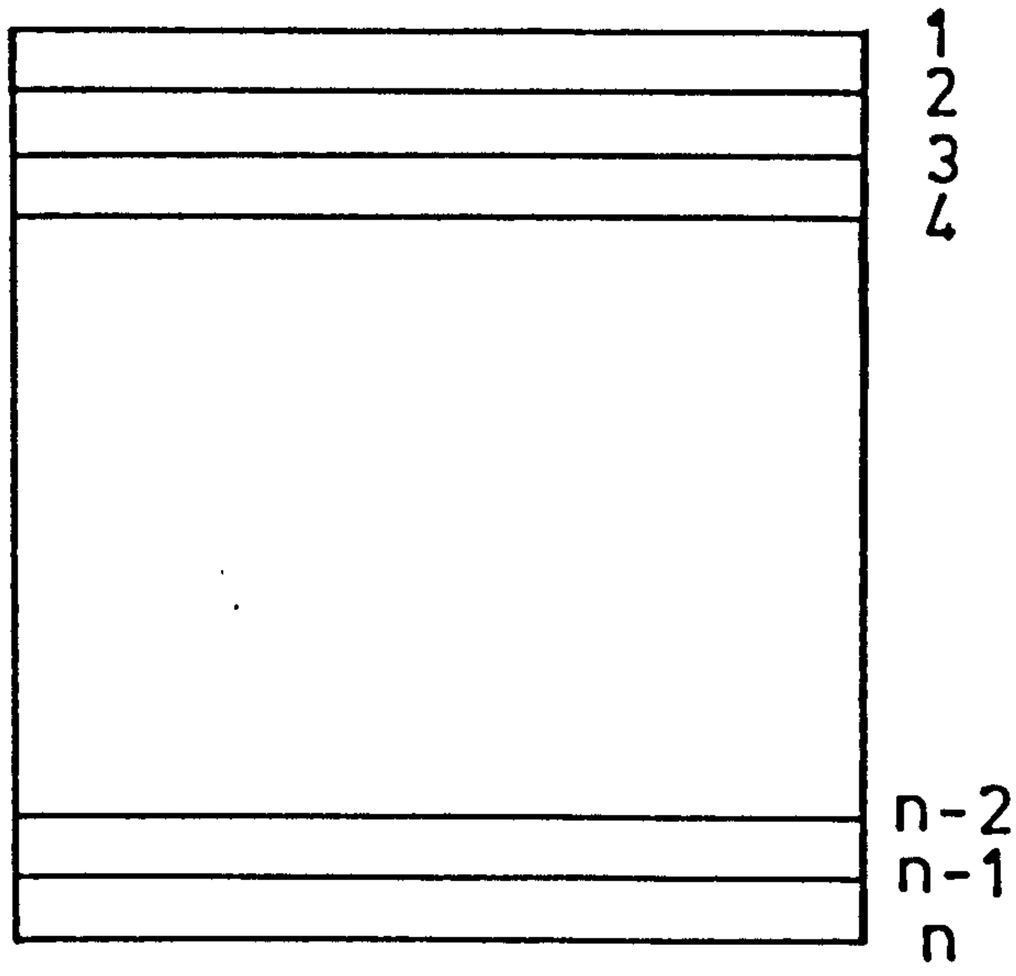

Fig 3.9 A Structure divided into strips

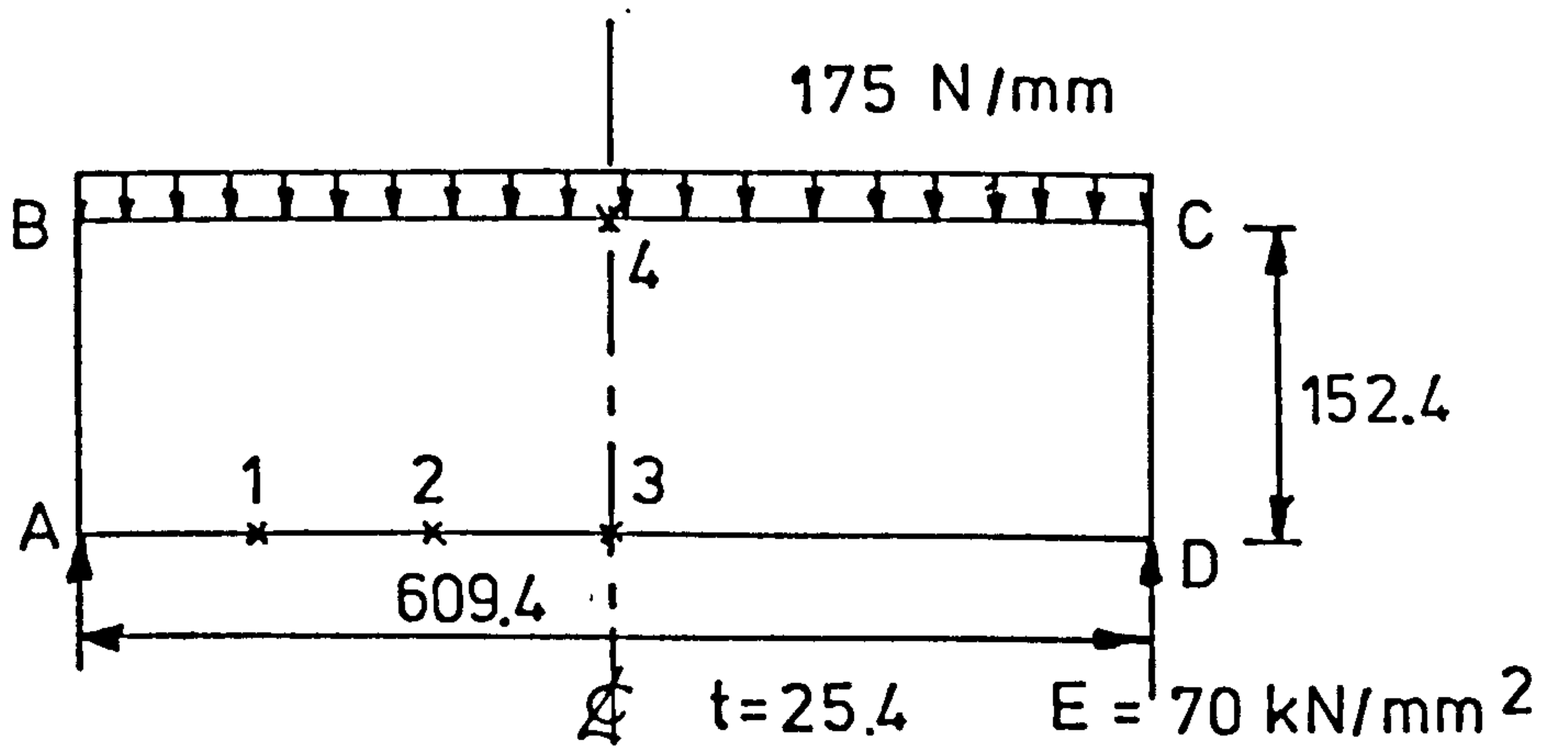

Fig 3.10 Plane stress simple supported deep beam

Deflection Point	Vertical Deflection	
	Finite Strip	Finite Element
1	0.3072	0.2902
2	0.5841	0.5797
3	0.6705	0.6539
4	0 6785	0 6464

Table 3.1 Comparison of Finite Strip and Finite Element for a Deep Beam

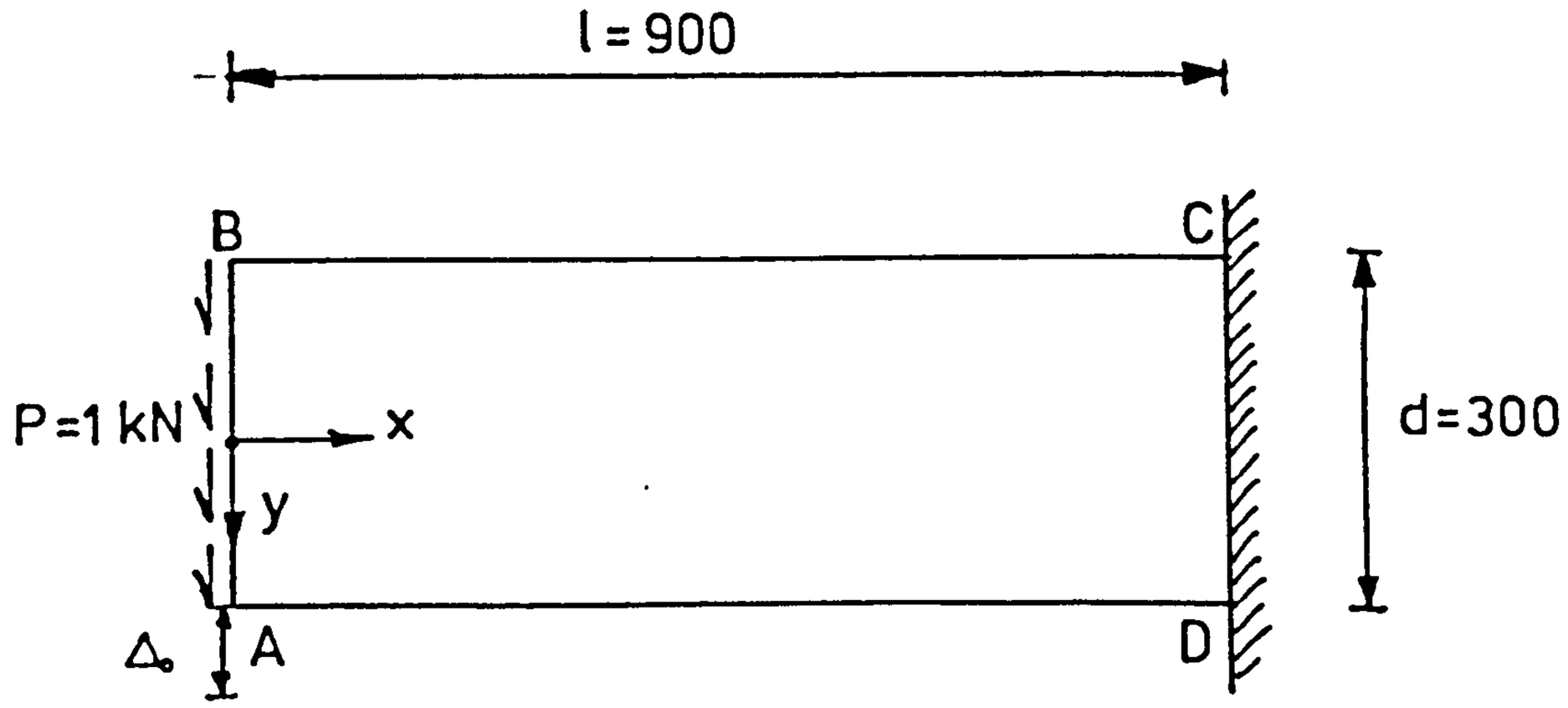

$\nu = 0.34$ $E = 1\,kN/mm^2$

$t = 1mm$

Fig 3.11 Dimension of deep cantilever

Finite Strip	Δ_o
6 strips	103.2
10 strips	109.2
15 strips	112.4
Timoshenki [38]	119.7
Finite Element [39]	
Macleod element	115.5
Argyis element	110.1
Cheung element	112.0

} Aspect ratio of one for elements

Table 3.2 Deflection of a deep cantilever (Δ_o)

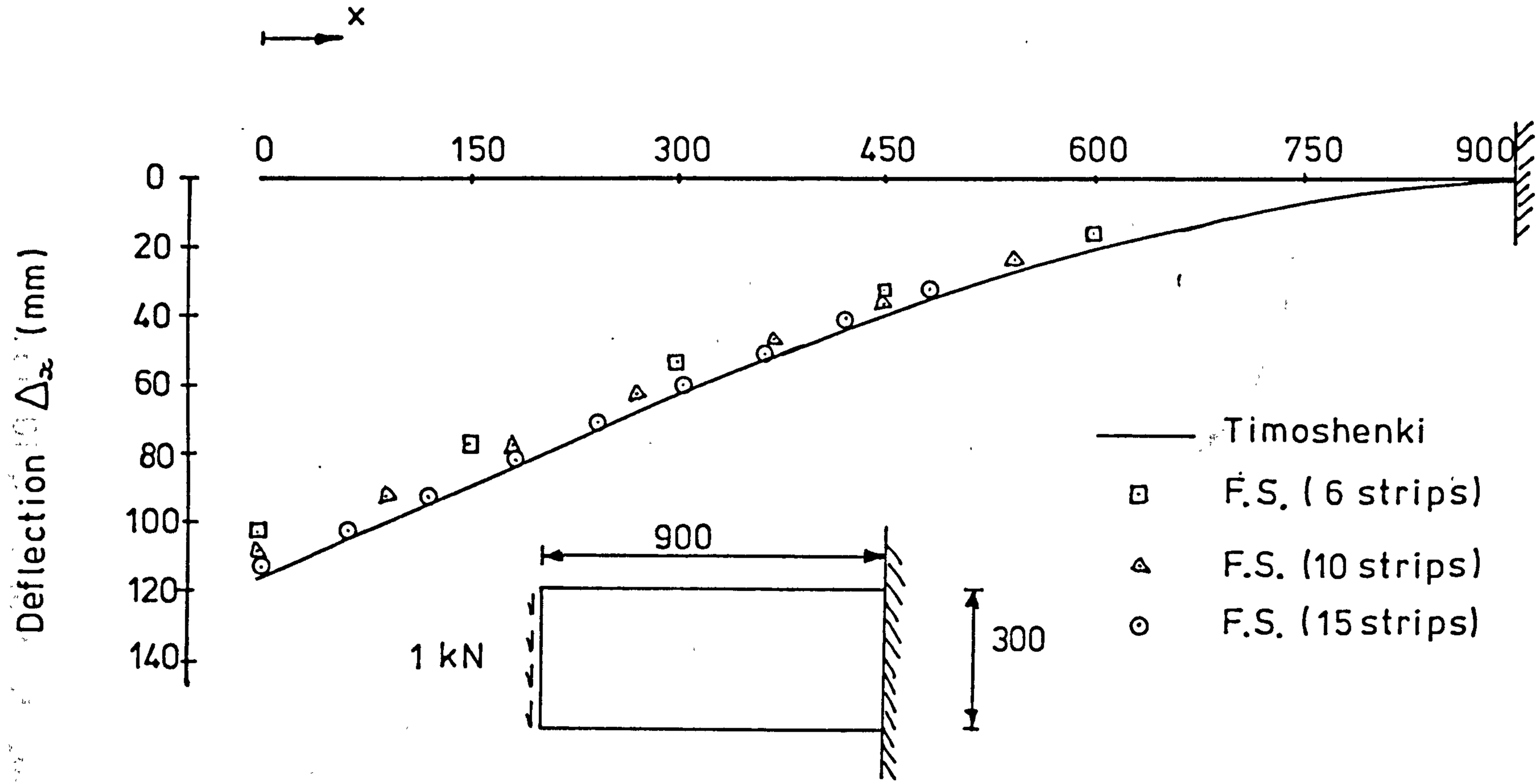

Fig 3.12 Deflection curves for deep cantilever

Self weight = 4.3 kN/m^2

E = 20.69 kN/mm^2

ν = 0.0

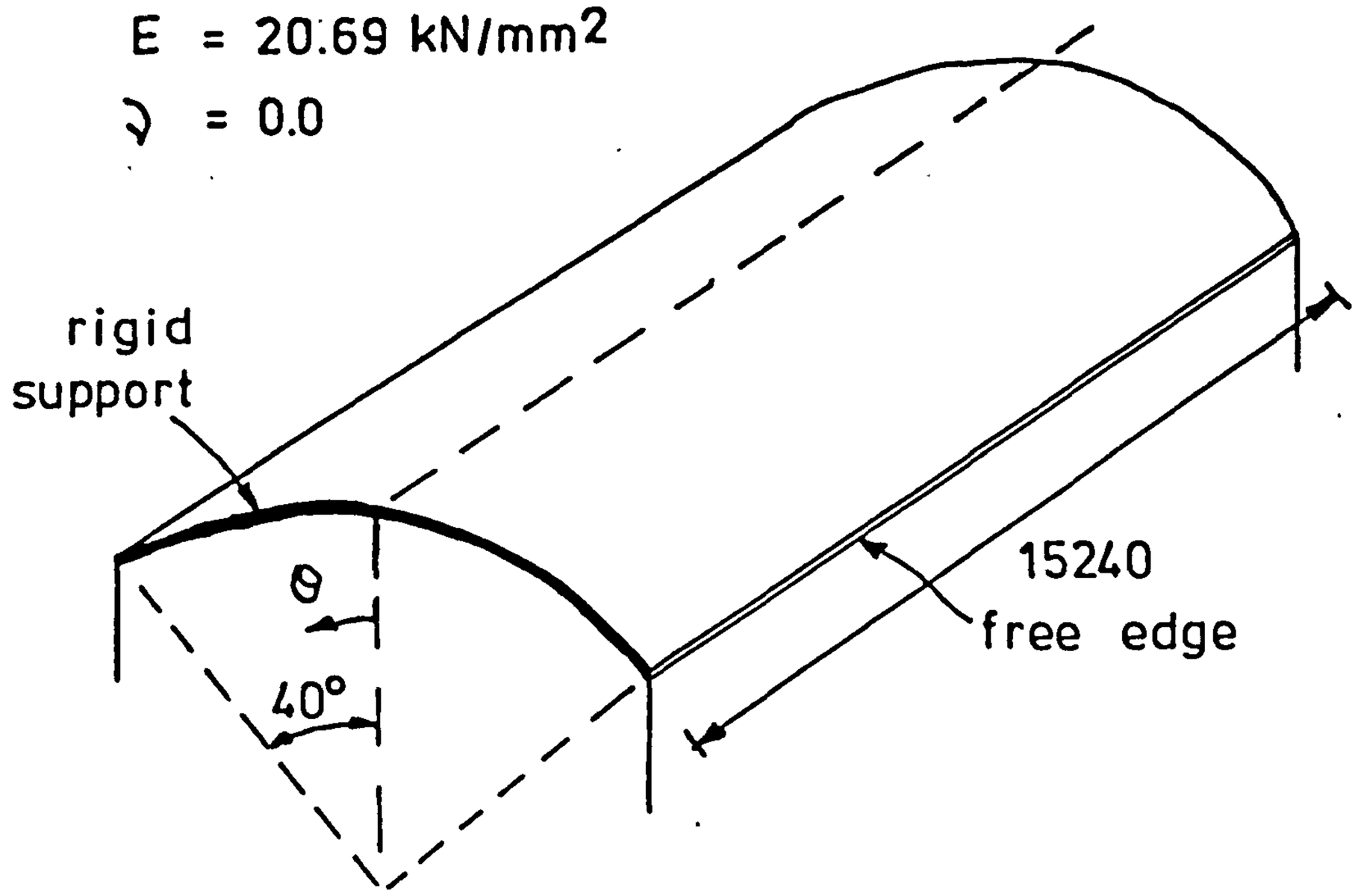

Fig 3.13 Layout of Cylindrical Shell

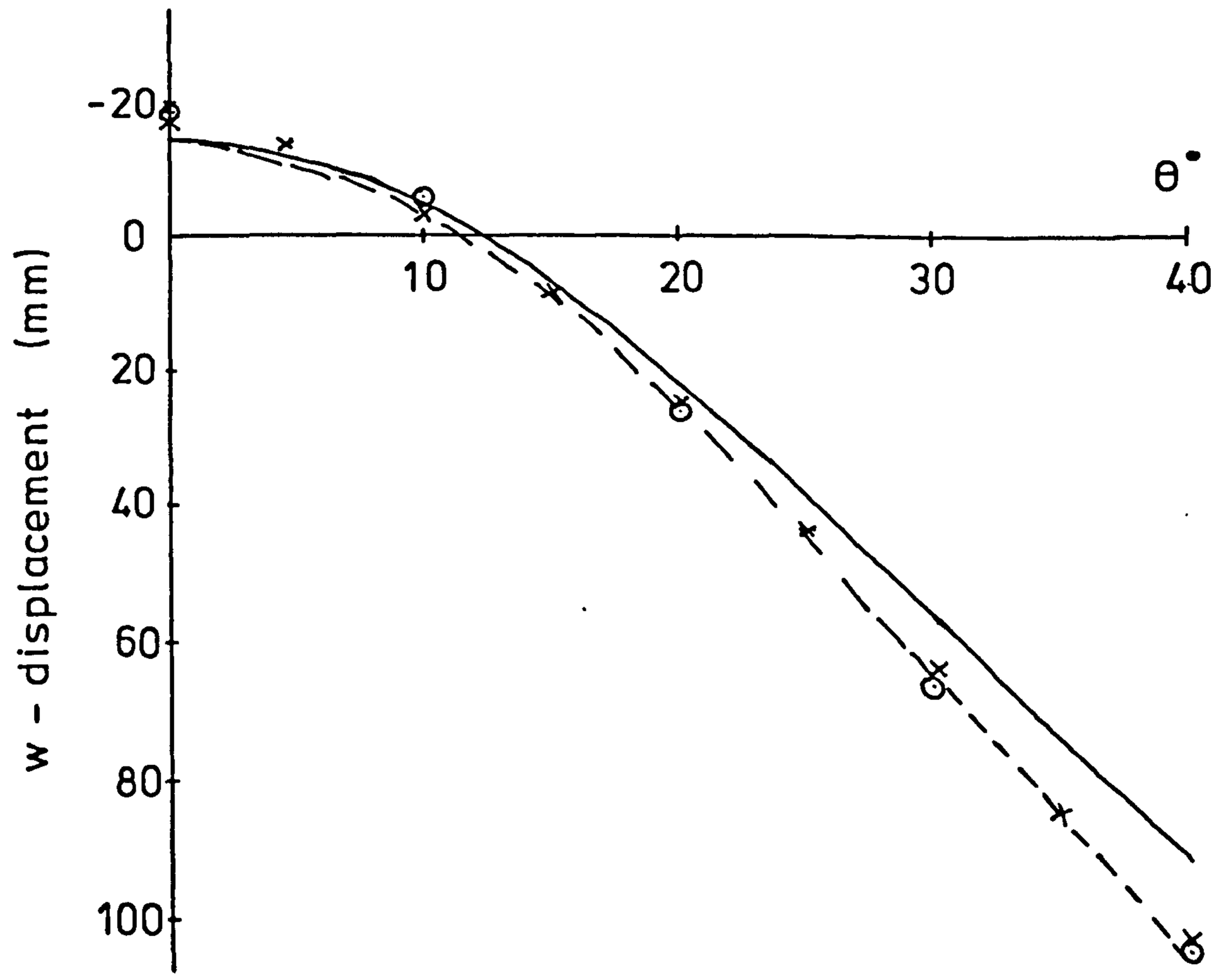

Fig 3.14a Vertical Displacement at centre of span

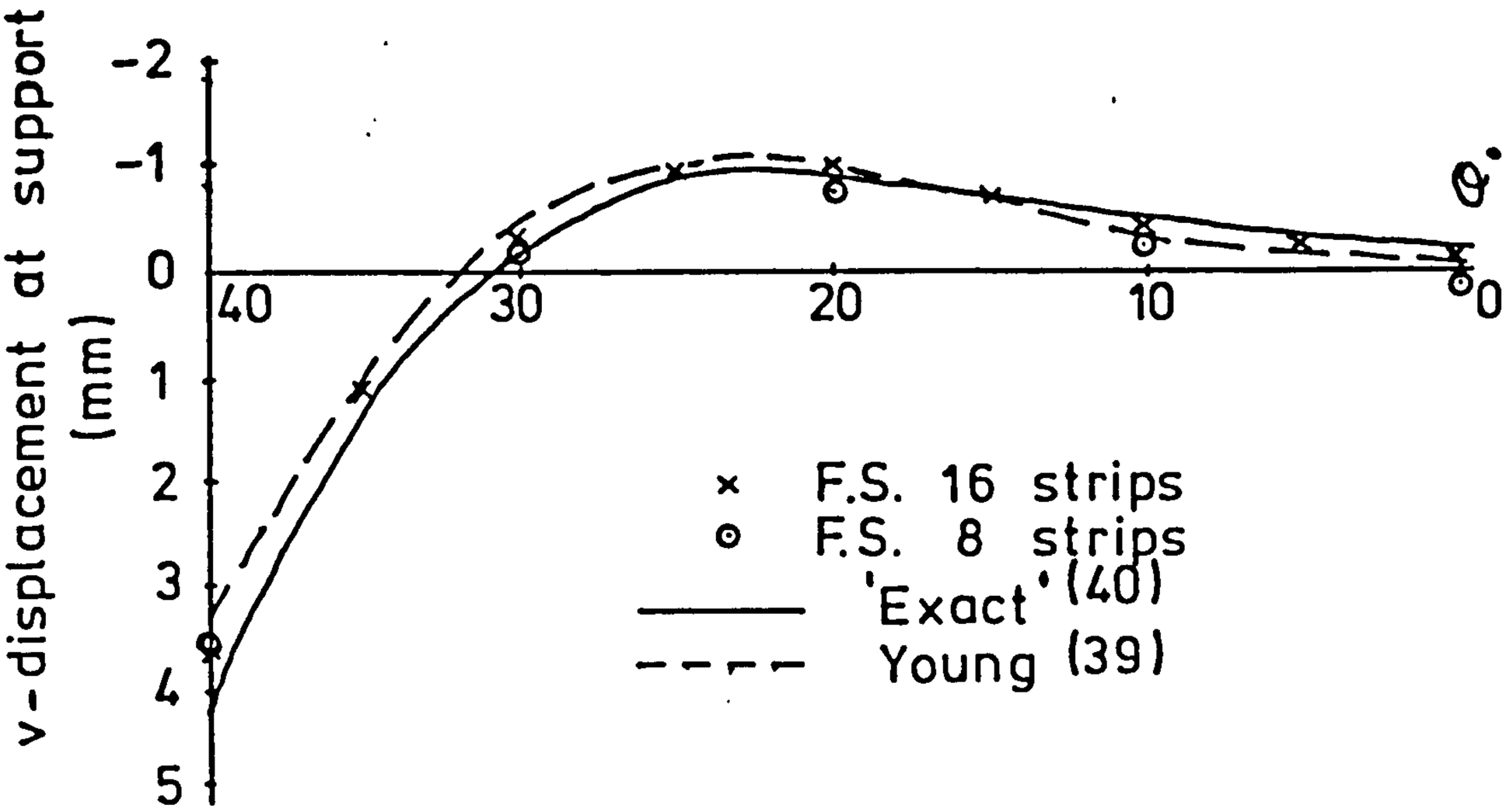

Fig 3.14b Lateral Displacement at Support

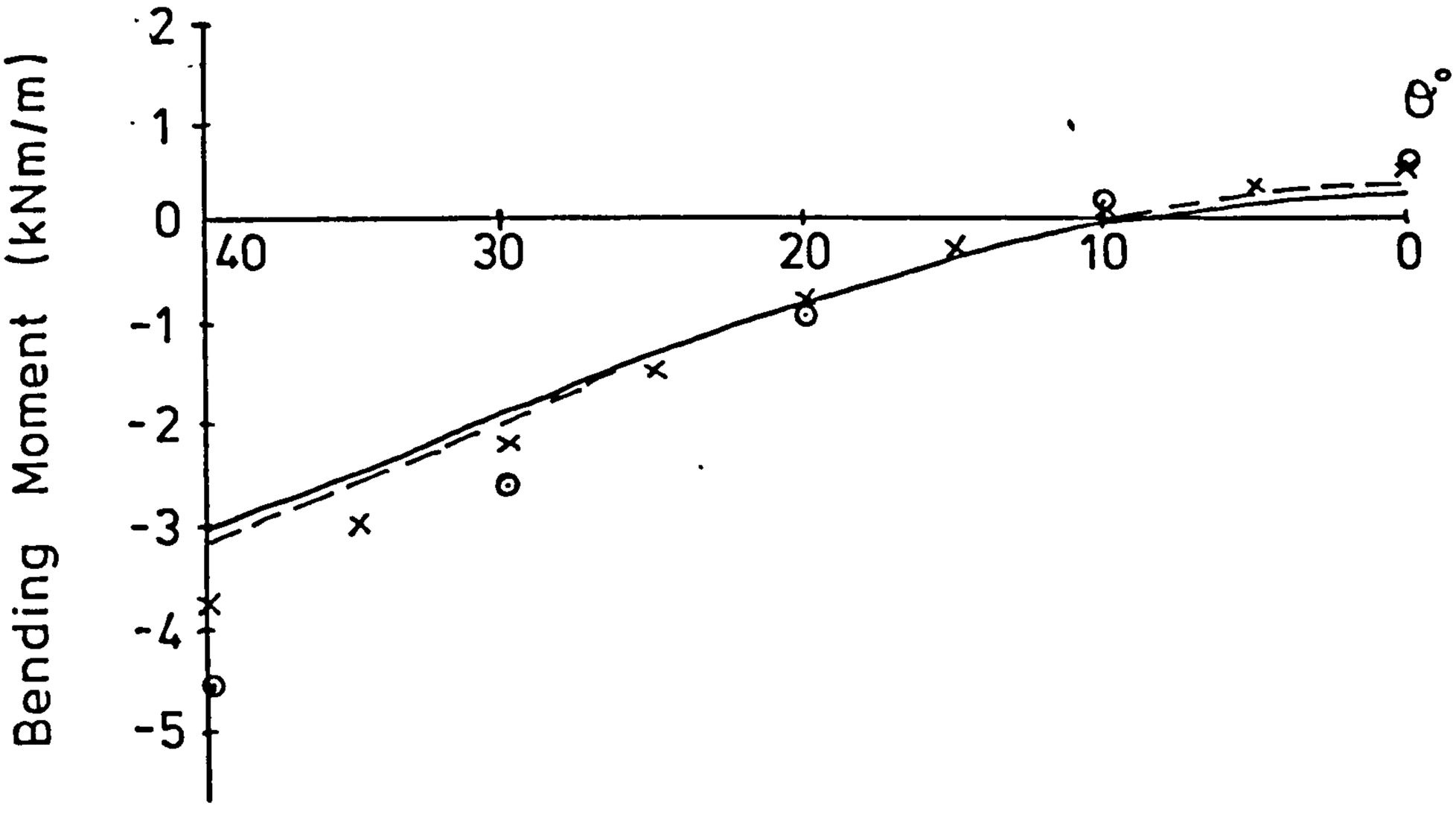

Fig 3.14c Long. Bending Moment at centre

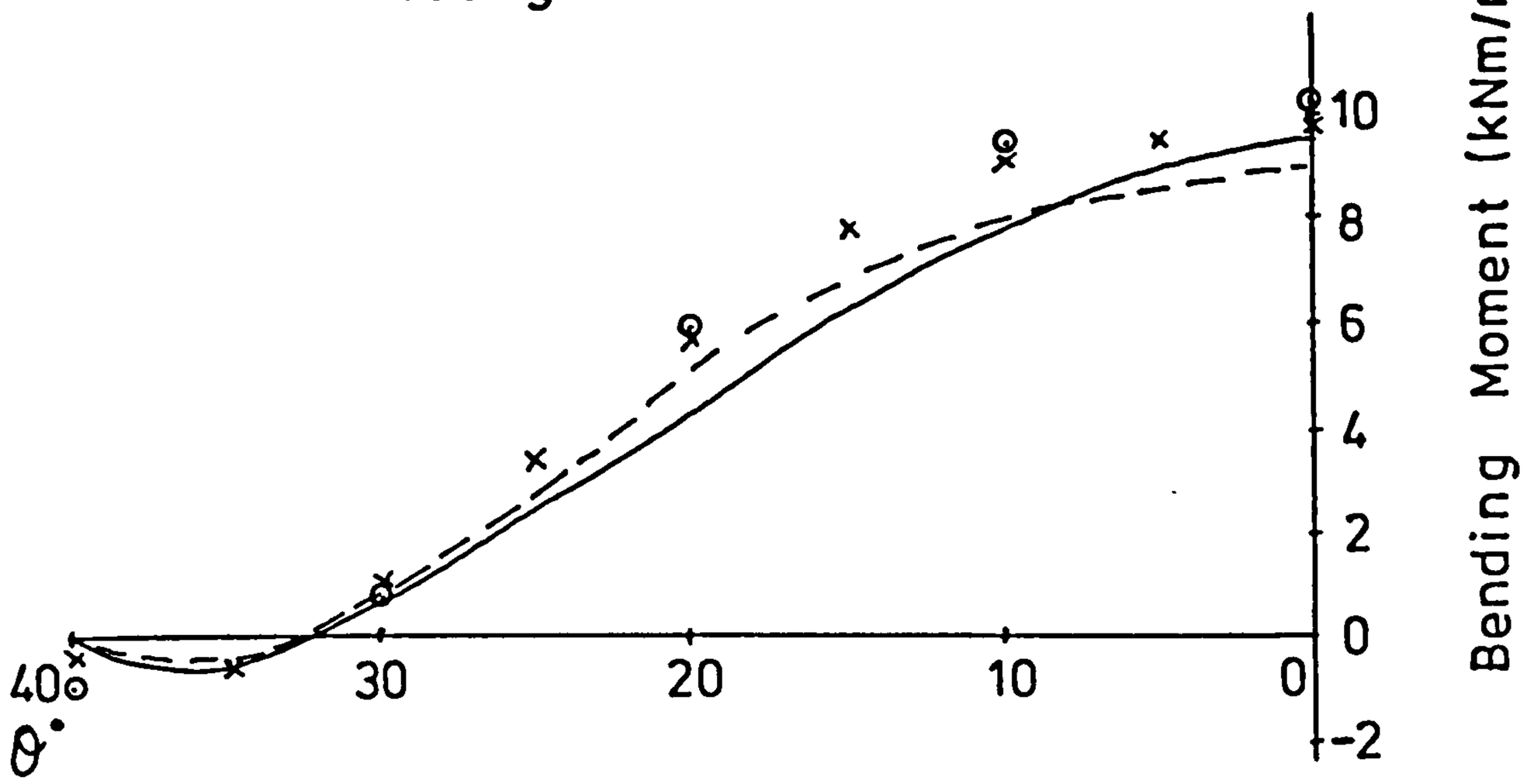

Fig 3.14d Transverse Bending Moment at centre

4. Finite Strip Analysis of Profiled Sheeting under the Action of a Shear Flow

4.1 Introduction

In the previous chapter, the development of a Finite Strip Program was described and verified for problems that have standard solutions as determined by both the Theory of Elasticity and the Finite Element Method. The main purpose of the development however, was to analyse profiled sheeting under the action of a shear flow. This has previously been undertaken by a number of researchers, their work to be described later, but, due to the methods employed and the scope of the computer, only a small number of corrugations within a large diaphragm could be considered.

Since work first started on the use of profiled steel sheeting acting as a diaphragm in resisting lateral loads, researchers have undertaken work to determine the flexibility of a corrugated panel. Until the early 1960's, the only method of obtaining the value of this flexibility was from actual test results [3]. Clearly this is far to expensive for most practical applications.

Work on the theoretical analysis of profiled panels was undertaken by Bryan [22] and was later modified [6]. Bryan's analysis identified the possible components of the flexibility of the diaphragm as

1. the distortion of the profile under the action of a shear flow, $C_{1.1}$
2. the shear strain of the material, $C_{1.2}$
3. the slip of the sheet / purlin fasteners, $C_{2.1}$
4. the slip of the seam fasteners, $C_{2.2}$

5. the slip of the sheet / shear connectors, $C_{2.3}$

and 6. the axial strain of the supporting structure, C_3

It has been found, from test results and theoretical investigations, that the $C_{1.1}$ component for the shear distortion of the profile is of paramount importance for practical diaphragms. A large proportion of the work predicting the flexibility has therefore been concerned with obtaining realistic methods of analysing the distortional shear movement of the profile.

4.2 Review of Work on the Distortion of Profiles

The distortion of a corrugated profile is the resultant deformation that occurs when the centre of shear resistance of the profile is different from the plane of application of the force - in this case the fastener force. The profile is twisted out of shape by the resulting shear flow, which causes the individual plates to rotate and bend inplane, producing longitudinal warping and thus the shear displacement.

Bryan and his fellow workers obtained an expression for the distortion $C_{1.1}$ of a single corrugation, Fig. 4.1, as :

$$C_{1.1} = \frac{0.144 \quad a \quad d^4 \quad K_B}{E \; t^3 \; b^3} \qquad (4.1)$$

where a and b are the overall dimensions of the diaphragm

d is the pitch of the corrugation

t is the thickness of the sheeting

E the Elastic Modulas

and K_B a constant for a particular profile

The above expression was based on experimental observation of a short single corrugation, which showed that the fold lines remain straight, Fig. 4.2, and is termed "rigid plate movements".

From full scale tests and more detailed analysis it has been found that there are large non-linear deformations near the region of the fasteners which Bryan, in the discussion of his work, states as a limitation of the analysis. So the assumption of linear plate movement breaks down in such cases.

Horne and Raslan [41] developed a more general approach to the analysis by again equating the internal and external work. They identified three basic displacements of the profile, Fig. 4.3 when under the action of a shear flow. A sinusoidal term was included, in addition to Bryan's analysis, in the displacement functions as follows :

$$\left.\begin{aligned} U_T &= C\,y + \frac{C_1\,b}{\pi}\,\mathrm{Sin}\,\frac{\pi\,y}{b} \\ U_B &= \frac{C_2\,b}{\pi}\,\mathrm{Sin}\,\frac{\pi\,y}{b} \\ \text{and}\quad U_s &= \frac{C_3\,b}{\pi}\,\mathrm{Sin}\,\frac{\pi\,y}{b} \end{aligned}\right\} \qquad (4.2)$$

with $y = 0$ at the centre of the corrugation

As a point of note, for the term for U_s, the analysis assumes no side plate movement at the ends of the corrugation. For a practical corrugation one end will remain zero, but consequently, as a result of the asymmetrical displacement patterns, the opposite end will have some significant value. The above displacement pattern was a means of obtaining some correlation with the actual test displacement in the region of the end purlins, Fig. 4.4.

Horne and Raslan do not compare any experimental results with the theory developed, but give a comparison with an equilibrium solution [42] that they developed. The additional term in the displacement function allowed the authors to consider non-linear plate movements. Bryan's analysis for rigid plate movements was shown to be valid up to 2 metres in length, but beyond this, non-linear movement in the region of the fastener required the additional term to be included. Consequently as a result of this non-linear movement, the shear flow is now no longer constant along the sheeting, and can be determined from the transverse bending moments.

Davies and Lawson [7] [8] further extended the analysis to include additional terms in the displacement functions and to allow for asymmetrical displacements of U_s in the unpropped condition, so

$$U_T = a_1 y + \sum_{n=1}^{5} a_{n+1} \frac{b}{2n\pi} \sin \frac{2\pi ny}{a}$$

$$U_s = a_7 y + \sum_{n=1}^{5} a_{n+7} \frac{b}{2n\pi} \sin \frac{2\pi ny}{a} \quad \ldots\ldots(43)$$

and $$U_B = \sum_{n=1}^{5} a_{n+12} \frac{b}{2n\pi} \sin \frac{2\pi ny}{a}$$

From their results it was found that the $C_{1.1}$ expression derived by Bryan was incorrect and they proposed a new expression of

$$C_{1.1} = \frac{a\ d^{2.5}\ \bar{K}}{E\ t^{2.5}\ b^2} \qquad (4.4)$$

A comprehensive study was undertaken into the effect of purlin restraint at the ends of the corrugation, intermediate purlins, and the results included in the $\bar{K}$ factor. The results were compared extensively with Finite Element and experimental results, which for large diaphragms were found to agree. For

small diaphragms however, the effect of the edge members were found to dominate as a result of rigid plate movements from the edge members.

Lawson[43] also undertook an extensive literature study of the previous analyses.

Libove[13] and his fellow workers undertook the analysis of the shear distortion from a different approach. They again considered bending of the cross-section, longitudinal plate flexure, shear and torsional energies, with differential equations being formed, such as

$$\left(\frac{d^2 U_T}{dy^2}\right)^2 \cdot \frac{2}{3} \cdot b_T^3 \; t \; E \qquad (4.5)$$

for the bending energy of the top plate in the U_T direction

The total energy is then expressed in terms of differential parameters, and by applying the calculus of variations, six differential equations are obtained corresponding to the minimised total potential energy. Libove solved the differential equations in terms of a complementary function and particular integral for varying boundary conditions to represent the methods of fastening.

4.3 The Work of Lawson

Lawson[43] has undertaken the most extensive study todate into the analysis of corrugated diaphragm, and in particular the distortional behaviour of the profile. The approach for the

analysis of the profiled sheeting was to divide the problem into the analysis for a single corrugation fastened and the analysis for multiple corrugations fastened. The multiple corrugations having an additional distortion pattern from the every corrugation as a result of the absence of the intermediate fasteners.

Considering a single corrugation the total strain energy for the profile is obtained from the displacements U_T, U_s and U_B in equation (4.3) and the inplane shear strains. This energy is expressed as the sum of the energies due to the following :

a. bending of the cross section

$$E_b = \int_0^b \left[C(1,1)\, U_T^{\,2} + C(1,2)\, U_s\, U_T + C(1,3)\, U_T\, U_B + C(2,2)\, U_s^{\,2} + C(2,3)\, U_s\, U_B + C(3,3)\, U_B^{\,2} \right] dy \qquad \ldots\ldots(4.6)$$

where $C(1,1)$ etc., have been derived by Horne and Raslan[4]

b. energy due to longitudinal bending of the plates

$$E_B = \sum_i \frac{E I_i}{2} \int_{-b/2}^{b/2} \left(\frac{d^2 Ui}{dy^2} \right)^2 \qquad (4.7)$$

where i refers to the top, side and bottom plates

c. energy due to longitudinal axial strain of the plates.

This is a result of the incompatibility of the longitudinal strain caused by the longitudinal bending of the plates, and is easily obtained from the following strain expression :

$$\varepsilon_A = \frac{1}{2} \left(b_T \cdot \frac{d^2 U_T}{dy^2} + b_T \cdot \frac{d \gamma_T}{dy} - b_L \cdot \frac{d^2 U_B}{dy^2} - b_L \cdot \frac{d \gamma_B}{dy} \right)$$

..... (4.8)

where γ_T and γ_B are the axial strain expressions.

d. energy due to the shear strain in the plates

$$Es = \frac{G}{2} \int_{0}^{s} \int_{-b/2}^{b/2} \gamma^2 \, ds. \, dy \qquad (4.9)$$

where s refers to the appropriate plate widths

b_ℓ, b_T, b_s

e. energy due to torsion of the plates. This is an additional energy not included in previous analyses.

$$E_T = \frac{t^2 . G}{3} \left[\left(\frac{1}{b_i} + \frac{1}{b_T} \right) \int_{-b/2}^{b/2} \left(\frac{d\, U_s}{dy} \right)^2 dy \right.$$

$$\left. + \frac{1}{2bs} \int_{-b/2}^{b/2} \left(\frac{dU_r}{dy} - \frac{dU_s}{dy} \right)^2 dy \right] \ldots . (4.10)$$

The total energy can then be expressed in terms of the parameters (a_i) in the displacement functions (4.3). By considering small variations in the parameters da_i, and allowing zero strain along the centre lines of the bottom plates, we obtain 17 simultaneous equations with 17 unknowns.

The computed values can then be substituted back into the expressions for total energy E_{TOT}, from which shear flexibility $C_{1.1} + C_{1.2}$ is obtained as follows :

$$C_{1.1} + C_{1.2} = \frac{\Delta^2}{2.\ E_{TOT}} \qquad (4.11)$$

where Δ is the shear displacement.

In dealing with the alternate corrugations, Lawson assumed that the shear flexibility is the resultant of two separate modes of distortion, Fig. 4.5, these are :

1. the flexibility when every corrugation is fastened, as described previously.
2. the flexibility due to the concertina deformation when the force in the missing fastener is reversed.

It is therefore only necessary to determine the flexibility due to the concertina action and add this to the flexibility due to the every corrugation fastened, so

$$K = Ka + Ke \qquad (4.12)$$

where Ka is the concertina sheeting factor

Ke is the sheeting factor for every corrugation

For the concertina action, Lawson again developed the analysis based on non-linear movements and redefined the bottom plate movement into two separate expressions, Fig. 4.6 :

$$U_{B1} = a_1 y + \frac{a_2 b}{2\pi} \cdot \sin \frac{2\pi y}{b} + \frac{a_3 b}{4\pi} \sin \frac{4\pi y}{b}$$

$$+ \frac{a_4 b}{6\pi} \sin \frac{6\pi y}{b}$$

$$U_{B2} = \frac{a_5 b}{2\pi} \sin \frac{2\pi y}{b} + \frac{a_6 b}{4\pi} \sin \frac{4\pi y}{b}$$

$$+ \frac{a_7 b}{6\pi} \sin \frac{6\pi y}{b}$$

. . . . . (4.13)

The top plate movement is assumed to be the average of the neighbouring bottom plates.

$$U_T = \frac{1}{2}\left(U_{B1} + U_{B2}\right) \qquad (4.14)$$

The development is now similar to the every corrugation in the determination of the shear flexibility expression.

The analysis described previously has been shown to be adequate in comparison with experimental results and the Finite Element Method. In particular it has shown that Bryan's factor K_B varies considerably with the length of the sheeting. However, there are certain limitations to the theory and this does restrict the method's use, namely :-

1. that the analysis gives no indication as to whether all the internal energies have been considered. Lawson did include an additional term for the torsion of the side plates, as compared with previous work, but the total internal energies may still not be included. Though Lawson's comparison with a similar Finite Element model does seem to confirm that the total internal energy has been considered.

2. as the length of the sheeting increases further terms are required in the displacement function to adequately predict the displaced form. For any additional terms in the displacement function the parameters a_i have to be re-determined and so the method is not self-generating.

3. Lawson also determined the propping restraint forces fór a linear plate movement, and, as shown by the unpropped analysis, the effect of non-linear plate movements are of paramount inportance in the analysis. It will be shown by the Finite Strip Method that the use of non-linear plate movements does predict the Finite Element and experimental results more closely.

4. no effect of edge members are included, as the analysis only considers a single corrugation in a "large field of corrugations". The effect of the edge member was stated by Lawson to be the reason for this discrepancy between the test and theoretical results. The edge member influences the results by preventing bottom plate movement of the displacement U_B at the shear connectors.

4.4 Determination of the Propping Force from the Finite Strip Analysis

The actual deformation of the profile under the action of a shear flow is not purely asymmetrical, as the edge purlins have the effect of restricting the downwards displacement of the profile, Fig. 4.4. However, points restraints can not be applied to the Finite Strip Method directly as the nodes are considered to be two dimensional, whereas in the Finite Element Method the nodes are one dimensional in nature. The method commonly employed to overcome this problem in the Finite Strip Method is to use the "flexibility" approach. This method was first employed in a program by Loo[44], who analysed bridge decks with discrete columns.

The structure in Fig. 4.7 is loaded by externally applied forces and restrained at certain points by "n" forces. The displacements at these points 1, 2, 3 . . . . , n - 1, n are zero. The method of determining the propping forces consists of relaxing the restraints, thus producing the deflections ∇i at each of the restrained points due to the external load. This is termed the primary structure.

$$\{\nabla\} = \begin{Bmatrix} \nabla_1 \\ \nabla_2 \\ \vdots \\ \nabla_{n-1} \\ \nabla_n \end{Bmatrix} \quad \text{. . . . . (4.15)}$$

Unit loads are then applied to the structure individually and the respective displacements $[f]_{ij}$ at each of the restrained nodes are obtained from :

$$[f]_{ij} = \begin{bmatrix} f_{11} & f_{12} & & f_{1n} \\ f_{22} & & & \\ & & & \\ f_{n1} & & & f_{nn} \end{bmatrix} \quad \text{---(4.16)}$$

where i refers to the loaded point

and j refers to the deflection point

From compatibility requirements of the displacements at the restrained points we obtain :

$$[f]\{R\} + \{\nabla\} = \{0\} \quad \text{-------(4.17)}$$

from which the reactions $\{R\}$ can be easily obtained

4.5 Comparison of the Finite Strip Method and the Work of Lawson

Before any analysis by the Finite Strip Method can be undertaken for the profiled sheeting, the correct boundary conditions for each strip in the profile must be identified. In

the analysis by Lawson the boundary conditions for U_s, U_T and U_B were defined by the displacement functions 4.3. Together with these defined boundary conditions, boundary values were implied for the bottom plates in the region of the fasteners. These boundary conditions are identified as the restriction of the vertical displacements alon the nodes A and B in Fig. 4.8 (a) for the every corrugation case and Fig. 4.8 (b) for the alternate corrugation case.

An additional requirement, stated by Lawson, is that the longitudinal strain which can be expressed as

$$\frac{d\,\Delta}{dy} = 0 \qquad (4.18)$$

where Δ is the shear displacement

along node A. This is required so that the analysis of a single profile models the effect of a single profile in a large diaphragm. This can be easily instigated in the program by restraining the inplane displacements (V) except for the second harmonic which is a constant displacement function.

Having determined the boundary conditions, the analysis of the profiled sheeting can now be compared with the work of Lawson. The results of the study, carried out on the profile given in Fig. 4.9., are shown in Fig. 4.10 and 4.11 for the every corrugation and alternate fastened cases respectively. The diagrams give the

variation of Bryan's factor K_B with the length of the sheeting (b), where Bryan's factor is determined from :

$$K_B = \frac{C_{1.1.} \quad E \quad t^3 \quad b^3}{0.144 \quad a \quad d^4} \qquad (4.19)$$

where a is the width of the diaphragm, in this case the pitch of the profile · d

b is the length of the sheeting

E is the Elastic Modulas

t is the thickness of the sheeting

and $C_{1.1}$ is the shear distortional flexibility

It should be noted that the value of K_B was determined only up to the 12^{th} harmonic, as the computer was not able to store matrices above this value. In both fastener arrangements correlation of the three methods (Finite Strip, Finite Element and Lawson's energy method) was found to be excellent. However, for the alternate arrangement case, the results of the Finite Strip, show that for short lengths of profile (under 2.5 metres) there is a slight divergence of the results. This could be accounted for by the fact that for short lengths of sheeting the internal energy in the profile may not be fully included in the analysis. Also the type of finite elements adopted could cause a divergence of the results. Even though both comparisons do differ from the

Finite Strip solutions, the results for this method are stiffer, and this is acceptable in most results.

The energy method of Lawson's could only consider the asymmetrical displacements for non-linear movements. In the propped arrangement, Lawson applied a linear analysis based on compatibility of displacements at the propped nodes. The Finite Strip and Finite Element solutions do show a shift from Lawson's energy method for these results, but, this error is not significant for design purposes and the tables given by Lawson do not need to be modified in this respect.

A repeat of the convergence study, carried out by Lawson, has also been undertaken for both fastener configerations to investigate the accuracy of the results for a varying number of harmonics. Only the unpropped arrangement has been analysed, as the propped case would only produce corresponding results.

For the every corrugation arrangement, the results shown in Fig. 4.12, give identical results to those of the previous work[43]. This is logical, as the displacement functions for the energy method and the Finite Strip Method are similar. In the alternate corrugation arrangement, given in Fig. 4.13, there is no limiting value of K_B for each harmonic as the length of the sheeting increases. This contradicts the results of Lawson who showed that a limiting value does occur of K_B in the alternate corrugation case. This can be explained by the fact that this study includes the combined distortional movement of the concertina action and the every corrugation cases of Lawson. The Finite Strip results having been shown previously to correspond to the combined results of Lawson's work.

As the curves in the alternate case have no plateau, an

acceptable result could be obtained for less harmonics, and this also shows that there is less distortional behaviour of the profile near to the fasteners against the much larger distortional behaviour for the every corrugation.

Having obtained the convergence for the number of harmonics it was felt that a study of the number of strips per plate of the profile and the number of profiles could have an effect on the results. From this investigation there was found to be no variation in the results compared with the single corrugation with one strip per plate. So for all future studies this arrangement of the strips will be considered.

4.6 The Influence of Edge Members on the Shear Distortion

In the analysis of the shear distortion factor $\bar{K}$ Lawson showed that many factors influenced the value of a particular profile. These factors included the number of purlins, the overlapping of the sheet lengths, and the number of fastener in each corrugation. Comparing the theoretical and experimental results, Lawson also concluded that the effect of the edge member influenced the $\bar{K}$ factor, though, due to the limitations of the energy method, a riourous analysis could not be undertaken. The Finite Strip program that has been developed is able to analyse diaphragms in which there are more than one corrugation, and thus the influence of the edge members can be fully investigated.

The effect of the edge member is to restrict the lateral movement U_B at the shear connectors. This displacement has been shown by previous work to be the predominate.factor that contributed to the shear distortion. In the energy method Lawson restricted this movement U_B at certain points to

investigate an increasing number of purlins on the value of $\bar{K}$. For the case of an infinite number of purlins, this fully restricted the U_B movement, and was shown to cause a considerable reduction in the $\bar{K}$ value. The case of an infinite number of purlins in the Lawson analysis can be likened to that of a single corrugation between two edge members. As the number of corrugations are increased, the restriction of the U_B movement at the end of the diaphragm would tend to be less effective on the value of Lawson's $\bar{K}$. There would then be a point at which the effect of the edge members would have diminished from the $\bar{K}$ factor.

Before the investigation could be carried out using the program, a selection of profiles had to be decided from among the many available profiles. The author used a number of the profiles investigated by Lawson together with a deeper profile, the profile dimensions of which are given in Fig. 4.14. A standard length of profile of 5 metres was selected for the investigation which was within the convergence accuracy of twelve harmonics, and this was not considered to be classed as a short profile, i.e., it was not a profile in which a linear displacement function was adequate to predict the shear displacement

Firstly, considering the results of the every corrugation case, which are given in Fig. 4.15 - 4.18, it can be seen that with increasing number of corrugations the value tends towards the single profile analysed without any edge effect included. For all profiles in the study the conclusions are that, after the 8^{th} corrugation, the influence of the edge members need not be considered. If a 5% cut off, for design purposes, is also considered, then after five corrugations the edge member need

not be considered.

Again, for the alternate corrugation case, the results given in Fig. 4.19 - 4.21 show that with about eight corrugations the consideration of the edge member need not be included in the design. However, comparing the rate of convergence of the two fastener arrangements, it is seen that they do not converge at the same rate and their extent of divergence is not similar. This is most likely due to the greater influence that the concertina deformation pattern has on the alternate corrugations case.

4.7 The Influence of Friction on the Shear Distortion of the Profile

The work of Lawson[43] has shown, for the alternate corrugation case that the test results are overstiff. One of the factors that has been shown to influence the test results is that of the edge members, which were considered in the previous section. An additional factor which could vary the shear distortion for the alternate corrugation case is due to the friction of the bottom plate which include no fastener. This plate is restricted against vertical movement by the purlin, Fig. 4.22, and as the plate moves horizontally, there is an induced friction force on the profile. In turn, due to the asymmetrical displacement of the profile a couple is formed as shown in Fig.4.22. This couple is opposite to the lateral displacement of the bottom plate and so will reduce the shear distortion of the profile.

An analysis of this reduction can be undertaken in one of

two ways. Firstly, applying Lawsons's criteria of two displacement patterns, the friction couple will only be concerned with the concertina mode and the every corrugation deformation pattern will remain unchanged. By first analysing the profile without the friction force the purlin force P_2 can be obtained. This results in a friction force P_f of

$$P_f = \mu \cdot P_2 \tag{4.20}$$

where μ is the coefficient of friction between the two materials.

So for a unit shear flow, the value of P_f can be compared with the concertina fastener force d. The percentage reduction is obtained simply by

$$\frac{100\ \mu \cdot P_2}{d} \tag{4.21}$$

and the value of Lawsons factor $\bar{K}$ is given by

$$\bar{K} = \left(1 - \frac{\mu P_2}{d}\right) \overline{Ka} + \overline{Ke} \tag{4.22}$$

This is only an approximate value of the friction force as no account of the comparative values of every and concertina shear distortion factors are included.

Another method of analysis is to use the Finite Strip Program and by applying a couple, obtained from the previous analysis, to the profile. A number of profiles have been analysed in this way using a value of the coefficient of friction of 0.3. From the results the maximum reduction in the Lawson $\bar{K}$ factor was found to be only 2.5%. Therefore in design this does not need to be considered, though from a theoretical point of view it may slightly effect experimental results.

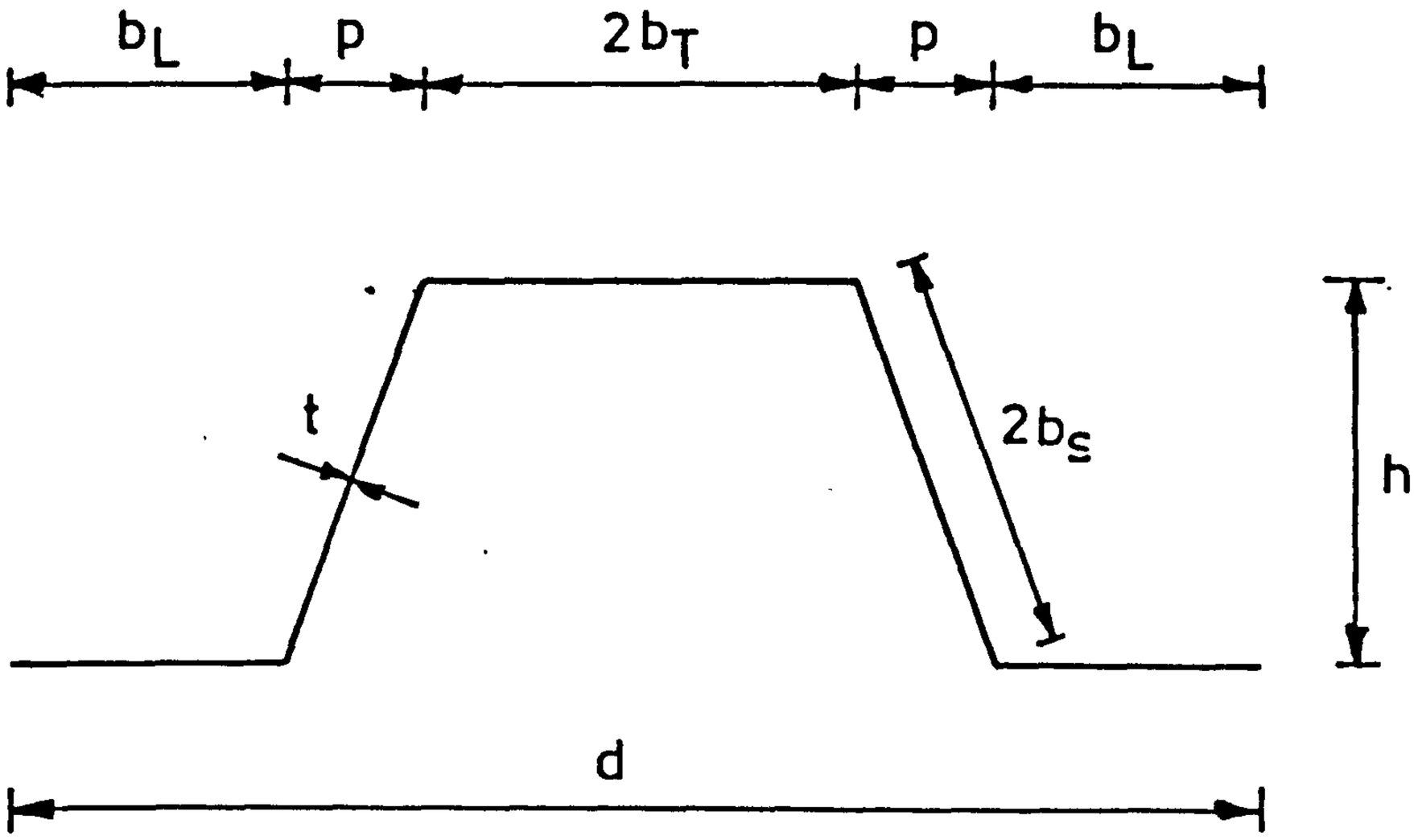

Fig 4.1 Notation of Profile

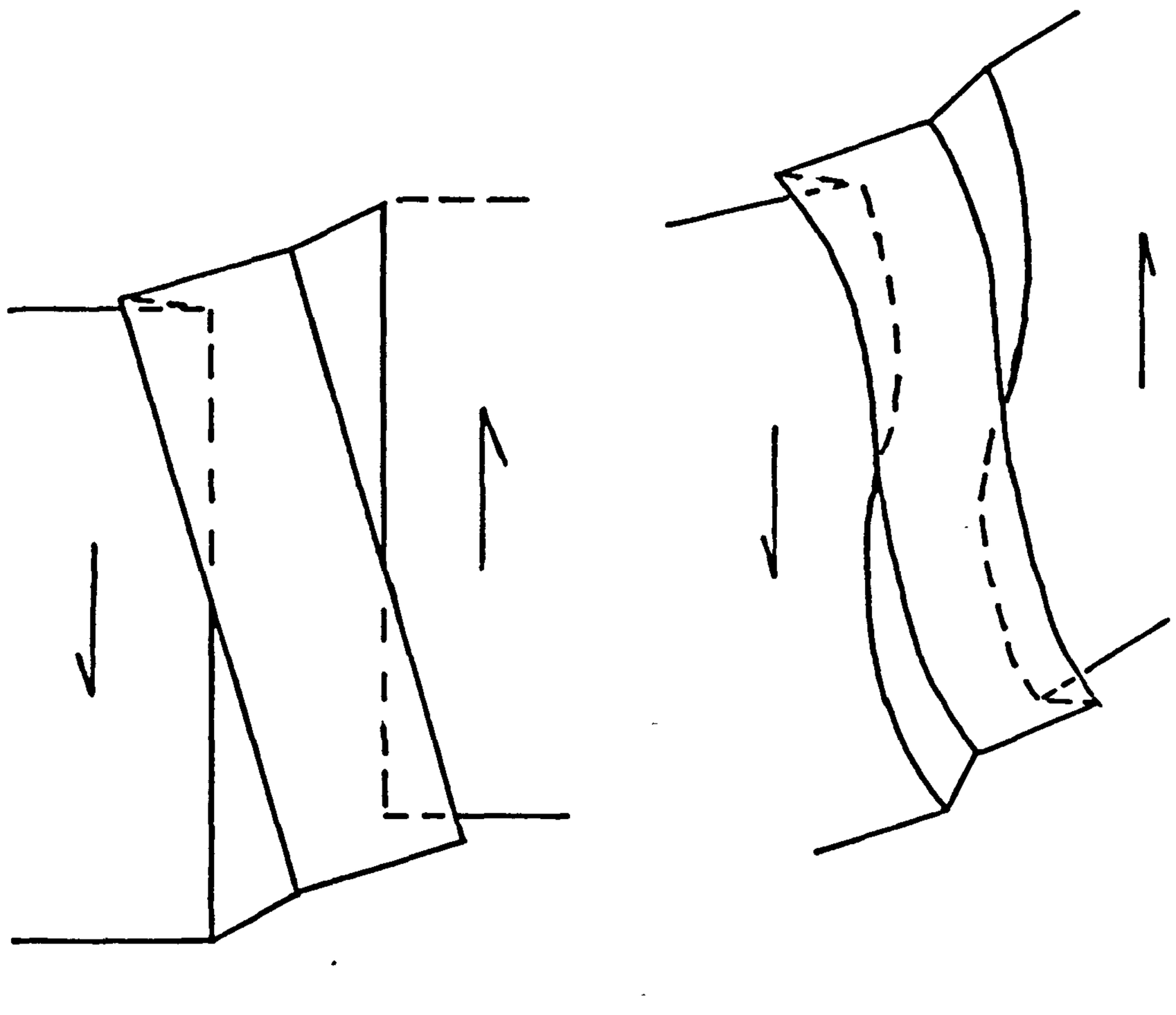

(a) Fold lines remain straight

(b) Fold lines remain free to curve

Fig 4.2 Plan Distortion of Profile

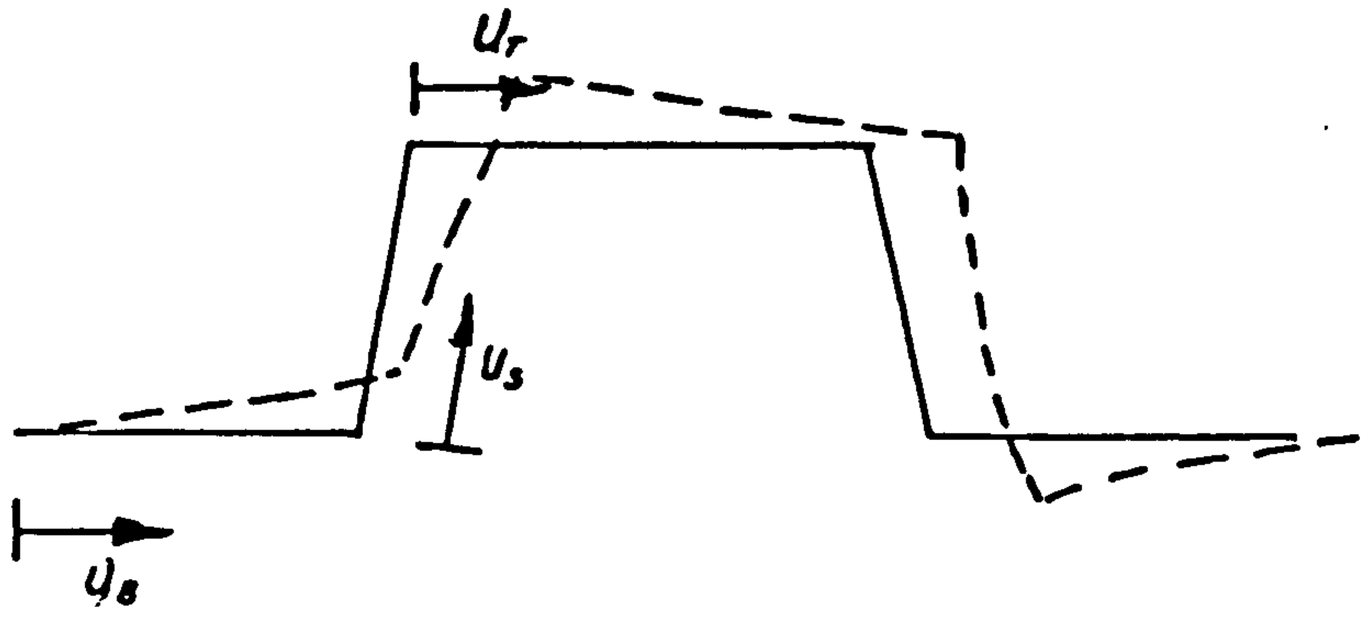

Fig 4.3 Definition of Displacements

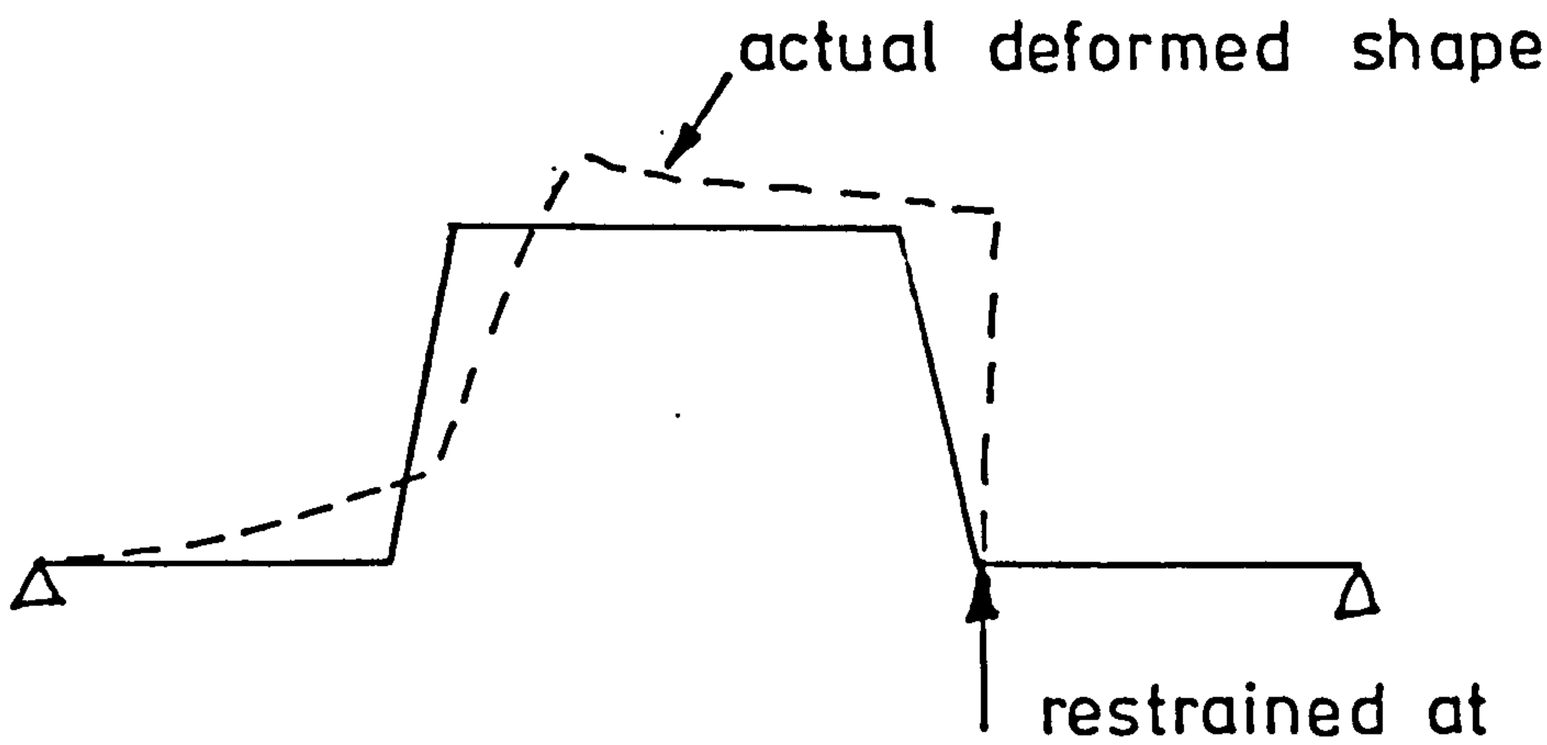

Fig 4.4 Actual Deformation at end of Profile

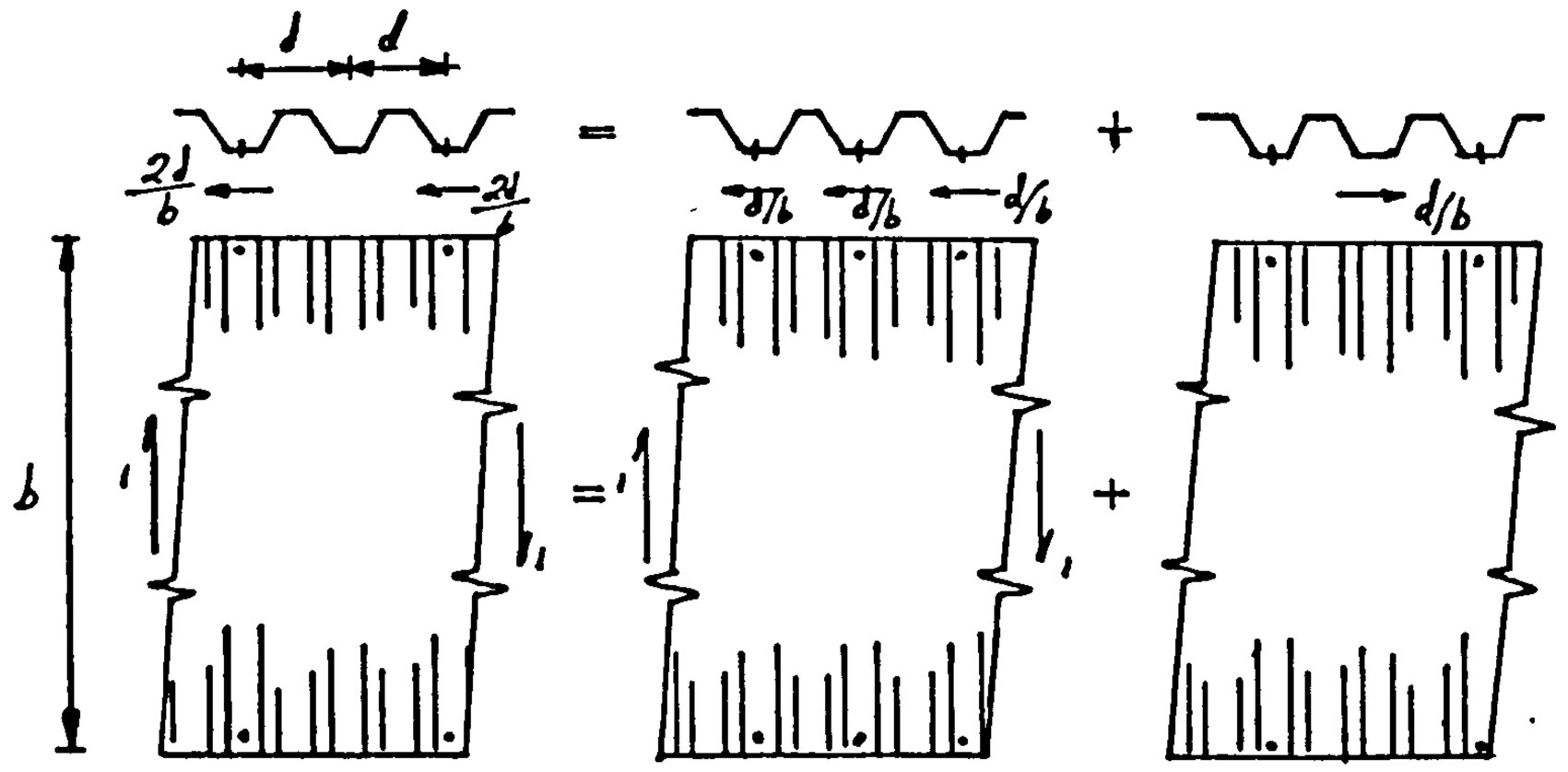

Fig.4 5 Analytical procedure for fasteners in alternate troughs

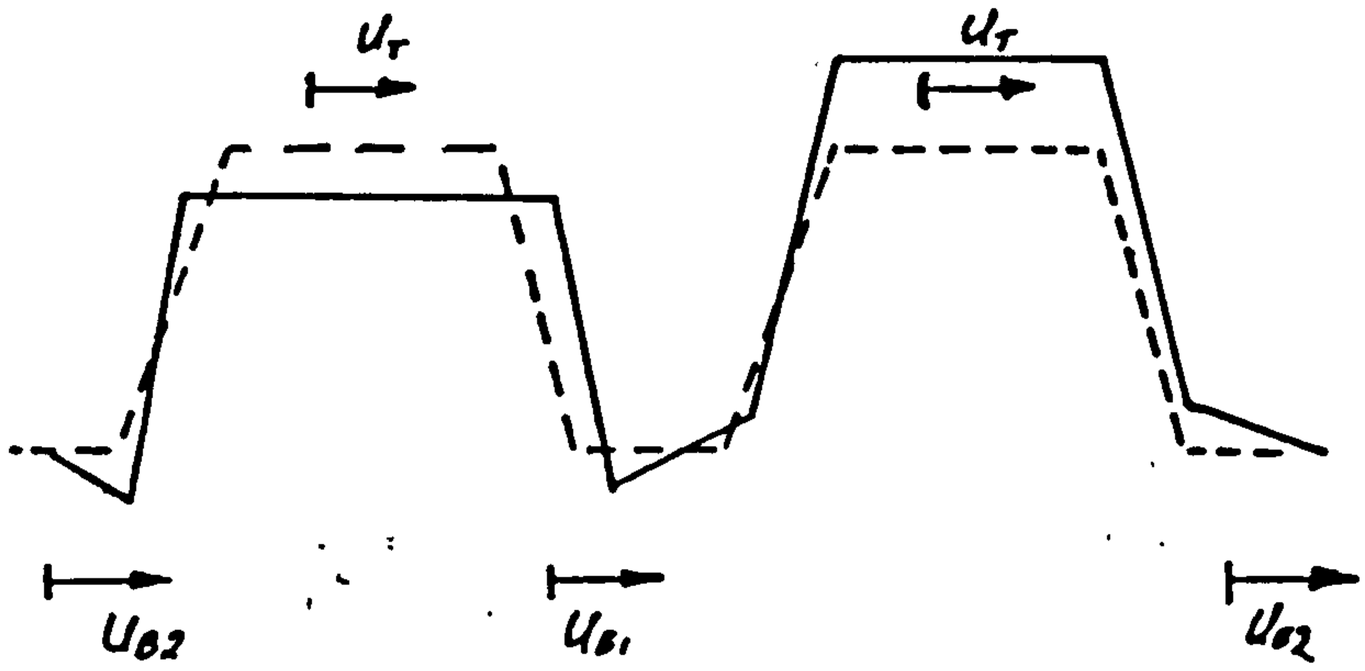

Fig 4.6 Profile Displacements for alternate corrugations fastened

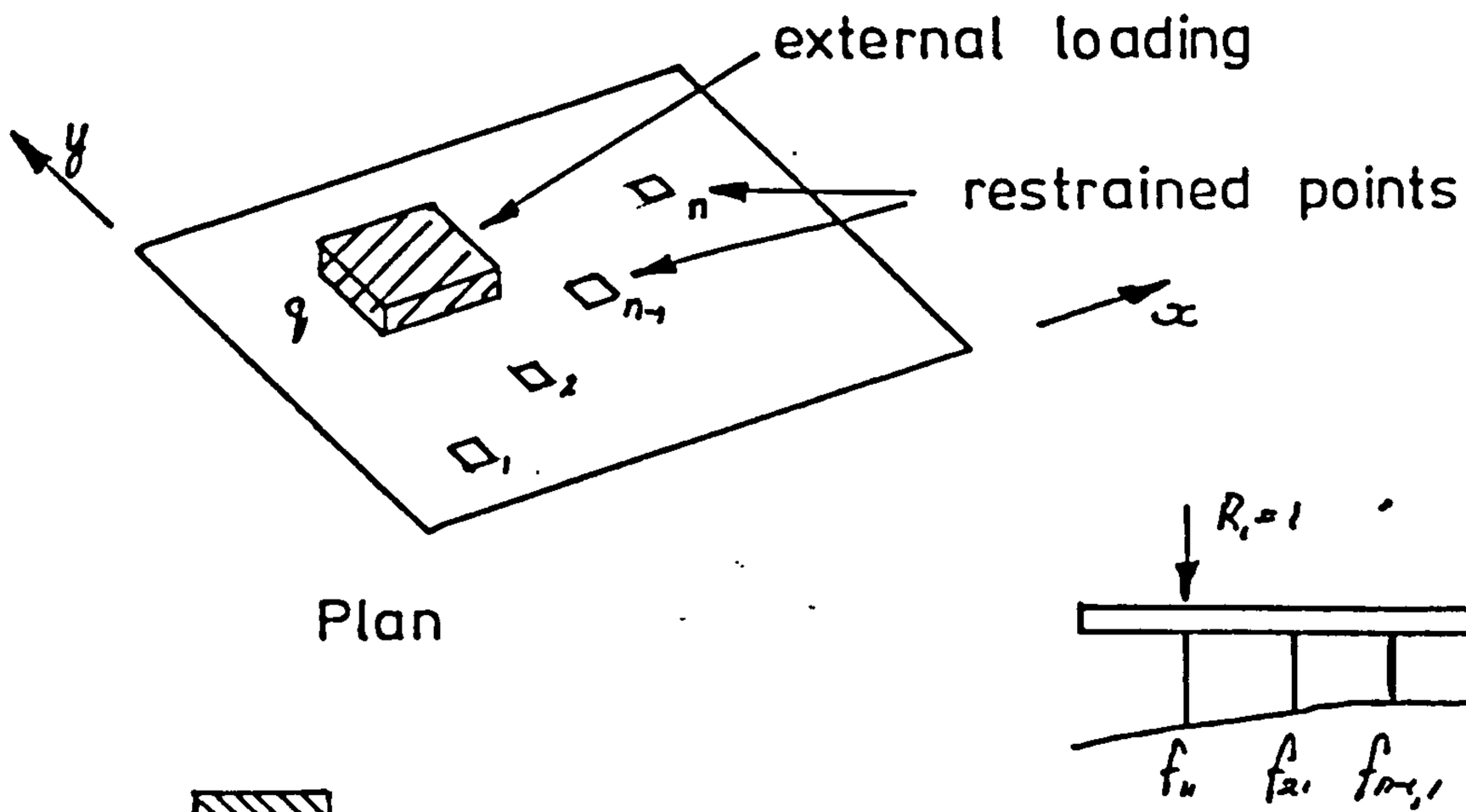

Fig 4.7 Loading Combinations for Propping Forces

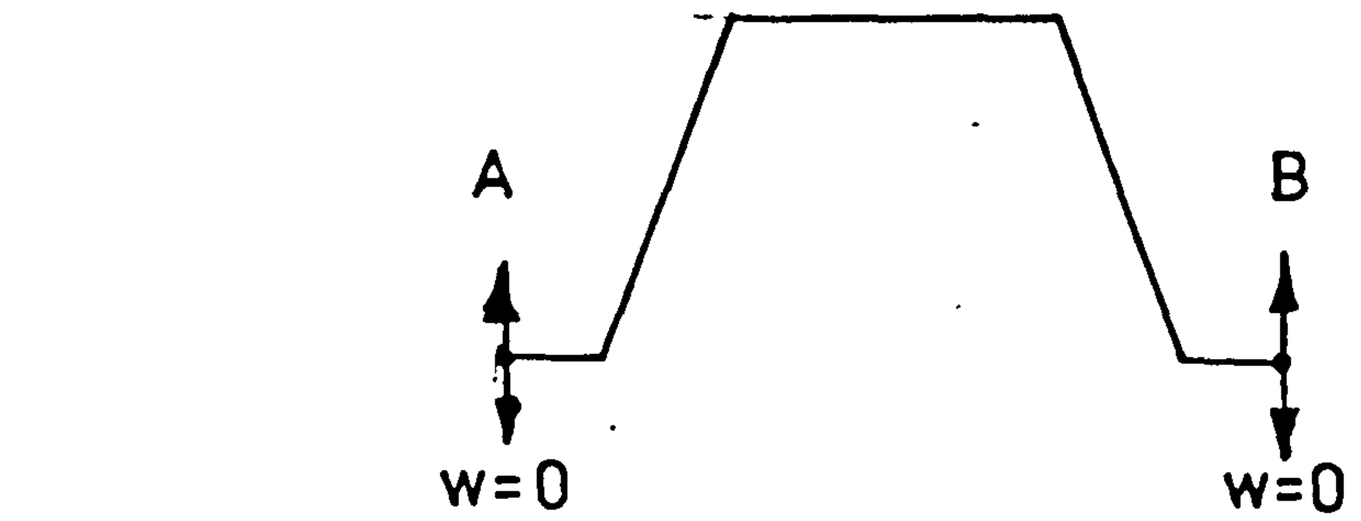

(a) every corrugation

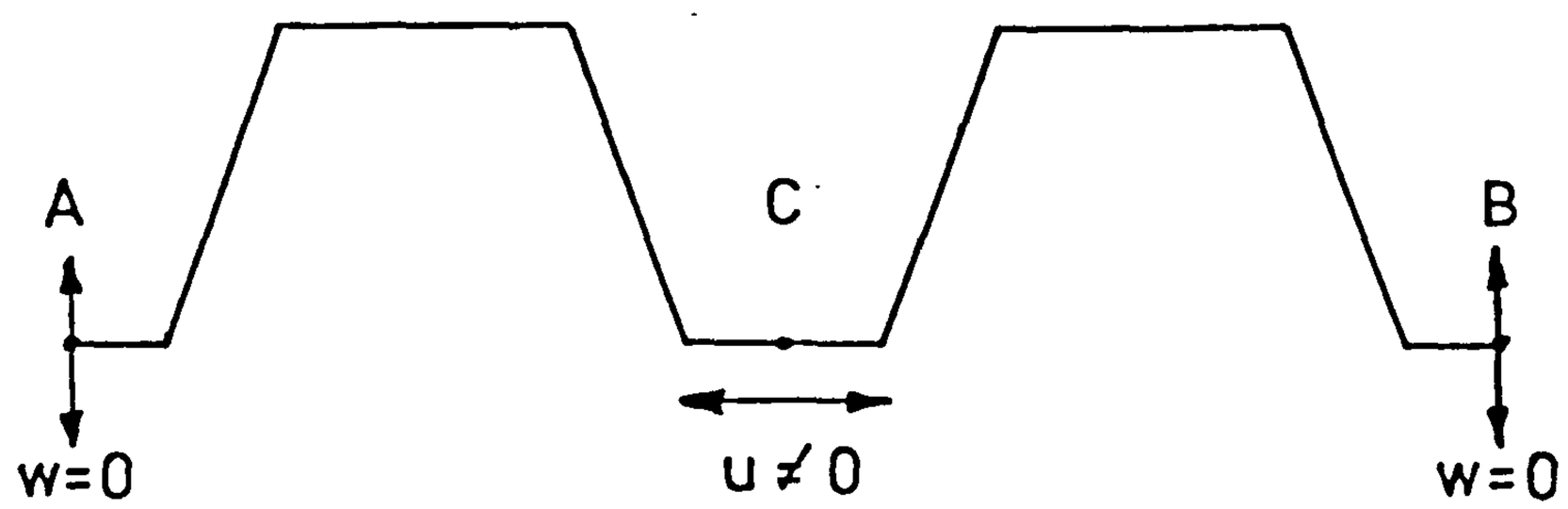

(b) alternate corrugation

Fig 4.8 Degree's of Freedom

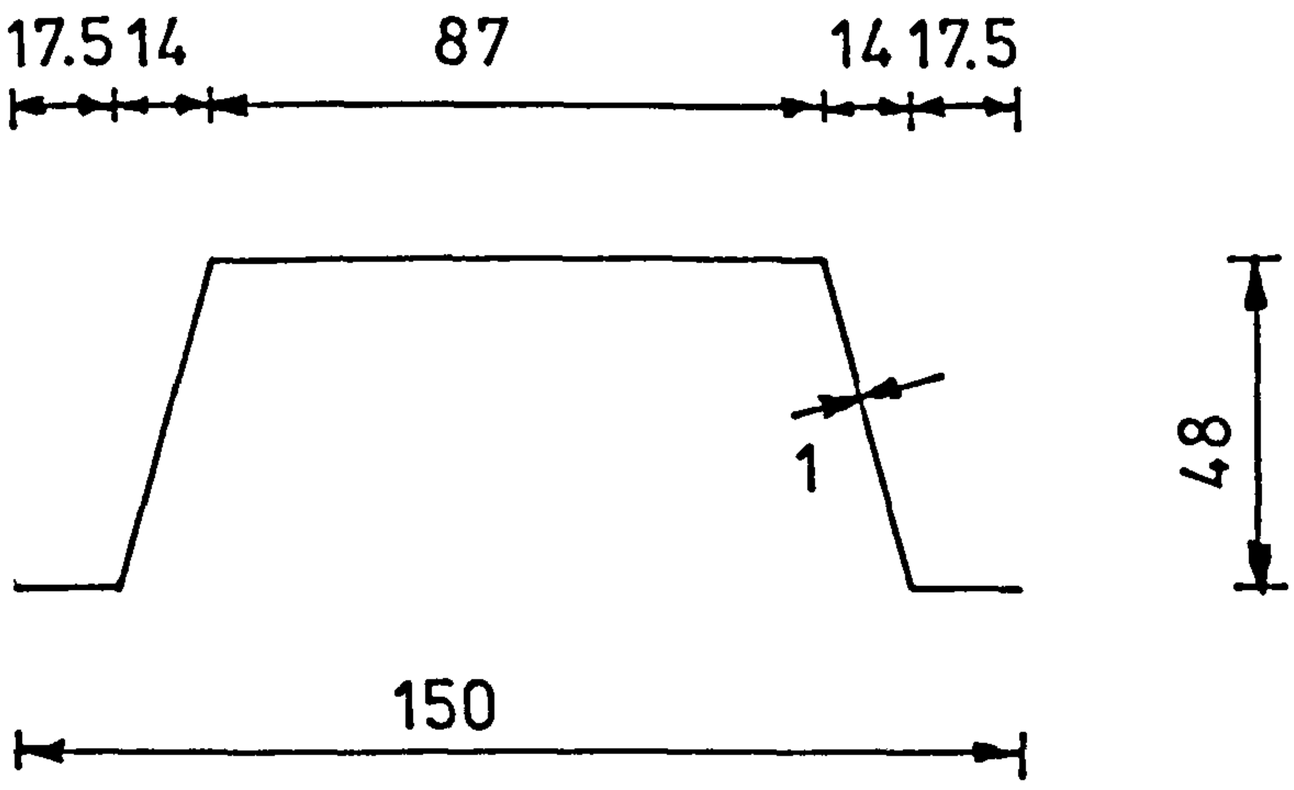

Fig 4.9 Dimension of Profile

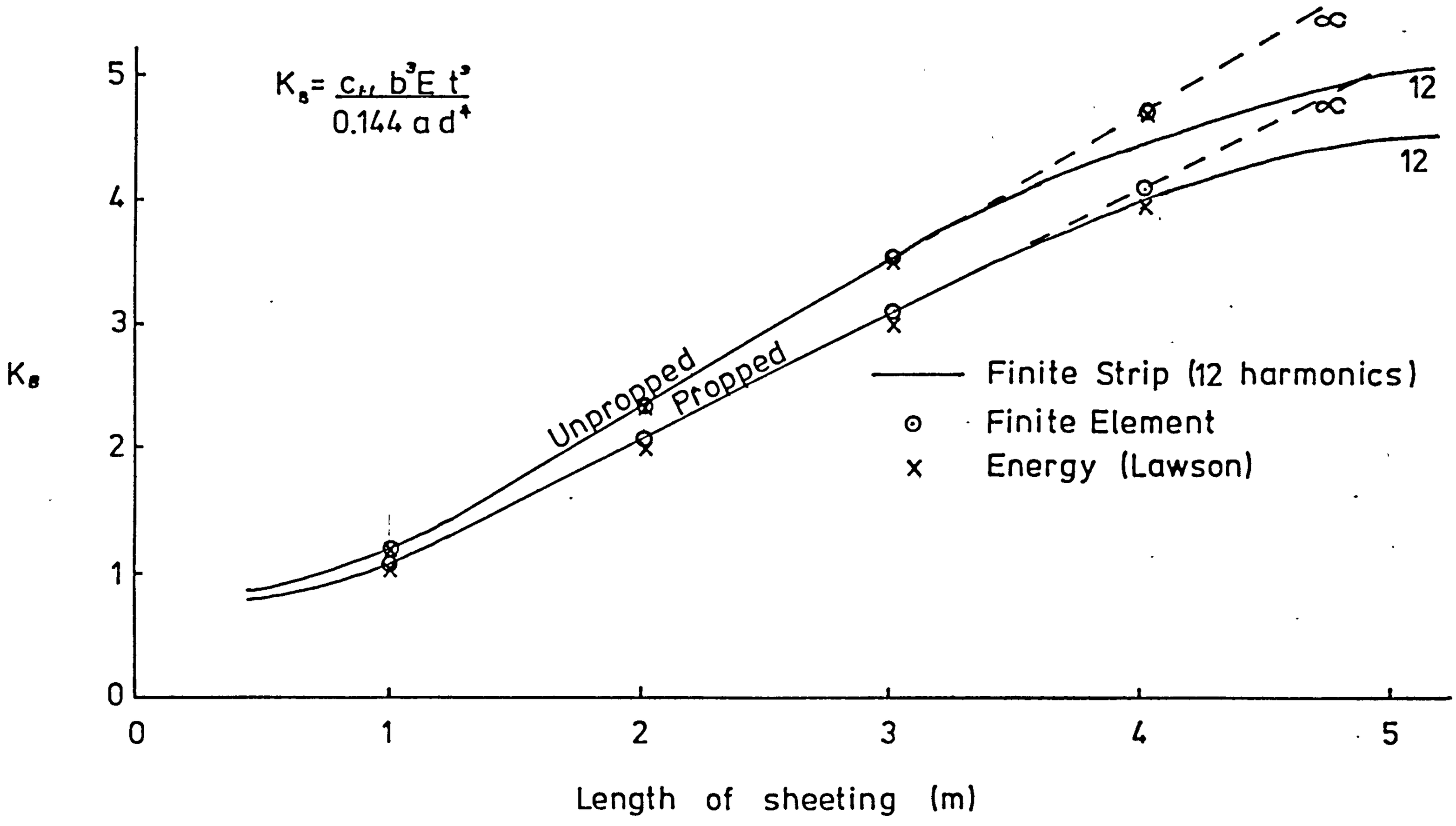

Fig. 4.10 Variation of K_s with sheeting length for every corrugation fastened

Fig 4.11 Variation of K_8 with sheeting length for alternate corrugations

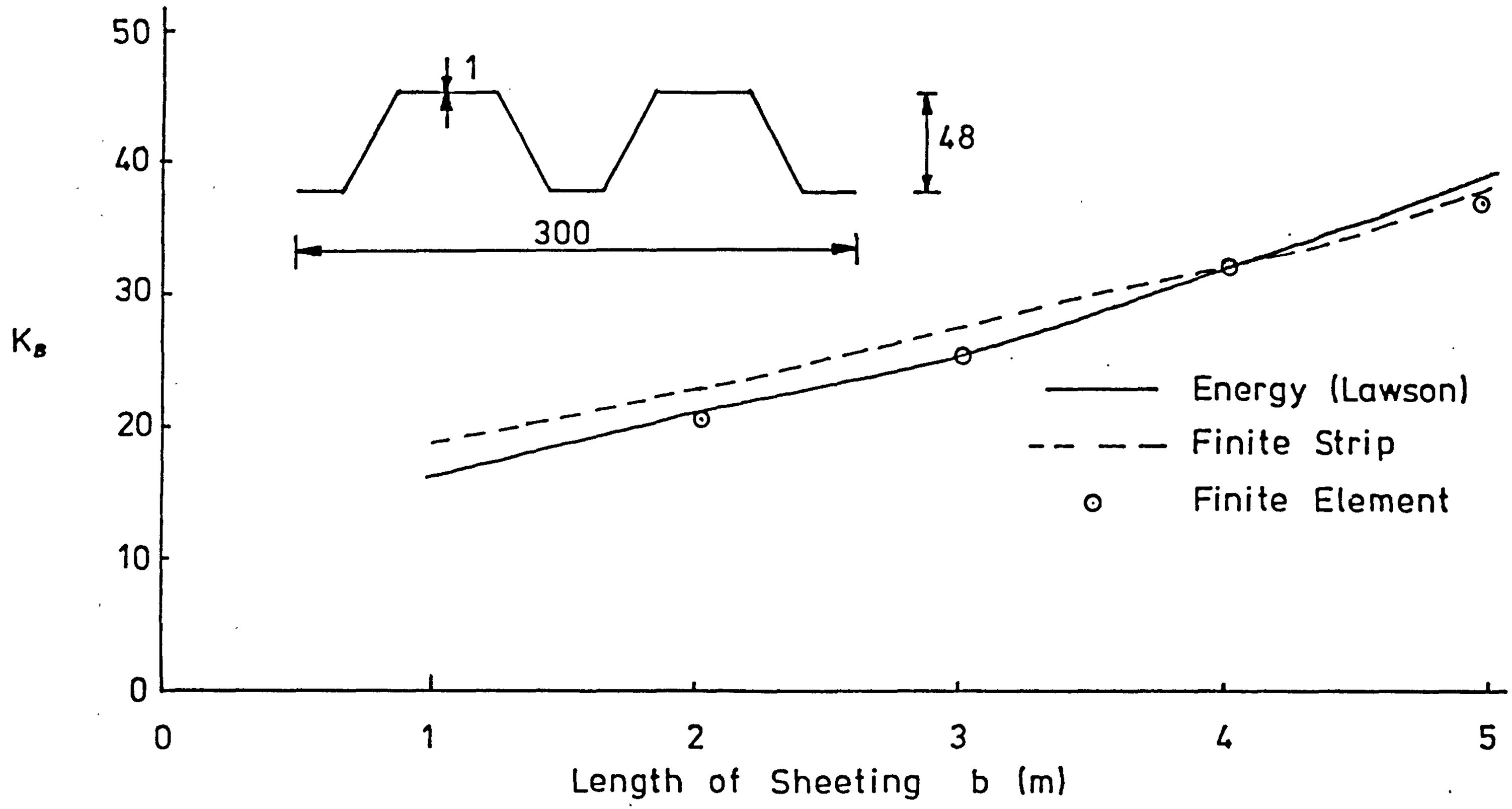

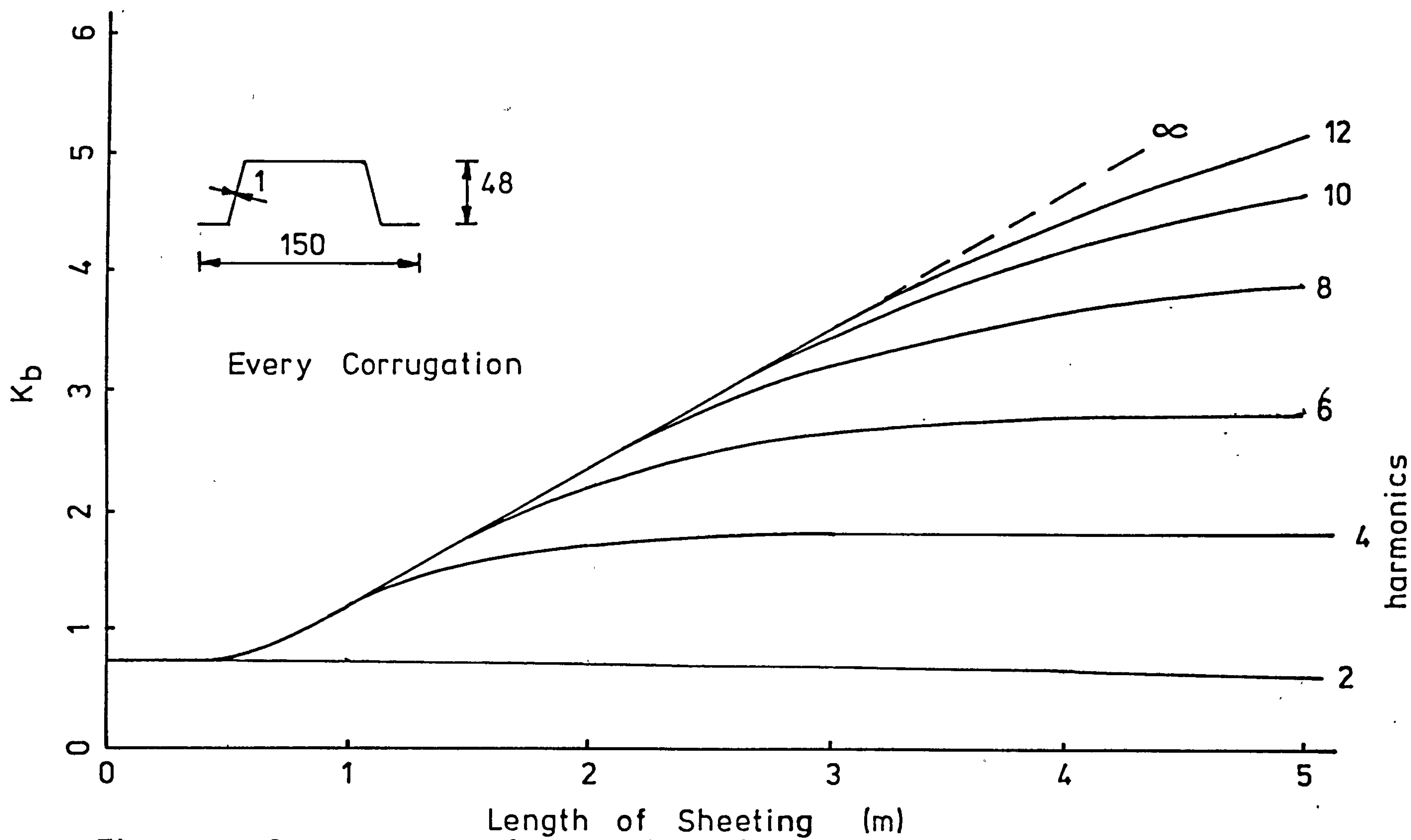

Fig 4.12 Convergence of K_b value with increasing numbers of harmonics

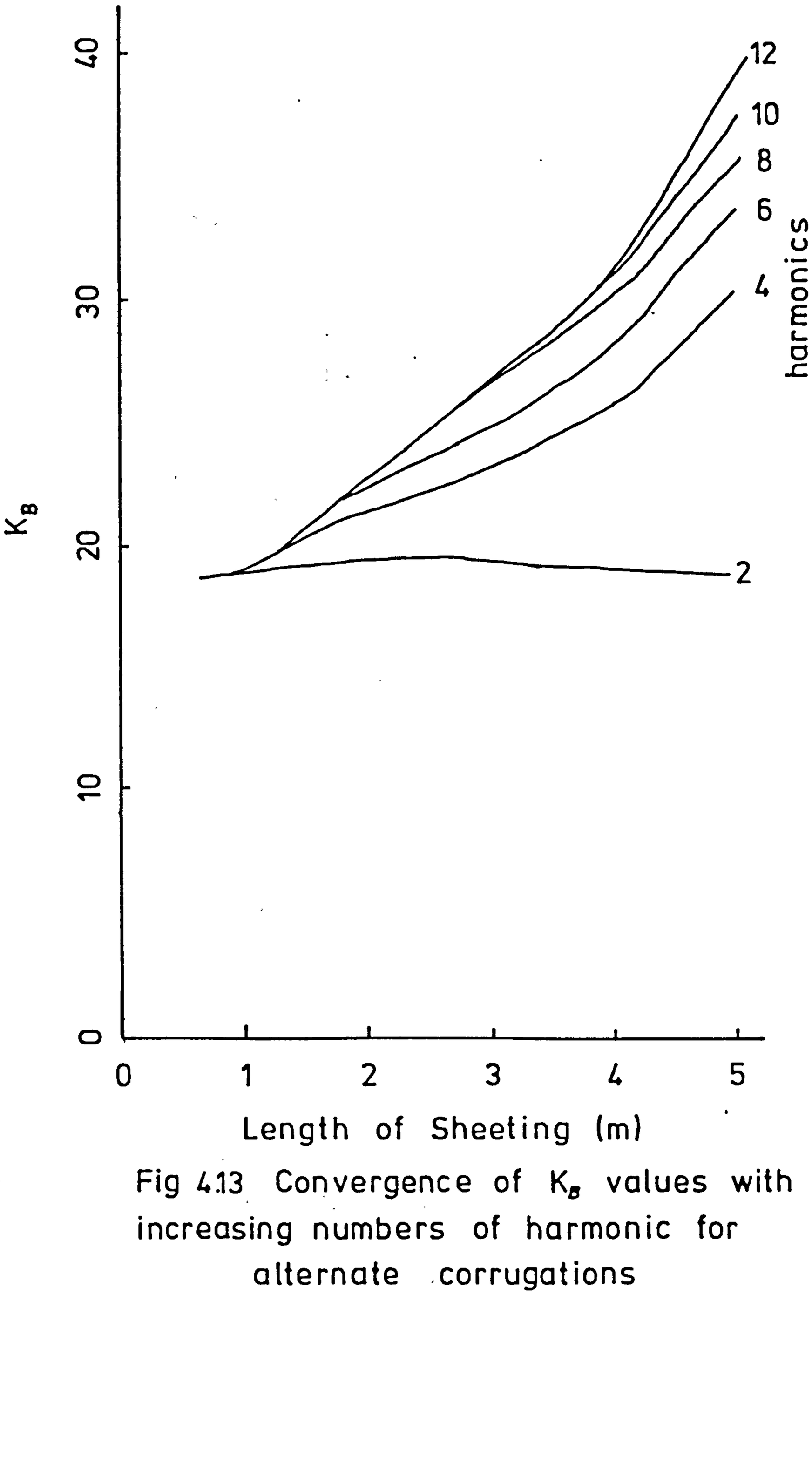

Fig 4.13 Convergence of K_B values with increasing numbers of harmonic for alternate corrugations

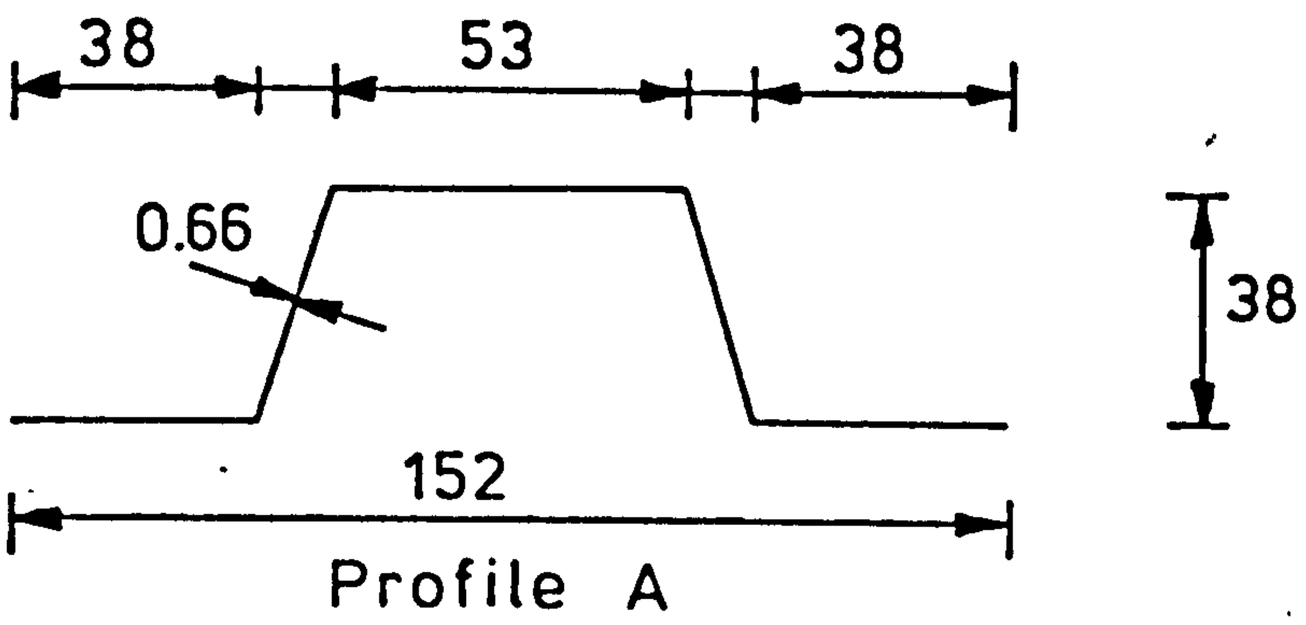

Fig 4.14 Dimension of Profiles

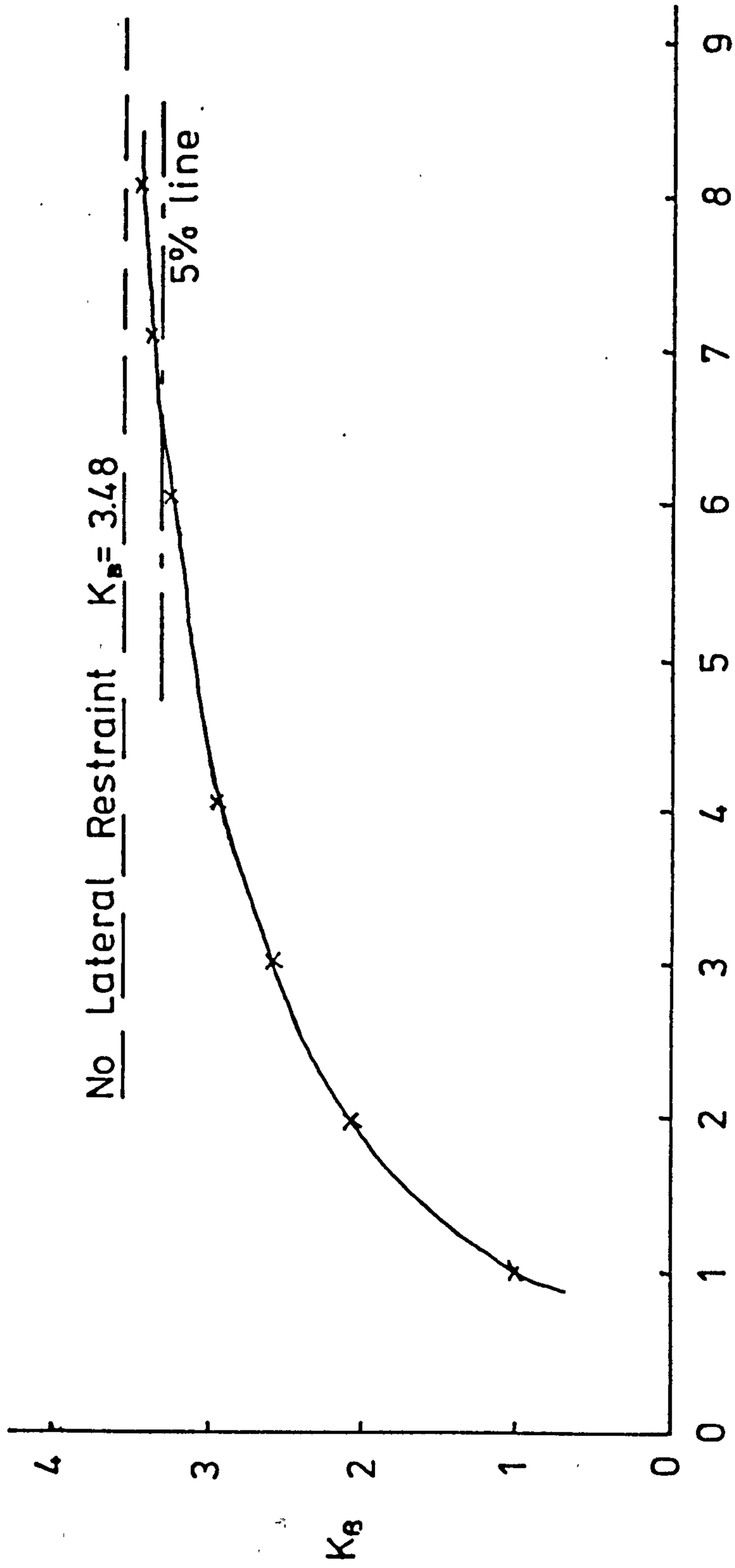

Fig 4.15 Variation of K_s for increasing number of corrugations including edge effects for Profile A

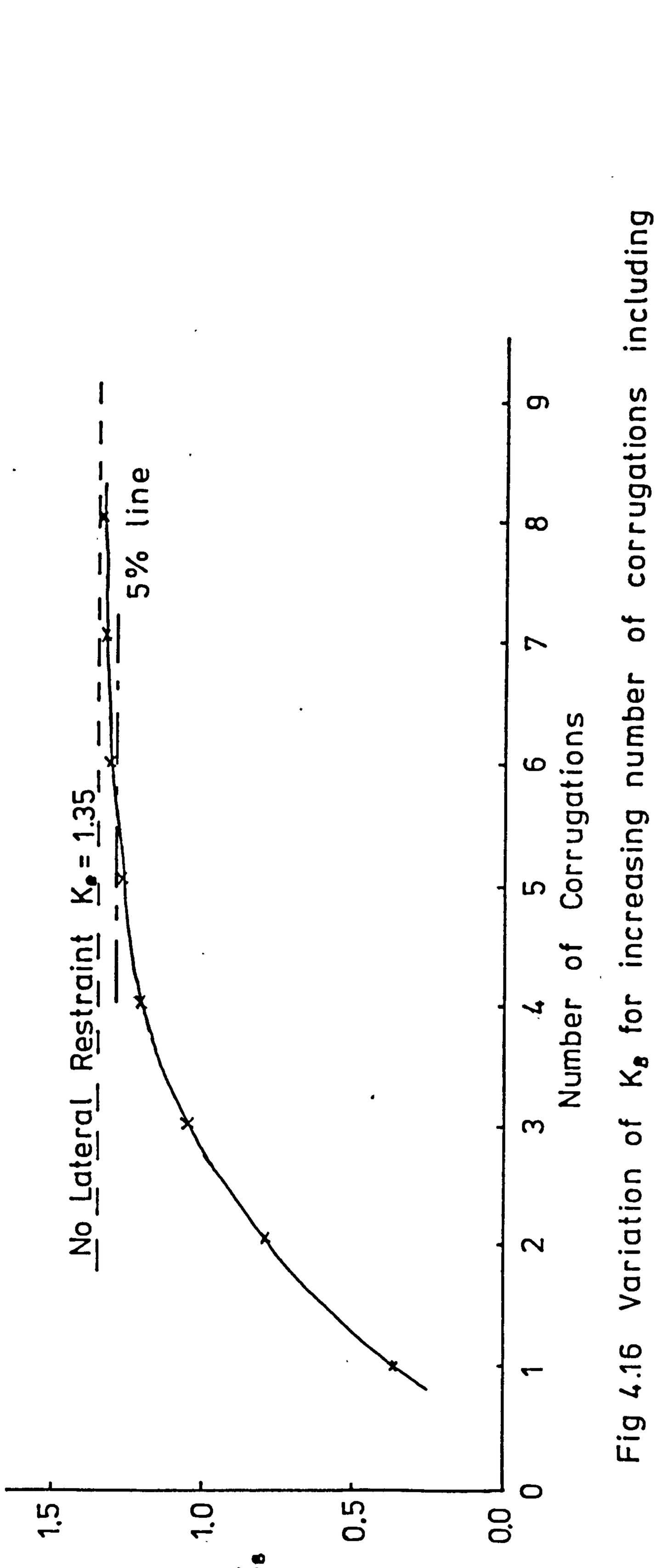
No Lateral Restraint $K_\bullet = 1.35$
5% line
$K_\bullet$
1.5
1.0
0.5
0.0
0
1
2
3
4
5
6
7
8
9
Number of Corrugations
Fig 4.16 Variation of $K_\bullet$ for increasing number of corrugations including edge effects for Profile B

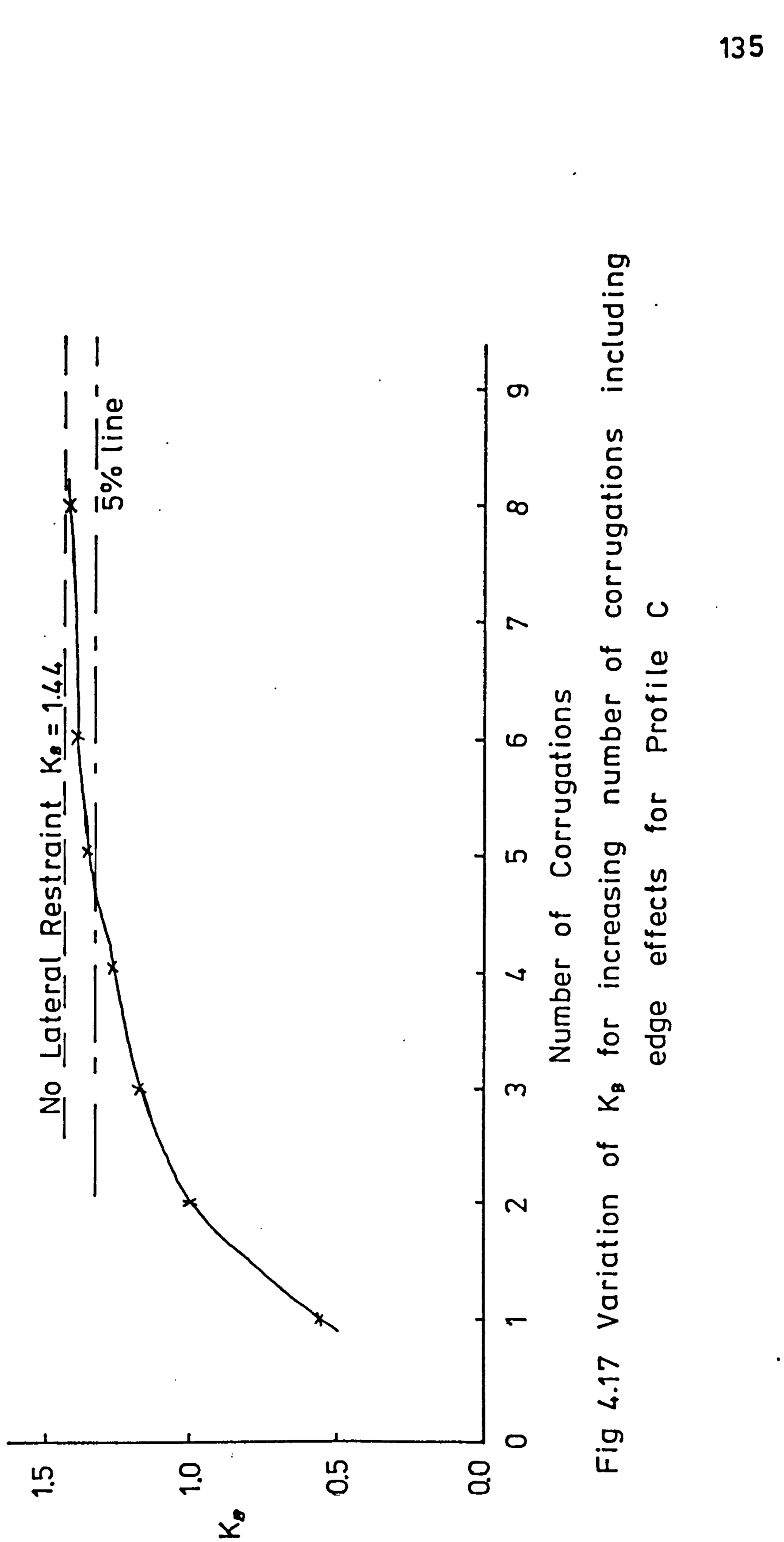
No Lateral Restraint
Lateral Restraint $K_\theta = 1.44$
5% line
K_θ
1.5
1.0
0.5
0.0
0
1
2
3
4
Number of Corrugations
5
6
7
8
9
Variation of K_θ for increasing number of corrugations including edge effects for Profile C

Fig 4.17

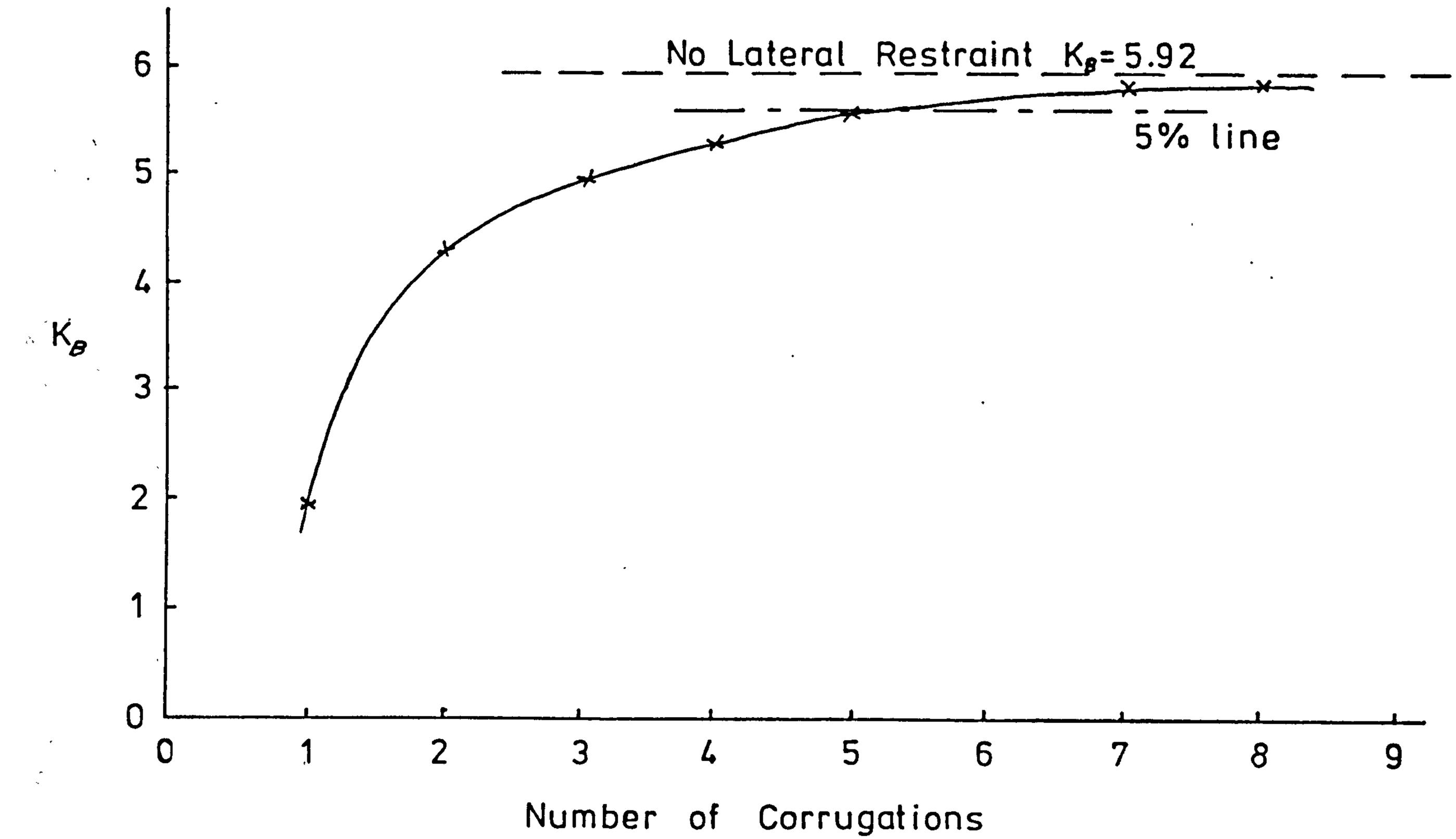

Fig 4.18 Variation of K_β for increasing number of corrugations including edge effects for Profile D

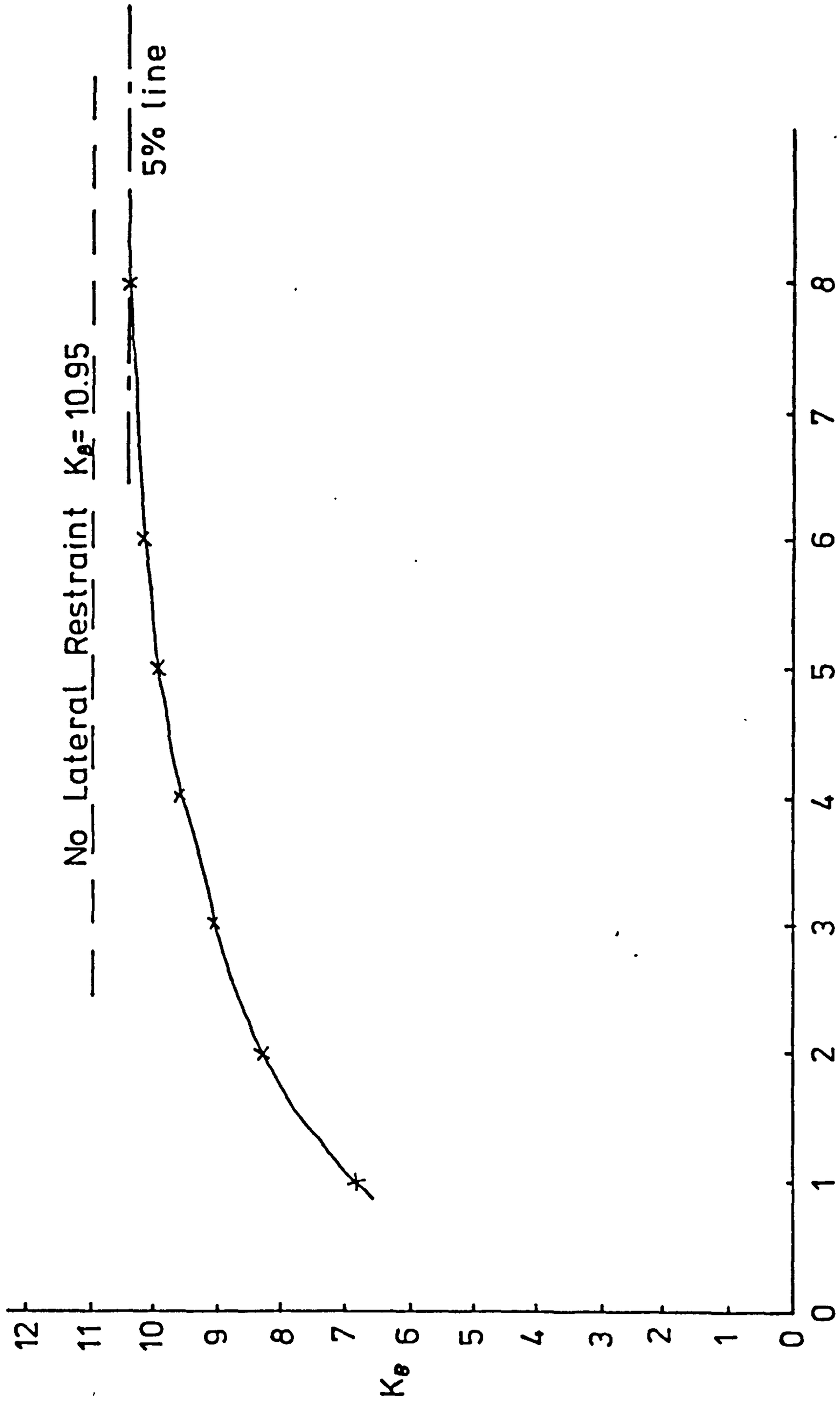

Fig 4.19 Variation of K_θ for increasing number of corrugations including edge effects for Profile B

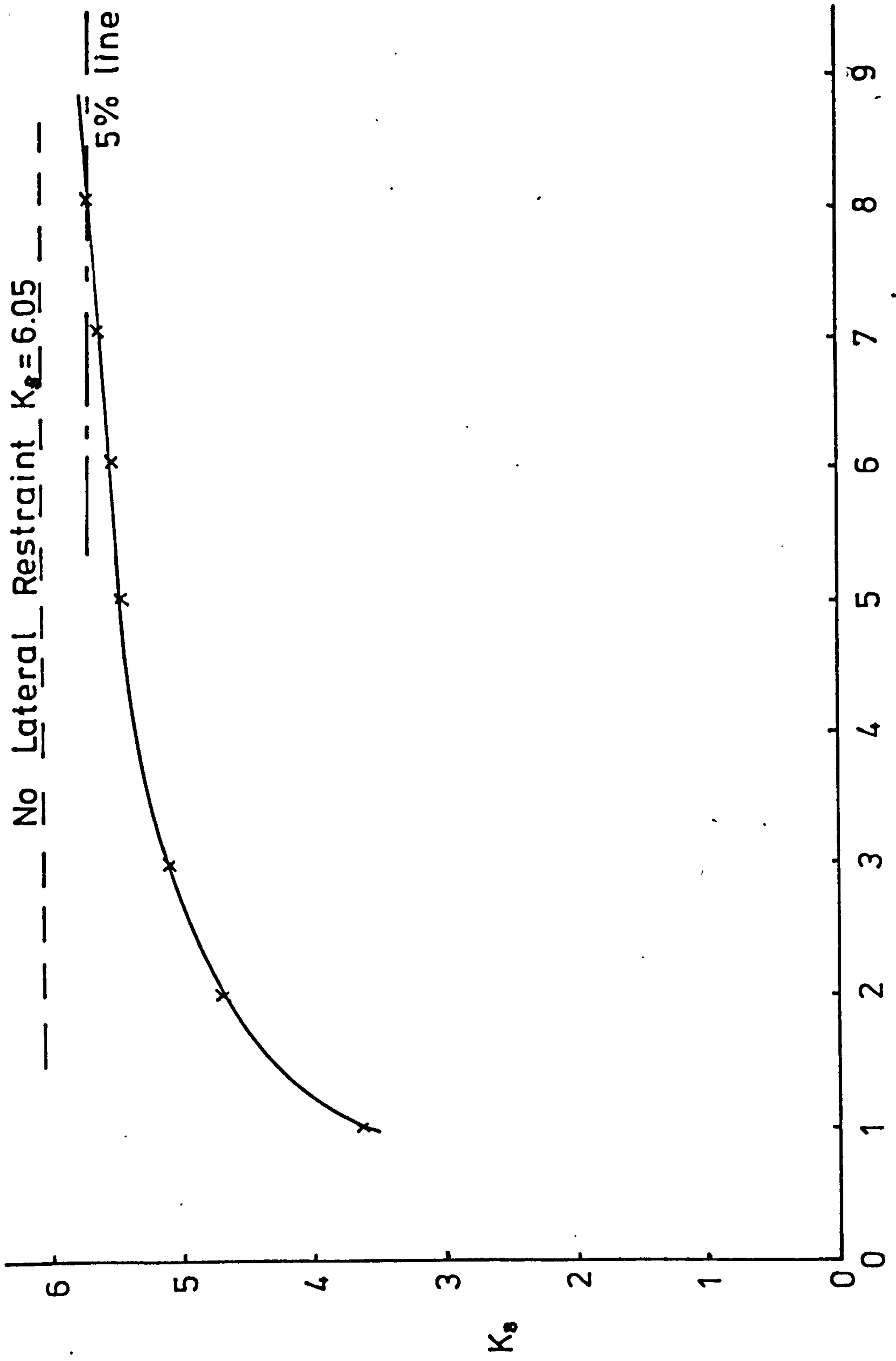

Fig 4.20 Variation of K_β for increasing number of corrugations including edge effects for Profile C

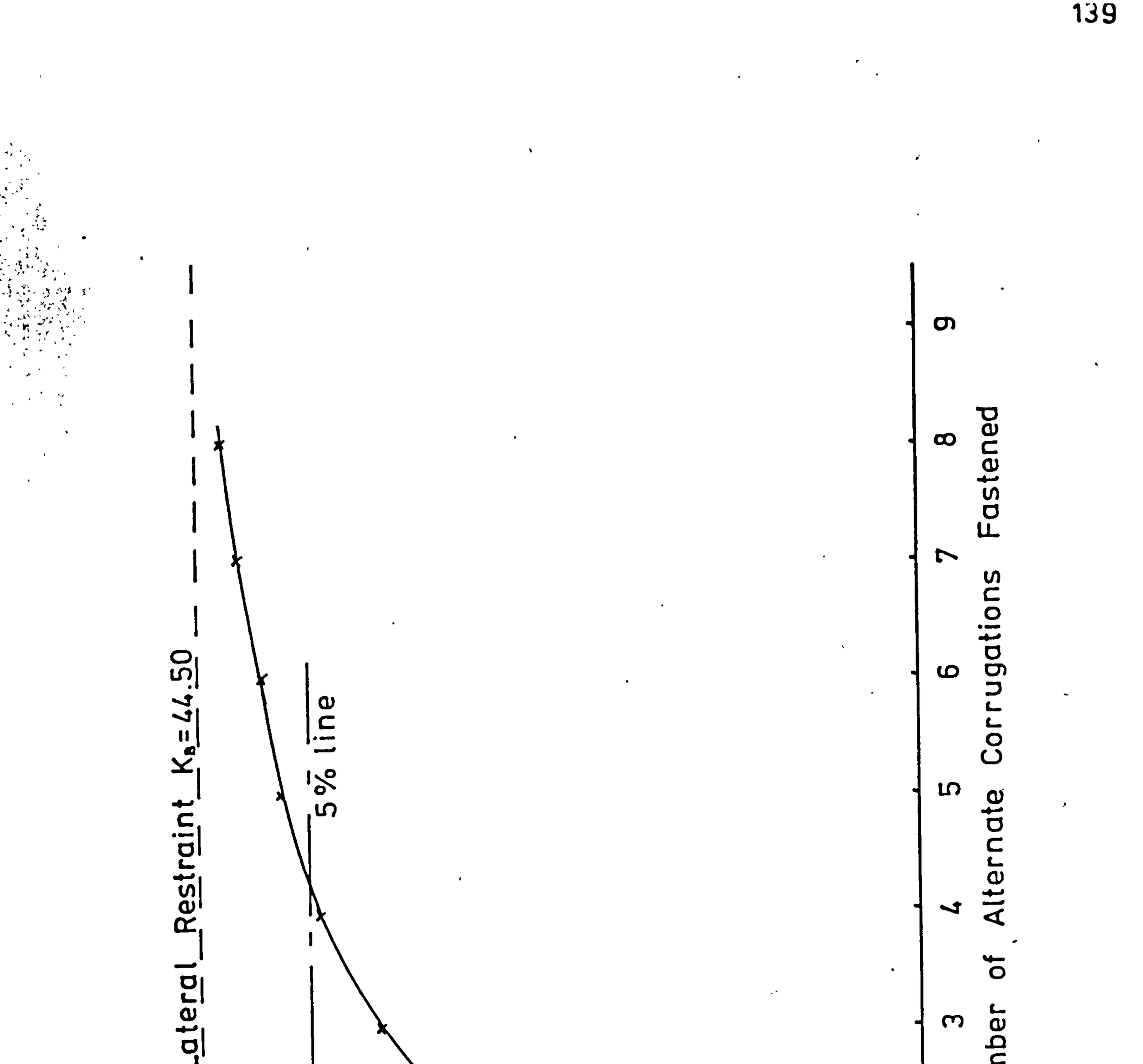

Fig 4.21 Variations of K_B for increasing number of corrugations including edge effects for Profile D

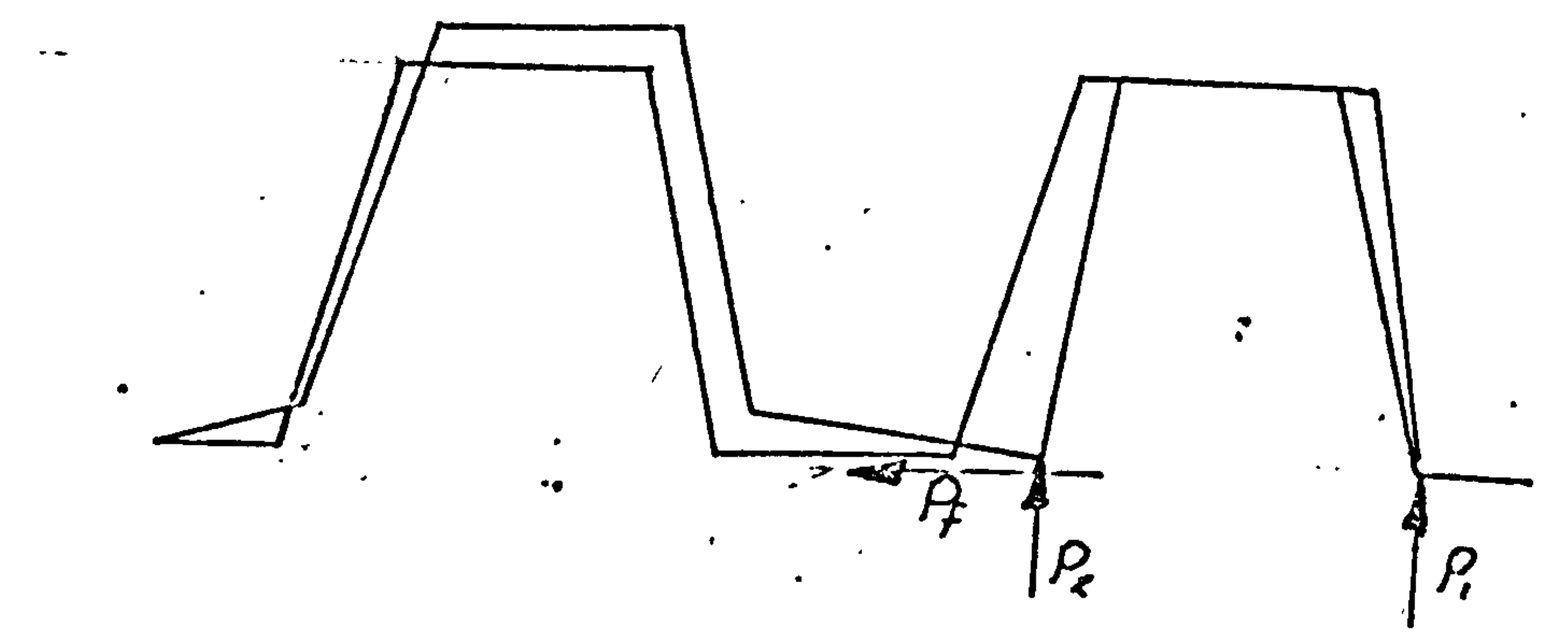

Elevation

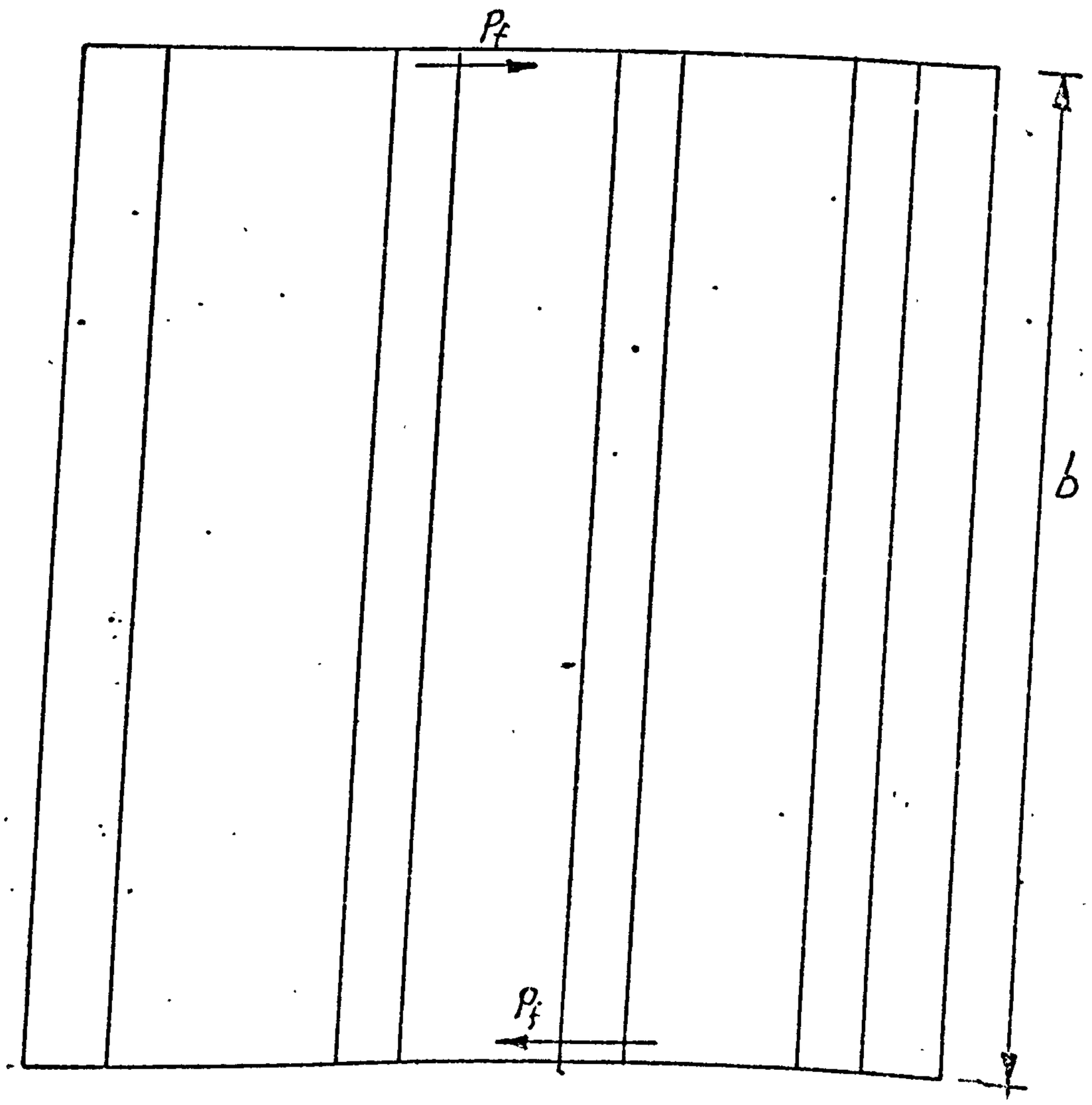

Plan

Fig 4.22. Friction couple for Alternate Profile

5 End Failure of Profiled Steel Diaphragms

5.1 Introduction

To predict the strength of a diaphragm it is necessary to consider a number of possible failure modes. These failure modes can be classified into two main groups; those involving ductile failure and those leading to a more brittle type of failure. It is desirable that diaphragms are designed so that failure is ductile, and this usually occurs when there is tearing of the sheeting at the fasteners, and in particular at the seam fasteners. From experience however, there are a number of other ductile failure modes which have been identified and included in the overall stressed skin theory.

There are at present three methods available to predict the strength of diaphragms. The first is the full scale testing of the diaphragm as described by Nilson [3]. Clearly, this is not only time consuming but also expensive in the actual testing and only a limited amount of data can be obtained from each test. Secondly, there is the finite element method [9,10] which takes account of the individual components of the diaphragm, namely, the sheeting, framing members and the fasteners. Due to the complexity of the method and the size of the computer required this method of analysis is not generally available to designers. However, it can give much detailed information into the distribution of internal forces and has been advantageously used by researchers. The final method was developed by Bryan [22], who derived simple expressions for predicting the strength of the components of a diaphragm. The ultimate strength of a diaphragm is determined by considering each components' own mode of failure and choosing

the least value. Following the work of Bryan and Davies [6], who later refined Bryan's work, the following failure modes are usually considered :-

1. seam failure between adjacent sheets
2. failure of the sheet / shear connectors
3. failure of the sheet / purlin fasteners
4. overall buckling of the sheeting
5. failure due to axial tension or compression in the outermost purlin.

Much work has been carried out to determine expressions for these failure modes, and this recently culminated in the publication of the European Recommendations on Stressed Skin Design of Steel Structures [45]. The design expressions given in the recommendations include :-

a. failure of the sheeting by tearing at the fasteners.

In this group there are a number of failure modes that are dependent on the various fastener groups, that are defined in Fig. 5.1. These are :-

1. failure of the fasteners between the adjacent sheets, known as seam fasteners in which the failure load is given by :-

$$Vult = \frac{(ns.\ Fs + np.\ Fp)\ (2ns.\ Sp + g_1.\ np.\ Ss)}{(2ns.\ Sp + np.\ Ss)} \qquad \ldots\ldots\ldots (5.1)$$

2. failure of the sheet / shear connectors, in which the failure load is given by :-

$$Vult = n_{sc}.\ F_{sc} \qquad (5.2)$$

As can be seen in Fig. 5.1, there is an additional fastener group - that of the sheet / purlin fasteners. However, the recommendations do not at present allow for failure to occur in this fastener group. So that failure does not occur in this group the recommendations specify the following criteria :-

$$(n_f - 1)\ Fp \geq \frac{1.25\ V.a.\alpha_3}{b.\ n_{sh}} \qquad (5.3)$$

where V is the least value of Vult in equations (5.1) and (5.2).

b. failure due to the overall buckling of the diaphragm. this usually occurs where there is a shallow deck or the fastener spacings are close. The expressions in the recommendations are those of Easley [21] and for the every corrugations fastened, the critical shear load is given by :-

$$Vcrit = 36\ Dx^{\frac{1}{4}}.\ Dy^{\frac{3}{4}} \qquad (5.4)$$

where $Dx = \dfrac{Et^3\ d}{12\ (1 - \nu^2)\ u}$

$$Dy = \frac{E.\ Iy}{d}$$

From these expressions the strength of a diaphragm can be ascertained. However, for certain aspect ratio's of the diaphragm and fastener spacings, failure in the sheet / purlin fasteners can be critical and it is useful to be able to predict more accurately what the failure load for this case should be. The 25% extra strength capacity required by the European Recommendations takes account of secondary effects, which cannot at present be accurately assessed. Thus, if failure of the sheet / purlin fasteners can be more accurately predicted and be shown to be ductile, then it may be possible to design more economical diaphragms.

5.2 Previous work associated with end failure of diaphragms

End failures of profiled steel diaphragms are those failures that occur in the region of the sheet / purlin fasteners. As the

stressed skin theory has developed, failure modes associated with the diaphragms have been identified and included in the overall theory. However, in the case of end failures, this has not been the case due to a number of reasons, namely :-

a. the state of the art for the overall diaphragm was not developed sufficiently to justify work in this region of the sheet / purlin fasteners.

b. a lack of knowledge of the fastener force distributions and the characteristics of the sheet / purlin fasteners.

Over the years a number of researchers have considered these possible failure modes, but did not include the work into the comprehensive theory that was developed by Bryan. From these studies three basic end failure modes can be identified, these are namely :-

a. failure of the sheet / purlin fastener, which were first identified in the early studies of Bryan. As a result of the proportions of the diaphragms tested, few failures occurred in these fasteners. Thus, attention was diverted to the more likely failure modes.

b. failure by buckling of the profile web as shown in Fig. 5.3. This mode has been studied by Falkenberg (46), who derived simple expressions for the failure and buckling criteria. Much of the work carried out by Falkenberg was undertaken before the more recent work by Davies and Lawson (7) on the distortion of the profile and this is shown in his expression for the purlin restraint force of

$$P = q \cdot h \qquad \ldots\ldots\ldots (5.5)$$

The criteria for buckling is limited to its application in that only a pure shear mode is considered. For realistic criteria, two additional factors need to be included in the model, namely :-

1. the effect of the compressive stresses induced in the web by the purlin restraint, Fig 5.2.

and

2. to define the buckled shape of the web.

As in all buckling expressions, the effective length is one of the critical factors. The effect of the shear flow is to induce moments in the profile, and, as common with all buckling analyses, the effective length is defined as the length between points of contraflexure. However, there is only one point of contraflexure, which can be clearly defined as shown in Fig. 5.2, and this consideration complicates the analysis.

c. the lateral sway of the profile. Unlike the two previous failure modes this mode cannot be classified as an ultimate limit state. For this failure mode the diaphragm can continue to carry additional load, but due to the excessive distortion of the profile, Fig. 5.4, a limiting value must be placed on this movement. Schardt and Strehl [47] considered this "serviceability" failure criteria and assumed a limiting value of lateral sway to be not greater than $h/20$ for any particular profile.

This approach does not take into account the types of fastener arrangement, that is the every and alternate corrugation cases, and does seem to be on an arbitrary value. A more precise criteria could be that due to the formation of plastic hinges in the profile. This criteria is the basis of the method proposed in this study.

5.3 Test Programme

Investigation of the failure modes that are classified by the author as "end failures" show that there are certain deficiencies in the present theories. A test programme was instigated to clarify the work of the previous research and to obtain information necessary to determine the empirical expressions that will be developed in due course.

As stated previously, certain aspect ratio's of profiled steel diaphragms can cause failure in the region of the sheet / purlin fasteners. Applying the expressions (5.1) ⟶ (5.4), previously obtained from the European Recommendations a possible range of aspect ratio's were determined for failure of the sheet / purlin fasteners. A test rig was then constructed so that suitable variation was possible in both the length and the width of the tested panel, as shown in Fig. 5.5. Using this rig, diaphragms with length varying from 1.5 metres to 3.0 metres, and width from 0.75 metres to 1.5 metres could be considered. Fig. 5.6 shows the test rig with sheeting in position ready for testing. The structural form of the test rig is that of a cantilever, developed by Nilson [3] and in this form is bolted to the "structural" floor together with a reaction frame.

For a particular diaphragm and profile, the test procedure involved first attaching the sheeting to the frame with the required fasteners; self-drilling, self-tapping fasteners for the perimeter fasteners, and blind rivets for the seam fasteners. So that an accurate predicted strength of the diaphragm could be obtained separate shear tests on the fasteners, as defined in the European Recommendations [23], were undertaken.

The test itself involved first loading in increments up to a load in excess of 50% of the predicted failure load, or in certain cases to a load in which a change in stiffness of the load / deflection curve was observed. As will be described later this is the result of the attainment of plastic bending at the end of the sheeting profile. At this point the load was removed gradually, and the subsequent reloaded until failure occured.

The shear deflection (Δ) was obtained from the reading of the four dial gauges shown in Fig. 5.5 and a graph of deflection / load was plotted.

$$\Delta = \delta_1 - \delta_2 - \frac{a}{b} (\delta_3 + \delta_4) \qquad (5.6)$$

Some typical load / deflection curves are shown in Fig. 5.7 and Fig. 5.8. For each test the actual failure load together with the load at which plasticity occurs in the profile were noted.

5.4 Investigation of the interaction between shear and tension on the sheet / purlin fasteners

Comparison of the test results and the predicted failure loads for the sheet / purlin fasteners show that there is a reduced shear capacity for these fasteners. The most likely cause for this reduction is the influence of the tension force on the fastener that results from the distortion of the profile , Fig. 5.2. The effect of the tension force can be likened to that previously found for bolts [48], where an interaction relationship between the shear and tension capacity of the bolt has been shown to exist.

For diaphragm action the predominate factor is the shear capacity of the fasteners. As a result of the tension force on the fastener an investigation was undertaken to determine the reduction of this shear capacity. No previous experimental work was known to the author into a shear / tension interation curve for self-drilling, self-tapping fasteners. However, the European Recommendations on Stressed Skin Design do specify a circular interaction curve for a fastener with shear / tension load of the form below :-

$$\left(\frac{S}{Su}\right)^2 + \left(\frac{T}{Tu}\right)^2 \leqslant 1 \qquad (5.7)$$

where S is the design shear load

Su is the shear strength when T = 0

T is the design tension load

Tu is the tension strength when S = 0

In order that an interaction curve could be obtained a testing procedure had to be formulated. At present there are two specific testing methods for self-drilling fasteners, as given by the European Recommendations [23]. These are the simple lap test for determination of the shear capacity of the fasteners and the tension test to simulate the suction force on the sheeting. These tests however, give no guidance to the actual test arrangement for the shear / tension interaction curve. The lap test was designed to simulate a line of fasteners, thus two or more fasteners need to be tested at any one time. The tension test was again designed to simulate suction loads and would cause prying of the sheeting around the fastener from more than one direction. Whereas the prying action only occurs in one direction from the distortion of the profile, as shown in Fig. 5.9. The lap test can be of some use in allowing a comparison with the results obtained from the interaction curve.

A test arrangement, Fig. 5.10, was constructed to simulate varying shear and tension forces on the fastener. The test rig consisted of a self-stressing frame with a swivel base, which is clamped by bolts to allow for varying angles between the applied force and the fastener / sheeting surface. Measurement of the applied force was undertaken by means of an electrical transducer.

In the study a number of parameters were varied so that the general characteristics of the interaction curve could be fully investigated. The parameters that were considered included the thickness of the thinnest material and cases with and without

TEST	THICKNESS (mm)	WASHER	SHEAR (kN)	TENSION (kN)
1	0.85	Y	5.35	4.250
2	0.85	N	4.32	2.855
3	0.75	Y	4.57	3.725
4	0.75	N	4.21	2.570

Table 5.1 Pure Shear and Tension Failure Loads for Interaction Curve

neoprane washers in the self-drilling, self-tapping fasteners. The interaction curve for all the tests is given in Fig. 5.11 on a dimensionless basis. The actual pure shear and tension failure loads are given in Table 5.1.

From the tests a number of points of interest should be noted, namely :-

a. for the design shear strength there is a slight reduction in the value for the case of no washers. This reduction is mostly to be a result of the change in the initial force applied to the fastener by clamping together of the two materials by the fastener.

b. in the case of the tension strength there is a considerable reduction when washers are not included. This reduction is as a result of the reduced contact area that the fasteners have with the sheeting.

and c. a good resemblence is shown between each interation curve in terms of their shape for the tests with and without washers.

There is evidence of experimental scatter, as would be expected, but the circular design curve in certain regions is found to be conservative and a new design curve "A" in Fig. 5.11 appears to be more suitable.

5.5 Analysis of End Failures

5.5.1 Forces on the Sheet / Purlin Fasteners

Expressions for the prediction of this failure have been derived in previous work. However, there have been significant disparities between the actual failure load and the predicted

failure load. The previous work was based on the shear force acting on the fasteners and no account of the tension force, resulting from the distortion of the profile, was considered. The following analysis extends the previous work to include the tension force on the fastener.

The shear force on the sheet / purlin fastener can best be accurately determined by the use of a finite element model [9] [10] due to the high degree of indeterminacy of this group of fasteners. The finite element model is not well suited to an application in design, but has been given much useful information into the distribution of forces in each of the fastener groups. The main purpose of the model has been as a base to verify the simple design methods [6] [22] that have been developed. These simple methods have separated the force in the sheet / purlin fasteners into respective components as shown in Fig. 5.12, from which the design expressions have been obtained.

For the purpose of this study the components of shear will be termed the longitudinal and transverse shear as shown in Fig. 5.12. The longitudinal shear is assumed to be as a direct result of the shear flow on the profile, whereas the transverse shear is a function of the fastener spacings.

Considering a corrugation fastened in every trough, the notation is as given in Fig. 5.13 (a) with a shear flow of unity acting on the surface and restrained at B to vertical movement. The end forces Fx, Fy etc., are determined by considering the equilibrium of the profile. However, this structure is one degree indeterminate and is reduced to its primary structure by removal of the propping restraint. The end forces then become :-

$$\left.\begin{aligned} Fx &= \frac{2h}{d}\left(2b_r + p\right) \\ \text{and } Fy &= {}^{d}/_{2} \end{aligned}\right\} \quad \ldots\ldots\ldots (5.8)$$

The propping force P is then determined by considering the propping conditions m_1 and m_2, Fig. 5.13 (c) and (d), respectively, and by applying the principle of virtual work we obtain :-

$$P = \frac{2\int_{o}^{s/2} \left(m_o \quad m_1\right) d_s}{\int_{o}^{s/2} \left(m_1 \quad m_1\right) d_s + \int_{o}^{s/2} \left(m_2 \quad m_2\right) d_s} \quad \ldots\ldots (5.9)$$

where $\int_{o}^{s/2}$ signifies the integral around half the profile.

Having obtained an expression (5.9) for the redundant propping force the actual end forces become

$$\text{longitudinal shear } (Fs_{\ell}) = d + \frac{P}{2} Fy2 \qquad (5.10)$$

$$\text{where } Fy2 = \frac{b \quad (bs + b_{\tau})}{h \quad (\frac{2bs}{3} + b_{\tau})}$$

for a unit shear flow around the profile.

For a general case, therefore, the shear flow must be related to the diaphragm load Q. As a consequence of the primary shear force Q interacting with the distortion of the profile, the profile tends to bend as a whole in the x-direction shown in Fig. 5.14. The bending induces internal shear forces in the profile rising to a maximum of $\frac{Qd}{b}$ at the ends. The resulting shear at the ends is therefore statically determinate, giving

$$q = \frac{Q}{b} \qquad (5.11)$$

where Q is the diaphragm load.

then

$$Fs_{\ell} = \frac{Qd}{b} + \frac{PQ}{2b} \cdot Fy2 \qquad (5.12)$$

The propping force is examined in greater detail in Appendix 4, where tables are given for the force in terms of a dimensional parameter k . The force is then given by

$$P = kd \qquad \ldots\ldots\ldots (5.13)$$

$$\text{so} \qquad F_{sL} = \frac{Qd}{b}\left(1 + \frac{k\,F_{y2}}{2}\right) \ldots\ldots\ldots (5.14)$$

or, using the symbols of the European Recommendations [45]

$$F_{sL} = \frac{Qa\,\alpha_3 \quad \left(1 + \frac{k\,F_{y2}}{2}\right)}{(n_f - 1)\,.\,b\,.\,n_{sh}} \qquad (5.15)$$

The resultant tension F_T on the fastener is given by :-

$$F_T = F_x.\,q + \frac{Pq}{2}\,(F_{x2} - F_{x1}) \qquad (5.16)$$

where

$$F_x = \frac{2h}{d}\,.\,(2b_T + p)$$

$$F_{x1} = \frac{2}{d}\,.\,(b_T + p)$$

$$F_{x2} = 1$$

which can be modified for the general case to give

$$F_T = \frac{Qd}{b}\left[\frac{Fx}{d} + \frac{k}{2}\cdot(1 - Fx_1)\right] \quad \ldots\ldots(5.17)$$

The expressions (5.14) and (5.17) are only applicable to diaphragms with every corrugation fastened. In the case where alternate corrugations are fastened, similar expressions can be developed, but noting that in this case there are two purlin restraints.

Considering the profile in Fig. 5.15 the expression for longitudinal shear is :-

$$Fs_L = \frac{Qd}{b}\left[2 + \frac{k_1\ Fy2}{2} + \frac{k_2\ Fy4}{2}\right] \qquad (5.18)$$

where $Fy2 = \frac{b_L}{h}\left[\frac{bs + b_T}{\frac{2bs}{3} + b_T}\right]$

$$Fy4 = \frac{d}{4h}\left[\frac{bs + b_T}{\frac{2bs}{3} + b_T}\right]$$

k_1 and k_2 are the propping force coefficients obtained from Appendix 4

The tension force F_T on the fastener is

$$F_T = \frac{Qd}{b}\left[\frac{Fx}{d} + \frac{k1}{2}\left(1 - Fx_1\right) + \frac{k2}{2}\left(1 - Fx_3\right)\right] \quad \ldots (5.19)$$

where $$Fx = \frac{2h}{d}\left(2b_T + p\right)$$

$$Fx_1 = \frac{d - b_L}{d}$$

$$Fx_3 = \frac{b_L}{d}$$

The previous analysis only took account of the forces in the plane of the corrugations. Davies [6] has shown that within each sheeting panel there are out of plane forces acting on the fastener, which are termed transverse shear forces. Expressions for the fastener forces were not given by Davies in his work, but can easily be derived from the expressions that are given in his text.

Davies considered a number of fastener variations, which are as follows :-

a. the direct transfer case, where the fasteners are attached on all four sides of the diaphragm.

and b. the indirect transfer case, where the fasteners are attached on only to opposite sides of the diaphragm.

In the development of the transverse fastener forces only the direct transfer case will be considered, even though other variations can easily be derived. Davies shows that, due to the bending of the purlins, the maximum shear force occurs in the end sub-panels. Thus the diaphragm shown in Fig. 5.16 is divided into sub-panels, which are designated end sub-panels and intermediate sub-panels.

Considering an intermediate sub-panel, Fig. 5.17, moment equilibrium gives :-

$$= \frac{Q.\ \ Ss.\ \ S}{(2ns.\ S + g_1\ \ n_p\ \ S_s)} \qquad (5.20)$$

where $g_1 = \sum_{i=1}^{\frac{nf-1}{2}} \left(\frac{2i}{nf-1}\right)^2$

for a linear distribution of the transverse fastener force

or $g_1 = \sum_{i=1}^{\frac{nf-1}{2}} \left(\frac{2i}{nf-1}\right)^3$

for a quadratic variation in the transverse fastener force.

It was found that both force distributions compared well with the finite element model.

Having obtained a relationship between the seam slip 2Δ and the applied force Q the end sub-panel, Fig. 5.18, is now considered for vertical equilibrium :-

$$\Delta e = \frac{\Delta \cdot s}{Ss} \left(\frac{2n_s \; Ssc - n_{sc} \cdot Ss}{n_{sc} \cdot S + g2 \; np \cdot Ssc} \right) \qquad (5.21)$$

where $g_2 = \sum_{i=1}^{\frac{nf-1}{2}} \left(\frac{2i}{nf-1} \right)$ linear distribution

or $g_2 = \sum_{i=1}^{\frac{nf-1}{2}} \left(\frac{2i}{nf-1} \right)^2$ quadratic distribution

The slip of the end fastener $(\Delta + \Delta e)$ was shown by Davies to be :-

$$\Delta + \Delta e = 1 + \frac{S}{Ss} \left(\frac{2n_s \; Ssc - n_{sc} \cdot Ss}{n_{sc} \cdot S + g_2 \; np \cdot Ssc} \right) \ldots (5.22)$$

from which the end fastener force, the maximum transverse fastener force, is :-

$$F_{\frac{nf-1}{2}} = \frac{\Delta + \Delta e}{s} \qquad (5.23)$$

Combining expression (5.23), (5.22) and (5.20) we can obtain an expression for $F_{\frac{nf-1}{2}}$ in terms of the fastener distribution and slip characteristics as follows :-

$$F_{\frac{nf-1}{2}} = Q \left[Ss + S \left(\frac{2n_S \cdot Ssc - n_{sc} \cdot Ss}{n_{sc} \cdot Ss + g2\ np\ Ssc} \right) \cdot \left(\frac{1}{2n_S \cdot S + g1\ np\ Ss} \right) \right] \quad \ldots\ldots (5.24)$$

The resultant shear force on the end fastener, derived from the two components of shear, can be obtained by summation of the force vectors.

$$F_R = (Fs_L)^2 + (F_{\frac{nf-1}{2}})^2 \qquad \ldots\ldots\ldots\ldots (5.25)$$

5.5.2 Buckling of the Profile Web at the End Purlin

An expression has now been given (5.9) for the propping force at the end purlin, and in Appendix 4 tables for its value has been determined in terms of the factors $2b_r/d$, h/d and theta. In the course of the test series carried out on a number of profiles, buckling of the profile web at the end purlin occurred, Fig 5.3. In order that this can be predicted in terms of the propping force already obtained, a buckling criteria must be determined. Falkenberg [46] suggested that a simple expression, similar to that for compressive failure, could be developed. However, in this approach, only the effect of the shear flow was considered. A more realistic development would include the effect of the restraint that is induced by the unbuckled region of the web, and the effective length of the buckled section.

This would require a complex analysis and in order to obtain a simple design expression the problem is best solved by obtaining an empirical relationship between the effective length of the web and some physical property of the profile. This effective length, based on Euler's expression, was therefore determined for each of the tests in which buckling took place.

The effective length (l_{eff}) as a proportion of the length of the web (2bs) has been plotted against the non-dimensional ratio of the height to the thickness of the profiles (h/t) and can be seen in Fig 5.20. Inspection of the diagram shows that there is a simple empirical relationship between these parameters. However, the result for the profile

which includes the web stiffener, shown on the diagram by the triangular symbol, compared with the general trend of the curve gives grounds for an alternative curve in this region for profiles without web-stiffeners. This is due to the fact that a column with lateral cranks have a lower buckling load than a normally straight column. So for a similar profile without the web stiffener a considerable increase in the buckling load of the web may be expected.

Further tests will have to be carried out, but in the present state of the art there seems to be two curves of which Fig 5.20 is a combination of these curves.

Clearly for the majority of profiles produced by manufacturers the curve given in Fig 5.20 can adequately predict the buckling failure load.

Thus if Pf is the buckling load, then the effective stress σ_{eff} is obtained from the expression:-

$$\frac{Pf}{t(bp+bsp)} \qquad (5.26)$$

where bp = the width of the purlin

bsp = the assumed spread of the purlin restraint force.

This distance was found from observation of the tests to be the position of maximum stress in the web, Fig 5.9. From the actual tests this has been found to be approximate equal to a quarter of the web length = bs/2.

The critical stress for buckling can be obtained from Euler's expression.

$$\sigma_{crit} = \frac{\pi^2 E t^3}{12(1-\nu^2)(\ell_{eff})^2} \qquad (5.27)$$

So equating σ_{eff} and σ_{crit}, the effective length is given by:-

$$\ell_{eff} = \pi t^2 \sqrt{\frac{E(bp+bs/2)}{12(1-\nu^2)\,Pf}} \qquad (5.28)$$

The bucling load for a given diaphragm is therefore

$$P = \frac{\pi^2 E t^4 (bp + bs/2)}{12(1-\nu^2)\,(\ell_{eff})^2} \qquad (5.29)$$

where ℓ_{eff} is obtained from Fig 5.20.

This can then be compared with the purlin restraint force obtained from

$$P = \frac{k\,Qd}{b} \qquad (5.30)$$

5.5.3. Lateral Sway of the Profile

5.5.3.1 Identification of the Problem

When a profile is distorted under the action of a shear flow the displacements at the ends of the profile can become excessive. This constitutes a failure and must be considered at the design stage. Schardt and Strehl [47] have proposed a method of restricting the displacement of the profile based on the elastic bending moments in the profile and a deflection criterion. There are certain limitations in this, in that the method takes no account of the redistribution that will occur in the bending moments at the end of the profile. Furthermore, the value of the lateral displacement was restricted by the authors to a value of $h/20$. This seems to be an arbitary value and not based on any rigous analysis.

Instead of limiting the lateral displacement of the profile an alternative criterion would be the formation of a plastic mechanism at the ends of the profile. However, the analysis of this mechanism is not as easy as one might at first imagine. In all plastic analyses [49] the three conditions of equilibrium, yield and mechanism have to be satisfied. So, when a plastic mechanism is formed, a slight increase in load would in theory produce large deflections. In fact this is not the case for this collapse as the sheeting exerts a restraining force on the profile. The problem is therefore a plastic collapse restrained by an elastic region of the sheeting.

The method of analysis has been to allow the actual end elastic bending moments in the profile to redistribute to an equilibrium condition, which in this case is the assumed plastic mechanism. The end bending moments can be considered in this way as there is little spread of plasticity into the profile.

The initial work equation for this sytem is therefore

$$\Sigma M_{ai}\,\theta_i = \Sigma M_{pi}\,\theta_i \qquad (5.31)$$

where θ_i - hinge rotation at points hi

M_{pi} - the corresponding plastic moment at joints i

and M_{ai} - the actual corresponding elastic bending moment at joints i

Davies [50] has proposed a profile constant for the load at which plasticity occurs, similar to the constant in wide use at present for the distortion of the profile, of

$$Qp = \frac{t^{1.5}\,\sigma_y\,\sqrt{d}\;b}{a\,\bar{p}} \qquad (5.32)$$

where Qp - the load at which plasticity occurs

t - the thickness of the sheeting

σ_y - the yield stress of the material

d - the pitch of the corrugation

b - length of the sheeting

a - width of the sheeting

$\bar{p}$ - the plastic constant

5.5.3.2 Analysis for every trough fastened

A unit depth of profile, Fig 5.21 under the action of the shear flow and restrained to vertical moment at E will be

considered. Neglecting the effect of the resultant slip of the fasteners, the structure is two degree's indeterminate, and so there must be three plastic hinges to form a complete mechanism.

For the mechanism under consideration plastic hinges are assumed to form at B, C and E and free hinges occur at A and F in Fig 5.21.

The instantaneous centre is at E and the resultant mode of deformation is as shown in Fig 5.22(a).

The moment diagram shown in Fig 5.22(b) gives the internal forces in the profile for this deformation.

The internal work of the profile is given by

$$\Sigma M_{pi}\,\theta_i = 2m\,\theta_1 + m\,\theta_2$$

and by compatibility at B

$$\theta_2 = \frac{2\theta_i\,(b_r + \rho)}{b_c}$$

The sign convention for the every and alternate corrugation cases, is that all plastic moments are assumed positive and that rotation in an opposite direction to the moment are also considered positive .

$$\text{so } \Sigma M_{pi}\,\theta_i = \frac{m\,\theta_1\,d}{b_c} \qquad (5.33)$$

where m = plastic moment = $\dfrac{t^2\,\sigma_y}{4}$

The internal work based on the plastic moments, can then be equated to the equivalent work done when the elastic bending moment distribution undergoes an identical virtual displacement.

So for a unit diaphragm force applied to a profile the elastic bending moments Mai can be related to the internal work by

$$\sum M_{pi}\,\theta_i = Q_p \sum M_{ai}\,\theta_i \qquad (5.34)$$

where Qp is the plastic load

$$\text{Therefore } Qp = \frac{\sum M_{pi}\,\theta_i}{\sum M_{ai}\,\theta_i}$$

The external work in equation 5.34 is given by

$$\frac{\theta_1}{b_L}\left[2m_B\left(b_T + p\right) + b_L\left(m_B + m_E\right)\right] \qquad (5.35)$$

Substituting equation (5.33)(5.34) and (5.35), we obtain

$$Q_p = \frac{m.d}{2m_B\left(b_T + p\right) + b_L\left(m_B + m_E\right)} \qquad (5.36)$$

As stated previously, Davies has proposed a profile constant for the plastic load Qp. An investigation was therefore undertaken to verify Davies expression of

$$Q_p = \frac{t^{1.5}\sigma_y\sqrt{d}\;b}{\alpha\,\bar{p}} \qquad (5.37)$$

In expression 5.36 the elastic bending moments can be determined from a number of sources including the finite element method and energy methods.

Profile	Thickness (mm)	Length (b) (mm)	Qp (kN)	$\bar{p}$
A	0.75	1500	6.41	3.171
A	0.75	3000	13.16	3.089
A	0.75	4500	20.22	3.016
A	0.75	6000	27.15	2.995
A	0.75	7500	33.81	3.006
A	0.75	9000	40.40	3.019
A	0.10	7500	1.59	4.948
A	0.25	7500	6.43	3.042
A	0.40	7500	13.15	3.010
A	0.55	7500	22.22	2.872
A	0.90	7500	44.53	3.000
A	1.10	7500	60.34	2.992
B	0.80	1500	6.47	3.322
B	0.80	3000	16.02	2.683
B	0.80	4500	24.61	2.620
B	0.80	6000	32.70	2.629
B	0.80	7500	41.04	2.618
B	0.80	9000	49.43	2.609
B	0.10	7500	1.73	2.745
B	0.25	7500	7.14	2.629
B	0.40	7500	14.41	2.636
B	0.55	7500	23.26	2.633
B	0.90	7500	40.09	2.612
B	1.10	7500	66.53	2.604

Table 5.2 Values of $\bar{p}$ for Every Corrugation Fastened.

However, the program previously described for analysing trapedzoidal profiles in chapters 3 and 4 was found to be inadequate for this purpose. This is due to the fact that only slope compatibility was included in the strip matrices and a further requirement of curvature would also be required. The actual program used for this analysis was developed by Professor J.M. Davies and is based on energy methods.

A parameter study using this program and equation 5.37 was undertaken to determine the validity of the expression for a variation of length and thickness of the sheeting. Figures 5.23 and 5.24 show the variation of the plastic load Qp for both the length and the thickness of the sheeting respectively. It can be concluded that both figures verify Davies' expression except for short lengths of profile where there is a non-linear relationship, similar to the results for the shear distortion factor for short length of profile.

Table 5.2 gives the value of $\bar{p}$, equation 5.3, for the profiles in the study and as can be seen there is a convergence of $\bar{p}$ for a particular profile as both the thickness and length of the sheeting are increased.

5.5.3.3 Analysis for alternate trough fastened

As with the case of every corrugation fastened, the analysis for alternate corrugations fastened considers a unit depth of profile, Fig 5.25, under the action of a shear flow and restrained against vertical movement at B and E. If the effect of the resultant slip of the fasteners is neglected,

the structure is three degree's indeterminate and so there must be four plastic hinges to form a complete mechanism. A number of alternative collapse mechanisms exist, however, noting the typical deformed shape of the alternate fastened profile under the action of a shear flow, the mechanism show in Fig 5.26(a) is proposed as typifying the deformed shape.

For the mechanism under consideration plastic hinges are assumed to form at B,C,F and H and free hinges occur at A and J in Fig 5.26(a). Two instanteous centres occur at I_1 and I_2 with rotations θ_1 and θ_2 respectively, and rotations of θ_3 and θ_4 at the nodes B and J follow by simple geometry. The moment diagram shown in Fig 5.26(b) gives the internal forces in the profile for this deformed shape.

The internal work of the profile is given by

$$\Sigma M_{pi}\,\theta_i = m(2\theta_1 + 2\theta_3 + \theta_4) \qquad (5.38)$$

where m = plastic moment = $\frac{t^2\sigma_y}{4}$

By compatibility the relationship between the rotations can be easily obtained. However, due to the length of the alegbra relationship they have been omitted.

The internal work can now be related to the applied load by considering the elastic bending moments in an equivalent system, such that

$$Q_p = \frac{\Sigma M_{pi}\,\theta_i}{\Sigma M_{ai}\,\theta_i} \qquad (5.39)$$

$$\text{where} \quad \Sigma M_{ai}\,\theta_i = \Big[m_H(\theta_2+\theta_4) + m_F(\theta_1-\theta_2) + m_C(\theta_1+\theta_3) + m_B\theta_3 \Big] \tag{5.40}$$

where m_B, m_C, m_F and m_H are the elastic bending moments related to figure 5.25.

Substituting equations 5.38, 5.40 in 5.39 we obtain

$$Q_p = \frac{m(2\theta_1 + 2\theta_3 + \theta_4)}{m_H(\theta_2+\theta_4) + m_F(\theta_1-\theta_2) + m_C(\theta_1+\theta_3) + m_B\theta_3} \tag{5.41}$$

A parameter study was again undertaken with the elastic bending moments obtained from the program developed by Professor J.M. Davies. Figures 5.27 and 5.28 show the variation of Qp for both the thickness and the length of the sheeting. As with the every corrugation the figures verify Davies' expression. However, the non-linear portion of the graphs extend further along the sheeting length than for the every corrugation case. This is a similar result to that found for the shear distortion factor $\bar{K}$ when comparing alternate corrugation with every corrugation.

Table 5.3 gives the value of $\bar{p}$ for the parameters in the study and again there is convergence of the value of $\bar{p}$ as the sheeting length and thickness are increased.

Profile	t (mm)	b (mm)	Qp	$\bar{p}$
A	0.75	1500	3.46	5.638
A	0.75	3000	9.54	4.090
A	0.75	4500	16.16	3.622
A	0.75	6000	21.96	3.553
A	0.75	7500	27.42	3.557
A	0.75	9000	32.94	3.553
A	0.10	7500	1.11	4.278
A	0.25	7500	5.11	3.674
A	0.40	7500	10.63	3.574
A	0.55	7500	17.19	3.563
A	0.90	7500	36.13	3.549
A	1.10	7500	48.97	3.538
B	0.75	1500	3.49	5.590
B	0.75	3000	10.60	3.680
B	0.75	4500	20.24	2.892
B	0.75	6000	31.29	2.495
B	0.75	7500	42.09	2.317
B	0.75	9000	51.91	2.255
B	0.10	7500	0.33	14.390
B	0.25	7500	5.71	11.446
B	0.40	7500	14.56	2.609
B	0.55	7500	25.19	2.432
B	0.90	7500	56.31	2.277
B	1.10	7500	76.88	2.254

Table 5.3 Values of $\bar{p}$ for Alternate Corrugation Fastened

5.5.3.4 Test Programme

In the tests carried out, section 5.3, to determine the various failure modes associated with "end failures" of trapezoidal sheeting, the sway of the profile was considered as a possible failure.

From the experimental tests carried out in the study, the collapse load Qp was determined by noting the change in stiffness of the load/deflection curve. This change in stiffness is as a result of the formation of a plastic region in the profile. The profile then has less resistance to the shear flow, so causing an effective reduction in the sheeting length and hence the stiffness of the sheeting. Figures 5.7 and 5.8 show the load/deflection curves for two typical tests noting the change in the slope of the curves. In the alternate corrugation case this change is slight as the sheeting is relatively more flexible initially than the every corrugation case. At this point it should be noted that both diaphragms still have capacity to carry load after the plastic load Qp has been attained. Therefore the formation of a plastic mechanism only contributes to the serviceability of the diaphragm.

5.6 Discussion of Results

From the tests carried out in this study, three failure modes were identified of which only one includes failure by tearing of the sheeting at the fasteners. A number of profiles were tested two of which exhibited this failure mode. Table 5.4 gives the predicted and experimental results for these profiles, together with the shear strength values for the fastener with and without the effect of the tension force on the fastener columns (e) and (c) respectively.

The modified results give a more accurate prediction of the failure load, although there is some discrepancy in a number of the results. This can be attributed to the redistribution of the forces in the sheet / purlin fasteners at failure. However, the predicted results do occur on the conservative side. The redistribution of the forces in the sheet / purlin fasteners take place as there is a large slip value for the sheeting between the point of attaining the ultimate load and the tearing load, Fig. 5.29. As further load is applied to the diaphragm, after the end fasteners have reached their ultimate value, the end fastener does not carry any additional load but is allowed to continue to slip along the load / slip curve for the fastener. In practice there is a reduction in the load carried by the fastener. The additional load now applied to the diaphragm, is distributed to the adjacent fasteners which have not attained their ultimate load carrying capacity. This progresses to the other sheet / purlin fasteners until the end fastener has attained the tearing slip value. At this point there is a progressive failure with a transfer of energy

(a) TEST	(b) THICKNESS OF SHEETING (mm)	(c) SHEAR STRENGTH (2 LAP TEST) (kN)	(d) TENSION IN FASTENER (kN)	(e) MODIFIED SHEAR STRENGTH (kN	(f) PREDICTED FAILURE (NO TENSION) (kN)	(g) PREDICTED FAILURE (MODIFIED SHEAR) (kN)	(h) ACTUAL FAILURE LOAD (kN)
A1	0.75	4.47	1.242	4.18	34.6	32.1	30
A3	0.75	4.47	1.242	4.18	34.6	32.1	31
E1	0.80	5.45	2.004	4.95	66.9	60.7	57
E2	0.80	5.40	2.460	4.8	37.1	31.7	35

For details of profiles see Appendix 6.

Table 5.4 Comparison of Experimental and Predicted Result for the Failure of the Sheet / Purlin Fasteners

from the fasteners to the sheeting, causing the sheeting to buckle.

At present the European Recommendations [45] specify a 25% factor of safety on this brittle failure to accommodate redistribution and the effect of the tension forces on the fastener. From the profiles tested, the percentage reduction in the shear strength was found to be 7% for the A-series, 38mm deep profile and 11% for the E-series, 90mm deep profile. So the 25% factor of safety is adequate and a re-evaluation of this figure can now be undertaken for the failure of the sheet / purlin fasteners.

In the tests associated with the buckling of the profile web, Table 5.5, the complex stresses induced in the profile and the buckled shape required that the test results be used to obtain an empirical solution. In the case of the test, which included a stiffener in the web there was found to be a considerable reduction in the failure load compared with a similar profile without the stiffener. Before any design results can be formulated for this type of profile further tests will have to be carried out.

A comparison of the theoretical and experimental values for the plastic load are given in Table 5.6. The theoretical values are based on the plastic mechanism criteria described previously. Also included in the table is the load $Q_{(h/20)}$ at which the criteria of Schardt and Strehl [47] occurs in that the top plate movement is restricted to h/20.

Profile	h/t	Length of sheeting (mm)	Diaphragm load at buckling (kN)	$\ell_{eff}/2bs$
B	87.5	1500	26	0.880
B	87.5	3000	50	0.950
C	153.3	3000	33	0.481
D	27.6	2000	96	3.120
E	112.5	1500	35	0.554
F	66.2	3000	74	1.231

Table 5.5 Buckling load of the Profile Web.

TEST E-EVERY A-ALTERNATE	LENGTH OF SHEETING (mm)	HEIGHT OF SHEETING (mm)	SWAY OF PROFILE (Δ_u) (mm/ N)	Q(h/20) (kN)	Qp (theoretical) (kN)	Qp (experimental) (kN)
B(E)	3000	70	0.1734	20.2	16.01	25.0
E1(E)	3000	90	0.2190	20.6	15.80	36.0
E2(E)	1500	90	0.5150	8.7	5.60	18.5
F1(E)	3000	48	0.1900	12.6	15.70	36.5
F2(E)	1500	48	0.4000	6.0	6.94	18.0
F3(A)	3000	48	2.03	1.18	6.33	13.5
F4(A)	1500	48	6.14	0.39	2.49	5.2
A2(A)	1500	38	7.54	0.25	6.69	6.5
G(A)	3000	63	4.64	0.68	6.30	8.4

For details of profiles see Appendix 6.

Table 5.6 Comparison of Lateral Sway Criteria.

The value of $Q_{(h/20)}$ was obtained using the Finite Strip Program in which the value of the top plate movement was used in the every corrugation fastened case. For the alternate corrugation fastened case the top plate movement could again be the basis for the deflection criteria. Schardt and Strehl do not give any guidance for other fastener arrangements, as they based most of their work on the every corrugation use. Therefore, since this is a serviceability criteria and the bottom plate movement is greater than the top plate movement, it would seem realistic to base the deflection criteria on the unrestrained bottom plate movement in the alternate corrugation case.

Comparison of the experimental plastic load with the deflection and plastic criteria shows that both are conservative by differing margins. In the case of the every corrugation fastened case the plastic criteria is more conservative than the deflection criteria, whereas for the alternate corrugation case the plastic criteria produces realistic results. The difference between the two criteria and the experimental results can be explained by a number of factors,

(1) the accuracy of the experimental plastic load cannot be fully guaranteed.

(2) the theories on which both the criteria are based assume a point load restraint at the end purlin. This is not the case in the actual tests, in which the propping force is spread over the full width of the purlin. The resulting spread of the propping force will cause a variation in the end bending moments and deflections, which are the

basis for the two criteria.

(3) the assumed shape of the stress/strain curve for the plastic criteria, Fig 5.30, will result in a lower bound failure compared with the actual stress/strain curve.

When there is a possibility of end failures in a diaphragm one of the above failure modes will be critical. So as to help an engineer identify the most likely mode of failure, Table 5.7 gives an indication of the most likely failure mode for a particular type of diaphragm.

5.7 Design Recommendations

Following the work carried out on the failure modes associated with end failures, three specific recommendations are proposed for inclusion in the European Recommendations on Stressed Skin Design. These are:-

a. that at present a 25% reserve of strength is required in the recommendations to allow for additional forces on the sheet / purlin fasteners. The present study has shown this to be conservative and there are two means of reducing this value. One proposal is to use a 12½% reserve of strength instead of the 25% value. The second proposal is to incorporate the tensile force in the calculations and to obtain a reduced shear capacity based on the proposed shear / tension

MODE OF FAILURE

Sheet/Purlin Fasteners	Buckling of Profile Web	Laterial Sway of the Profile
Usually occurs when Profiles of a height less than 40mm are used. Possible failure when heights are greater than 75mm and the ratio $2\ b_T/d$ is less than 0.3	Buckling will usually occur when lengths of sheeting less than 5m are considered.	Will normally be critical when alternate corrugations are considered.

Table 5.7 Indication of Possible Failure Modes.

interaction curve. An expression for the tension and shear forces on the fasteners are given by

$$Fs = \frac{Qd}{b}\left(1 + \frac{k\,Fy2}{2}\right) \qquad (5.42)$$

for the longitudinal shear force

and
$$F_T = \frac{Qd}{b}\left(\frac{Fx}{d} + \frac{k}{2}\left(1 - F_{x1}\right)\right) \qquad (5.43)$$

for tension force

where
$$Fy2 = \frac{b_L\,(bs + b)}{h\,(2bs + b)}$$

$$\frac{}{3}$$

$$Fx = \frac{2h}{d}\,(2b_T + p)$$

$$Fx_1 = \frac{2}{d}\,(b_T + p)$$

It must be noted that these expressions should only be applied to the every corrugation arrangements.

b. the buckling of the profile web is only a secondary consideration. This failure load is given by

$$P_B = \frac{\pi^2 E t^4 (bp + bs/2)}{12 (1 - \nu^2) (\ell eff)^2} \qquad (5.44)$$

where ℓeff is obtained for Fig. 5.21

bp is the width of the purlin

bs is half the web length

t is the thickness of the profile

This can then be compared with the actual purlin restrain force given by

$$P = \frac{k Q d}{b} \qquad (5.45)$$

where k is obtained from Appendix 4

Q is the diaphragm load

giving a design criterion that if P is less than P_B, failure will not occur by buckling of the profile web.

As a consequence of the large deflected shape of the profile in the alternate corrugation fastened case, this requirement need only be considered in the case of every corrugation fastened.

c. the lateral sway of the profile need only be considered as a serviceability requirement as further load can be applied to the diaphragm until the ultimate load criteria is obtained. An expression for the plastic load Qp, defined as the load at which a change in shape in the load / deflection curve is obtained, for the every corrugation fastened case is given by

$$Qp = \frac{m\ d}{2m_B(b_T + p) + b_L(m_B + m_E)} \qquad (5.46)$$

where m = plastic moment of sheeting

$$= \frac{t^2 \sigma_y}{4}$$

m_B and m_E are the actual bending moments at the ends of the sheeting, Fig. 5.21.

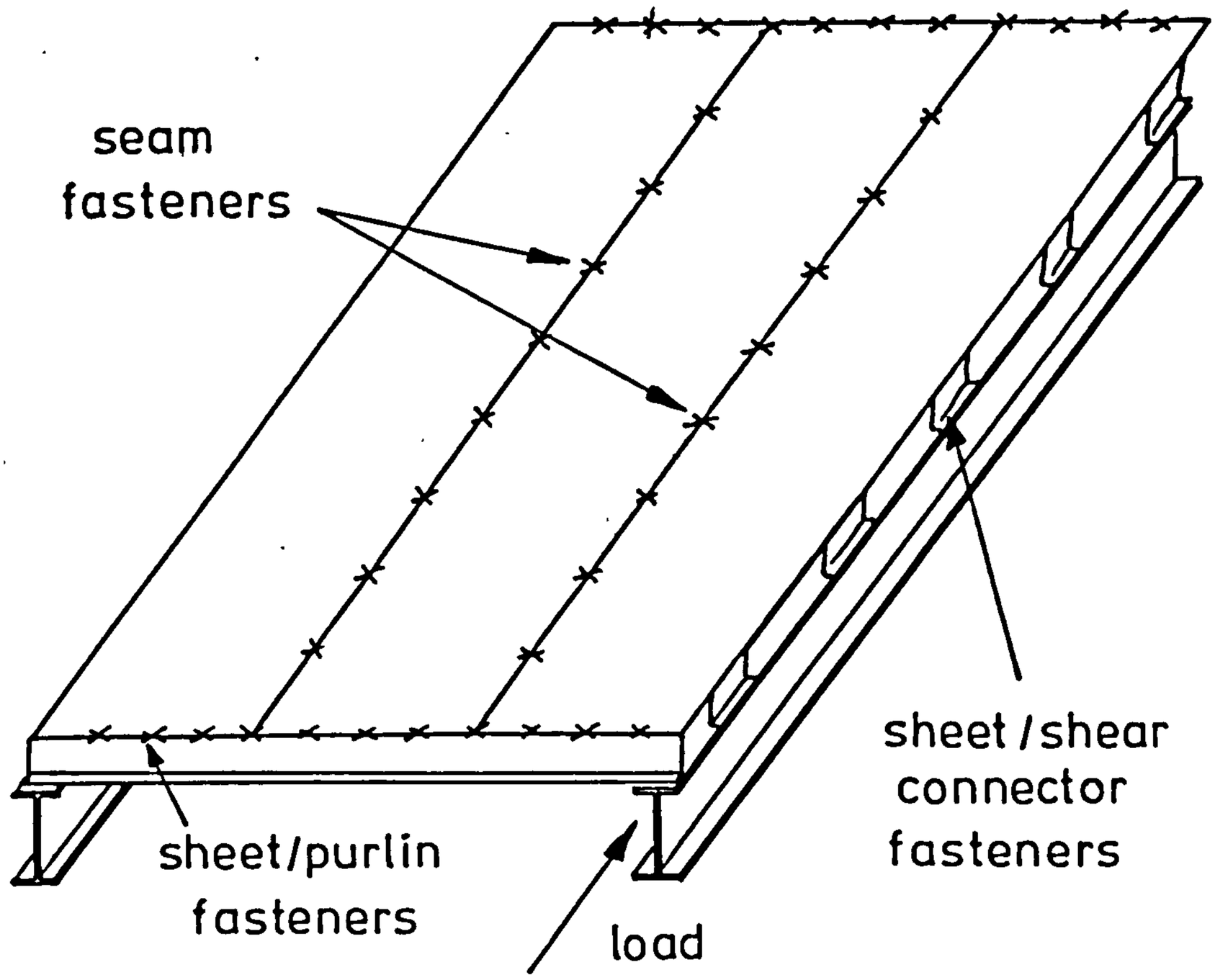

Fig 5.1 Individual diaphragm and the fastener groups

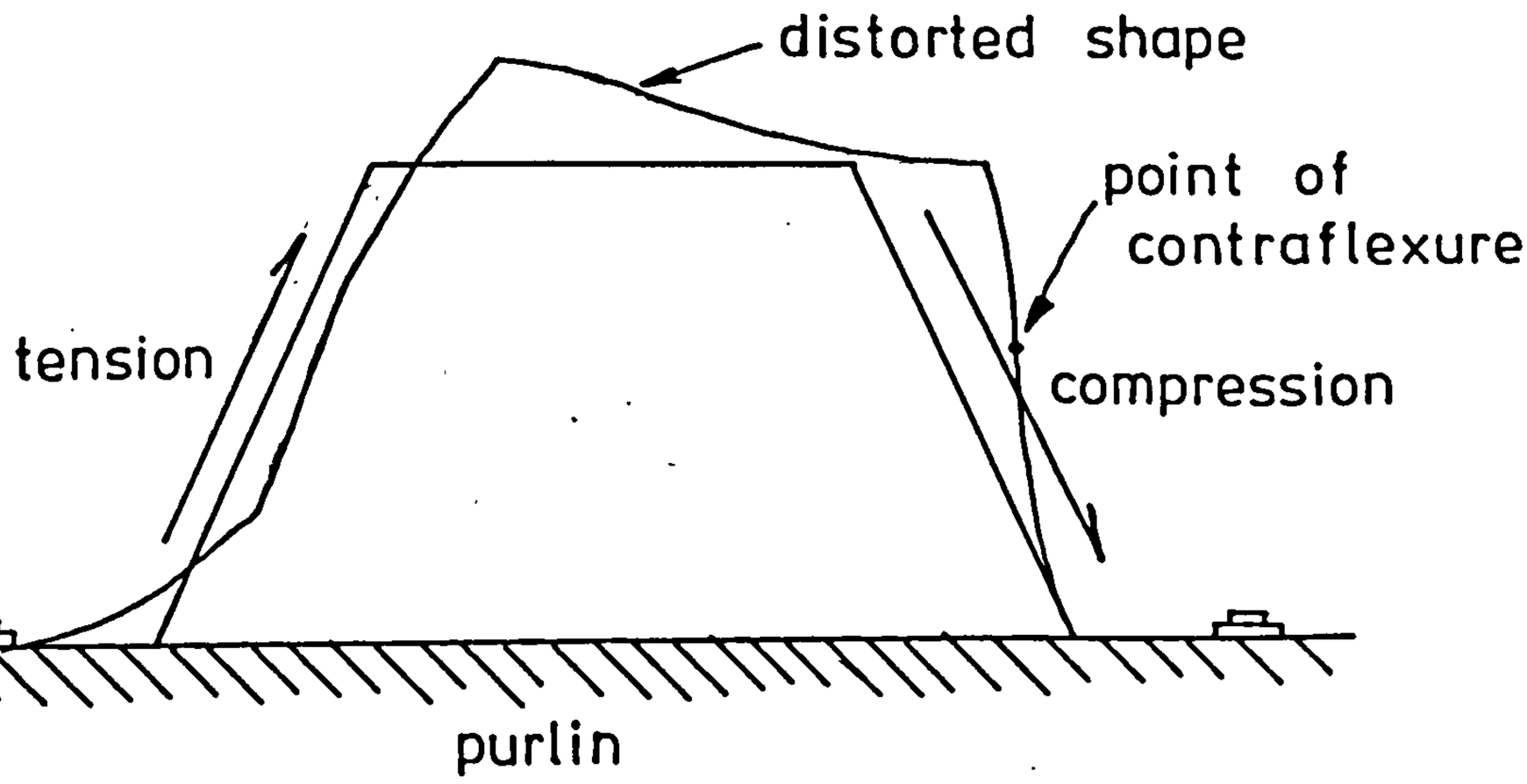

Fig 5.2 Local forces on profile at end of sheeting

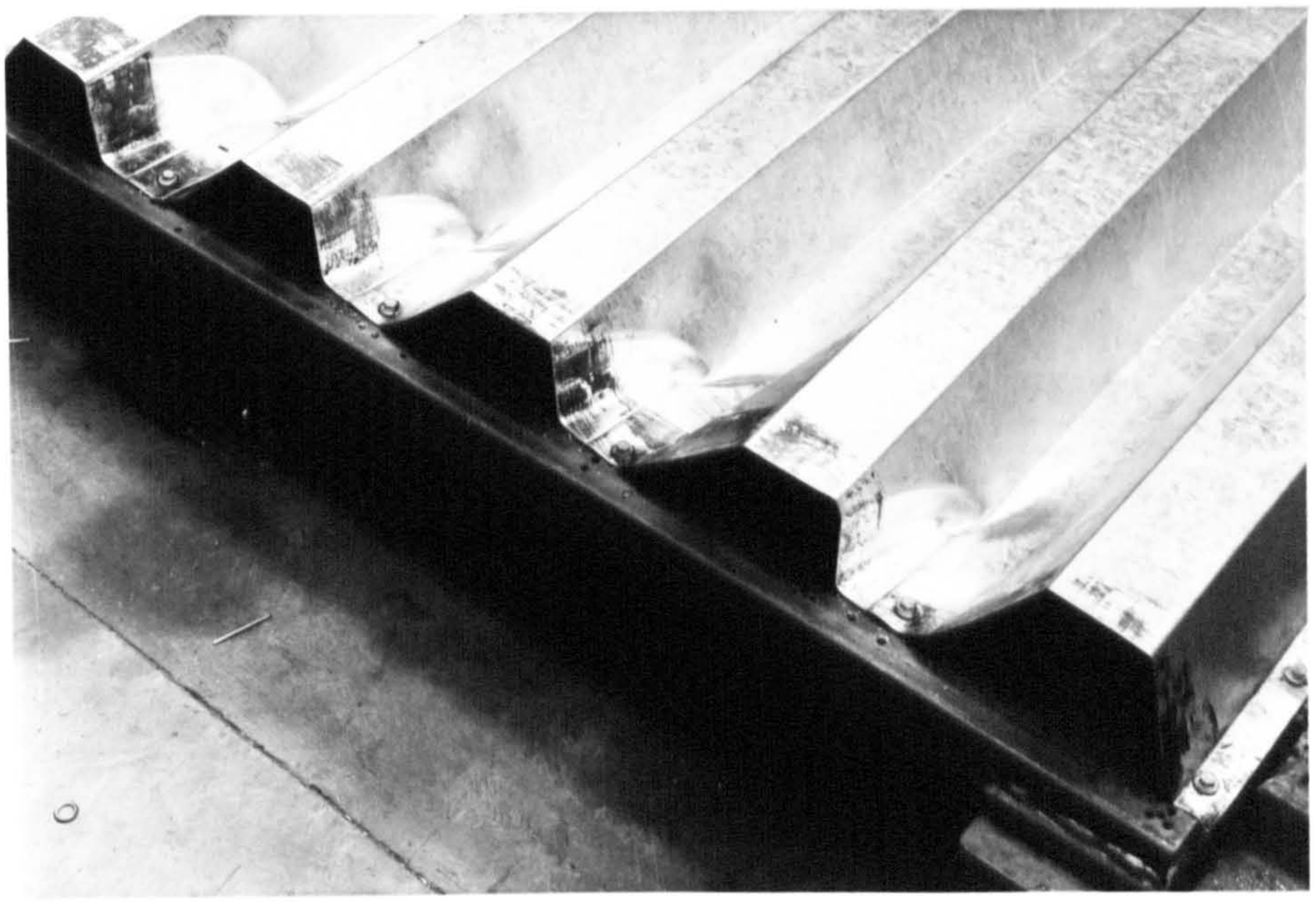

Fig 5.3 Buckling of profile at end purlin

Fig 5.4 Excessive distortion of profile

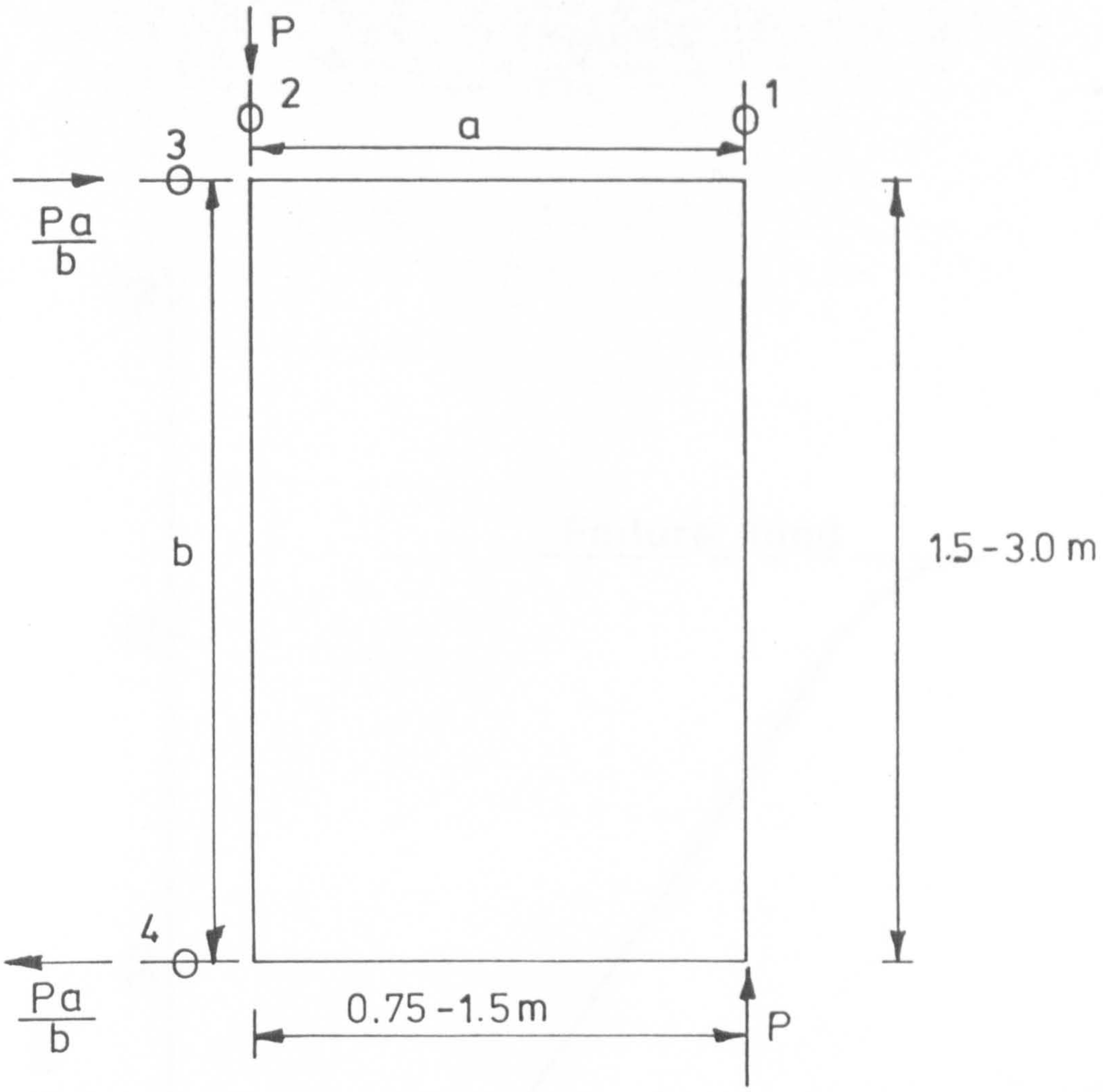

Fig 5.5 Arrangement of test rig

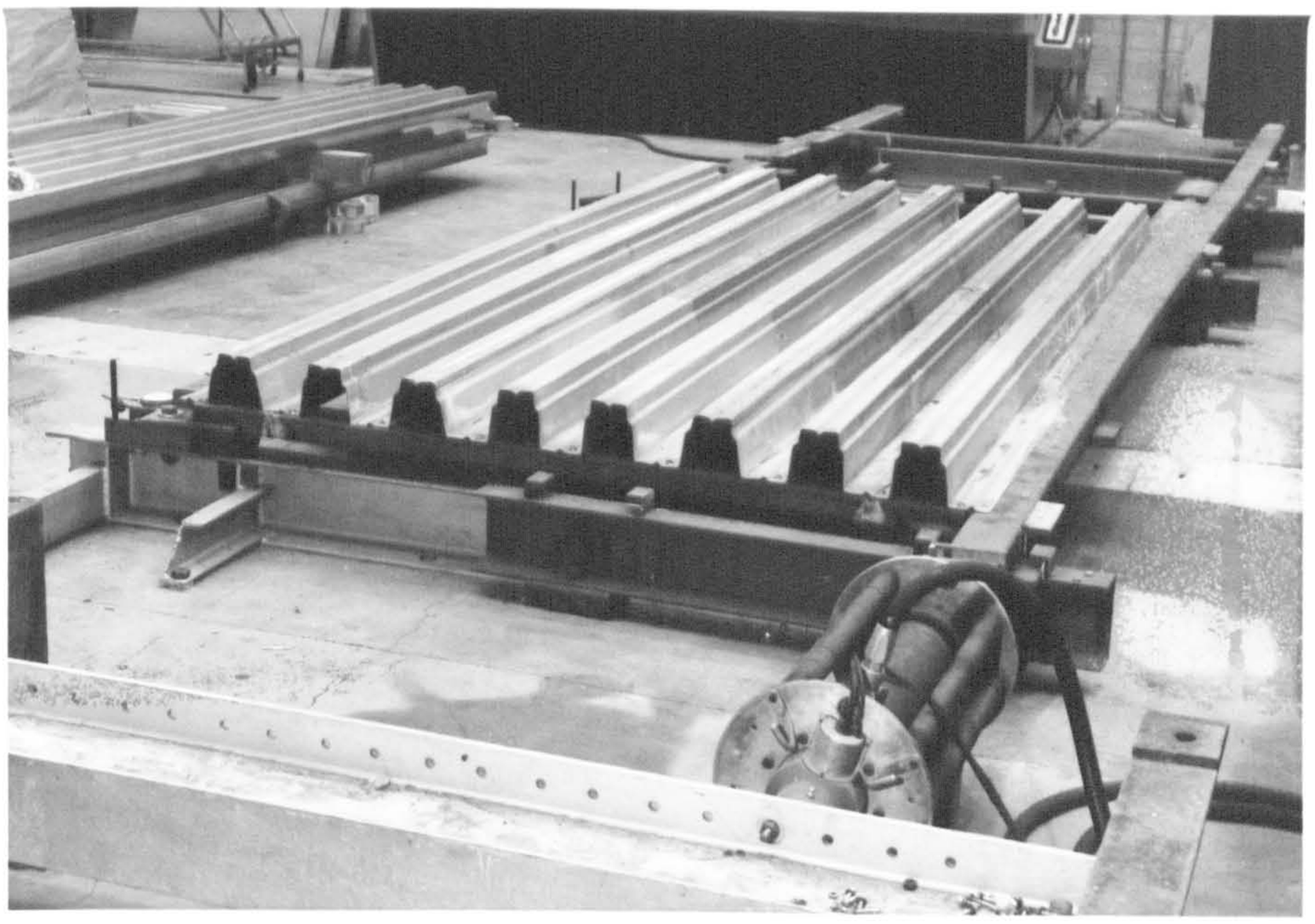

Fig 5.6 Test rig with sheeting in position

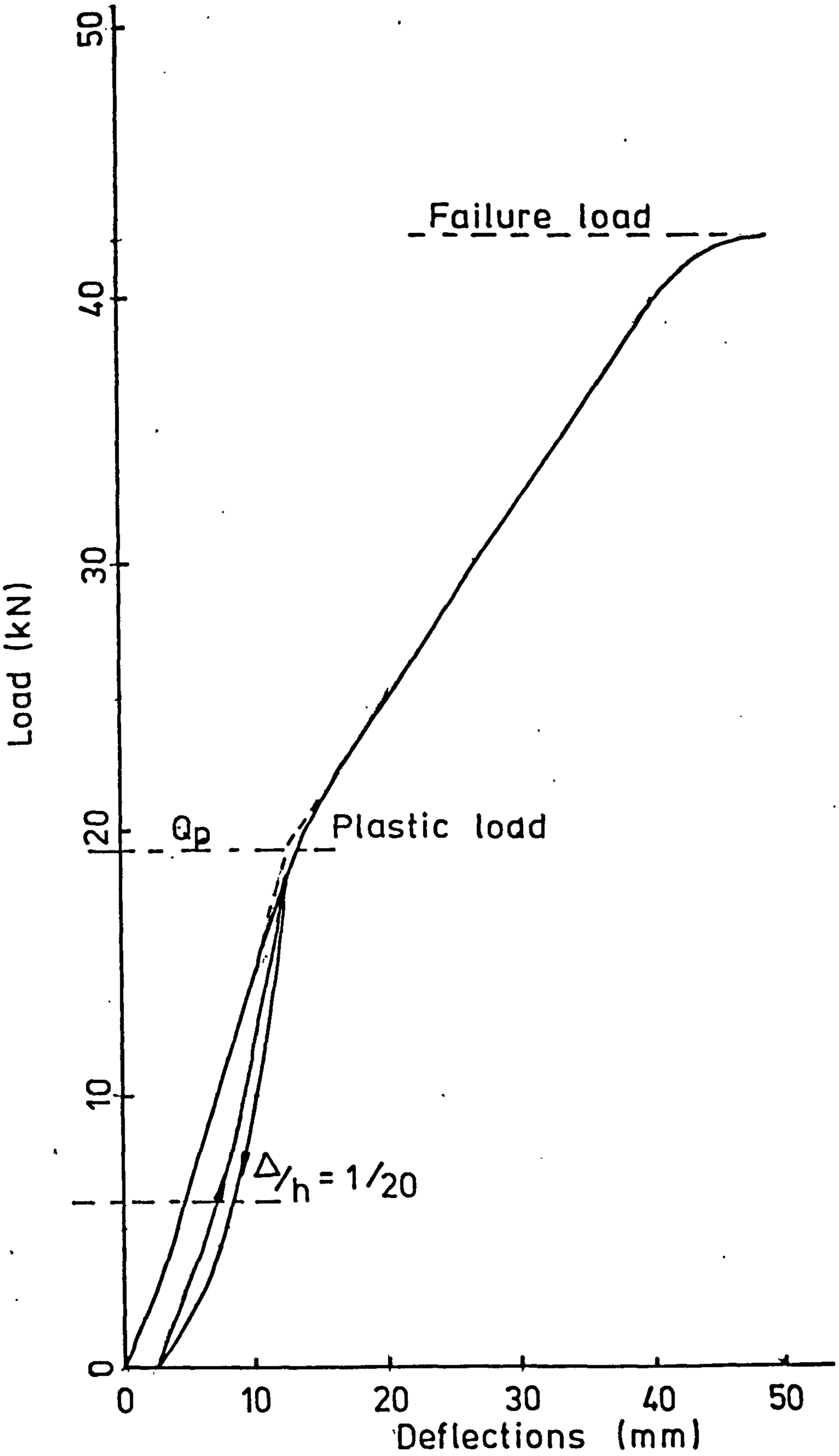

Fig 5.7 Load v deflection curve for Test F2

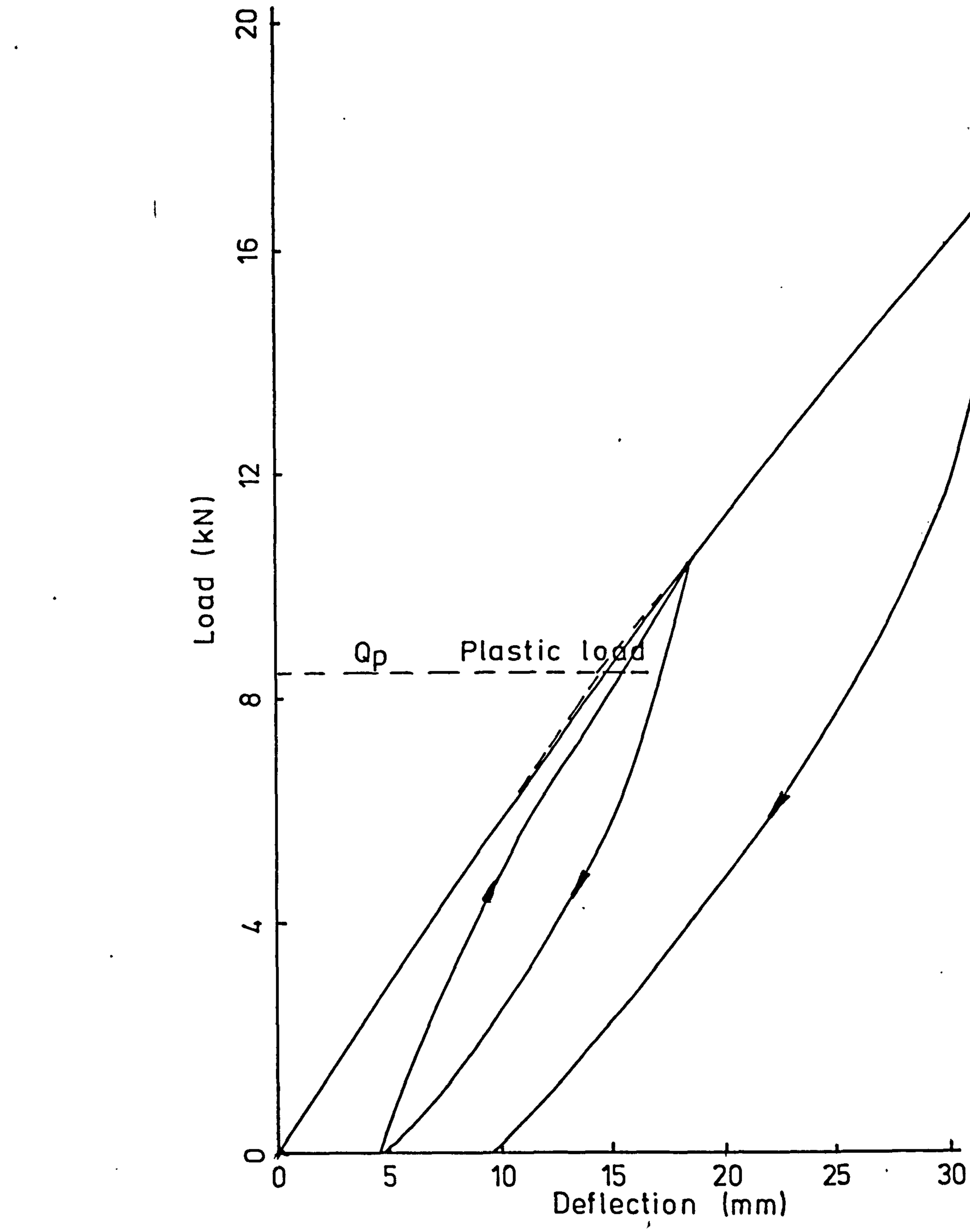

Fig 5.8 Load v deflection curve for Test G

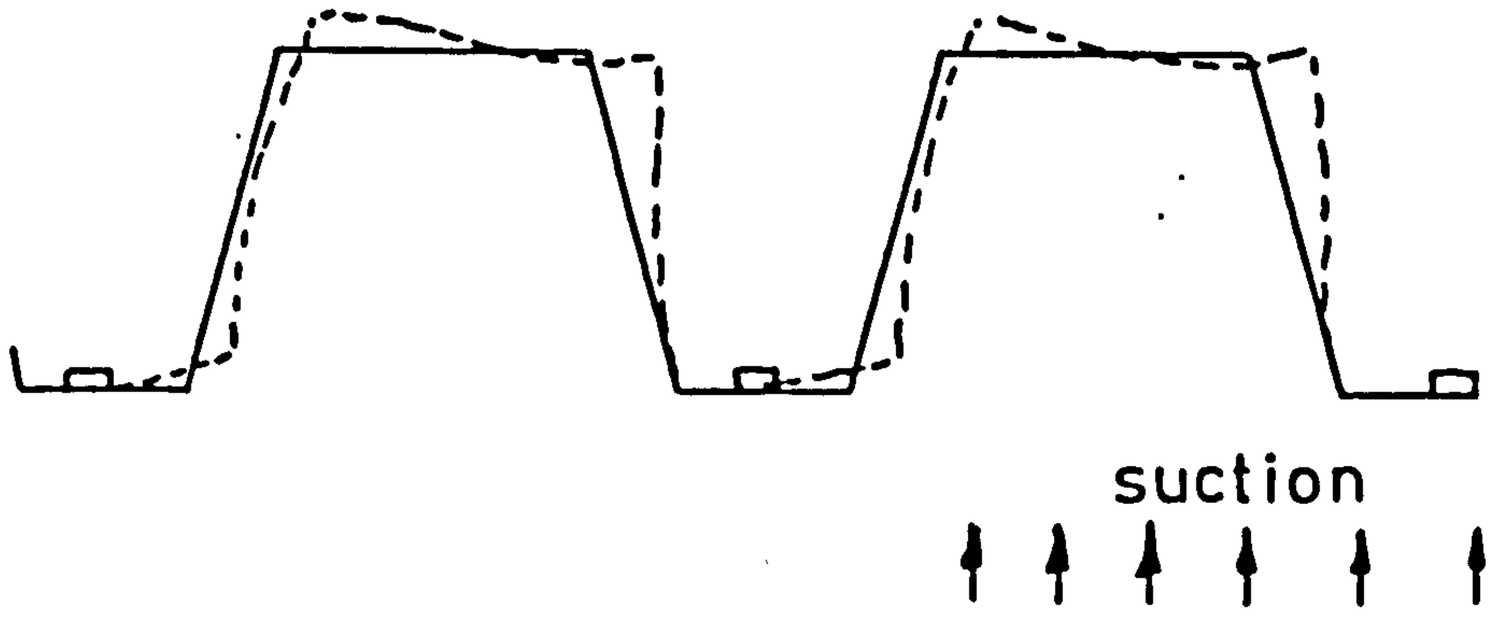

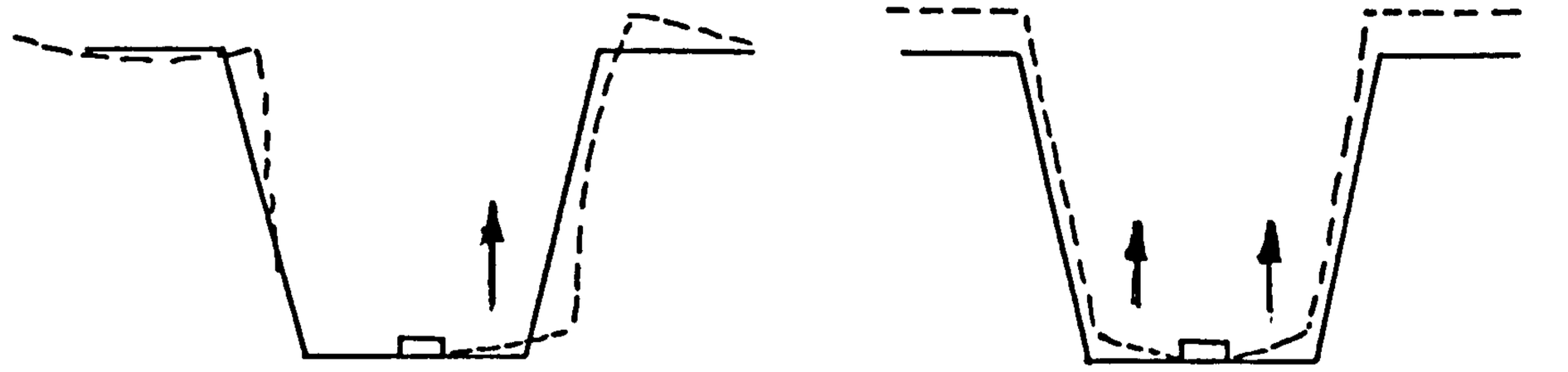

Fig 5.9 Possible tension forces on fastener jack

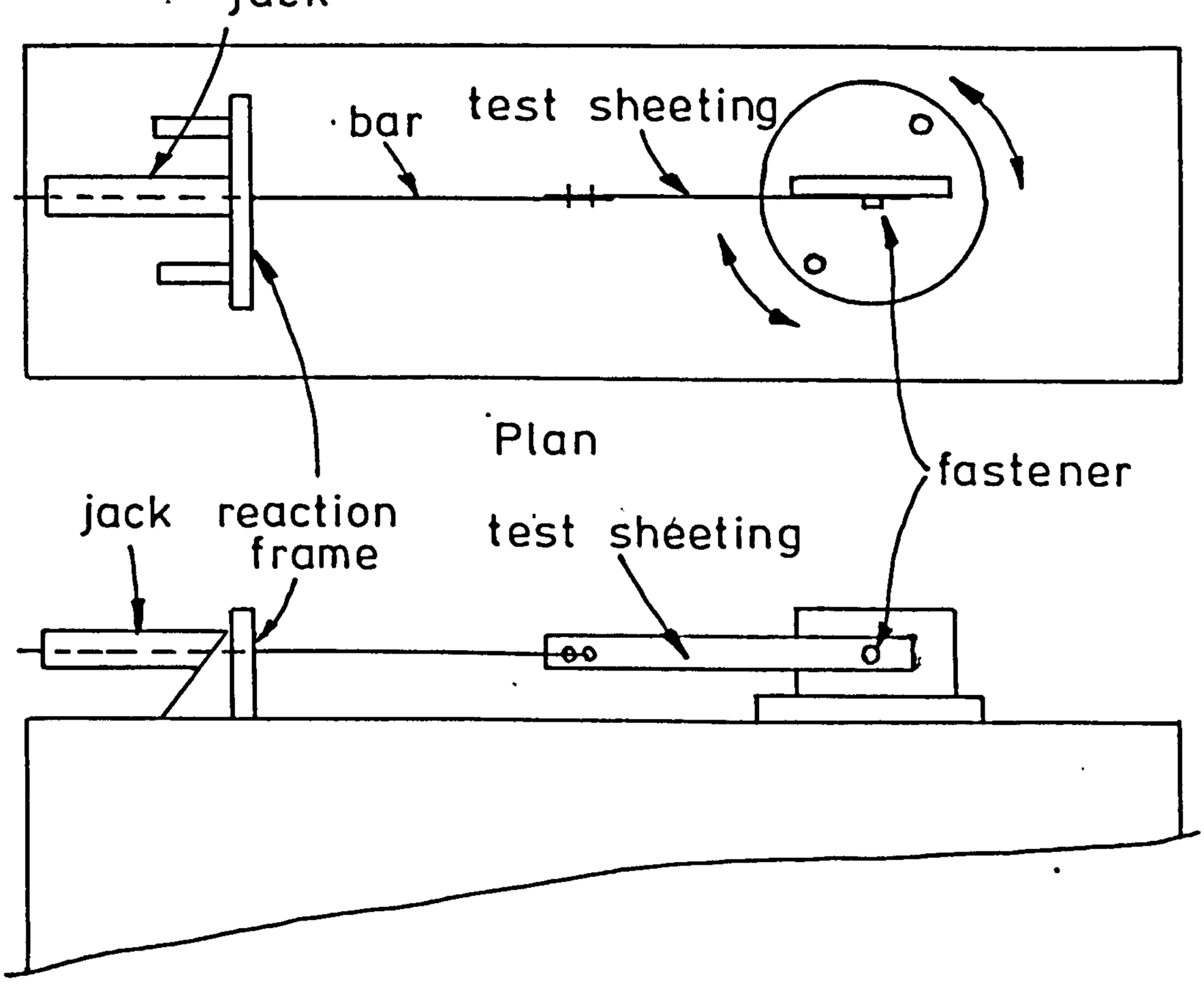

Fig 5.10 Test arrangement for shear/tension interaction curve

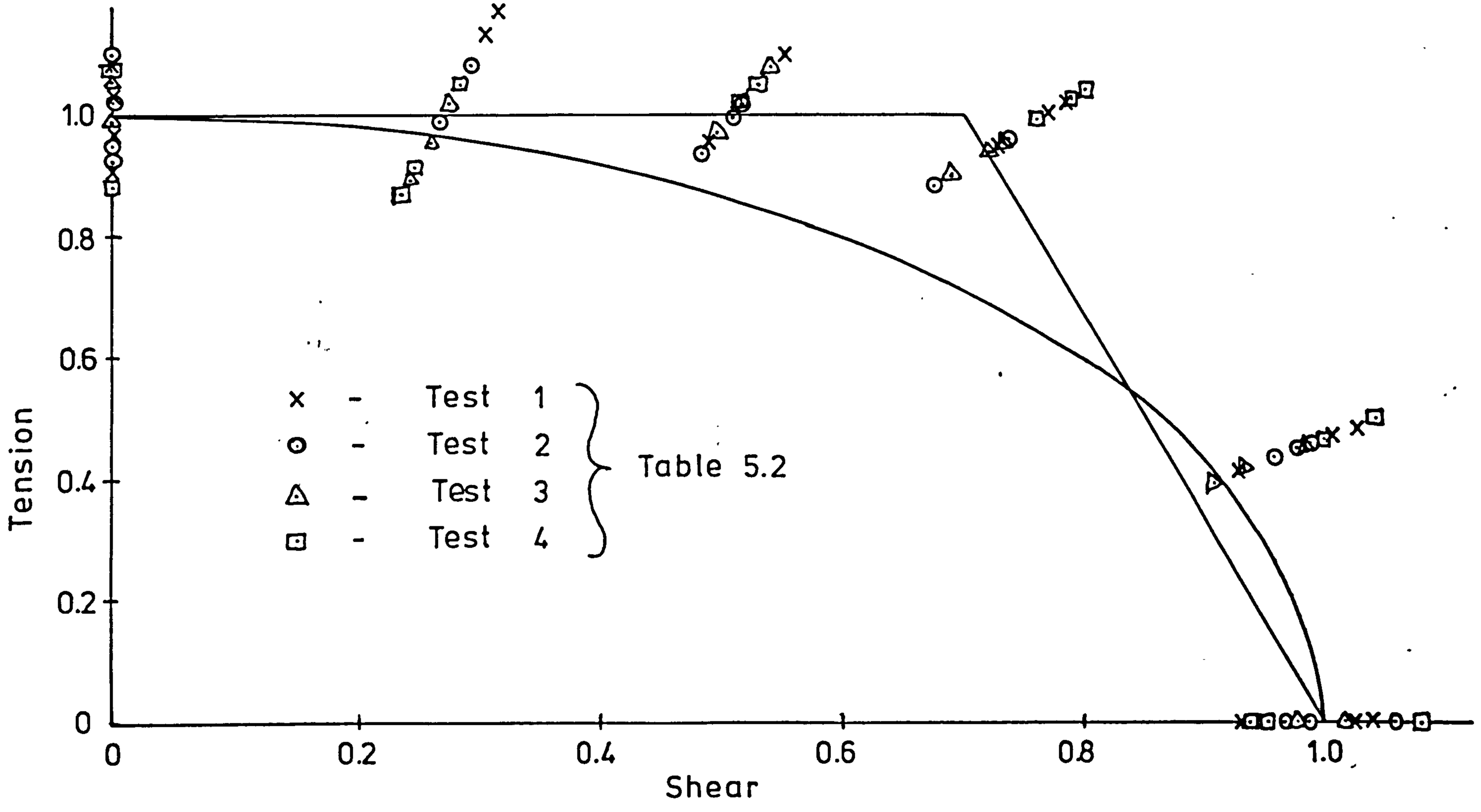

Fig 5.11 Interaction curve for shear/tension forces on sheet/purlin fasteners

F_{sl} - Longitudinal shear force

F_{st} - Transverse shear force

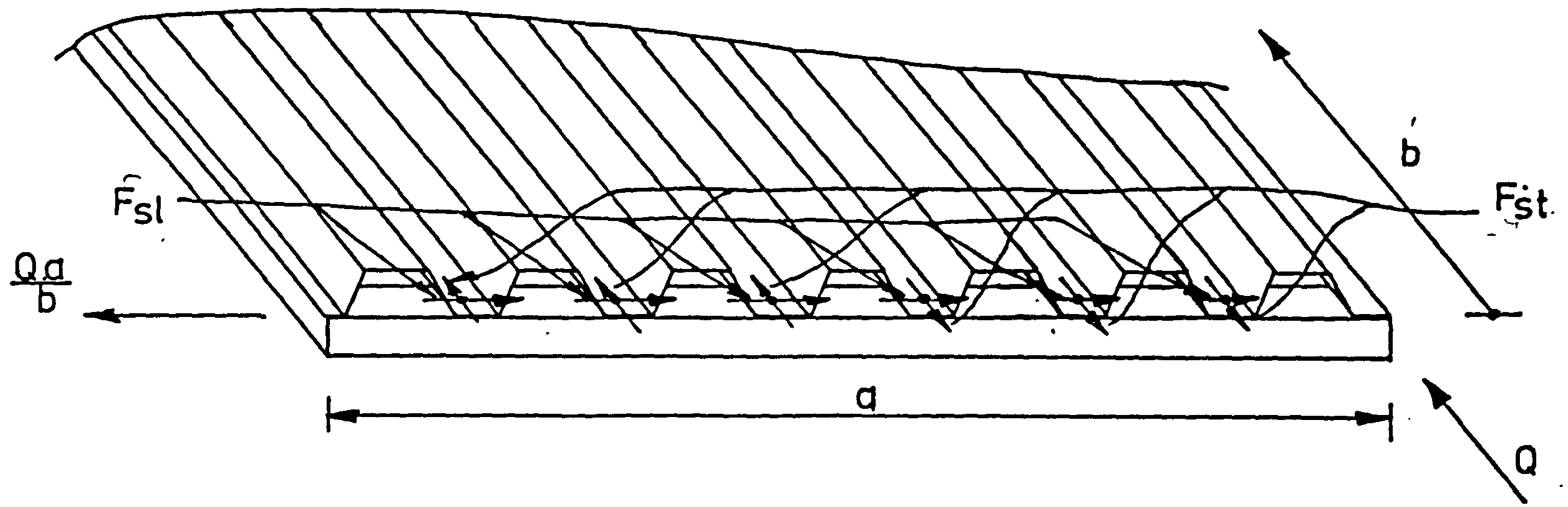

Fig 5.12 Components of shear in a diaphragm

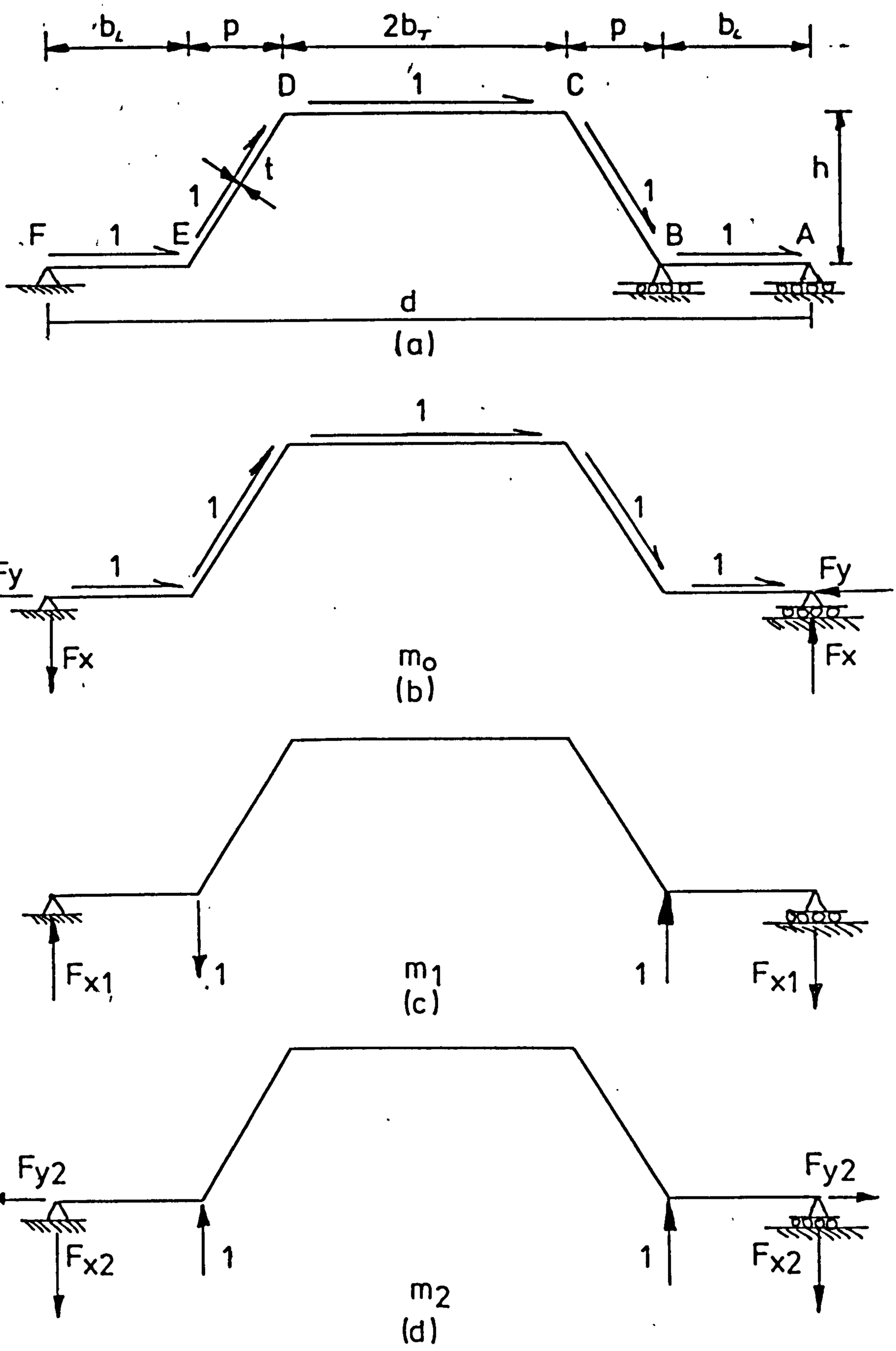

Fig 5.13 Analysis of End Forces for Every Corrugation Fastened

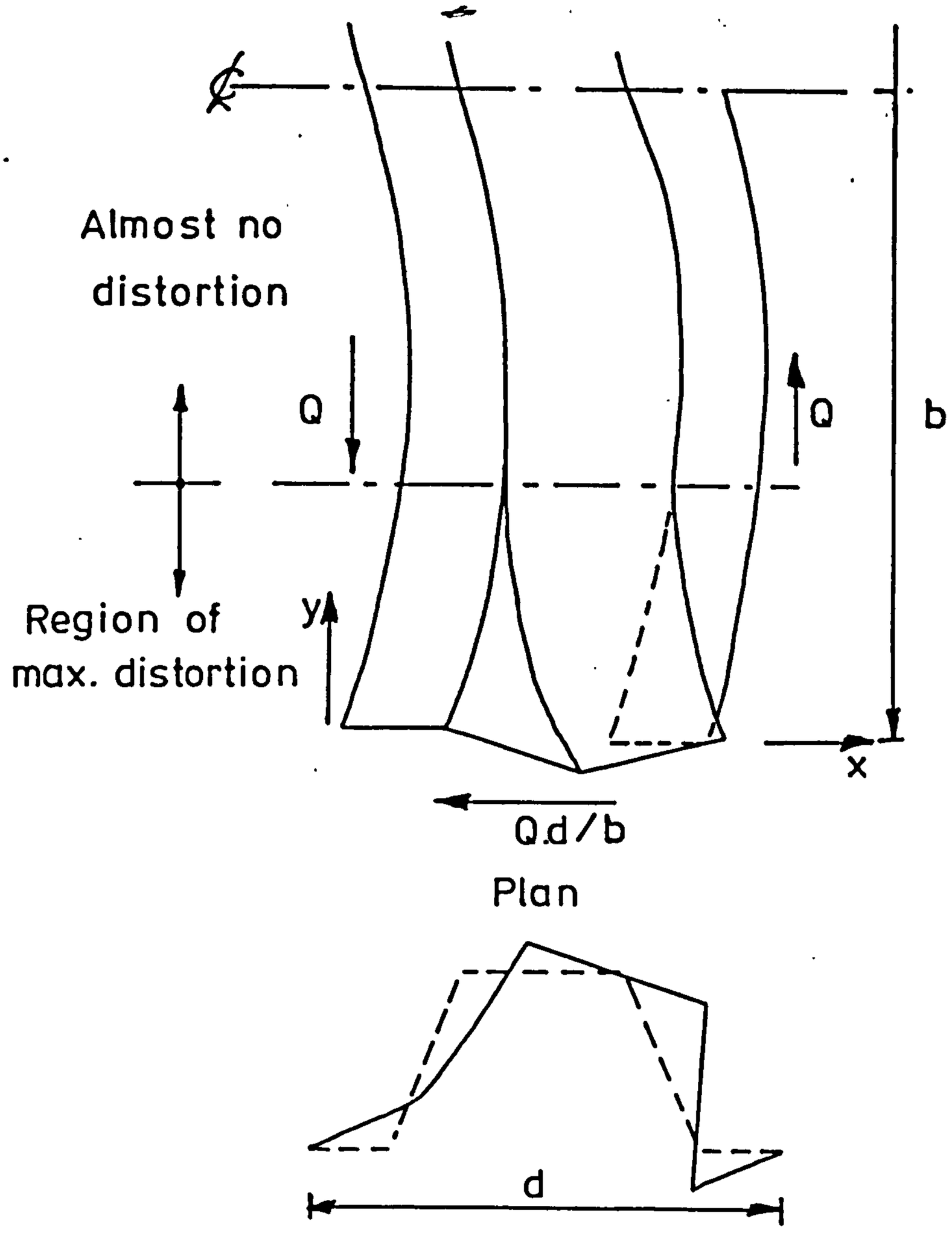

Fig 5.14 Distortion of a Profile

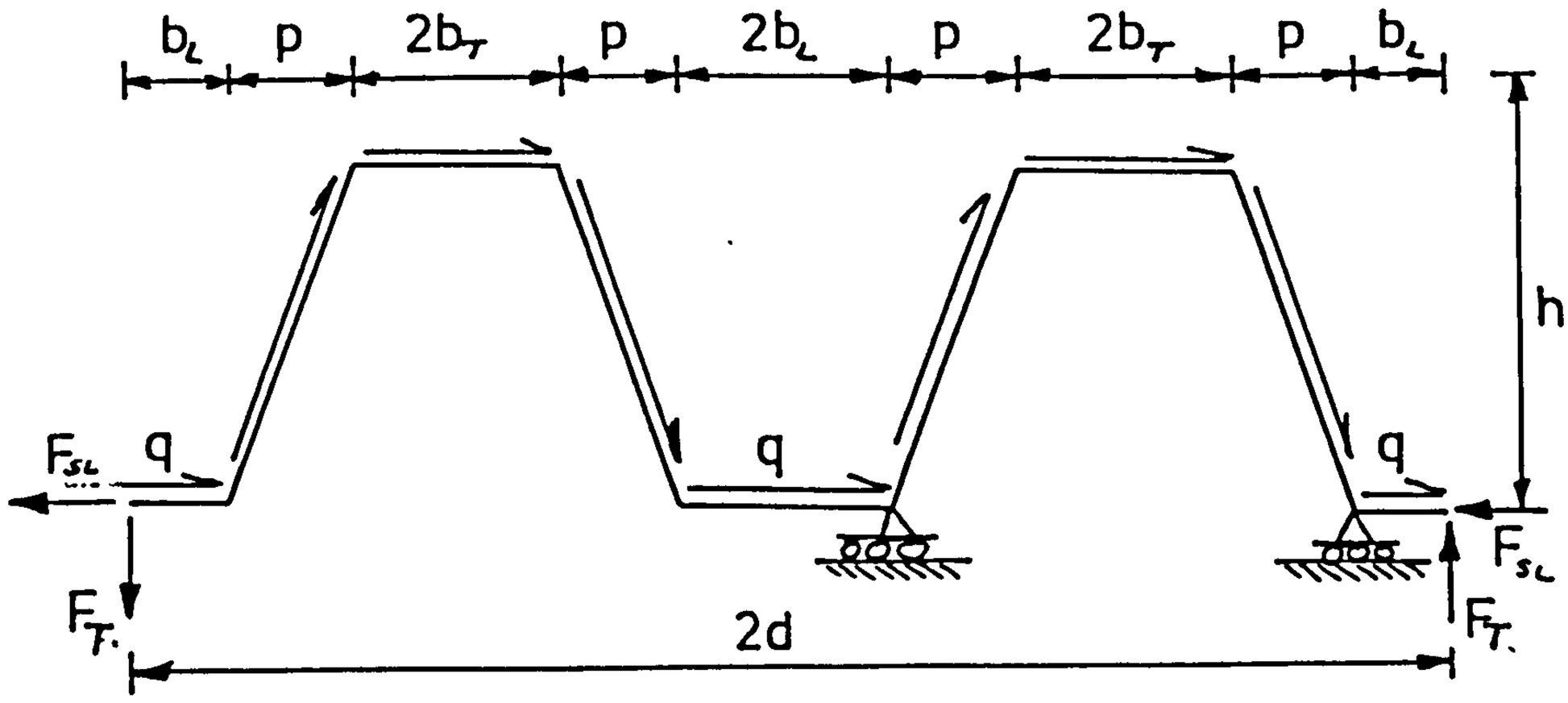

Fig 5.15 Alternate Corrugations Fastened

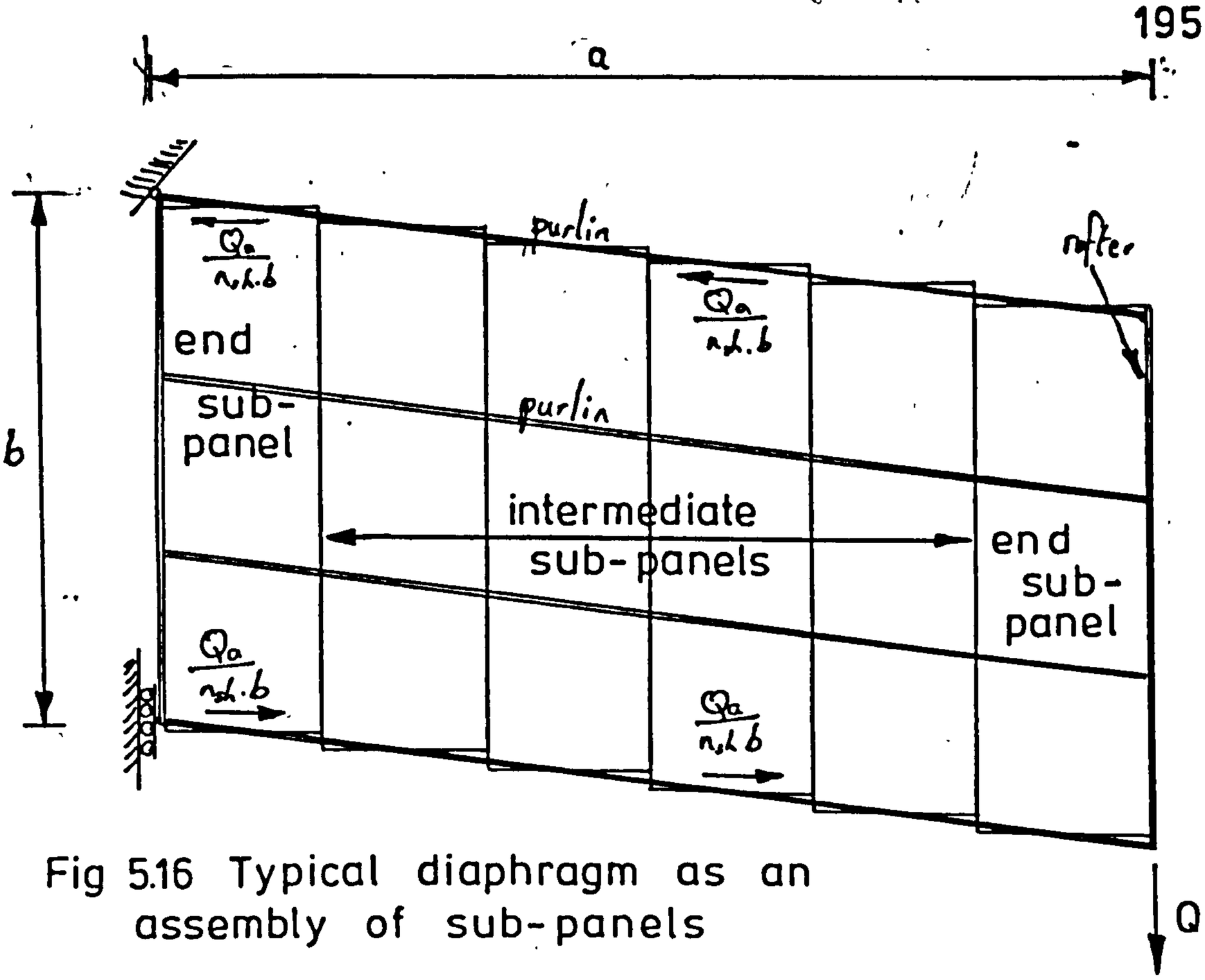

Fig 5.16 Typical diaphragm as an assembly of sub-panels

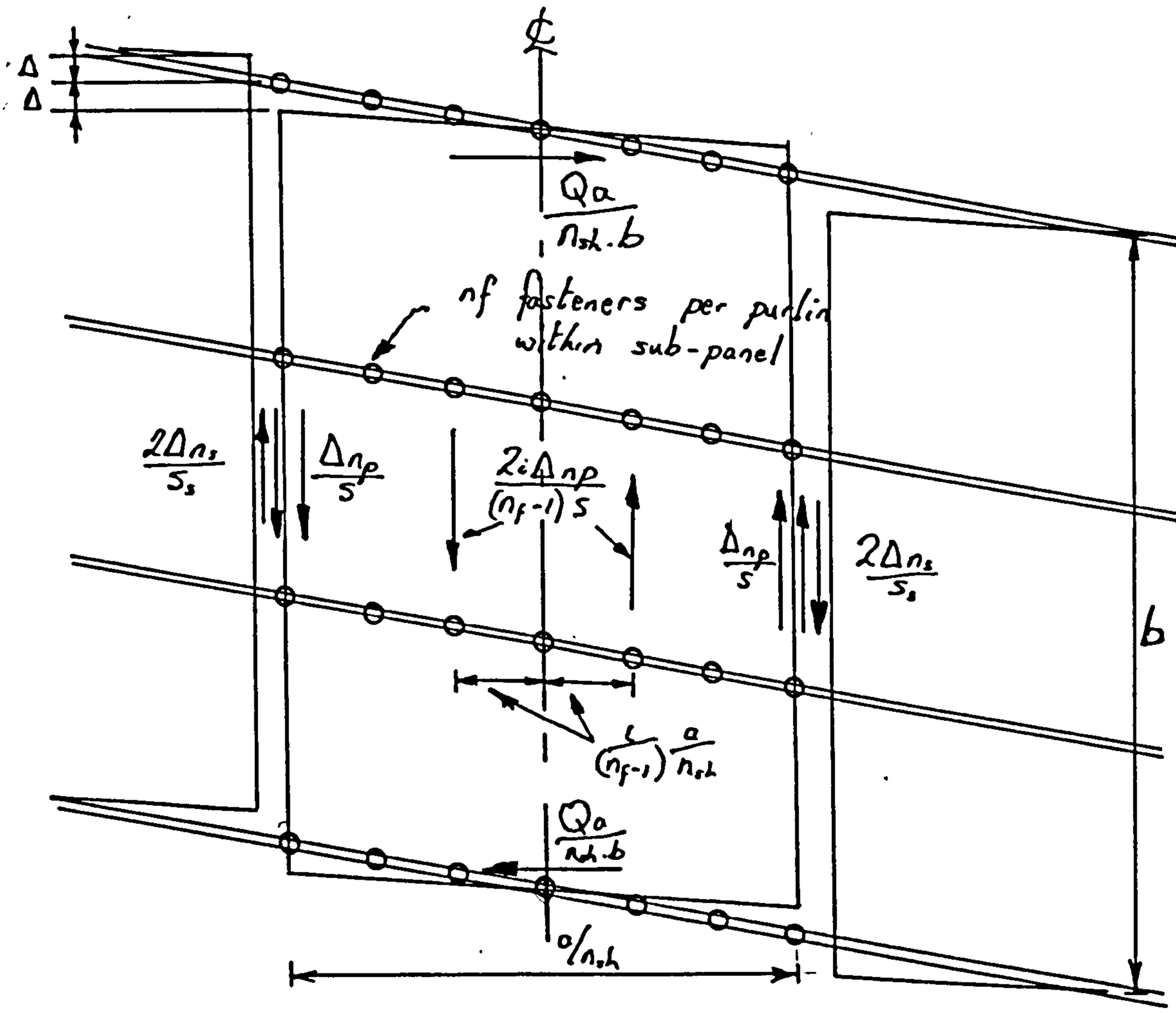

Fig 5.17 Forces and deformations assumed for an intermediate sub-panel

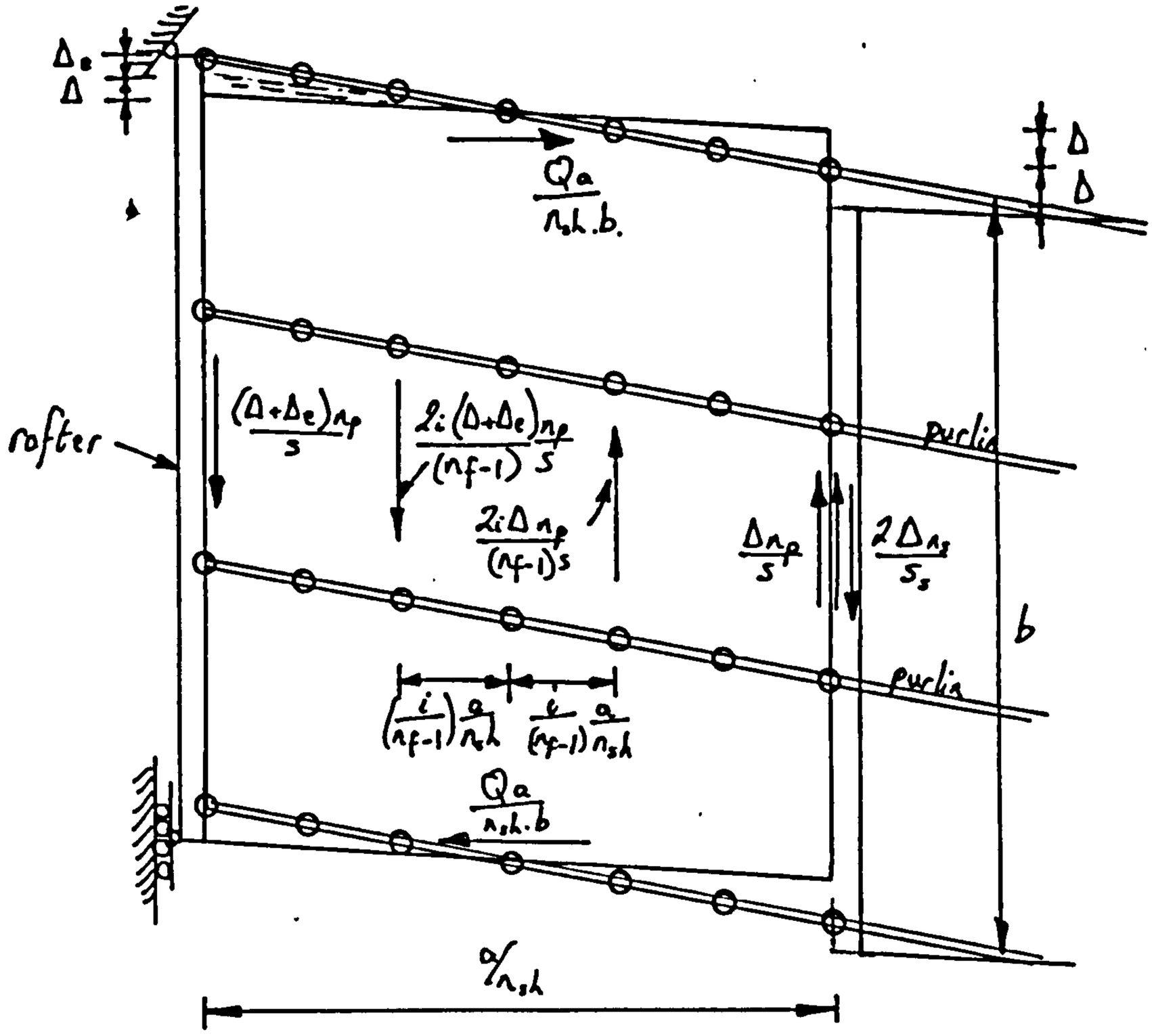

Fig 5.18 Forces and deformations assumed for end sub-panel

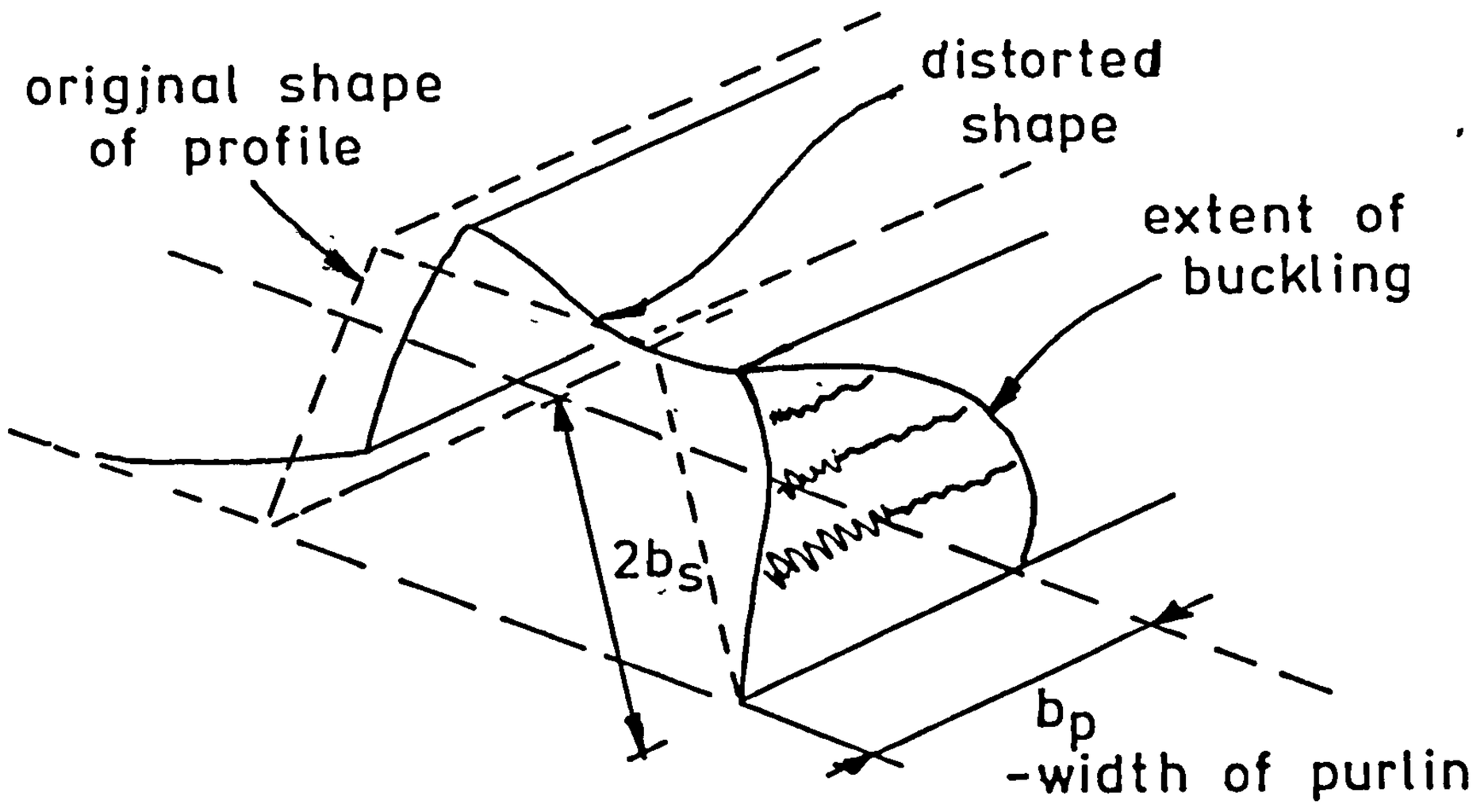

Fig 5.19 Buckling of profile at end purlin

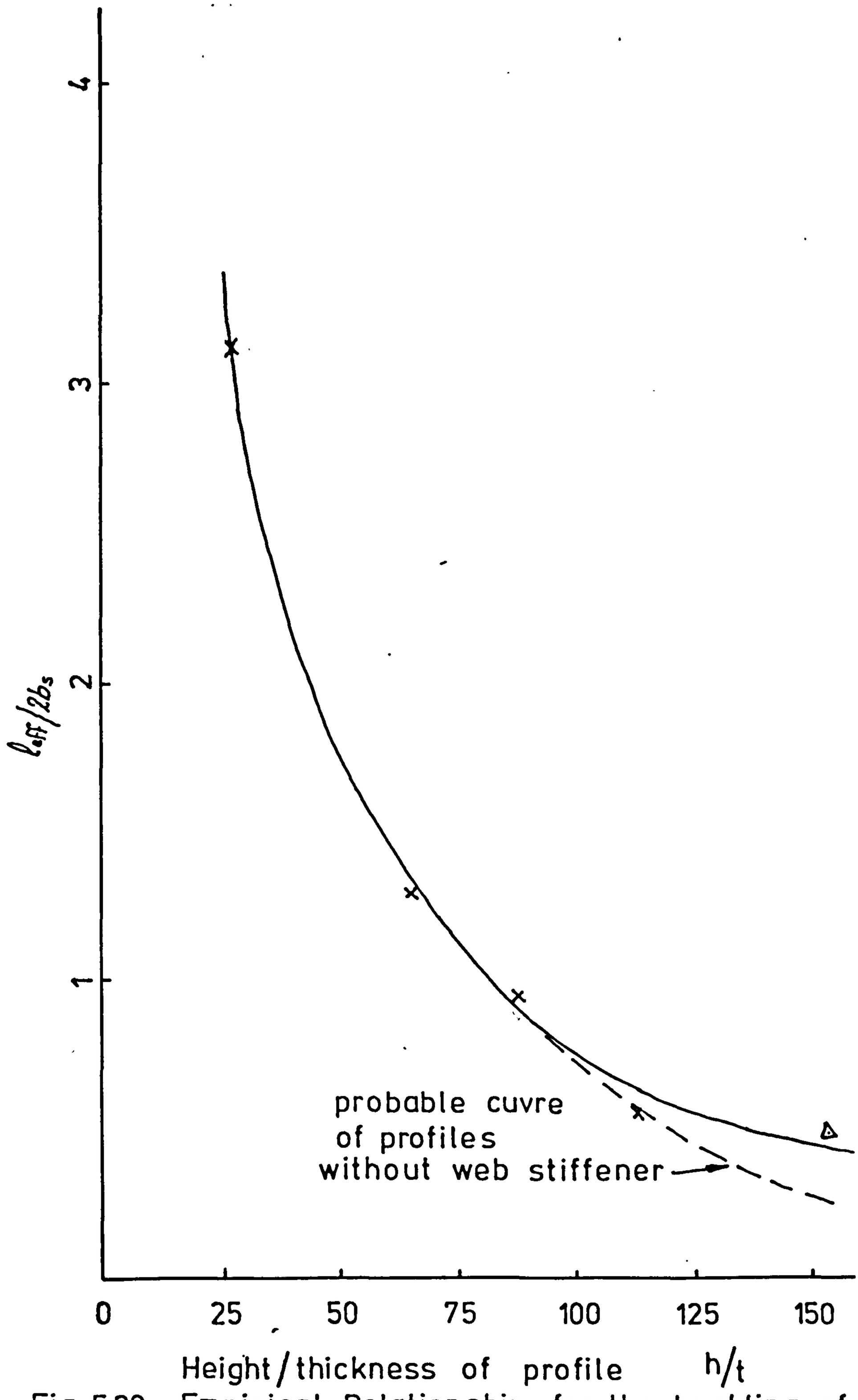

Fig 5.20 Empirical Relationship for the buckling of the profile web

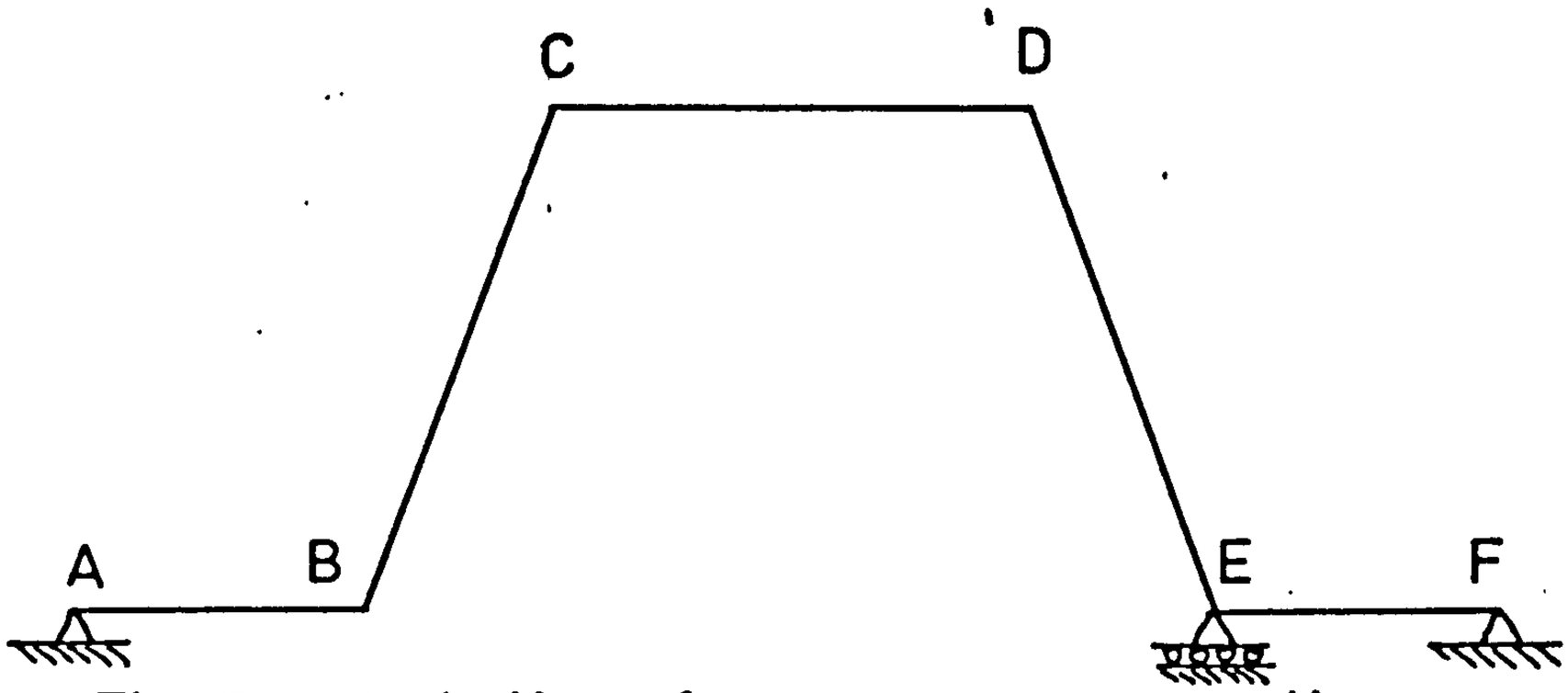

Fig 5.21 Notation for every corrugation

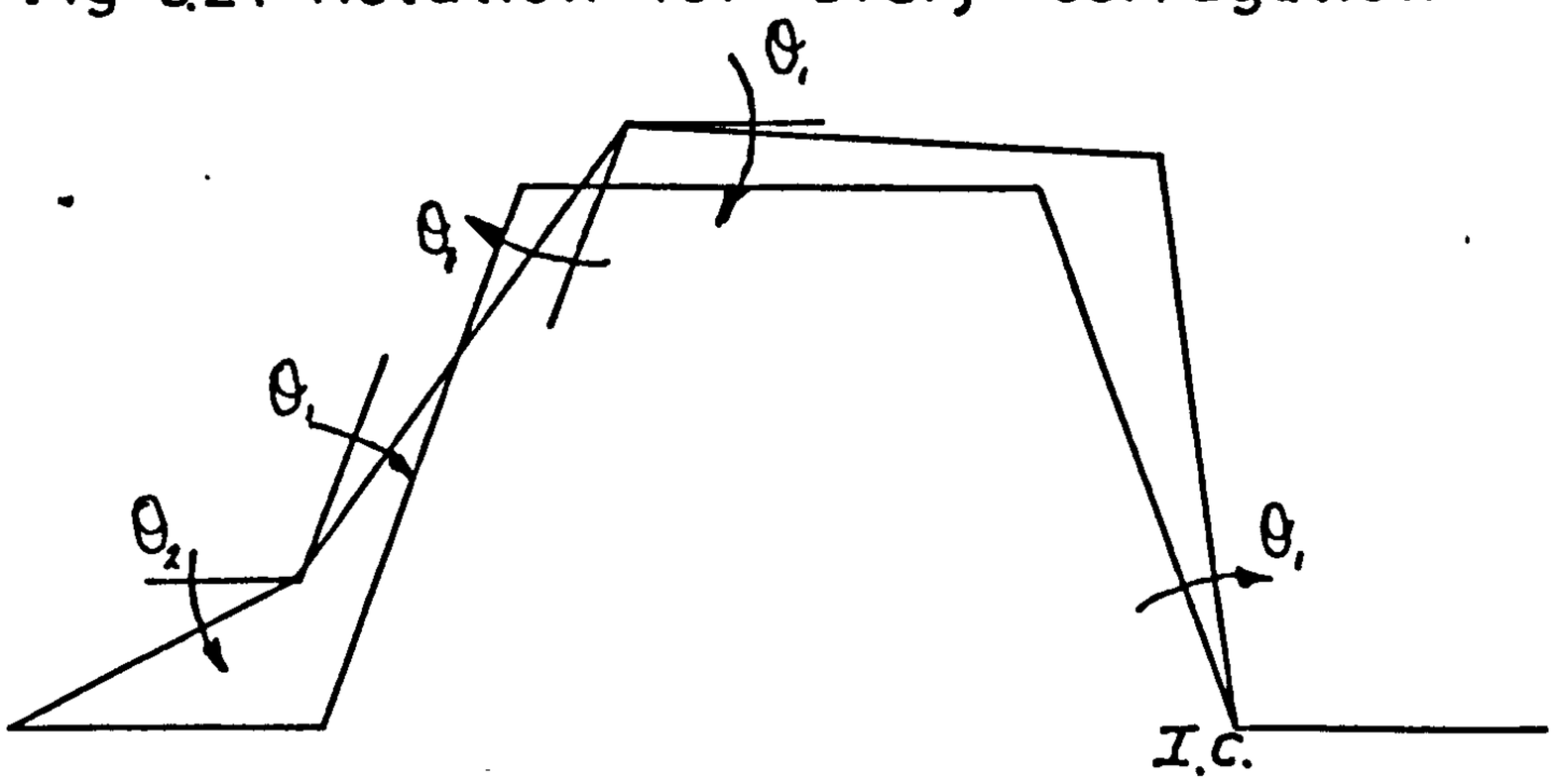

Fig 5.22(a)Deformed Shape

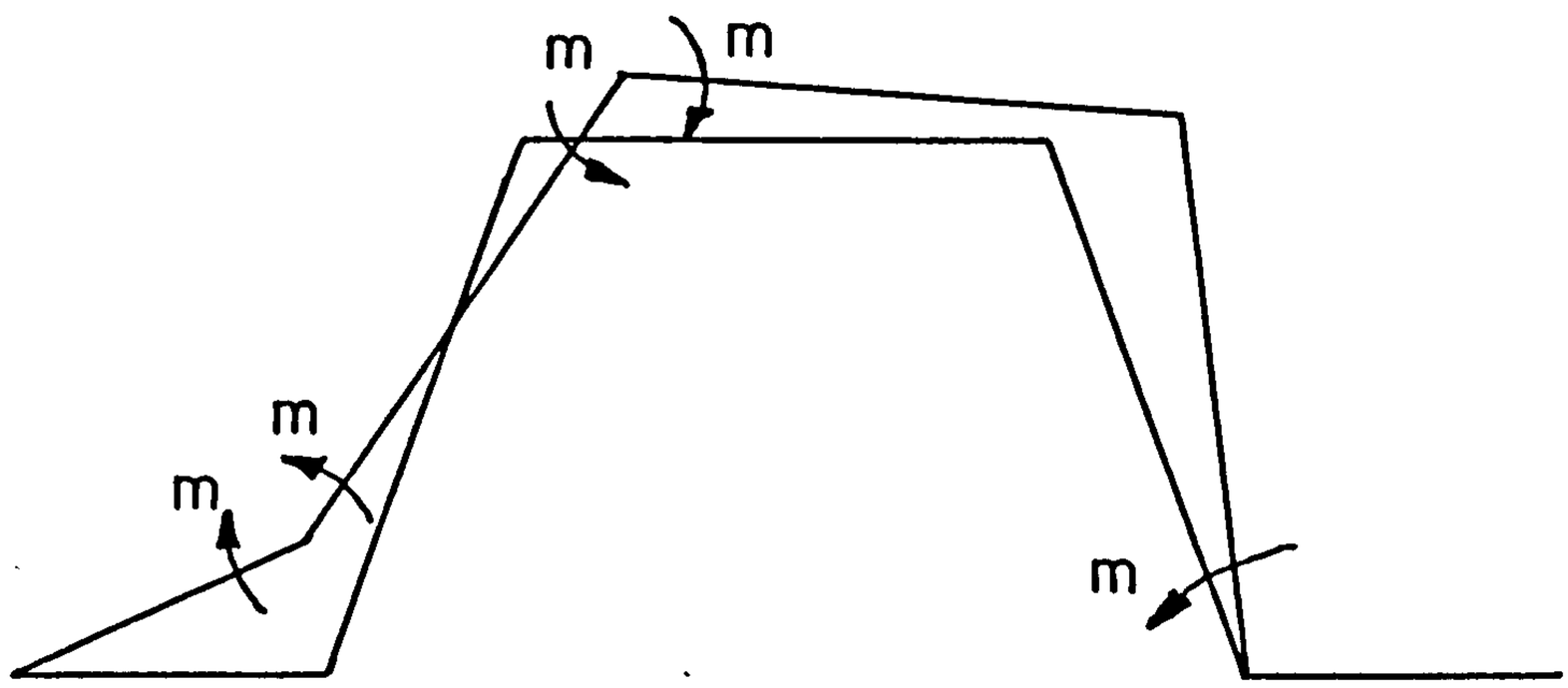

Fig 5.22(b) Moment Diagram

See Appendix 6
for profiles

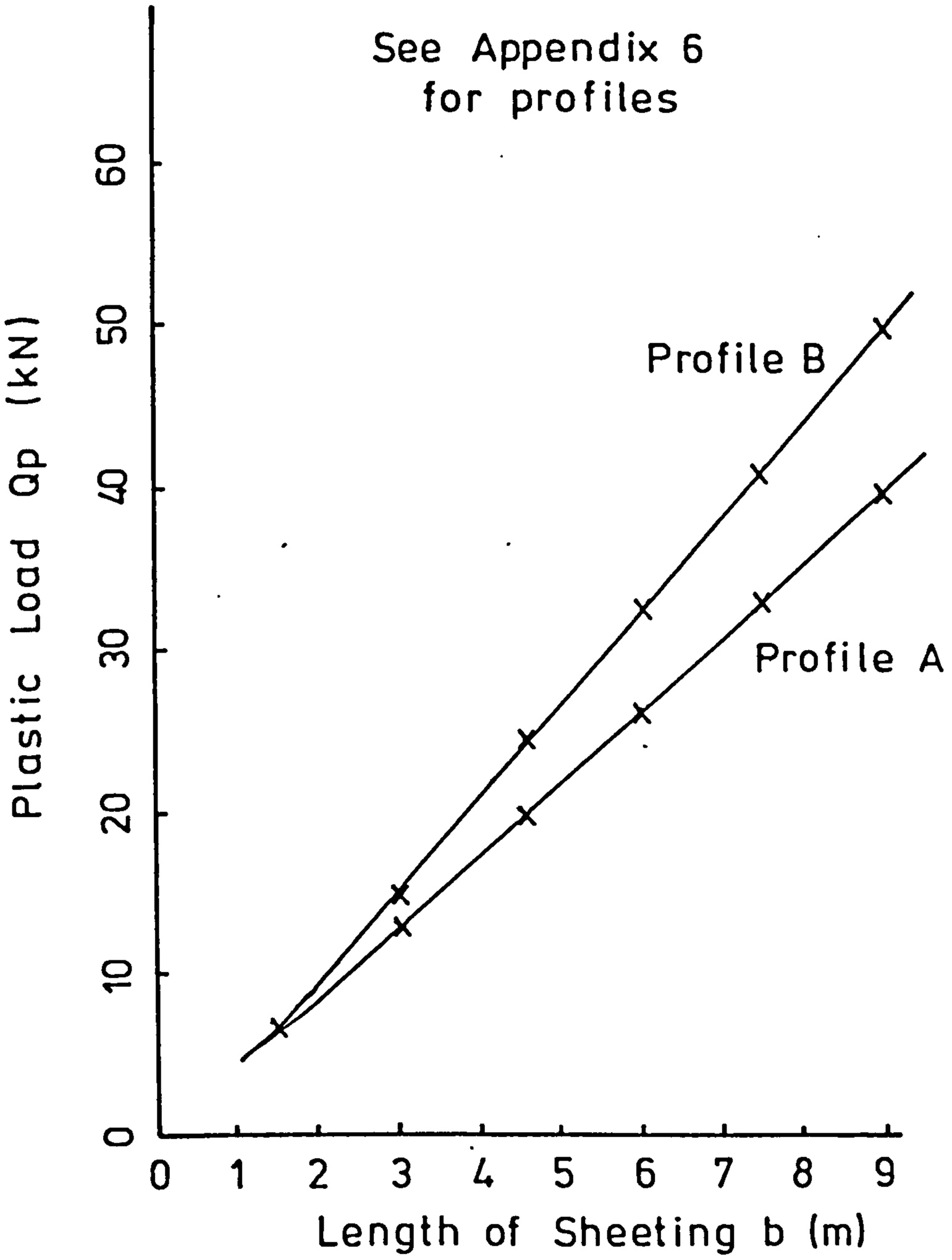

Fig 5.23 Variation of Qp against length
for profiles A and B (every case)

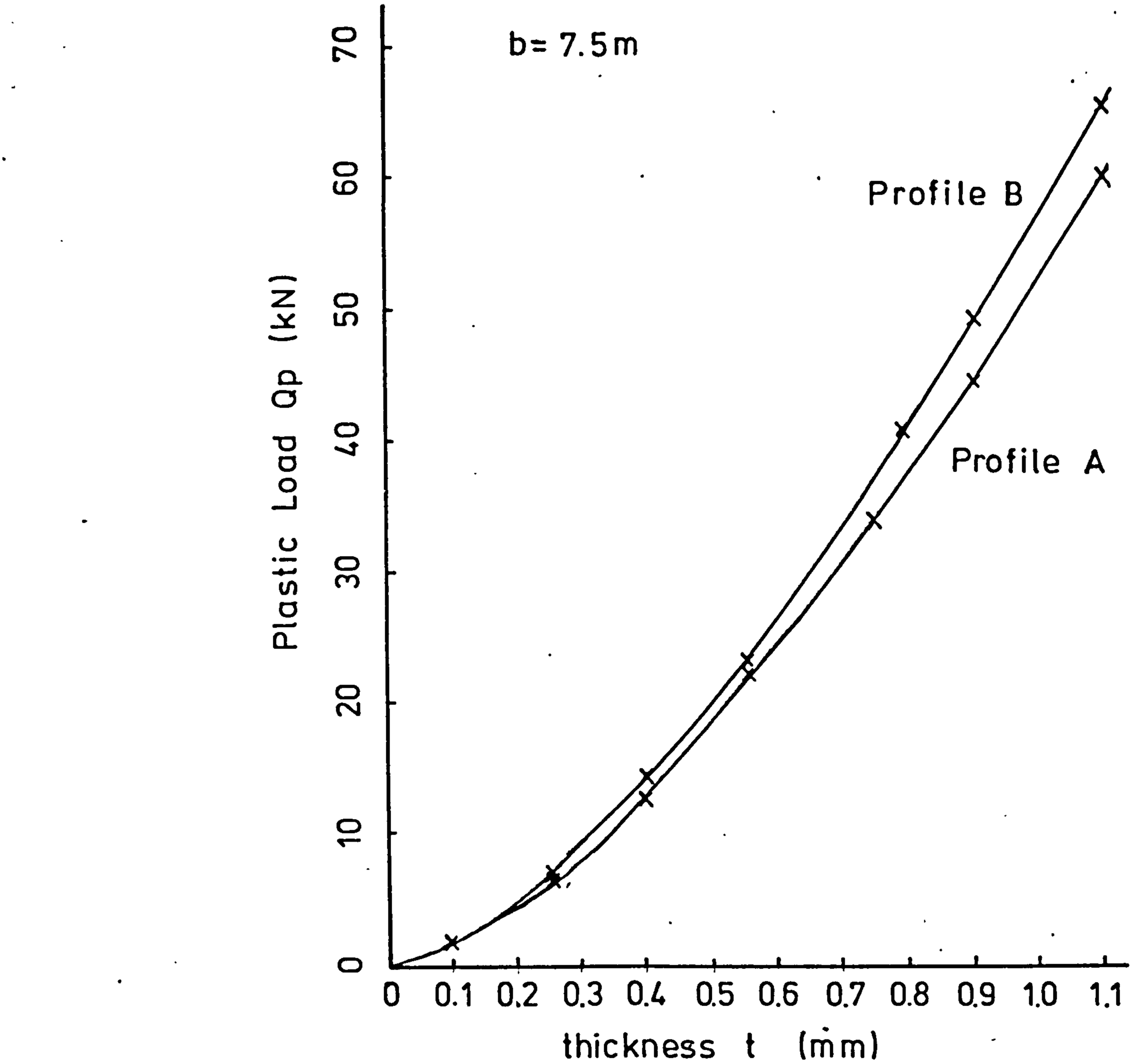

Fig 5.24 Variation of Qp against thickness for profiles A and B (every case)

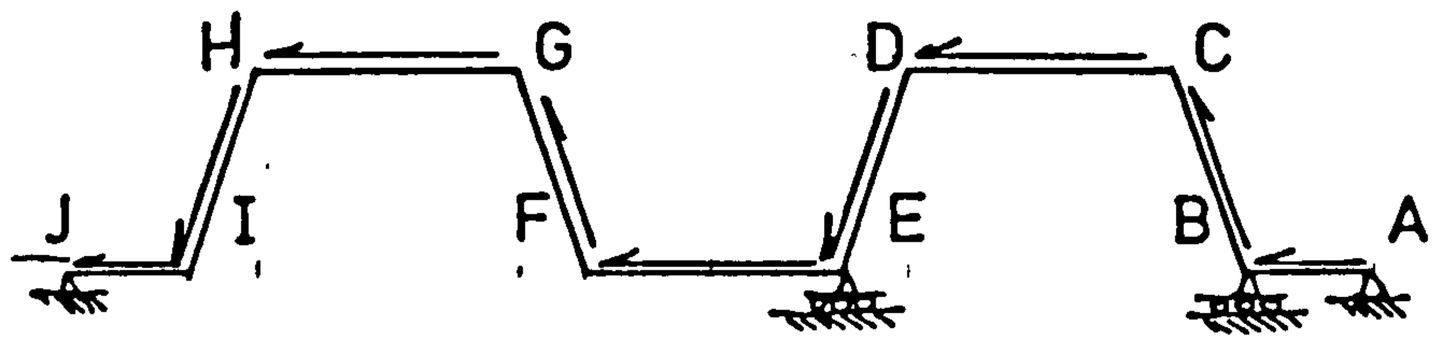

Fig 525 Notation and points of restraint for alternate corrugation

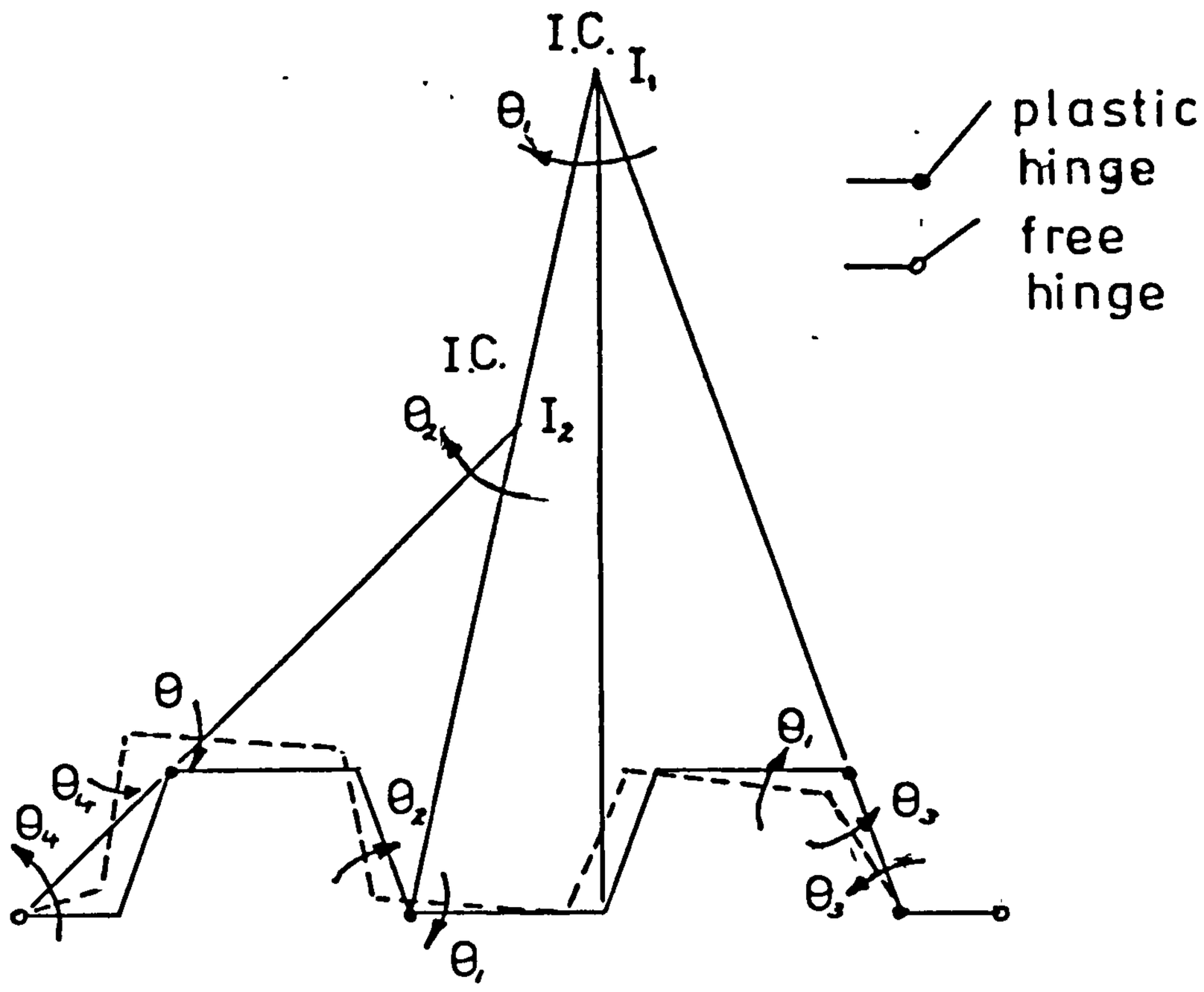

Fig 5.26a Alternate corrugation mechanism - rotations

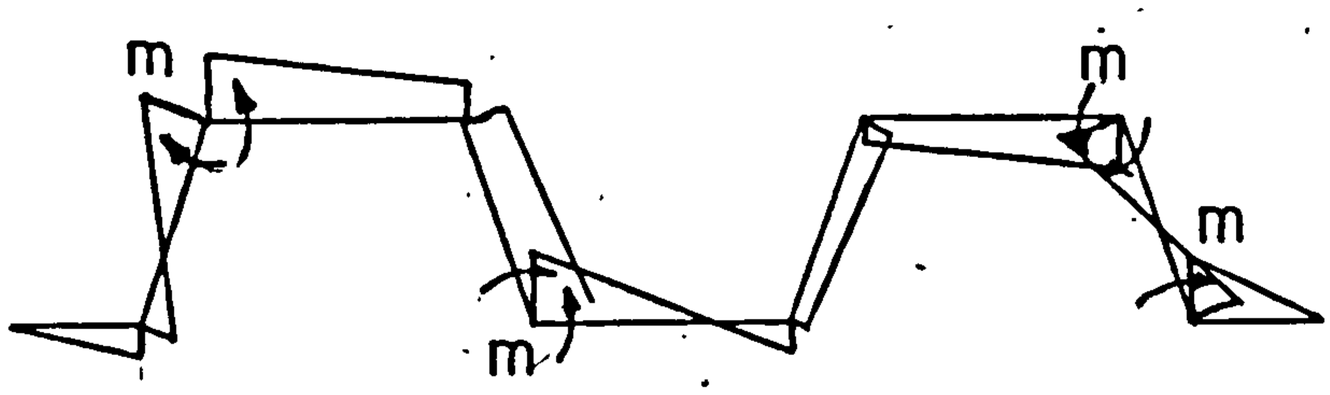

Fig 526b Alternate corrugation mechanism - moments

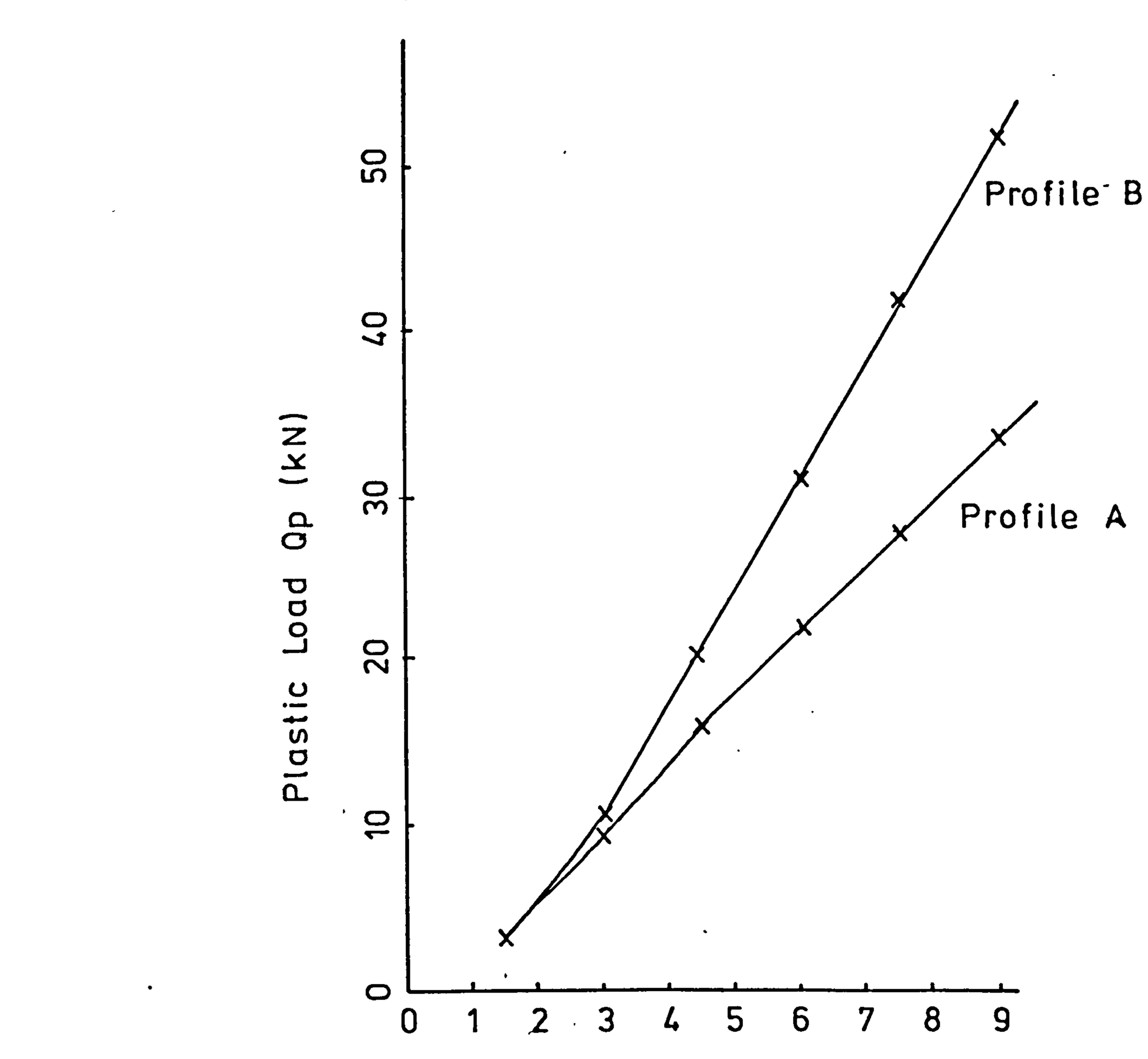

Fig 5.27 Variation of Qp against length for profiles A and B (alternate case)

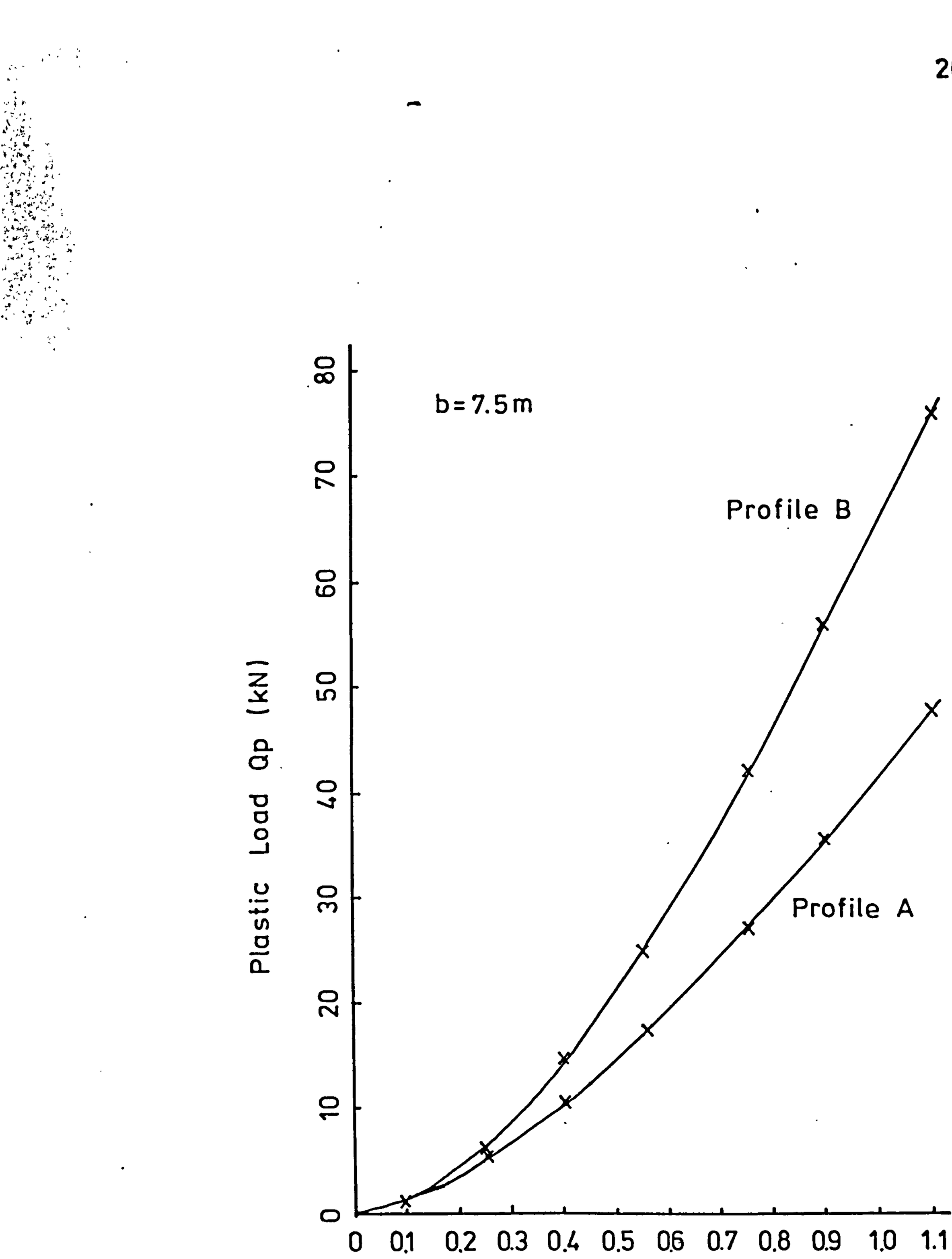

Fig 5.28 Variation of Qp against thickness for profiles A and B (alternate case)

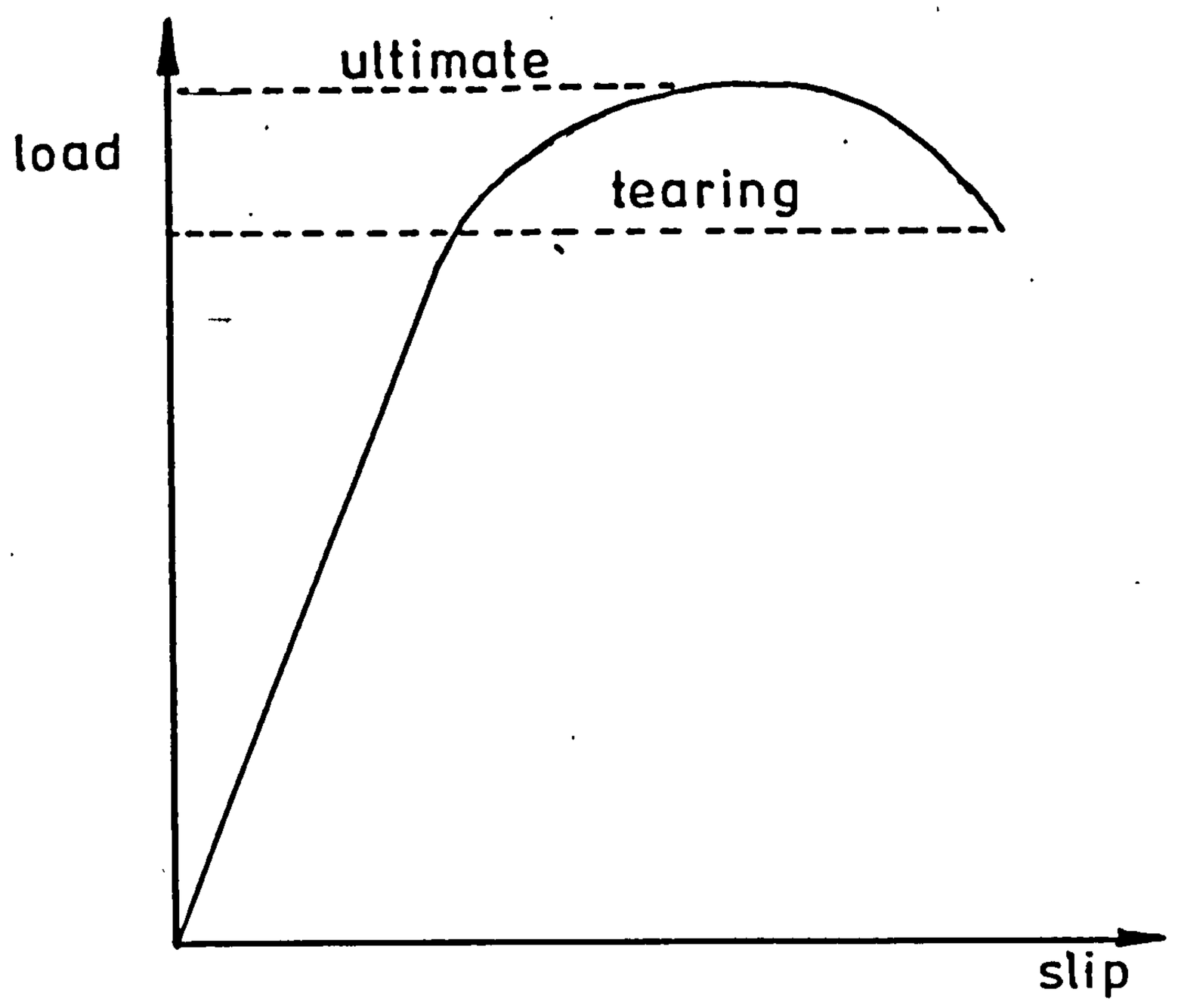

Fig 5.29 Load/slip characteristics of self-drilling fasteners

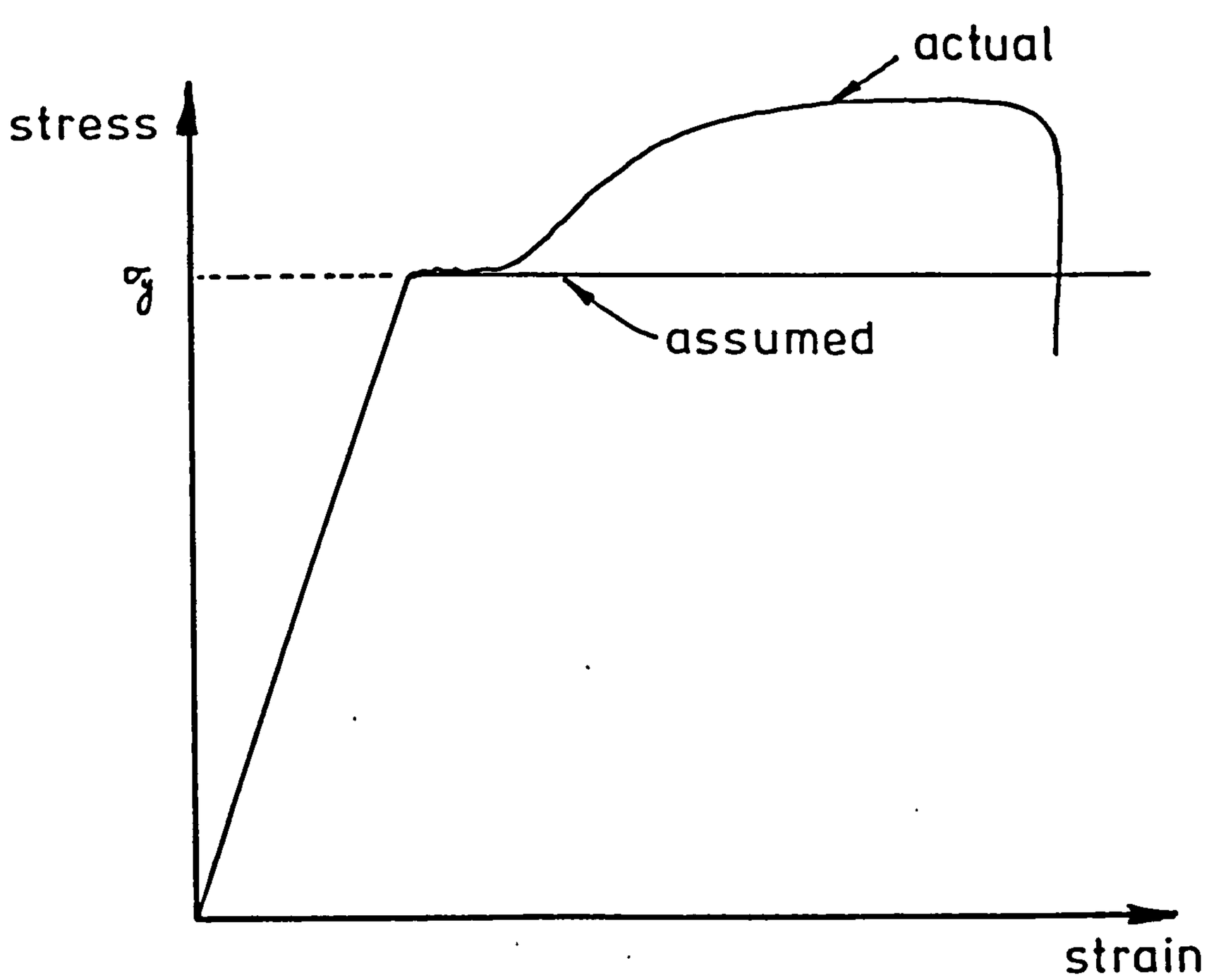

Fig 5.30 Idealised and actual stress/strain curve as applied to plastic mechanism

6. Conclusion to Thesis

6.1 Introduction

The work carried out in this thesis has been concerned with investigating certain aspects of "stressed skin theory". The areas of study have been concerned with the diaphragm action of composite slabs, the shear distortion of profiled sheeting and end failures in profiled steel diaphragms. As a result of this work, stressed skin theory has been extended to include further failure modes and the introduction of new materials namely, composite diaphragms into the theory.

6.2 Composite Diaphragms

For composite diaphragms, two types of fastener arrangements have been defined, namely :-

a. diaphragms in which the steel sheeting is fastened to the supporting structure and there is no direct attachment of the concrete to the supporting structure.

and b. diaphragms incorporating shear connectors. No work has been undertaken in this area although many buildings do incorporate composite beams in their construction.

The work in this study has been concerned with the first type and the following points can now be noted from the work :-

1. that expressions for the ultimate load of the composite slab have been presented and verified experimentally. Three failure modes have been identified and all three are possible in cantilever diaphragms. In the case of simply supported diaphragms only the first mode is

possible.

2. the flexibility of the diaphragm has been predicted for only the reloading of the slabs. For this condition the flexibility has been shown to be dependent on

   a. the elastic strain of the diaphragm

   b. the flexibility of the side fasteners

   c. the flexibility of the longitudinal fasteners

and d. the axial strain of the supporting structure.

The initial deformation of the slab was shown to include a non-linear portion which was found to be a result of the shrinkage of the concrete away from the sheeting.

3. that the composite slabs acting as horizontal diaphragms has a considerable influence on the distribution of the forces in multi-storey buildings. A computer model has been presented for analysing these buildings.

Further work is still required in the area of composite slabs before they can be an acceptable design material. These area s can be summarized as :-

   a. varying the aspect ratio of the diaphragm to verify further the above formulae.

and b. only slabs with self-drilling, self-tapping fasteners have been tested, whereas there are many fastener arrangements used, especially in North America where the practice is to use welded diaphragms, which have higher failure loads. Failure could then, not only occur in the fastener but in the concrete or at the connection between the steel and concrete.

As a consequence of the possibility of rotation of the composite slab over the supporting frame cantilever composite diaphragms behave differently from simply supported diaphragms. It is recommended that in further experimental studies simply supported diaphragms should be used despite the great increase in cost.

6.3 Shear Distortion of Profiled Sheeting

A Finite Strip Program has been written to analyse profiled sheeting under the action of a shear flow. At present there are two forms of analysis recognised, although, there are certain limitations apparent. The method that has been presented overcome these limitations, in that :-

a. more detailed information of deflections and stresses are available compared with the Energy Method (43), although consuming more computer time and storage.

and b. the method gives similar information to the Finite Element Method but produces this information in a reduced computer time for a similar machine.

A further advantage over the energy method is that non-linear plate movements are considered in the propped condition and they have been shown to predict the experimental and Finite Element results more accurately.

The influence of the edge member on the shear distortion has also been investigated and it can be concluded that, in the case of sheeting over five corrugations for the every corrugation fastened, and over six fastener spacings for the alternate corrugation case the edge member need not be considered.

6.4 End Failure of Profiled Steel Diaphragms

Profiled steel diaphragms have been shown to include additional failure modes in the region of the sheet/purlin fasteners, and together with the failure of these fasteners have been classified into "End Failures". From the work in the study there are a possibility of three failure modes, namely :-

a. failure by tearing of the sheeting at the sheet / purlin fasteners. Here the previous work has been extended to include the tension force acting on the fastener, as a result of the distortion of the profile. A shear / tension interaction curve for the sheet / purlin fastener has also been determined.

In order to avoid end failures the current European Recommendations [45] specify a 25% increase in strength for failure at the sheet / purlin fasteners. To deal with the effect of the tensile force, it has been shown that a more acceptable value could be a 12½% increase in strength for these fasteners.

b. failure by buckling of the profile web at the outermose purlin. An empirical expression for the buckling load has been developed incorporating a factor ℓ_{eff} based on test results.

c. failure by excessive distortion of the profile. The analysis has been based on the formation of a plastic mechanism in the profile, although as a result of the elastic portion of the sheeting it is not a pure mechanism. Design expressions for diaphragms with every and alternate corrugations fastened have been derived.

The last two failure modes are not primary modes as the diaphragm would still have load carrying capacity. They are therefore more in the nature of serviceability requirements.

Bending Stiffness Matrix :-

$$[BLO]_{mn} = \frac{1}{420\ b^3}$$

$5040\ Dx\ I_1$ $-504\ b^2\ D1\ I_2$ $-504\ b^2\ D1\ I_3$ $156\ b^4\ Dy\ I_4$ $2016\ b^2\ Dxy\ I_5$	$2520\ b\ Dx\ I_1$ $-462\ b^3\ D1\ I_2$ $-42\ b^3\ D1\ I_3$ $22\ b^5\ Dy\ I_4$ $168\ b^3\ Dxy\ I_5$	$-5040\ Dx\ I_1$ $504\ b^2\ D1\ I_2$ $504\ b^2\ D1\ I_3$ $54\ b^4\ Dy\ I_4$ $-2016\ b^2\ Dxy\ I_5$	$2520\ b\ Dx\ I_1$ $-42\ b^3\ D1\ I_2$ $-42\ b^3\ D1\ I_3$ $-13\ b^5\ Dy\ I_4$ $168\ b^3\ Dxy\ I_5$
$2520\ b\ Dx\ I_1$ $-462\ b^3\ D1\ I_3$ $-42\ b^3\ D1\ I_2$ $22\ b^5\ Dy\ I_4$ $168\ b^3\ Dxy\ I_5$	$1680\ b^2\ Dx\ I_1$ $-56\ b^4\ D1\ I_2$ $-56\ b^4\ D1\ I_3$ $4\ b^6\ Dy\ I_4$ $224\ b^4\ Dxy\ I_5$	$-2520\ b\ Dx\ I_1$ $42\ b^3\ D1\ I_2$ $42\ b^3\ D1\ I_3$ $13\ b^5\ Dy\ I_4$ $-168\ b^3\ Dxy\ I_5$	$840\ b^2\ Dx\ I_1$ $14\ b^4\ D1\ I_2$ $14\ b^4\ D1\ I_3$ $-3\ b^6\ Dy\ I_4$ $-56\ b^4\ Dxy\ I_5$
$-5040\ Dx\ I$ $504\ b^2\ D1\ I_2$ $504\ b^2\ D1\ I_3$ $54\ b^4\ Dy\ I_4$ $-2016\ b^2\ Dxy\ I_6$	$-2520\ b\ Dx\ I_1$ $42\ b^3\ D1\ I_2$ $42\ b^3\ D1\ I_3$ $13\ b^5\ Dy\ I_4$ $-168\ b^3\ Dxy\ I_5$	$5040\ Dx\ I_1$ $-504\ b^2\ D1\ I_2$ $-504\ b^2\ D1\ I_3$ $156\ b^4\ Dy\ I_4$ $2016\ b^2\ Dxy\ I_5$	$-2520\ b\ Dx\ I_1$ $462\ b^3\ D1\ I_2$ $42\ b^3\ D1\ I_3$ $-22\ b^5\ Dy\ I_4$ $-168\ b^3\ Dxy\ I_5$
$2520\ b\ Dx\ I$ $-42\ b^3\ D1\ I_2$ $-42\ b^3\ D1\ I_3$ $-13\ b^5\ Dy\ I_4$ $168\ b^3\ Dxy\ I_5$	$840\ b^2\ Dx\ I_1$ $14\ b^4\ D1\ I_2$ $14\ b^4\ D1\ I_3$ $-3\ b^6\ Dy\ I_4$ $-56\ b^4\ Dxy\ I_5$	$-2520\ b\ Dx\ I_1$ $462\ b^3\ D1\ I_3$ $42\ b^3\ D1\ I_2$ $-22\ b^5\ Dy\ I_4$ $-168\ b^3\ Dxy\ I_5$	$1680\ b^2\ Dx\ I_1$ $-56\ b^4\ D1\ I_2$ $-56\ b^4\ D1\ I_3$ $4\ b^6\ Dy\ I_4$ $224\ b^4\ Dxy\ I_5$

$$[PLO2]_{mn} = t * \begin{array}{|c|c|c|c|} \hline K1 * L1 / B & -K2 * L1 / 2 & -K1 * L1 / B & -K2 * L2 / 2 \\ +K4 * B * L4 / 3 & -K4 * L3 / 2 & +K4 * B * L4 / 6 & +K4 * L3 / 2 \\ \hline -K2 * L5 / 2 & K3 * L7 * B / 3 & K2 * L5 / 2 & K3 * L7 * B / 6 \\ -K4 * L6 / 2 & +K4 * L8 / B & -K4 * L6 / 2 & -K4 * L8 / B \\ \hline -K1 * L1 / B & K2 * L2 / 2 & K1 * L1 / B & K2 * L2 / 2 \\ +K4 * B * L4 / 6 & -K4 * L3 / 2 & +K4 * L4 * B / 3 & +K4 * L3 / 2 \\ \hline -K2 * L5 / 2 & K3 * L7 * B / 6 & K5 * L5 / 2 & K3 * B * L7 / 3 \\ +K4 * L6 / 2 & -K4 * L8 / B & +K4 * L6 / 2 & K4 * L8 / B \\ \hline \end{array}$$

K1 = Ex / (1 - νx νy); K3 = EY / (1 - νx νy); K2 = νx Ey / (1 - νx νy); K4 = Gxy

$$[B]_m =$$

$-\frac{Y_m}{b}$	0	0	0	Y_m/b	0	0	0
0	$(1-\bar{x})X_m'$	0	0	0	$\bar{x}X_m'$	0	0
$(1-\bar{x})Y_m'$	$-\frac{X_m}{b}$	0	0	$\bar{x}Y_m'$	X_m/b	0	0
0	0	$\frac{6}{b^2}(1-2\bar{x})Y_m$	$\frac{2}{b}(2-3\bar{x})Y_m$	0	0	$\frac{6}{b^2}(-1+2\bar{x})Y_m$	$\frac{2}{b}(1-3\bar{x})Y_m$
0	0	$-(1-3\bar{x}^2+2\bar{x}^3)Y_m''$	$-x(1-2\bar{x}+\bar{x}^2)Y_m''$	0	0	$-(3\bar{x}^2-2\bar{x}^3)Y_m''$	$-x(\bar{x}^2-\bar{x})Y_m''$
0	0	$\frac{2}{b}(-6\bar{x}+6\bar{x}^2)Y_m'$	$2(1-4\bar{x}+3\bar{x}^2)Y_m'$	0	0	$\frac{2}{b}(6\bar{x}-6\bar{x}^2)Y_m'$	$2(3\bar{x}^2-2\bar{x})Y_m'$

Folded Plate Strain Matrix

$$[BO]_{mn} =$$

PLO2(1,1)	PLO2(1,2)	0	0	PLO2(1,3)	PLO2(1,4)	0	0
PLO2(2,1)	PLO2(2,2)	0	0	PLO2(2,3)	PLO2(2,4)	0	0
0	0	BLO(1,1)	BLO(1,2)	0	0	BLO(1,3)	BLO(1,4)
0	0	BLO(2,1)	BLO(2,2)	0	0	BLO(2,3)	BLO(2,4)
PLO2(3,1)	PLO2(3,2)	0	0	PLO2(3,3)	PLO2(3,4)	0	0
PLO2(4,1)	PLO2(4,2)	0	0	PLO2(4,3)	PLO2(4,4)	0	0
0	0	BLO(3,1)	BLO(3,2)	0	0	BLO(3,3)	BLO(3,4)
0	0	BLO(4,1)	BLO(4,2)	0	0	BLO(4,3)	BLO(4,4)

Folded Plate Stiffness Matrix for each term

Appendix 2 -
Product integrals for bending and plane stress matrices

Applying the principle of minimum potential energy we obtain the stiffness matrices given in Appendix 1. From the matrices a number of product integrals were obtained and the explicit solution to these twelve expressions are now given. Where expressions for the integrals are not given the values are to be assumed zero.

Bending Integrals

$$I_1 = \int_0^b Y_m . Y_n \, dy$$

$$\mu_m = (m-2)\pi$$
$$\mu_n = (n-2)\pi$$

$m = n = 1$

$$I_1 = \int_0^b 1 . 1 \, dy = b$$

$m = 1 \quad n = 3$ or more

$$I_1 = \int_0^b 1 . \sin \frac{\mu_n y}{a} \, dy$$

$$= \frac{b}{\mu_n}\left[1 - \cos \mu_n\right]$$

$m = 3$ or more $\quad n = 1$

$$I_1 = \int_0^b \sin \frac{\mu_m y}{b} . 1 \, dy$$

$$= \frac{b}{\mu_m}\left[1 - \cos\mu_m\right]$$

$m = 2 \quad n = 3$ or more

$$I_1 = \int_0^b \left(1 - \frac{2y}{b}\right) \sin\frac{\mu_n y}{b}\, dy$$

$$= \frac{b}{\mu_n}\left[1 + \cos\mu_n\right]$$

$m = 3$ or more $\quad n = 2$

$$I_1 = \int_0^b \sin\frac{\mu_m y}{b} \cdot \left(1 - \frac{2y}{b}\right) dy$$

$$= \frac{b}{\mu_m}\left[1 + \cos\mu_m\right]$$

$m = 3 \quad n = 3$ or more

$$I_1 = \int_0^b \sin\frac{\mu_m y}{b} \sin\frac{\mu_n y}{b}\, dy$$

$$= \frac{b}{2}$$

$$I_2 = \int_0^b Y_m'' \cdot Y_n\, dy$$

$m = 3$ or more $\quad n = 1$

$$I_2 = \int_0^b -\left(\frac{\mu_m}{b}\right)^2 \sin\frac{\mu_m y}{b}\, dy$$

$$= -\left(\frac{\mu_m}{b}\right)^2 \left(1 - \cos\mu_m\right)$$

$m = 3$ or more $\quad n = 2$

$$I_2 = \int_0^b -\left(\frac{\mu_m}{b}\right)^2 \sin \frac{\mu_m y}{b} \cdot \left(1 - \frac{2y}{b}\right) dy$$

$$= -\frac{\mu_m}{b}\left[1 + \cos \mu_m\right]$$

$m = n = 3$ or more

$$I_2 = \int_0^b -\left(\frac{\mu_m}{b}\right)^2 \sin \frac{\mu_m y}{b} \cdot \sin \frac{\mu_n y}{b} \, dy$$

$$= -\left(\frac{\mu_m}{b}\right)^2 \frac{b}{2}$$

$$I_3 = \int_0^b Y_m Y_n'' \, dy$$

$m = 1 \quad n = 3$ or more

$$I_3 = \int_0^b \left(-\frac{\mu_n}{b}\right)^2 \sin \frac{\mu_n y}{b} \, dy$$

$$= -\left(\frac{\mu_n}{b}\right)^2 \left[1 - \cos \mu_n\right]$$

$m = 2 \quad n = 3$ or more

$$I_3 = \int_0^b -\left(1 - \frac{2y}{b}\right)\left(\frac{\mu_n}{b}\right)^2 \sin \frac{\mu_n y}{b} \, dy$$

$$= -\left(\frac{\mu_n}{b}\right)\left[1 + \cos \mu_n\right].$$

$m = n = 3$ or more

$$I_3 = \int_0^b -\left(\frac{\mu_n}{b}\right)^2 \sin\frac{\mu_n y}{b} \sin\frac{\mu_m y}{b}\, dy$$

$$= -\left(\frac{\mu_n}{b}\right)^2 \frac{b}{2}$$

$$I_4 = \int_0^b Y_m'' Y_n''\, dy$$

$m = n = 3$ or more

$$I_4 = \int_0^b \left(\frac{\mu_m}{b}\right)^4 \sin\frac{\mu_m y}{b} \cdot \sin\frac{\mu_n y}{b}\, dy$$

$$= \left(\frac{\mu_m}{b}\right)^4 \frac{b}{2}$$

$$I_5 = \int_0^b Y_m' Y_n'\, dy$$

$m = n = 2$

$$I_5 = \int_0^b \left(-\frac{2}{b}\right)\left(-\frac{2}{b}\right) dy$$

$$= \frac{4}{b}$$

$m = n = 3$ or more

$$I_5 = \int_0^b \left(\frac{\mu_m}{b}\right)^2 \sin\frac{\mu_m y}{b} \sin\frac{\mu_n y}{b}\, dy$$

$$= \left(\frac{\mu_m}{b}\right)^2 \frac{b}{2}.$$

Plane Stress Integrals

$$L_1 = \int_0^b Y_m Y_n \, dy$$

as for I_1

$$L_2 = \int_0^b Y_m X_n' \, dy$$

$m = n = 1$

$$L_2 = \int_0^b 1 \cdot -\frac{2}{b} \, dy$$

$$= -b$$

$m = 1 \quad n = 3$ or more

$$L_2 = \int_0^b 1 \cdot \left(-\frac{\mu_n}{b}\right) \sin \frac{\mu_n y}{b} \, dy$$

$$= \cos \mu_n - 1$$

$m = 2 \quad n = 3$ or more

$$L_2 = \int_0^b \left(1 - \frac{2y}{b}\right)\left(-\frac{\mu_n}{b}\right) \sin \frac{\mu_n y}{b} \, dy$$

$$= -\left(1 + \cos \mu_n\right)$$

$m = 3$ or more $\quad n = 1$

$$L_2 = \int_0^b \sin \frac{\mu_m y}{b} \left(-\frac{2}{b}\right)$$

$$= -\frac{2}{\mu_m}\left[1 - \cos \mu_m\right]$$

$m = n = 3$ or more

$$L_2 = \int_0^b \sin \frac{\mu_m y}{b} \left(-\frac{\mu_n}{b}\right) \sin \frac{\mu_n y}{b}\, dy$$

$$= -\frac{\mu_m}{2}$$

$$L_3 = \int_0^b X_n Y_m'\, dy$$

$m = 3$ or more $\quad n = 1.$

$$L_3 = \int_0^b \left(\frac{\mu_m}{b}\right) \cos \frac{\mu_m y}{b}\, dy$$

$$= \frac{2}{\mu_m}\left(1 - \cos \mu_m\right)$$

$m = n = 2$

$$L_3 = \int_a^b 1 \cdot \left(-\frac{2}{b}\right) dy$$

$$= -2$$

$m = n = 3$ or more

$$L_3 = \int_0^b \cos \frac{\mu_n y}{b} \cdot \left(\frac{\mu_m}{b}\right) \cos \frac{\mu_m y}{b}\, dy$$

$$= \frac{\mu_m}{b}$$

$$L_4 = \int_0^b Y_m' Y_n'\, dy$$

as for I_5

$$L_5 = \int_0^b X_m' Y_n \, dy$$

$m = n = 1$

$$L_5 = \int_0^b \left(-\frac{2}{b}\right) dy$$

$$= -2$$

$m = 1 \quad n = 3$ or more

$$L_5 = \int_0^b \left(-\frac{2}{b}\right) \sin \frac{\mu_n y}{b} \, dy$$

$$= -\frac{2}{\mu_n}\left[1 - \cos \mu_n\right]$$

$m = 3$ or more $\quad n = 1$

$$L_5 = \int_0^b -\left(\frac{\mu_m}{b}\right) \sin \frac{\mu_m y}{b} \, dy$$

$$= \left[\cos \mu_m - 1\right]$$

$m = 3$ or more $\quad n = 2$

$$L_5 = \int_0^b \left(-\frac{\mu_m}{b}\right) \sin \frac{\mu_m y}{b}\left(1 - \frac{2y}{b}\right) dy$$

$$= -\left[1 + \cos \mu_m\right]$$

$m = n = 3$ or more

$$L_5 = \int_0^b \left(\frac{\mu_m}{b}\right) \sin \frac{\mu_n y}{b} \sin \frac{\mu_n y}{b} \, dy$$

$$= -\frac{\mu_m}{2}$$

$$L_6 = \int_0^b X_m Y_n' \, dy$$

$m = 1 \quad n = 3$ or more

$$L_6 = \int_0^b \left(1 - \frac{2y}{b}\right)\left(\frac{\mu_n}{b}\right) \cos \frac{\mu_n y}{b} \, dy$$

$$= \frac{2}{\mu_n}\left[1 - \cos \mu_n\right]$$

$m = n = 2$

$$L_6 = \int_0^b 1 \cdot \left(-\frac{2}{b}\right) dy$$

$$= -2$$

$m = n = 3$ or more

$$L_6 = \int_0^b \cos \frac{\mu_n y}{b}\left(\frac{\mu_m}{b}\right) \cos \frac{\mu_n y}{b} \, dy$$

$$= \frac{\mu_m}{2}$$

$$L_7 = \int_0^b X_m' \, X_n' \, dy$$

$m = n = 1$

$$L_7 = \int_0^b \left(-\frac{2}{b}\right)\left(-\frac{2}{b}\right) dy$$

$$= \frac{4}{b}$$

$m = 1 \quad n = 3$ or more

$$L_7 = \int_0^b \left(-\frac{2}{b}\right)\left(-\frac{\mu_n}{b}\right) \sin \frac{\mu_n y}{b} \, dy$$

$$= \frac{2}{b}(1-\cos\mu_n)$$

$m = 3$ or more $\quad n = 1$

$$L_7 = \int_0^b \left(-\frac{\mu_m}{b}\right) \sin\frac{\mu_m y}{b} \left(-\frac{2}{b}\right) dy$$

$$= \frac{2}{b}\left[1-\cos\mu_m\right]$$

$m = n = 3$ or more

$$L_7 = \int_0^b -\left(\frac{\mu_m}{b}\right) \sin\frac{\mu_m y}{b} \left(-\frac{\mu_n}{b}\right) \sin\frac{\mu_n y}{b}\, dy$$

$$= \left(\frac{\mu_m}{b}\right)^2 \frac{b}{2}$$

$$L_8 = \int_0^b X_m X_n\, dy$$

$m = n = 1$

$$L_8 = \int_0^b \left(1-\frac{2y}{b}\right)^2 dy$$

$$= \frac{b}{3}$$

$m = 1 \quad n = 3$ or more

$$L_8 = \int_0^b \left(1-\frac{2y}{b}\right) \cos\frac{\mu_n y}{b}\, dy$$

$$= \frac{2b}{\mu_n^2}\left(1-\cos\mu_n\right)$$

$m = 3$ or more $\quad n = 1$

$$L_8 = \int_0^b \cos\frac{\mu_m y}{b}\left(1 - \frac{2y}{b}\right) dy$$

$$= \frac{2b}{\mu_m^2}\left[1 - \cos\mu_m\right]$$

$m = n = 2$

$$L_8 = \int_0^b 1 \cdot 1 \, dy$$

$$= b$$

$m = n = 3$ or more

$$L_8 = \int_0^b \cos\frac{\mu_m y}{b} \cos\frac{\mu_n y}{b} \, dy$$

$$= \frac{b}{2}$$

```
C   ***************************************************************
C
C        FINITE  STRIP  PROGRAM  DEVELOPED  BY  J.FISHER
C        THAT CAN BE  USED TO  ANALYSE
C             (1)  BENDING  ONLY  PROBLEMS
C             (2)  PLANE  STRESS  ONLY  PROBLEMS
C             (3)  FOLDED  PLATE  PROBLEMS
C             (4)  DISTORTION  OF  CORRUGATED  PROFILES
C
C   ***************************************************************
      PROGRAM STRIP(INPUT,OUTPUT,MAG1,MAG2,MAG3,
     2TAPE1=INPUT,TAPE2=OUTPUT,
     1TAPE3=MAG1,TAPE4=MAG2,TAPE5=MAG3)
      DIMENSION SS(96,96),BLO(4,4),PLO2(4,4),F(4),BETA(100)
     1,SK(96,96),FF(96,2),FK(96),R(2000),FX(56),SB(6,8),SR(6)
     2,RI(8,8),RIT(8,8),BOL(8,8),POL2(8,8),FQ(4),XZ(100)
     3,AC(2000),XF(10,10),DELTA(10),AX(10),AY(10),IZ(10)
     4,XU(100),XV(10,10),ZZ(10),RR(2000),H(100),AL(100),K5(100)
     5,QZ(100),QU(100),QB(100),RS(8),OB(8,8),BO(8,8),BG(2000,7)
     6,RRS(8),AB(30)
      COMMON /BL2/FK,R/BL3/RI,RIT/BL1/SS,SK/BL60/AC
     +/BL4/BLO/BL5/PLO2/BL6/I1,I2,I3,I4,I5/BL8/LL
     +/BL10/IR,X2,X3,Y1,Y2,JO,NV,NA,K5/BL12/IZ,AX,AY
      REAL I1,I2,I3,I4,I5,J1,K,NC,K1,K2,K3,K4
      LEVEL 2,SS,SK,AC
      DATA NNN,LZ,LV/1,0,0/,XX,T1,A2,B1,NC,QY1,Q1,
     1P1,XI1,YI1/10*0.0/,IA,JA,IL,JL/100,100,100,100/
900   READ (1,20) LL,NN1,NN2,N3,IP
20    FORMAT (5I2)
      IF (LL.LT.0) GO TO 999
      XX=0.0
      READ (1,5) (AB(I),I=1,15)
5     FORMAT (1X,15A4)
      WRITE (2,10)
10    FORMAT (1H1,///,19X,46(1H*),/,19X,12H**********  ,
     134HFINITE  STRIP  PROGRAM  **********,/,19X,46(1H*),///)
      WRITE (2,15) (AB(I),I=1,15)
15    FORMAT (1H ,10X,15A4///)
C
C     LL=0   BENDING
C     LL=1   PLANE
C     LL=2   BENDING + PLANE
C     NN1=0    U.D.L.
C     NN1=1   POINT LOAD
C     NN1=2   PROPPING
C     NN1=3   NODAL  FORCES
C     NN1=4   DISTORTION OF PROFILE
C     NN1=5   DATA  GENERATOR FOR SHELL ROOFS
C     NN2=0   LIMITED OUTPUT
C     NN2=1   SK MATRIX AND K MATRIX ALSO OUTPUT
C     N3=0   SYMMETRICAL
C     N3=1   UN-SYMMETRICAL
C
      INPROP=1
      AQ=40.
      IR=1
```

```
      H(1)=0.0
      AL(1)=0.0
      IF (NN1.NE.5) GO TO 643
C
C     READ  STATEMENT  FOR  CYLINDRICAL  SHELLS
C
      READ (1,642) E,PV,A,RE,T,NS,MM,Q,Q2
642   FORMAT (F10.2,F3.1,3F10.2,2I4,2F10.2)
      QX=0.0
643   IF (LL.EQ.0) GO TO 25
      IF (LL.EQ.1) GO TO 25
      IF (LL.EQ.2) GO TO 30
      GO TO 999
25    N1=4
      N2=2
      GO TO 35
30    N1=8
      N2=4
35    IF (N3.EQ.0) GO TO 640
      IF (N3.EQ.1) GO TO 645
      GO TO 999
640   NCC=2
      GO TO 655
645   NCC=1
655   IF (NN1.NE.5) GO TO 644
      CALL CYMESH (NS,AQ,RE,NEC,II,JJ,XSUM,XSUM1)
      GO TO 44
644   READ (1,40) E,NS,PV,A,MM,T,Q,QX,Q2
40    FORMAT (F10.2,I2,F3.1,F10.4,I4,F10.5,3F10.8)
      READ (1,45) X3,X2,Y1,Y2
45    FORMAT (4F10.2)
44    IH=N1*MM
      IG=IH/2
      H(NNN+1)=Y2-Y1
      AL(NNN+1)=X2-X3
      B=SQRT((H(NNN+1)**2)+(AL(NNN+1)**2))
      IF (NNN.EQ.1.AND.NN1.EQ.4) QX=1./A
      QZ(NNN)=Q*1000.
      QU(NNN)=Q2*1000.
      QB(NNN)=0.0
      IF (NN1.NE.3) QB(NNN)=QX*1000.
      QB(NS+1)=0.0
      IF (NN1.EQ.3) QB(NS+1)=QX*1000.
      ID=1.5*IH
      IF (AL(NNN+1).LT.0.0.AND.H(NNN+1).EQ.0.0) GO TO 56
      IF (AL(NNN+1).EQ.0.0.AND.H(NNN+1).LT.0.0) GO TO 54
      IF (AL(NNN+1).EQ.0.0.AND.H(NNN+1).GT.0.0) GO TO 559
      BETA(NNN)=ATAN (H(NNN+1)/AL(NNN+1))
      GO TO 53
56    BETA(NNN)=2*1.5707963
      GO TO 53
54    BETA(NNN)=-1.5707963
      GO TO 53
559   BETA(NNN)=1.5707963
53    IF(E.LE.0.0) GO TO 999
      IF(XX.NE.0.0) GO TO 51
```

```
      NX=N2*MM*(NS+1)
      IF (NX.GT.2000) WRITE (2,950)
950   FORMAT (1X,32HSTORAGE  TO  SMALL  FOR  PROBLEM)
824   WRITE (2,55) NS,MM
55    FORMAT (1X,24HNUMBER  OF  STRIPS     -,I2,//,1X,
     124HNUMBER  OF  HARMONICS  -,I4,///)
51    PK=1.0
50    IF (NNN.NE.1) GO TO 61
      WRITE (2,60)
60    FORMAT (1X,12H STRIP  DATA,/,1X,7H  STRIP,7X,6HLENGTH,7X,
     15HWIDTH,7X,9HTHICKNESS,4X,16HELASTIC  MODULAS,3X,
     216HPOISSON'S  RATIO,10X,4HBETA,9X,2HPK,/,16X,4H(MM),8X,
     34H(MM),10X,4H(MM),9X,10H(KN/MM**2),31X,9H(RADIANS),/)
61    WRITE (2,62) NNN,A,B,T,E,PV,BETA(NNN),PK
62    FORMAT (1X,2X,I3,5X,F10.1,3X,F10.1,3X,F10.2,7X,F10.3,13X,
     1F3.1,16X,F7.4,8X,F3.1)
      DO 71 I=1,IH
71    FF(I,2)=0.0
      IF (XX.NE.0.0) GO TO 65
      DO 70 I=1,IH
      DO 72 II=1,2
72    FF(I,II)=0.0
      FX(I)=0.0
      DO 70 J=1,IH
      SK(I,J)=0.0
70    SS(I,J)=0.0
      NX=N2*MM*(NS+1)
      DO 75 I=1,IH
75    FK(I)=0.0
65    G=E/(2.0*(1.+PV))
      DX=PK*E*(T**3.)/(12.*(1.-(PV**2.)))
      DY=DX
      D1=PV*DX
      DXY=G*PK*(T**3.)/12.
      IF (NN1.EQ.5) GO TO 81
      READ (1,80) NEC,II,JJ,IHOLD,JHOLD,NPROP
80    FORMAT (6I2)
      K5(NNN)=IHOLD
      IF (NNN.EQ.NS) K5(NNN+1)=JHOLD
81    IF (NN1.NE.1) GO TO 85
      READ (1,90) XI,YI,P
85    IF (XX.EQ.0.0) GO TO 95
      IF(T.NE.T1)GO TO 95
      IF(A.NE.A2)GO TO 95
      IF(B.NE.B1)GO TO 95
      IF(Q.NE.Q1) GO TO 95
      IF (Q2.NE.QY1) GO TO 95
      IF(QX.NE.QX1) GO TO 95
      IF (IP.NE.0) GO TO 95
       IF (BETA(NNN).NE.BETA(NNN-1)) GO TO 95
      IF (NN1.NE.1) GO TO 95
      IF (XI.NE.XI1) GO TO 95
      IF (YI.NE.YI1) GO TO 95
      IF (P.NE.P1) GO TO 95
      IF (IP.NE.0) GO TO 95
      GO TO 100
```

```
95      DO 105 I=1,IH
        DO 73 II=1,2
73      FF(I,II)=0.0
        FX(I)=0.0
        DO 105 J=1,IH
        SS(I,J)=0.0
        SK(I,J)=0.0
105     CONTINUE
        DO 104 I=1,4
104     FQ(I)=0.0
        XX=1.0
        DO 110 M=1,MM
        DO 110 N=1,MM
14      CALL INTE (A,NEC,M,N)
        IF (LL.EQ.1) GO TO 115
C
C        BENDING  STIFFNESS  MATRIX,  COMPATIBILITY OF SLOPE
C
        CALL BENDLO2 (B,DX,DY,D1,DXY)
        IF (NN1.EQ.1) GO TO 120
C
C        FORCE  MATRIX  FOR  U.D.L
C
        BET=BETA(NNN)
        CALL FORCE (Q,Q2,B,M,NEC,A,F,BET,FQ,LL,NCC)
        GO TO 115
C
C        FORCE  MATRIX  FOR DISTORTION  OF  PROFILES
C
90      FORMAT (3F10.3)
C
C        FORCE  MATRIX  FOR  POINT  LOAD
C
120     CALL POINT (P,B,A,XI,YI,F,NEC,M)
115     E1=E
        PV1=PV
        IF (LL.EQ.0) GO TO 125
C
C        PLANE STRESS  STIFFNESS  MATRIX
C
        CALL PLANL02 (E,E1,PV,PV1,G,B,A,T,NEC,M,N,K1,K2,K3,K4)
        IF (NN1.LE.2.OR.NN1.GT.5) GO TO 125
C
C        FORCE  MATRIX  FOR  NODAL  U.D.L.
C
        CALL PFORCE (QX,B,M,NEC,A,FQ,NCC)
125     IF (LL.NE.0) GO TO 160
150     DO 175 I=1,4
        NI=4*(M-1)+I
        IF (N.GT.1) GO TO 180
        FX(NI)=FX(NI)+F(I)
180     DO 175 J=1,4
        NJ=4*(N-1)+J
175     SS(NI,NJ)=SS(NI,NJ)+BLO(I,J)
        GO TO 110
160     IF(LL.EQ.2) GO TO 185
```

```
      DO 200 I=1,4
      NI=4*(M-1)+I
      IF (N.GT.1) GO TO 205
      FX(NI)=FX(NI)+FQ(I)
205   DO 200 J=1,4
      NJ=4*(N-1)+J
200   SS(NI,NJ)=SS(NI,NJ)+PLO2(I,J)
      GO TO 110
C
C       FORMATION  OF  FOLDED  PLATE  STIFFNESS  MATRIX
C
185   CALL COMB (BO,PLO2,BLO)
      BET=BETA(NNN)
      CALL ENT (BET,LL)
      CALL XMULT (8,8,8,BO,RIT,OB)
      CALL XMULT (8,8,8,RI,OB,BO)
      DO 112 I=1,8
      NI=8*(M-1)+I
      IF (N.GT.1) GO TO 113
      IF (I.LE.2) GO TO 106
      IF (I.LE.4) GO TO 107
      IF (I.LE.6) GO TO 108
      FX(NI)=FX(NI)+F(I-4)
      GO TO 113
106   FX(NI)=FX(NI)+FQ(I)
      GO TO 113
107   FX(NI)=FX(NI)+F(I-2)
      GO TO 113
108   FX(NI)=FX(NI)+FQ(I-2)
113   DO 112 J=1,8
      NJ=8*(N-1)+J
 112  SS(NI,NJ)=SS(NI,NJ)+BO(I,J)
110   CONTINUE
      LV=0
      LZ=0
C
C       RE-ARRANGEMENT  OF  INDIVIDUAL  STIFFNESS  MATRIX  FROM
C       HARMONIC  BASED  SYSTEM  TO  A  NODAL  BASED  SYSTEM
C
      IF(MM.EQ.1) GO TO 285
      KY=0
290   DO 295 I=1,MM
      KX=0
300   IF(KY.EQ.1) GO TO 305
      IS=(I*N2-N2)*2
      IX=(I-1)*N2
      I7=IS
      I8=IX
      GO TO 310
305   IS=(I*2-1)*N2
      IX=(I-1+MM)*N2
      I7=IS
      I8=IX
310   IF(KX.EQ.1) GO TO 315
      DO 325 III=1,N2
      IF(III.NE.1) GO TO 320
```

```
      IS=I7
      IX=I8
320   IS=IS+1
      IX=IX+1
325   FF(IX,1)=FF(IX,1)+FX(IS)
315   DO 330 J=1,MM
      IF(KX.EQ.1) GO TO 335
      JS=(J*N2-N2)*2
      IY=(J-1)*N2
      I9=JS
      I10=IY
      GO TO 340
335   JS=(J*2-1)*N2
      IY=(J-1+MM)*N2
      I9=JS
      I10=IY
340   DO 345 III=1,N2
      IF(III.NE.1) GO TO 350
      IS=I7
      IX=I8
350   IS=IS+1
      IX=IX+1
      DO 355 JJ=1,N2
      IF(JJ.NE.1) GO TO 360
      JS=I9
      IY=I10
360   JS=JS+1
      IY=IY+1
355   SK(IX,IY)=SK(IX,IY)+SS(IS,JS)
345   CONTINUE
      IF(J.EQ.MM) KX=KX+1
330   CONTINUE
      IF(KX.EQ.1) GO TO 300
      IF(I.EQ.MM) KY=KY+1
295   CONTINUE
      IF(KY.EQ.1) GO TO 290
285   IF (MM.NE.1) GO TO 370
      DO 375 I=1,IH
      FF(I,1)=FF(I,1)+FX(I)
      DO 375 J=1,IH
      SK(I,J)=SK(I,J)+SS(I,J)
375    CONTINUE
370    CONTINUE
      IF(NN2.EQ.0) GO TO 100
      DO 380 I=1,IH
      WRITE (2,385) I
385   FORMAT (1X,I2)
      WRITE (2,390) (SK(I,J),J=1,IH)
390   FORMAT (1X,4E15.5)
380   CONTINUE
      WRITE (2,390) (FF(I,1),I=1,IH)
C
C    ASSEMBLY OF OVERALL STIFFNESS MATRIX
C
100   NI=N2*MM*(II-1)
      QY1=Q2
```

```
      T1=T
      IA=1
      A2=A
      B1=B
      Q1=Q
      QX1=QX
      IF (NPROP.EQ.0) GO TO 101
      CALL PROP (IH,MM,NEC,A,B,LL,N2,NX,NP,BG,NN,M1,M2,NNN,
     1FF,INPROP)
      INPROP=INPROP+1
101   IF (NN1.NE.1) GO TO 102
      XI1=XI
      YI1=YI
      P1=P
102   CALL REST (IHOLD,JHOLD,IG,MM,N1)
      CALL PART (NNN,IH,IG,FF,BG,NS,INPROP,IP)
      IF (NS.EQ.NNN) GO TO 455
      NNN=NNN+1
      GO TO 35
455   WRITE (2,452)
      SUM1=0.0
      SUM2=0.0
      NA=NNN+1
      DO 453 I=1,NA
      SUM1=SUM1+AL(I)
      SUM2=SUM2+H(I)
453   WRITE (2,451) I,SUM1,SUM2,K5(I)
452   FORMAT (1X,//,14H   NODAL  DATA,//,1X,5X,4HNODE,10X,
     114HDIMENSION  (X),10X,14HDIMENSION  (Z),10X,
     29HRESTRAINT,//)
451   FORMAT (7X,I2,10X,F10.2,15X,F10.2,17X,I2)
      WRITE (2,414)
414   FORMAT (1X,//,3X,20H**LOADING  DETAILS**,/,4X,5HSTRIP,
     110X,19HOVERALL  U.D.L. (P),4X,19HOVERALL  U.D.L. (Q),/,
     224X,9H(N/MM**2),14X,9H(N/MM**2),/)
      DO 413 I=1,NNN
413   WRITE (2,412) I,QZ(I),QU(I)
412   FORMAT (6X,I2,15X,E10.4,13X,E10.4)
      WRITE (2,411)
411   FORMAT (1X,/,5X,4HNODE,10X,6HU.D.L.,13X,16HPOINT  LOAD  (N)
     1/,20X,6H(N/MM),8X,11HX-DIRECTION,4X,11HY-DIRECTION,/)
      DO 409 I=1,NA
      WRITE (2,408 ) I,QB(I)
408   FORMAT (7X,I2,8X,F10.3)
      IF (QB(I).EQ.0.0) GO TO 409
      IF (NN1.EQ.3.AND.NEC.EQ.1) WRITE (2,2001)
      IF (NN1.EQ.3.AND.NEC.EQ.2) WRITE (2,2002)
2001  FORMAT (1H+,60X,12H U-DIRECTION)
2002  FORMAT (1H+,60X,12H V-DIRECTION)
409   CONTINUE
C
C       SOLUTION  OF  SIMULTANEOUS  EQUATIONS
C
      CALL SOLVE (IH,IG,BG,1,NS,INPROP,IP)
      NP=NNN
      DO 403 II=1,INPROP
```

```
      DO 402 JJ=1,NX
402   R(JJ)=BG(JJ,II)
      IF (II.EQ.1) WRITE (2,476)
      IJ=II-1
      IF (II.NE.1) WRITE (2,477) IJ
477   FORMAT (1X,//,1X,30HDEFLECTION DUE TO PROP FORCE R,I2,//)
      CALL OUTPUT (R,NNN,MM,LL,N2)
403   NNN=NP
462   FORMAT (1X,/,60(1H*),//,24H  **DEFLECTION  OUTPUT**)
476   FORMAT (1X,//,1X,32HDEFLECTION DUE TO EXTERNAL LOADS)
      NP=NNN
C
C       DEFLECTION  OUTPUT
C
      IF (NN1.EQ.2) GO TO 484
      IF (NN1.EQ.4) GO TO 484
      GO TO 4800
484   II=0
      NZ=NN+1
      DO 490 I=1,NZ
      DO 480 J=1,NX
      II=II+1
480   AC(II)=BG(J,I)
490   CONTINUE
      DO 600 I=1,NN
      SUM=0.0
      Z=AX(I)
      W=AY(I)/A
      CI=C1(Z,B)
      CJ=C2(Z,B)
      CL=C3(Z,B)
      CK=C4(Z,B)
      KA=1
      IF (LL.EQ.2) KA=3
      DO 605 J=1,MM
      IB=N2*MM*IZ(I)+N2*(J-1)
      IA=N2*MM*(IZ(I)-1)+N2*(J-1)
      Y1=YM(NEC,W,J,0,A)
      SUM=SUM+AC(IA+KA)*Y1*CI
      SUM=SUM+AC(IA+KA+1)*Y1*CJ
      SUM=SUM+AC(IB+KA)*Y1*CL
      SUM=SUM+AC(IB+KA+1)*Y1*CK
605   CONTINUE
      DELTA(I)=SUM
      DO 610 L=1,NN
      SUM=0.0
      DO 615 J=1,MM
      IA=N2*MM*(IZ(I)-1)+NX*L+N2*(J-1)
      IB=N2*MM*IZ(I)+NX*L+N2*(J-1)
      Y1=YM(NEC,W,J,0,A)
      SUM=SUM+AC(IA+KA)*Y1*CI
      SUM=SUM+AC(IA+KA+1)*Y1*CJ
      SUM=SUM+AC(IB+KA)*Y1*CL
      SUM=SUM+AC(IB+KA+1)*Y1*CK
615   CONTINUE
      XF(I,L)=SUM
```

```
610   CONTINUE
600   CONTINUE
      I=0
      DO 700 J=1,NN
      DO 700 L=1,NN
      I=I+1
700   XZ(I)=XF(J,L)
      CALL INVERT1 (NN,XZ,XU)
      I=0
      DO 705 J=1,NN
      DO 705 L=1,NN
      I=I+1
705   XV(J,L)=XU(I)
      DO 710 I=1,NN
      ZZ(I)=0.0
      DO 710 J=1,NN
      ZZ(I)=ZZ(I)-DELTA(J)*XV(I,J)
710   CONTINUE
      WRITE (2,714)
714   FORMAT (1X,//,19H   PROPPING  FORCES/)
      WRITE (2,715) (ZZ(I),I=1,NN)
715   FORMAT (1X,4(4X,E15.5))
      DO 720  I=1,NN
      DO 720 II=1,NX
      J=NX*I+II
      AC(J)=AC(J)*ZZ(I)
720   CONTINUE
      DO 730 II=1,NX
      SUM=0.0
      NI=NN+1
      DO 725 I=1,NI
      J=(I-1)*NX+II
      SUM=SUM+AC(J)
725   CONTINUE
      R(II)=SUM
730   CONTINUE
      CALL OUTPUT (R,NP,MM,LL,N2)
C
C      SECTION  TO  OBTAIN  STRESS  AT  CETRE  OF  NODAL  LINES
C
4800  WRITE (2,481)
481   FORMAT (1X,/,60(1H*),//,20H  **STRESS  OUTPUT**/)
      Y=0.0
      DO 8000 IIX=1,5
      WRITE (2,8005) Y
8005  FORMAT (/13H --STRESS AT ,F10.3,2H--)
      DO 805 I=1,NS
      WRITE (2,829) I
829   FORMAT (1X,12H ++STRIP++  ,I3)
      DO 835 IX=1,MM
      IY=2
      IF (LL.EQ.0.OR.LL.EQ.1) GO TO 800
      DO 810 J=1,4
      NI=(I-1)*4*MM+(IX-1)*4+J
      NA=I*4*MM+(IX-1)*4+J
      NJ=J+4
```

```
      RS(J)=R(NI)
810   RS(NJ)=R(NA)
      BET=BETA(I)
      CALL ENT(BET,LL)
      CALL XMULT (8,8,1,RIT,RS,RRS)
      DO 801 IN=1,8
801   RS(IN)=RRS(IN)
      GO TO 815
800   IF (LL.EQ.1) GO TO 820
      DO 825 IU=1,IY
      NJ=(I-1)*2*MM+(IU-1)*MM*N2+(IX-1)*2
      NI=(IU-1)*4
      RS(NI+1)=0.0
      RS(NI+2)=0.0
      RS(NI+3)=R(NJ+1)
      RS(NI+4)=R(NJ+2)
 825  CONTINUE
      GO TO 815
820   DO 830 IU=1,IY
      NJ=(I-1)*2*MM+(IU-1)*MM*N2+(IX-1)*2
      NI=(IU-1)*4
      RS(NI+1)=R(NJ+1)
      RS(NI+2)=R(NJ+2)
      RS(NI+3)=0.0
      RS(NI+4)=0.0
 830  CONTINUE
815   X=0.0
      CALL SBBEND (B,DX,DY,D1,DXY,X,Y,A,SB,NEC,IX,K1,K2,K3,K4)
      CALL MULT1 (6,8,RS,SB,SR)
835   CALL STRESS (SR,IX,I)
      DO 840 IX=1,MM
      X=B
      IF (LL.EQ.0.OR.LL.EQ.1) GO TO 850
      DO 855 J=1,4
      NI=(I-1)*4*MM+(IX-1)*4+J
      NA=I*4*MM+(IX-1)*4+J
      NJ=J+4
      RS(J)=R(NI)
      RS(NJ)=R(NA)
855   CONTINUE
      BET=BETA(I)
      CALL ENT(BET,LL)
      CALL XMULT (8,8,1,RIT,RS,RRS)
      DO 854 IN=1,8
854   RS(IN)=RRS(IN)
      GO TO 860
 850  IF (LL.EQ.1) GO TO 865
      DO 870 IU=1,IY
      NJ=(I-1)*2*MM+(IU-1)*MM*N2+(IX-1)*2
      NI=(IU-1)*4
      RS(NI+1)=0.0
      RS(NI+2)=0.0
      RS(NI+3)=R(NJ+1)
      RS(NI+4)=R(NJ+2)
870   CONTINUE
      GO TO 860
```

```
865     DO 875 IU=1,IY
        NJ=(I-1)*2*MM+(IU-1)*MM*N2+(IX-1)*2
        NI=(IU-1)*4
        RS(NI+1)=R(NJ+1)
        RS(NI+2)=R(NJ+2)
        RS(NI+3)=0.0
        RS(NI+4)=0.0
875     CONTINUE
860     CALL SBBEND (B,DX,DY,D1,DXY,X,Y,A,SB,NEC,IX,K1,K2,K3,K4)
        CALL MULT1 (6,8,RS,SB,SR)
        NNN=I+1
840     CALL STRESS (SR,IX,NNN)
805     CONTINUE
        WRITE (2,804)
804     FORMAT (1X,60(1H*))
8000    Y=Y+A/8.
        NNN=1
        GO TO 900
999     STOP
        END
        SUBROUTINE PROP(IH,MM,NEC,A,B,LL,N2,NX,NP,BG,NN,M1,M2,NNN,
       1FF,I)
        DIMENSION BG(2000,7),FX(96),FF(96,2),FK(96),
       1R(2000),IZ(10),AX(10),AY(10),F(4)
        COMMON /BL12/IZ,AX,AY/BL2/FK,R
C
C       NO.  OF  PROPPING  FORCES
C
C
C       POSITION  OF  PROPPING  FORCES
C
        N1=IH/MM
        READ (1,500) NEC,AX(I),AY(I)
500     FORMAT (I2,2F10.2)
        IZ(I)=NNN
        DO 505 IN=1,IH
        FX(IN)=0.0
        FF(IN,2)=0.0
505     CONTINUE
        XS=AX(I)
        Z=AY(I)
        DO 510 M=1,MM
        CALL POINT (1.,B,A,XS,Z,F,NEC,M)
        DO 515 IL=1,4
        IF (LL.NE.2) GO TO 100
        NI=N1*(M-1)
        IF (IL.EQ.1) NI=NI+3
        IF (IL.EQ.2) NI=NI+4
        IF (IL.EQ.3) NI=NI+7
        IF (IL.EQ.4) NI=NI+8
        GO TO 515
100     NI=N1*(M-1)+IL
515     FX(NI)=FX(NI)+F(IL)
510     CONTINUE
511     IF (MM.EQ.1) GO TO 520
        KY=0
```

```
525     DO 530 J=1,MM
535     IF (KY.EQ.1) GO TO 540
        IS=(J*N2-N2)*2
        IX=(J-1)*N2
        I7=IS
        I8=IX
        GO TO 545
540     IS=(J*2-1)*N2
        IX=(J-1+MM)*N2
        I7=IS
        I8=IX
545     DO 550 III=1,N2
        IF (III.NE.1) GO TO 555
        IS=I7
        IX=I8
555     IS=IS+1
        IX=IX+1
550     FF(IX,2)=FF(IX,2)+FX(IS)
        IF (J.EQ.MM) KY=KY+1
530     CONTINUE
        IF (KY.EQ.1 ) GO TO 525
        GO TO 560
520     DO 565 J=1,IH
        FF(J,2)=FF(J,2)+FX(J)
565     CONTINUE
560     RETURN
        END
        SUBROUTINE INTE (A,NEC,M,N)
        COMMON /BL6/I1,I2,I3,I4,I5
C
C       SUBROUTINE FOR BENDING INTEGRALS
C
        REAL I1,I2,I3,I4,I5
        UM=(M-2)*3.1415926
        UN=(N-2)*3.1415926
        IF (M.EQ.N) GO TO 5
        IF (M.GT.2.AND.N.GT.2) GO TO 10
        IF (M.EQ.1.AND.N.EQ.2) GO TO 10
        IF (M.EQ.2.AND.N.EQ.1) GO TO 10
        IF (M.EQ.2.AND.N.GE.3) GO TO 35
        IF (M.GE.3.AND.N.EQ.2) GO TO 40
        IF (M.EQ.1.AND.N.GE.3) GO TO 15
        IF (M.GE.3.AND.N.EQ.1) GO TO 50
        GO TO 10
50      I1=A*(1.-COS(UM))/UM
        I2=-UM*(1.-COS(UM))/A
        I3=0.0
        I4=0.0
        I5=0.0
        GO TO 20
15      I1=A*(1.-COS(UN))/UN
        I2=0.0
        I3=-UN*(1.-COS(UN))/A
        I4=0.0
        I5=0.0
        GO TO 20
```

```
10      I1=0.0
        I2=0.0
        I3=0.0
        I4=0.0
        I5=0.0
        GO TO 20
5       IF (M.EQ.1) GO TO 25
        IF (M.EQ.2) GO TO 30
        I1=A/2.
        I2=-((UM/A)**2)*A/2.
        I3=I2
        I4=((UM/A)**4)*A/2.
        I5=-I2
        GO TO 20
30      I1=A/3.
        I2=0.0
        I3=0.0
        I4=0.0
        I5=4./A
        GO TO 20
35      I1=A*(COS(UN)+1.)/UN
        I2=0.0
        I3=-UN*(COS(UN)+1.)/A
        I4=0.0
        I5=0.0
        GO TO 20
40      I1=A*(COS(UM)+1.)/UM
        I2=-UM*(COS(UM)+1.)/A
        I3=0.0
        I4=0.0
        I5=0.0
        GO TO 20
25      I1=A
        I2=0.0
        I3=0.0
        I4=0.0
        I5=0.0
20      RETURN
        END
        SUBROUTINE BENDLO2(B,DX,DY,D1,DXY)
        COMMON /BL6/I1,I2,I3,I4,I5/BL4/BLO
        DIMENSION BB(24),BLO(4,4)
C
C        BENDING  STIFFNESS  MATRIX
C
        REAL I1,I2,I3,I4,I5
        BB(1)=5040.*DX*I1
        BB(2)=504.*(B**2)*D1*I2
        BB(3)=504.*(B**2)*D1*I3
        BB(4)=156.*(B**4)*DY*I4
        BB(5)=2016.*(B**2)*DXY*I5
        BB(6)=5040.*DX*B*I1/2.
        BB(7)=462.*(B**3)*D1*I2
        BB(8)=42.*(B**3)*D1*I3
        BB(9)=22.*(B**5)*DY*I4
        BB(10)=168.*(B**3)*DXY*I5
```

```
      BB(11)=42.*(B**3)*D1*I2
      BB(12)=13.*(B**5)*DY*I4
      BB(13)=54*(B**4.)*DY*I4
      BB(14)=462.*(B**3)*D1*I3
      BB(15)=1680.*(B**2)*DX*I1
      BB(16)=56.*(B**4)*D1*I2
      BB(17)=56.*(B**4)*D1*I3
      BB(18)=4.*(B**6)*DY*I4
      BB(19)=224*(B**4.)*DXY*I5
      BB(20)=BB(15)/2.
      BB(21)=14*(B**4.)*D1*I2
      BB(22)=14*(B**4.)*D1*I3
      BB(23)=3.*(B**6)*DY*I4
      BB(24)=56.*(B**4)*DXY*I5
      BLO(1,1)=BB(1)-BB(2)-BB(3)+BB(4)+BB(5)
      BLO(1,2)=BB(6)-BB(7)-BB(8)+BB(9)+BB(10)
      BLO(1,3)=-BB(1)+BB(2)+BB(3)+BB(13)-BB(5)
      BLO(1,4)=BB(6)-BB(11)-BB(8)-BB(12)+BB(10)
      BLO(2,1)=BB(6)-BB(14)-BB(11)+BB(9)+BB(10)
      BLO(2,2)=BB(15)-BB(16)-BB(17)+BB(18)+BB(19)
      BLO(2,3)=-BLO(1,4)
      BLO(2,4)=BB(20)+BB(21)+BB(22)-BB(23)-BB(24)
      BLO(3,1)=BLO(1,3)
      BLO(3,2)=BLO(2,3)
      BLO(3,3)=BLO(1,1)
      BLO(3,4)=-BLO(1,2)
      BLO(4,1)=BLO(1,4)
      BLO(4,2)=BLO(2,4)
      BLO(4,3)=-BLO(2,1)
      BLO(4,4)=BLO(2,2)
      DO 15 I=1,4
      DO 15 J=1,4
      BLO(I,J)=BLO(I,J)/(420.*(B)**3)
   15 CONTINUE
      RETURN
      END
      SUBROUTINE FORCE (Q,Q1,B,M,NEC,A,F,BETA,FQ,LL,NCC)
C
C       FORCE  MATRIX  FOR U.D.L.
C
      REAL J1,J3
      DIMENSION F(4),FQ(4)
      CALL FORINT (A,M,NEC,J1,J3,NCC)
      F(1)=Q*B*COS(BETA)*J1/2.
      F(2)=Q*B*B*COS(BETA)*COS(BETA)*J1/12.
      F(3)=F(1)
      F(4)=-F(2)
      IF (Q1.EQ.0.0) GO TO 25
      F(1)=F(1)+Q1*B*COS(BETA)*J1/2.
      F(2)=F(2)+Q1*B*B*J1/12.
      F(3)=F(3)+Q1*B*COS(BETA)*J1/2.
      F(4)=F(4)-Q1*B*B*J1/12.
   25 IF (LL.NE.2) GO TO 20
      FQ(1)=-Q1*B*SIN(BETA)*J1/2
      FQ(2)=0.0
      FQ(3)=FQ(1)
```

```
      FQ(4)=0.0
20    RETURN
      END
      SUBROUTINE PFORCE (QX,B,M,NEC,A,F,NCC)
      REAL J1,J3
C
C       FORCE  MATRIX  FOR  NODAL  U.D.L.
C
      DIMENSION F(4)
      UM=3.1415926*M
      CALL FORINT (A,M,NEC,J1,J3,NCC)
      F(1)=0.0
      F(2)=0.0
      F(3)=0.0
      F(4)=0.0
      IF (NEC.EQ.1) F(1)=QX*J1
      IF (NEC.EQ.2) F(4)=QX*J3
      RETURN
      END
      SUBROUTINE FORINT (A,M,NEC,J1,J3,NCC)
      REAL J1,J3,K
      J3=0.0
      PI=3.141592653
      IF (NCC.EQ.1) GO TO 2
1     K=(M-2)*PI
      IF (M.EQ.1) GO TO 20
      IF (M.EQ.2) GO TO 25
      J3=0.0
      J1=A*(1-COS(K))/K
      GO TO 10
20    J1=A
      J3=0.0
      GO TO 10
25    J3=A
      J1=0.0
      GO TO 10
2     IF (M.EQ.1) GO TO 11
      IF (M.EQ.2) GO TO 12
      K=(M-2)*PI
      J1=A*(1.-COS(K/2))/K
      GO TO 10
11    J1=A/2.
      GO TO 10
12    J1=A/4.
10    CONTINUE
      RETURN
      END
      SUBROUTINE SBBEND (B,DX,DY,D1,DXY,X,Y,A,SB,NEC,M,K1,K2,K3,K4
C
C       STRESS  MATRIX
C
      DIMENSION SB(6,8),BZ(3,4)
      COMMON /BL8/LL
      REAL K1,K2,K3,K4
      DO 15 I=1,6
      DO 15 J=1,8
```

```
15      SB(I,J)=0.0
        Z=Y/A
        Y1=YM(1,Z,M,0,A)
        Y2=YM(1,Z,M,1,A)
        Y3=YM(1,Z,M,2,A)
        Y4=YM(2,Z,M,0,A)
        Y5=YM(2,Z,M,1,A)
        XBAR=X/B
        IF (LL.EQ.1) GO TO 10
        BZ(1,1)=6.*(1.-2*XBAR)*Y1/(B**2)
        BZ(1,2)=2.*(2.-3*XBAR)*Y1/B
        BZ(1,3)=-BZ(1,1)
        BZ(1,4)=2.*(-3*XBAR+1)*Y1/B
        BZ(2,1)=-Y3*(1.-3*XBAR**2+2*XBAR**3)
        BZ(2,2)=-X*(1.-2*XBAR+XBAR**2)*Y3
        BZ(2,3)=-(3.*XBAR**2-2.*XBAR**3)*Y3
        BZ(2,4)=-X*((XBAR)**2-XBAR)*Y3
        BZ(3,1)=2.*Y2*(-6.*XBAR+6.*XBAR**2)/B
        BZ(3,2)=2.*Y2*(1.-4.*XBAR+3.*XBAR**2)
        BZ(3,3)=-BZ(3,1)
        BZ(3,4)=2*Y2*(3.*XBAR**2-2.*XBAR)
        SB(4,3)=DX*BZ(1,1)+D1*BZ(2,1)
        SB(4,4)=DX*BZ(1,2)+D1*BZ(2,2)
        SB(4,7)=DX*BZ(1,3)+D1*BZ(2,3)
        SB(4,8)=DX*BZ(1,4)+D1*BZ(2,4)
        SB(5,3)=D1*BZ(1,1)+DY*BZ(2,1)
        SB(5,4)=D1*BZ(1,2)+DY*BZ(2,2)
        SB(5,7)=D1*BZ(1,3)+DY*BZ(2,3)
        SB(5,8)=D1*BZ(1,4)+DY*BZ(2,4)
        SB(6,3)=DXY*BZ(3,1)
        SB(6,4)=DXY*BZ(3,2)
        SB(6,7)=DXY*BZ(3,3)
        SB(6,8)=DXY*BZ(3,4)
10      IF (LL.EQ.0) GO TO 20
        SB(1,1)=-K1*Y1/B
        SB(1,2)=K2*(1.-XBAR)*Y5
        SB(1,5)=-SB(1,1)
        SB(1,6)=K2*XBAR*Y5
        SB(2,1)=-K2*Y1/B
        SB(2,2)=K3*(1.-XBAR)*Y5
        SB(2,5)=-SB(2,1)
        SB(2,6)=K3*XBAR*Y5
        SB(3,1)=K4*(1.-XBAR)*Y2
        SB(3,2)=-K4*Y4/B
        SB(3,5)=K4*XBAR*Y2
        SB(3,6)=-SB(3,2)
20      CONTINUE
        RETURN
        END
        SUBROUTINE PLANLO2 (EX,EY,PVX,PVY,GXY,B,A,T,NEC,M,N,K1,K2,K3
        DIMENSION PLO2(4,4)
C
C        PLANE  STRESS  STIFFFNESS  MATRIX
C
        COMMON /BL5/PLO2
        REAL K1,K2,K3,K4,L1,L2,L3,L4,L5,L6,L7,L8
```

```
      K1=EX/(1.-PVX*PVY)
      K2=PVX*K1
      K3=EY/(1.-PVX*PVY)
      K4=GXY
      PI=3.141592653
      UN=(N-2)*PI
      UM=(M-2)*PI
      CALL INS (M,N,UN,UM,A,L1,L2,L3,L4,L5,L6,L7,L8)
      PLO2(1,1)=K1*L1/B+K4*L4*B/3.
      PLO2(1,2)=-K2*L2/2.-K4*L3/2.
      PLO2(1,3)=-K1*L1/B+K4*L4*B/6.
      PLO2(1,4)=-K2*L2/2.+K4*L3/2.
      PLO2(2,1)=-K2*L5/2.-K4*L6/2.
      PLO2(2,2)=K3*L7*B/3.+K4*L8/B
      PLO2(2,3)=K2*L5/2.-K4*L6/2.
      PLO2(2,4)=K3*L7*B/6-K4*L8/B
      PLO2(3,1)=PLO2(1,3)
      PLO2(3,2)=K2*L2/2.-K4*L3/2.
      PLO2(3,3)=K1*L1/B+K4*L4*B/3.
      PLO2(3,4)=K2*L2/2.+K4*L3/2.
      PLO2(4,1)=-K2*L5/2.+K4*L6/2.
      PLO2(4,2)=PLO2(2,4)
      PLO2(4,3)=K2*L5/2.+K4*L6/2.
      PLO2(4,4)=K3*B*L7/3.+K4*L8/B
      DO 15 I=1,4
      DO 15 J=1,4
      PLO2(I,J)=PLO2(I,J)*T
15    CONTINUE
      RETURN
      END
      SUBROUTINE INS(M,N,UN,UM,A,L1,L2,L3,L4,L5,L6,L7,L8)
      REAL L1,L2,L3,L4,L5,L6,L7,L8
C
C       INTEGRALS  FOR  PLANE  STIFFNESS  MATRIX
C
      IF(M.NE.N) GO TO 5
      IF(M.EQ.1) GO TO 10
      IF(M.EQ.2) GO TO 15
      L1=A/2.
      L2=-UM/2
      L3=-L2
      L4=((UM/A)**2)*L1
      L5=L2
      L6=L3
      L7=L4
      L8=L1
      GO TO 20
15    L1=A/3.
      L2=0.0
      L3=-2.
      L4=4./A
      L5=L2
      L6=L3
      L7=0.0
      L8=A
      GO TO 20
```

```
10      L1=A
        L2=-2.
        L3=0.0
        L4=0.0
        L5=L2
        L6=0.0
        L7=4./A
        L8=A/3.
        GO TO 20
5       IF (M.EQ.1.AND.N.EQ.2) GO TO 25
        IF (M.EQ.1.AND.N.GE.3) GO TO 30
        IF (M.EQ.2.AND.N.EQ.1) GO TO 25
        IF (M.GE.3.AND.N.EQ.1) GO TO 40
        IF (M.EQ.2.AND.N.GE.3) GO TO 45
        IF (M.GE.3.AND.N.EQ.2) GO TO 50
25      L1=0.0
        L2=L1
        L3=L1
        L4=L1
        L5=L1
        L6=L1
        L7=L1
        L8=L1
        GO TO 20
30      Y=1.-COS(UN)
        L1=A*Y/UN
        L2=-Y
        L3=0.0
        L4=0.0
        L5=-2*Y/UN
        L6=-L5
        L8=2*A*Y/(UN*UN)
        L7=2.*Y/A
        GO TO 20
40      Y=1.-COS(UM)
        L1=A*Y/UM
        L2=-2*Y/UM
        L3=2*Y/UM
        L4=0.0
        L5=-Y
        L6=0.0
        L8=2*A*Y/(UM*UM)
        L7=2*Y/A
        GO TO 20
45      Y=1+COS(UN)
        L1=A*Y/UN
        L2=-Y
        L3=0.0
        L4=0.0
        L5=0.0
        L6=0.0
        L7=0.0
        L8=0.0
        GO TO 20
50      Y=1+COS(UM)
        L1=A*Y/UM
```

```
      L2=0.0
      L3=0.0
      L4=0.0
      L5=-Y
      L6=0.0
      L7=0.0
      L8=0.0
   20 CONTINUE
      RETURN
      END
      SUBROUTINE XMULT (L,M,N,A,B,C)
      DIMENSION A(8,8),B(8,8),C(8,8)
      DO 2 I=1,L
      DO 2 J=1,N
      C(I,J)=0.
      DO 2 K=1,M
    2 C(I,J)=C(I,J)+A(I,K)*B(K,J)
      RETURN
      END
      SUBROUTINE ENT (BETA,LL)
C
C      TRANSFORMATION  MATRICES
C
      DIMENSION RI(8,8),RIT(8,8)
      COMMON /BL3/RI,RIT
      DO 10 I=1,8
      DO 10 J=1,8
      RI(I,J)=0.0
   10 CONTINUE
      RI(1,1)=COS(BETA)
      RI(1,3)=-SIN(BETA)
      RI(2,2)=1.0
      RI(3,1)=-RI(1,3)
      RI(3,3)=RI(1,1)
      RI(4,4)=1.0
      RI(5,5)=RI(1,1)
      RI(5,7)=RI(1,3)
      RI(6,6)=1.0
      RI(7,5)=-RI(1,3)
      RI(7,7)=RI(1,1)
      RI(8,8)=1.0
      DO 20 I=1,8
      DO 20 J=1,8
      RIT(I,J)=0.0
   20 CONTINUE
      RIT(1,1)=COS(BETA)
      RIT(1,3)=SIN(BETA)
      RIT(2,2)=1.0
      RIT(3,1)=-RIT(1,3)
      RIT(3,3)=RIT(1,1)
      RIT(4,4)=1.0
      RIT(5,5)=RIT(1,1)
      RIT(5,7)=RIT(1,3)
      RIT(6,6)=1.0
      RIT(8,8)=1.0
      RIT(7,7)=RIT(1,1)
```

```
      RIT(7,5)=-RIT(1,3)
      RETURN
      END
      FUNCTION YM(NEC,YA,M,IDC,A)
      PI=3.141592653
      IF (NEC.EQ.2) GO TO 2
    1 IF (M.EQ.1) GO TO 20
      IF (M.EQ.2) GO TO 25
      UM=(M-2)*PI
      IF(IDC.EQ.0)YM=SIN(UM*YA)
      IF(IDC.EQ.1)YM=(UM/A)*COS(UM*YA)
      IF(IDC.EQ.2) YM=-(UM*UM/(A*A))*SIN(UM*YA)
      GOTO 10
   20 IF (IDC.EQ.0) YM=1.
      IF (IDC.GT.0) YM=0.0
      GO TO 10
   25 IF (IDC.EQ.0) YM=1.-2.*YA
      IF (IDC.EQ.1) YM=-2./A
      IF (IDC.EQ.2) YM=0.0
      GO TO 10
    2 IF (M.EQ.1) GO TO 11
      IF (M.EQ.2) GO TO 12
      UM=(M-2)*PI
      IF (IDC.EQ.0) YM=COS(UM*YA)
      IF (IDC.EQ.1) YM=-(UM/A)*SIN(UM*YA)
      GO TO 10
   11 IF (IDC.EQ.0) YM=1.-2.*YA
      IF (IDC.EQ.1) YM=-2./A
      GO TO 10
   12 IF (IDC.EQ.0) YM=1.
      IF (IDC.EQ.1) YM=0.0
   10 RETURN
      END
      SUBROUTINE MULT1  (L,M,A,B,C)
      DIMENSION A(30),B(6,8),C(6)
      DO 2 I=1,L
      C(I)=0.0
      DO 2 K=1,M
    2 C(I)=C(I)+A(K)*B(I,K)
      RETURN
      END
      SUBROUTINE POINT(P,B,A,X,Y,BFP,NEC,M)
      DIMENSION BFP(4)
      Z=Y/A
      Y1=YM(NEC,Z,M,0,A)
      XC=X/B
      BFP(1)=P*Y1*(1.-3.*(XC)**2+2.*(XC)**3)
      BFP(2)=P*Y1*X*(1.-2.*XC+(XC)**2)
      BFP(3)=P*Y1*(3.*(XC)**2-2.*(XC)**3)
      BFP(4)=P*Y1*X*((XC)**2-XC)
      RETURN
      END
      FUNCTION C1(X,B)
C
      XC=X/B
      C1=1.-3.*(XC)**2+2.*(XC)**3
```

```
      RETURN
      END
      SUBROUTINE OUTPUT(R,NNN,MM,LL,NZ)
C
C       OUTPUT  MATRIX  FOR  DEFLECTIONS
C
      DIMENSION R(2000)
      NNN=NNN+1
      NO=NZ*6
      I=1
      L=1
20    IF (NNN-6.LE.0.0) GO TO 100
      N1=(I-1)*6+1
      N2=N1+1
      N3=N1+2
      N4=N1+3
      N5=N1+4
      N6=N1+5
      WRITE (2,10) N1,N2,N3,N4,N5,N6
10    FORMAT (1X,//,5X,4HNODE,8X,I2,5(17X,I2))
      WRITE (2,16)
16    FORMAT (1X,/,1X,9HHARMONICS,/)
      NX=NO*MM
      NN=NZ*MM
      II=0
      JJ=(L-1)*MM*NO
      DO 21 K=1,NN,NZ
      WRITE (2,17) (R(JJ+J),J=K,NX,NN)
      II=II+1
      WRITE (2,18) II
      M=K+1
      WRITE (2,17) (R(JJ+J),J=M,NX,NN)
      IF (LL.NE.2) GO TO 21
      M1=K+2
      WRITE (2,17) (R(JJ+J),J=M1,NX,NN)
      M2=K+3
      WRITE (2,17) (R(JJ+J),J=M2,NX,NN)
21    CONTINUE
      N=N-6
17    FORMAT (1X,7X,E15.5,5(4X,E15.5))
18    FORMAT (1H+,1X,5X,I1)
      NNN=NNN-6
      L=L+1
      I=I+1
      GO TO 20
100   WRITE (2,25)
25    FORMAT (1X,//,5X,4HNODE)
      N1=(I-1)*6+1
      N=NNN
      WRITE (2,30) N1
30    FORMAT (1H+,17X,I2)
      IF (N-1.EQ.0) GO TO 40
      N1=N1+1
      WRITE (2,35) N1
35    FORMAT (1H+,36X,I2)
      IF (N-2.EQ.0) GO TO 40
```

```
      N1=N1+1
      WRITE (2,45) N1
45    FORMAT (1H+,55X,I2)
      IF (N-3.EQ.0) GO TO 40
      N1=N1+1
      WRITE (2,50) N1
50    FORMAT (1H+,74X,I2)
      IF (N-4.EQ.0) GO TO 40
      N1=N1+1
      WRITE (2,55) N1
55    FORMAT (1H+,93X,I2)
      IF (N-5.EQ.0) GO TO  40
      N1=N1+1
      WRITE (2,60) N1
60    FORMAT (1H+,112X,I2)
40    CONTINUE
      WRITE (2,16)
      II=0
      NN=NZ*MM
      DO 22 K=1,NN,NZ
      JJ=(L-1)*NO*MM
      NX=NZ*MM*N
      WRITE (2,17) (R(JJ+J),J=K,NX,NN)
      II=II+1
      WRITE (2,18) II
      M=K+1
      WRITE (2,17) (R(JJ+J),J=M,NX,NN)
      IF (LL.NE.2) GO TO 22
      M1=K+2
      WRITE (2,17) (R(JJ+J),J=M1,NX,NN)
      M2=K+3
      WRITE (2,17) (R(JJ+J),J=M2,NX,NN)
22    CONTINUE
      RETURN
      END
      FUNCTION C2(X,B)
      XC=X/B
      C2=X*(1.-2.*(XC)+(XC)**2)
      RETURN
      END
      FUNCTION C3(X,B)
      XC=X/B
      C3=3*(XC)**2-2.*(XC)**3
      RETURN
      END
      FUNCTION C4(X,B)
      XC=X/B
      C4=X*((XC)**2-(XC))
      RETURN
      END
      SUBROUTINE INVERT(IP)
      DIMENSION B(2400),C(2400)
      COMMON /BL30/B,C
      LEVEL 2,B,C
      IF(IP.EQ.1) GO TO 9
      IW=IP*IP
```

```
      DO 2 I=1,IW
    2 C(I)=0.
      DO 3 I=1,IP
    3 C(I+IP*(I-1))=1.0
      IW=IP-1
      DO 5 IQ=1,IW
      K=IP-IQ+1
      AP=B(K+IP*(K-1))
      IK=K-1
      DO 5 I=1,IK
      AT=B(I+IP*(K-1))/AP
      DO 5 J=1,IP
      B(I+IP*(J-1))=B(I+IP*(J-1))-B(K+IP*(J-1))*AT
    5 C(I+IP*(J-1))=C(I+IP*(J-1))-C(K+IP*(J-1))*AT
C    MATRIX  NOW  REDUCED  TO  UPPER  TRIANGLE  FORM
      DO 6 IQ=1,IW
      AP=B(IQ+IP*(IQ-1))
      IK=IQ+1
      DO 6 I=IK,IP
      AT=B(I+IP*(IQ-1))/AP
      DO 6 J=1,IP
      B(I+IP*(J-1))=B(I+IP*(J-1))-B(IQ+IP*(J-1))*AT
    6 C(I+IP*(J-1))=C(I+IP*(J-1))-C(IQ+IP*(J-1))*AT
C   MATRIX  NOW  REDUCED  TO  DIAGONAL  FORM
      DO 7 I=1,IP
      DO 12 J=1,IP
   12 C(I+IP*(J-1))=C(I+IP*(J-1))/B(I+IP*(I-1))
    7 CONTINUE
      GO TO 8
    9 C(1)=1.0/B(1)
    8 RETURN
      END
      SUBROUTINE COMB (BO,PL02,BLO)
C
C       FOLDED  PLATE  STIFFNESS  MATRIX
C
      DIMENSION BO(8,8),PL02(4,4),BLO(4,4)
      DO 10 I=1,8
      DO 10 J=1,8
   10 BO(I,J)=0.0
      BO(1,1)=PL02(1,1)
      BO(1,2)=PL02(1,2)
      BO(2,1)=PL02(2,1)
      BO(2,2)=PL02(2,2)
      BO(5,1)=PL02(3,1)
      BO(5,2)=PL02(3,2)
      BO(6,1)=PL02(4,1)
      BO(6,2)=PL02(4,2)
      BO(3,3)=BLO(1,1)
      BO(3,4)=BLO(1,2)
      BO(4,3)=BLO(2,1)
      BO(4,4)=BLO(2,2)
      BO(1,5)=PL02(1,3)
      BO(1,6)=PL02(1,4)
      BO(2,5)=PL02(2,3)
      BO(2,6)=PL02(2,4)
```

```
      BO(5,5)=PLO2(3,3)
      BO(5,6)=PLO2(3,4)
      BO(6,5)=PLO2(4,3)
      BO(6,6)=PLO2(4,4)
      BO(3,7)=BLO(1,3)
      BO(3,8)=BLO(1,4)
      BO(4,7)=BLO(2,3)
      BO(4,8)=BLO(2,4)
      BO(7,7)=BLO(3,3)
      BO(7,8)=BLO(3,4)
      BO(8,7)=BLO(4,3)
      BO(8,8)=BLO(4,4)
      BO(7,3)=BLO(3,1)
      BO(7,4)=BLO(3,2)
      BO(8,3)=BLO(4,1)
      BO(8,4)=BLO(4,2)
      RETURN
      END
      SUBROUTINE STRESS (SR,I,N)
C
CC     STRESS  OUTPUT  SUBROUTINE
C
      DIMENSION SR(6)
      IF (I.NE.1) GO TO 20
      WRITE (2,5) N
5     FORMAT (1X,//,7H  NODE ,I2)
      WRITE (2,10)
10    FORMAT (1X,/,15X,7HZIGMA-X,10X,7HZIGMA-Y,10X,
     18HZIGMA-XY,10X,8HMOMENT-X,10X,8HMOMENT-Y,10X,
     29HMOMENT-XY,/,1X,9HHARMONICS,4X,10H(KN/MM**2),8X,
     310H(KN/MM**2),7X,10H(KN/MM**2),8X,7H(KN*MM),12X,7H(KN*MM)
     412X,7H(KN*MM)/)
20    WRITE (2,15) I,(SR(J),J=1,6)
15    FORMAT (5X,I2,3X,E15.5,3X,E15.5,3X,E15.5,2X,
     1E15.5,3X,E15.5,3X,E15.5)
      RETURN
      END
      SUBROUTINE DFORCE (A,B,F,FQ,M)
C
CC     DISTORTION  FORCE  MATRIX
C
      DIMENSION F(4),FQ(4)
      DO 5 I=1,4
5     F(I)=0.0
      FQ(1)=0.0
      FQ(2)=1.0
      IF (M.NE.2) FQ(2)=0.0
      FQ(3)=0.0
      FQ(4)=1.0
      IF(M.NE.2) FQ(4)=0.0
      RETURN
      END
      SUBROUTINE CYMESH(NS,AQ,R,NEC,II,JJ,XSUM,XSUM1)
C
CC     DATA  GENERATOR  FOR SHELL  ROOFS
C
```

```
      DIMENSION K5(20)
      COMMON /BL10/IR,X2,X3,Y1,Y2,J,NV,NA,K5
      IF (IR.GT.NS) GO TO 20
      X=3.1415925*AQ*R/(90*NS)
      IF (IR.NE.1) GO TO 10
      II=0
      NV=0
      XSUM=0.0
      XSUM1=0.0
10    X3=XSUM
      Y1=XSUM1
      ANGLE=AQ*(1.-(1.+2.*(IR-1))/NS)
      S=SIN(ANGLE)*X
      C=COS(ANGLE)*X
      XSUM=XSUM+C
      XSUM1=XSUM1+S
      X2=XSUM
      Y2=XSUM1
      IR=IR+1
      NEC=1
      II=II+1
      JJ=II+1
      GO TO 15
20    IF (J.EQ.NS+1) GO TO 25
      NA=1
      NV=NV+1
      K5(J)=1
      GO TO 15
25    NA=0
15    RETURN
      END
      SUBROUTINE INVERT1(IP,B,C)
      DIMENSION B(100),C(100)
      IF(IP.EQ.1) GO TO 9
      IW=IP*IP
      DO 2 I=1,IW
    2 C(I)=0.
      DO 3 I=1,IP
    3 C(I+IP*(I-1))=1.0
      IW=IP-1
      DO 5 IQ=1,IW
      K=IP-IQ+1
      AP=B(K+IP*(K-1))
      IK=K-1
      DO 5 I=1,IK
      AT=B(I+IP*(K-1))/AP
      DO 5 J=1,IP
      B(I+IP*(J-1))=B(I+IP*(J-1))-B(K+IP*(J-1))*AT
    5 C(I+IP*(J-1))=C(I+IP*(J-1))-C(K+IP*(J-1))*AT
C   MATRIX NOW REDUCED TO UPPER TRIANGLE FORM
      DO 6 IQ=1,IW
      AP=B(IQ+IP*(IQ-1))
      IK=IQ+1
      DO 6 I=IK,IP
      AT=B(I+IP*(IQ-1))/AP
      DO 6 J=1,IP
```

```
      B(I+IP*(J-1))=B(I+IP*(J-1))-B(IQ+IP*(J-1))*AT
6     C(I+IP*(J-1))=C(I+IP*(J-1))-C(IQ+IP*(J-1))*AT
C  MATRIX  NOW  REDUCED  TO  DIAGONAL  FORM
      DO 7 I=1,IP
      DO 12 J=1,IP
12    C(I+IP*(J-1))=C(I+IP*(J-1))/B(I+IP*(I-1))
7     CONTINUE
      GO TO 8
9     C(1)=1.0/B(1)
8     RETURN
      END
      SUBROUTINE PART (IY,NN,N,B,DB,IZ,IPROP,IP)
      DIMENSION A(96,96),B(96,2),BB(144,7),AA(144,144),ZZ(48,48)
     1,XX(48,48),R(2400),RR(2400),SY(48,48),BA(48,7),AB(48,7),
     2AZ(96,96),DB(2000,7),D(48,7),A5(48,48)
     3,BZ(144,7),YY(48,48)
      COMMON /BL1/AZ,A/BL30/R,RR/BL31/YY,SY/BL50/AA/BL65/BZ
      LEVEL 2,AZ,A,AA,R,RR,BZ
      IQ=2
      IF (IPROP.EQ.1) IQ=1
      IN=1
      IF (IY.NE.1) GO TO 61
      NQ=1.5*NN
      IPP=IP+1
      DO 210 I=1,NQ
      DO 220 II=1,IPP
220   BB(I,II)=0.0
      DO 210 J=1,NQ
210   AA(I,J)=0.0
      DO 20 I=1,NN
      DO 21 II=1,IQ
      IN=1
      IF (II.EQ.2) IN=IPROP
21    BB(I,IN)=BB(I,IN)+B(I,IQ)
      DO 20 J=1,NN
20    AA(I,J)=AA(I,J)+A(I,J)
      WRITE (3) ((A(I,J),J=1,N),I=1,N)
      WRITE (4) ((A(I,N+J),J=1,N),I=1,N)
      GO TO 500
61    DO 26 I=1,NN
      DO 27 II=1,IQ
      IN=1
      IF (II.EQ.2) IN=IPROP
27    BB(N+I,IN)=BB(N+I,IN)+B(I,II)
      DO 26 J=1,NN
26    AA(N+I,N+J)=AA(N+I,N+J)+A(I,J)
      IPP=1+IP
63    DO 25 I=1,N
      DO 25 J=1,N
      ZZ(I,J)=AA(I,J)
      YY(I,J)=AA(I,N+J)
25    XX(I,J)=AA(N+I,N+J)
      IF (IY.EQ.IZ+1) IY=IY+1
      II=0
      DO 30 I=1,N
      DO 30 J=1,N
```

```
      II=II+1
30    R(II)=ZZ(I,J)
      CALL INVERT (N)
      II=0
      DO 35 I=1,N
      DO 35 J=1,N
      II=II+1
35    ZZ(I,J)=RR(II)
      CALL  TRANS (N)
      CALL  MULTI (N,N,N,SY,ZZ,A5)
      DO 40 II=1,IPROP
      DO 40 I=1,N
40    BA(I,II)=BB(I,II)
      CALL XMULTI (N,N,IPROP,A5,BA,AB)
      DO 45 II=1,IPROP
      DO 45 I=1,N
45    BB(N+I,II)=BB(N+I,II)-AB(I,II)
      IPP=IP+1
      WRITE (5) ((BB(I,J),J=1,IPP),I=1,N)
      CALL MULTI (N,N,N,A5,YY,SY)
      DO 50 I=1,N
      DO 50 J=1,N
50    XX(I,J)=XX(I,J)-SY(I,J)
      WRITE (3) ((XX(I,J),J=1,N),I=1,N)
      WRITE (4) ((YY(I,J),J=1,N),I=1,N)
      DO 80 I=1,N
      NI=N+I
      DO 80 J=1,N
      NJ=N+J
80    AA(NI,NJ)=XX(I,J)
      DO 81 I=1,NN
      NI=N+I
      DO 79 II=1,IPROP
      BZ(I,II)=BB(NI,II)
79    CONTINUE
      DO 81 J=1,NN
      NJ=N+J
81    AZ(I,J)=AA(NI,NJ)
      NQ=1.5*NN
      DO 82 I=1,NQ
      DO 94 II=1,IPROP
94    BB(I,II)=0.0
      DO 82 J=1,NQ
82    AA(I,J)=0.0
      DO 83 I=1,NN
      DO 93 II=1,IPROP
93    BB(I,II)=BZ(I,II)
      DO 83 J=1,NN
83    AA(I,J)=AZ(I,J)
      IF (IY.EQ.IZ) IY=IY+1
      IF (IY.EQ.IZ+1) GO TO 63
      IF (IY.LT.IZ+1) RETURN
      WRITE (5) ((BB(I,J),J=1,IPP),I=1,N)
      IY=IY-2
      II=0
      DO 65 I=1,N
```

```
      DO 65 J=1,N
      II=II+1
65    R(II)=XX(I,J)
      CALL INVERT (N)
      II=0
      DO 70 I=1,N
      DO 70 J=1,N
      II=II+1
70    XX(I,J)=RR(II)
      DO 71 II=1,IPROP
      DO 71 I=1,N
71    AB(I,II)=BB(I,II)
      CALL XMULTI (N,N,IPROP,XX,AB,D)
      DO 75 II=1,IPROP
      DO 75 I=1,N
      NI=N*(IY)
75    DB(NI+I,II)=D(I,II)
500   RETURN
      END
      SUBROUTINE SOLVE (NN,N,DB,NX,NS,IPROP,IP)
      DIMENSION ZZ(48,48),XX(48,48),D(48,7),E(48,7),
     1DB(2000,7),R(2400),RR(2400),AB(48,7)
      COMMON /BL30/R,RR
      LEVEL 2,R,RR
      IX=NS
      DO 90 I=1,IX
      IXX=IX-(I-1)
      DO 110 II=1,IPROP
      DO 110 KI=1,N
      NI=N*IXX
110   D(KI,II)=DB(NI+KI,II)
      CALL BACK(2,3)
      READ (3) ((ZZ(J,K),K=1,N),J=1,N)
      CALL BACK (2,4)
      READ (4) ((XX(J,K),K=1,N),J=1,N)
      CALL XMULTI(N,N,IPROP,XX,D,E)
      II=0
      DO 105 K=1,N
      DO 105 J=1,N
      II=II+1
105   R(II)=ZZ(K,J)
      CALL INVERT (N)
      II=0
      DO 120 K=1,N
      DO 120 J=1,N
      II=II+1
120   ZZ(K,J)=RR(II)
      CALL BACK (2,5)
      IPP=IP+1
      READ (5) ((AB(II,JJ),JJ=1,IPP),II=1,N)
      DO 130 II=1,IPROP
      DO 130 K=1,N
130   AB(K,II)=AB(K,II)-E(K,II)
      CALL XMULTI (N,N,IPROP,ZZ,AB,D)
      DO 135 II=1,IPROP
      DO 135 K=1,N
```

```
      NI=N*(IXX-1)
135   DB(NI+K,II)=D(K,II)
90    CONTINUE
      RETURN
      END
      SUBROUTINE TRANS (N)
      DIMENSION A(48,48),B(48,48)
      COMMON /BL31/A,B
      DO 5 I=2,N
      LL=I-1
      DO 10 J=1,LL
      X=A(I,J)
      B(I,J)=A(J,I)
10    B(J,I)=X
5     CONTINUE
      DO 20 I=1,N
20    B(I,I)=A(I,I)
      RETURN
      END
      SUBROUTINE BACK (I,N)
      DO 10 J=1,I
10    BACKSPACE N
      RETURN
      END

      SUBROUTINE REST (NI,NJ,N,MM,N1)
      DIMENSION A(96,96),SS(96,96)
      COMMON /BL1/SS,A
      LEVEL 2,SS,A
C
C     NI,NJ=0  NODE  FREE
C   NI,NJ=1  NODE  S.S.
C   NI,NJ=2  NODE  FIXED
C   NI,NJ=3  NODE  S.S. AT  ENDS, V FREE
C   NI,NJ=4 NODE  S.S. AT ENDS, V FIXED
C    NI,NJ=5  NODE  S.S. AT  ENDS, U&V  FREE
C   NI,NJ,=6  AS NI,NJ=3, BUT WITH W RESTRAINED ALONG EDGE
C   NI,NJ=7  AS NI,NJ=4 BUT WITH W RESTRAINED ALONG EDGE
C   NJ=8  AS  NJ=6   RIGID  PLATE  MOVEMENT
C   NI=10  AS  NI=6   BUT  WITH  U1  AND  U2  NOT  =  ZERO
C
      IF (NI.EQ.0) GO TO 10
      IF (NI.EQ.1) GO TO 20
      IF (NI.EQ.2) GO TO 30
      IF (NI.EQ.3) GO TO 40
      IF (NI.EQ.4) GO TO 20
      IF (NI.EQ.5) GO TO 40
      IF (NI.EQ.6) GO TO 40
      IF (NI.EQ.7) GO TO 20
      IF (NI.EQ.10) GO TO 40
20    DO 25 I=1,N1
      IF (NI.EQ.7.AND.I.EQ.4) GO TO 25
      IF (NI.EQ.7.AND.I.EQ.8) GO TO 25
      A(I,I)=A(I,I)+1.E50
25    CONTINUE
      IF (NI.EQ.4.OR.NI.EQ.7) GO TO 50
```

```
      GO TO 10
30    DO 35 I=1,N
      A(I,I)=A(I,I)+1.E50
35    CONTINUE
      GO TO 10
40    DO 45 I=1,N1
      IF (NI.EQ.5.AND.I.EQ.1) GO TO 44
      IF (NI.EQ.6.AND.I.EQ.4) GO TO 44
      IF (NI.EQ.6.AND.I.EQ.8) GO TO 44
      IF (NI.EQ.5.AND.I.EQ.5) GO TO 44
      IF (NI.EQ.10.AND.I.EQ.4) GO TO 44
      IF (NI.EQ.10.AND.I.EQ.8) GO TO 44
      IF (NI.EQ.10.AND.I.EQ.1) GO TO 44
      IF (NI.EQ.10.AND.I.EQ.5) GO TO 44
      IF (I.EQ.6) GO TO 44
      A(I,I)=A(I,I)+1.E50
44    CONTINUE
45    CONTINUE
      IF (NI.EQ.10) NI=6
      IF (NI.EQ.6) GO TO 61
      GO TO 10
50    NZ=MM-2
      IF (MM.LE.2) GO TO 10
      DO 57 IP=1,NZ
      IN=4*(IP-1)+10
57    A(IN,IN)=A(IN,IN)+1.E50
      IF (NI.NE.7) GO TO 10
      DO 56 IP=1,NZ
      IN=4*(IP-1)+11
      A(IN-2,IN-2)=A(IN-2,IN-2)+1.E50
56    A(IN,IN)=A(IN,IN)+1.E50
      GO TO 10
61    DO 62 I=1,MM
      IN=4*(I-1)+3
      IF (I.EQ.2) GO TO 62
      A(IN-1,IN-1)=A(IN-1,IN-1)+1.E50
62    A(IN,IN)=A(IN,IN)+1.E50
10    IF (NJ.EQ.0) GO TO 60
      IF (NJ.EQ.1) GO TO 70
      IF (NJ.EQ.2) GO TO 80
      IF (NJ.EQ.3) GO TO 90
      IF (NJ.EQ.4) GO TO 70
      IF (NJ.EQ.5) GO TO 90
      IF (NJ.EQ.6) GO TO 90
      IF (NJ.EQ.7) GO TO 70
      IF (NJ.EQ.8) GO TO 90
70    DO 75 I=1,N1
      IF (NJ.EQ.7.AND.I.EQ.4) GO TO 75
      IF (NJ.EQ.7.AND.I.EQ.8) GO TO 75
      A(N+I,N+I)=A(N+I,N+I)+1.E50
75    CONTINUE
      IF (NJ.EQ.4.OR.NJ.EQ.7) GO TO 100
      GO TO 60
80    DO 85 I=1,N
      A(N+I,N+I)=A(N+I,N+I)+1.E50
85    CONTINUE
```

```
      GO TO 60
90    DO 95 I=1,N1
      IF (NJ.EQ.5.AND.I.EQ.1) GO TO 94
      IF (NJ.EQ.8.AND.I.EQ.8) GO TO 94
      IF (NJ.EQ.8.AND.I.EQ.4) GO TO 94
      IF (I.EQ.6) GO TO 94
      IF (NJ.EQ.5.AND.I.EQ.5) GO TO 94
      IF (NJ.EQ.6.AND.I.EQ.8) GO TO 94
      IF (NJ.EQ.6.AND.I.EQ.4) GO TO 94
      A(N+I,N+I)=A(N+I,N+I)+1.E50
94    CONTINUE
95    CONTINUE
      IF (NJ.EQ.6.OR.NJ.EQ.8) GO TO 91
      GO TO 60
100   NZ=MM-2
      IF (MM.LE.2) GO TO 60
      DO 107 IP=1,NZ
      IN=4*(IP-1)+10+N
107   A(IN,IN)=A(IN,IN)+1.E50
      IF (NJ.NE.7) GO TO 60
      DO 106 IP=1,NZ
      IN=4*(IP-1)+11+N
106   A(IN,IN)=A(IN,IN)+1.E50
      GO TO 60
91    DO 92 I=1,MM
      IN=4*(I-1)+3+N
      IF (NJ.EQ.8) A(IN-2,IN-2)=A(IN-2,IN-2)+1.E50
      IF (I.EQ.2) GO TO 92
      A(IN-1,IN-1)=A(IN-1,IN-1)+1.E50
92    A(IN,IN)=A(IN,IN)+1.E50
60    RETURN
      END
      SUBROUTINE MULTI (L,M,N,A,B,C)
      DIMENSION A(48,48),B(48,48),C(48,48)
      DO 2 I=1,L
      DO 2 J=1,N
      C(I,J)=0.
      DO 2 K=1,M
2     C(I,J)=C(I,J)+A(I,K)*B(K,J)
      RETURN
      END
      SUBROUTINE XMULTI(L,M,N,A,B,C)
      DIMENSION A(48,48),B(48,7),C(48,7)
      DO 2 I=1,L
      DO 2 J=1,N
      C(I,J)=0.0
      DO 2 K=1,M
2     C(I,J)=C(I,J)+A(I,K)*B(K,J)
      RETURN
      END
```

APPENDIX 4

Determination of Propping Forces

The distortion of a profile is restricted at the ends of the sheeting due to the influence of the purlins. Many methods are now available, amongst these the Finite Strip Method, to determine the forces. Most methods however, are costly in computer time with respect to the accuracy required in a design method. For the design charts, to be given later, a simple method was therefore necessary.

As the distortion mainly occurs at the ends of the sheeting it can be assumpted that the deformation of the plates die out at the same distance x_d along the sheeting length, shown in Fig. A4.1.

Considering Fig. A4.2, the uplift force P exerted by the purlin for the every corrugation fastened case is given by

$$P = - \frac{F \int_0^s M_1 M_o x_d}{d \int_0^s M_1 M_1 x_d}$$

so $P = k F$

where k is a constant depending only on the cross-sectional geometry of the profile,

and F is the fastener force = $q \cdot d$

To simplify the analysis, the propping moment diagram M_1 is separated into two moment diagrams M_2 and M_3, and the propping force P can then be given by

$$P = \frac{2.F. \int_0^{s/2} M_o \; M_2}{d \left[\int_0^{s/2} M_2 \; M_2 + \int_0^{s/2} M_3 \; M_3 \right]}$$

where $\int_0^{s/2}$ is the integration around half the profile.

The design tables are based on the above equation and a simple program was written to obtain the factor k for varying values of $2b_T / d$, h/d and theta θ.

In the case of the alternate corrugations, the purlin restrains the profile at two positions, Fig. A4.3. The assumption that the decay of the distortion is constant for all the plates has been shown to be incorrect. A modification factor γ of 2 has been chosen on the bases of Finite Element results undertaken by Lawson [4.3]. The propping forces can then be determined from the simultaneous equation

$$\begin{bmatrix} \int_0^{s/2} M_0 \; M_5 \; ds \\ \int_0^{s/2} M_0 \; M_7 \; ds \end{bmatrix} =$$

$$\begin{bmatrix} \left(\int_0^{s/2} M_5 \, M_5 \, ds + \gamma \int_0^{s/2} M_6 \, M_6 \, ds\right) & \left(\int_0^{s/2} M_5 \, M_7 \, ds + \gamma \int_0^{s/2} M_6 \, M_8 \, ds\right) \\ \left(\int_0^{s/2} M_5 \, M_7 \, ds + \gamma \int_0^{s/2} M_6 \, M_8 \, ds\right) & \left(\int_0^{s/2} M_7 \, M_7 \, ds + \gamma \int_0^{s/2} M_8 \, M_8 \, ds\right) \end{bmatrix}$$

$$\begin{bmatrix} P_1 / 2 \\ P_2 / 2 \end{bmatrix}$$

Again design tables were produced based on these equation, were

$$k_1 = \frac{P_1}{2d}$$

$$k2 = \frac{P_2}{2d}$$

It should be noted that certain values are not given in the design tables, this is for one of two reasons, namely :-

a. that the various combinations of the parameter $2b_T/d$, h/d and theta give an unrealistic profile

i.e.

$$2\,b_T + 2\,b_L + 2\,p > d$$

and b. that the value of the propping force is negative from the program and so the force should be taken as zero.

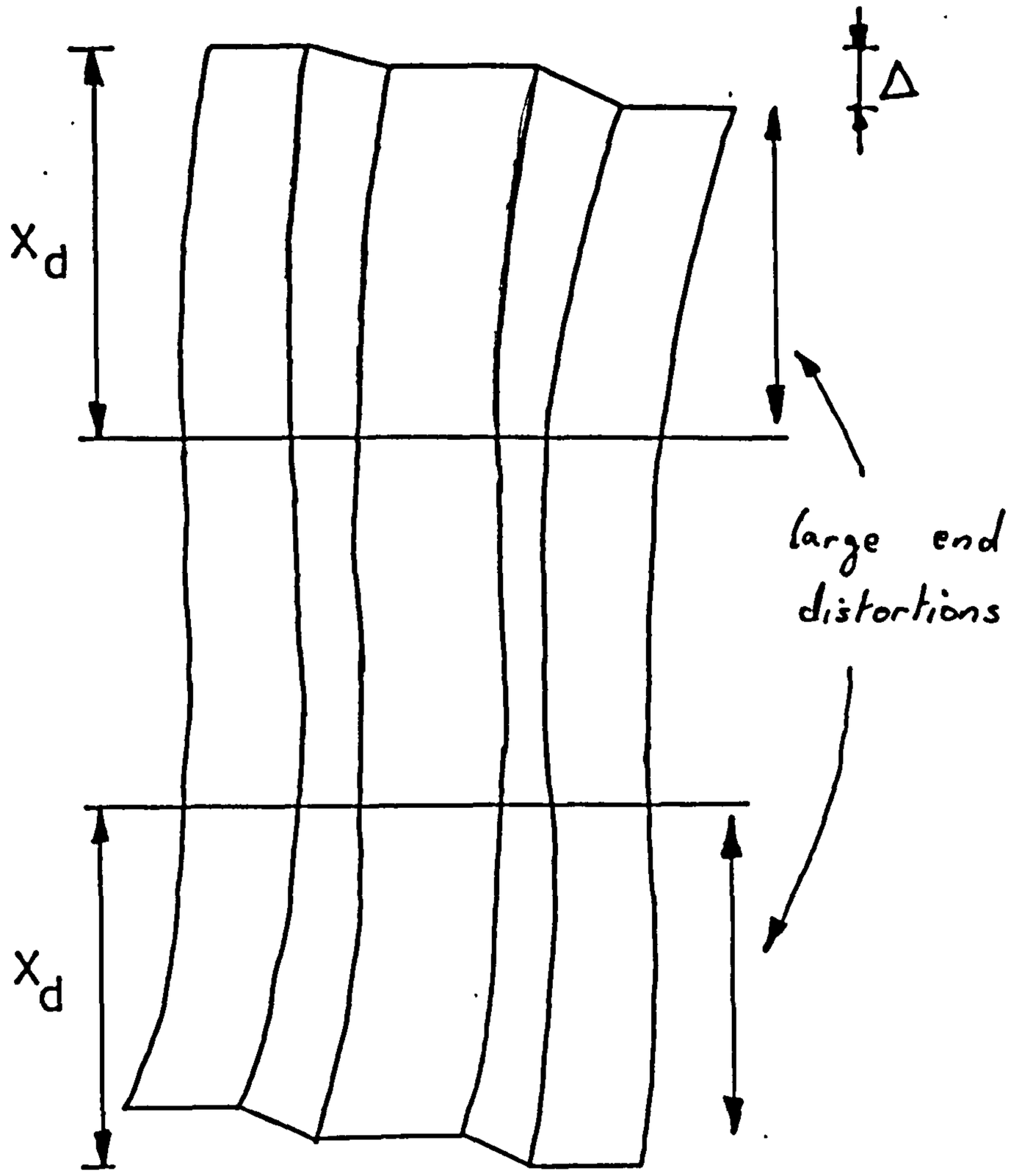

Fig A4.1 Plan View of the Distortion of Profile

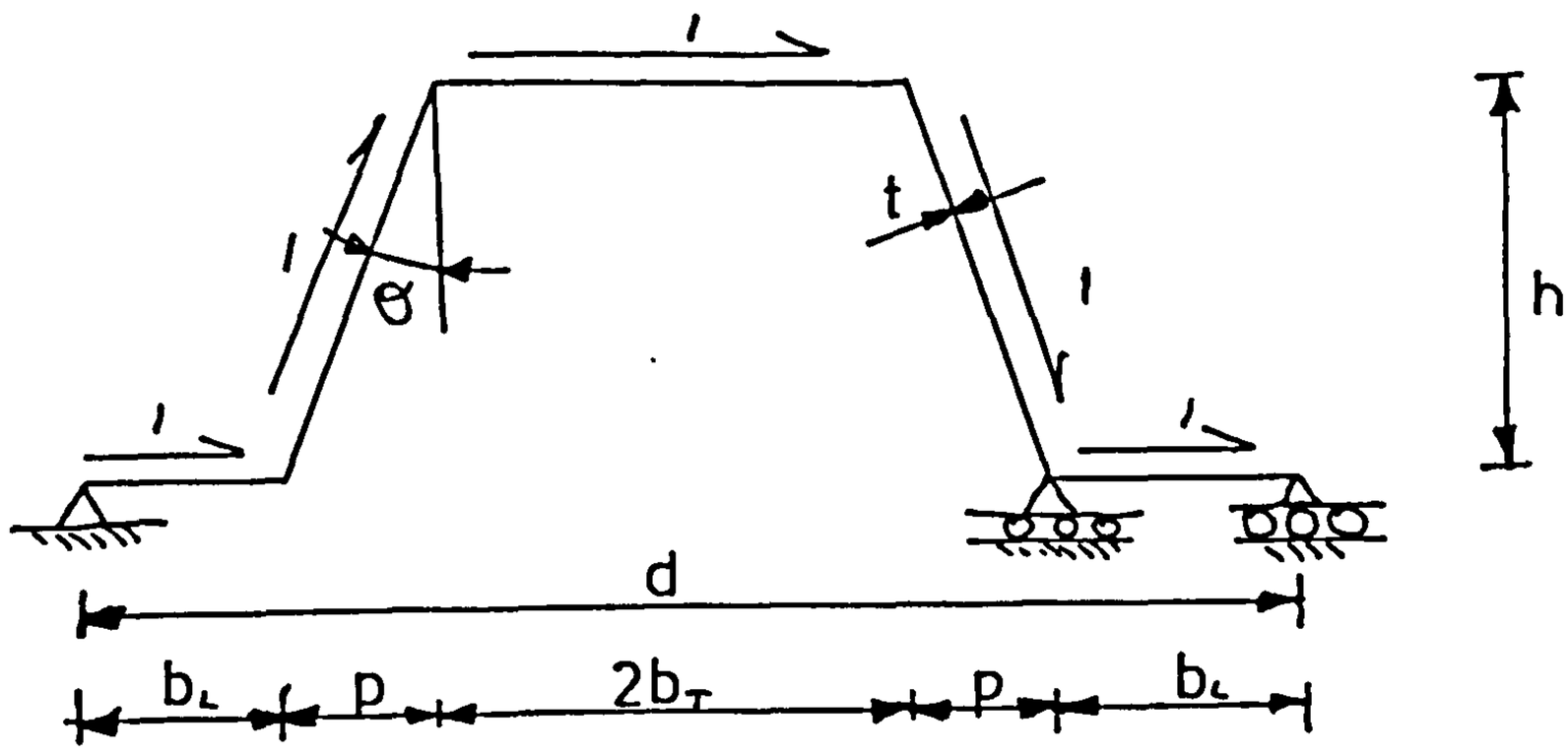

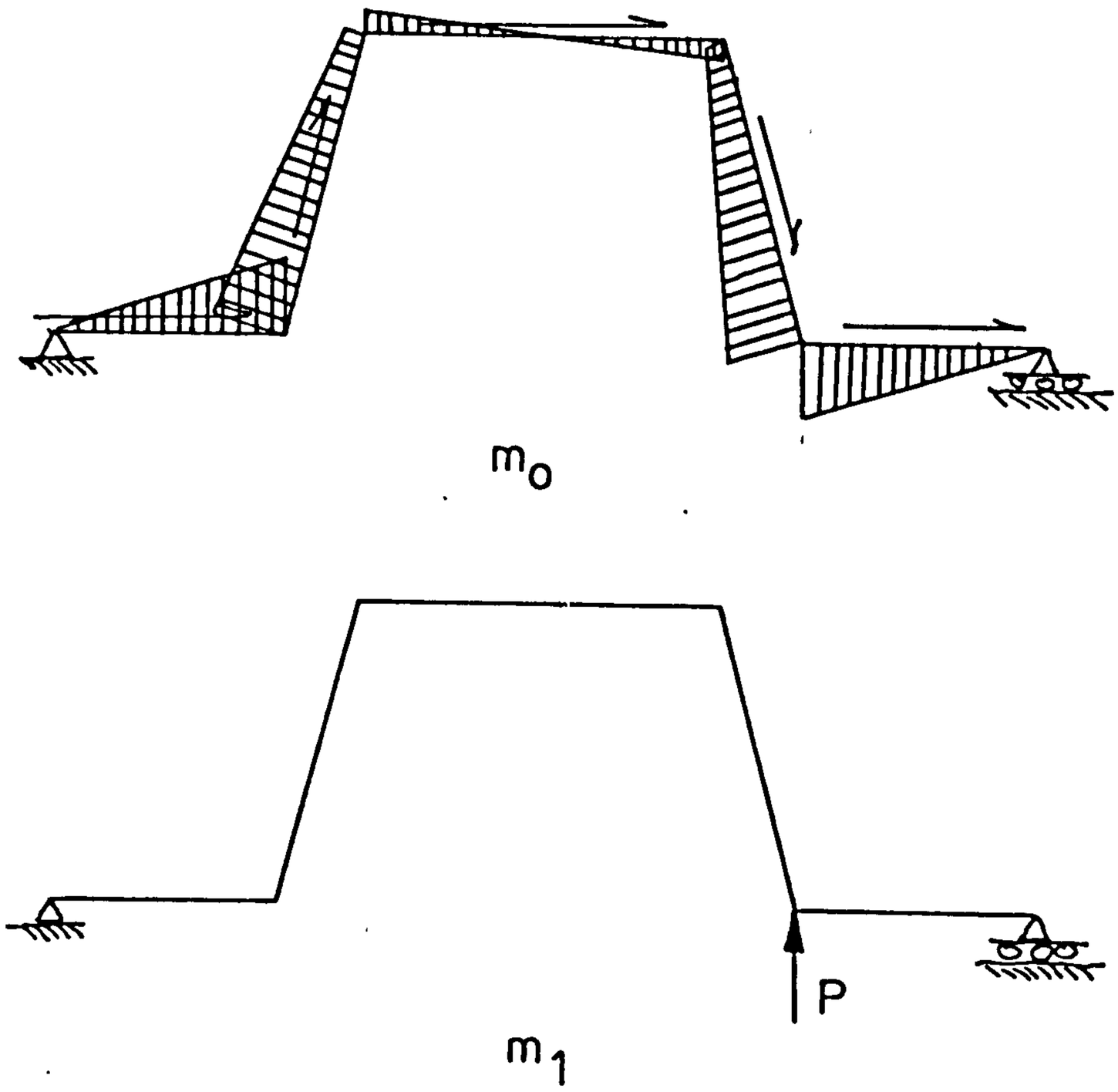

m_0

m_1

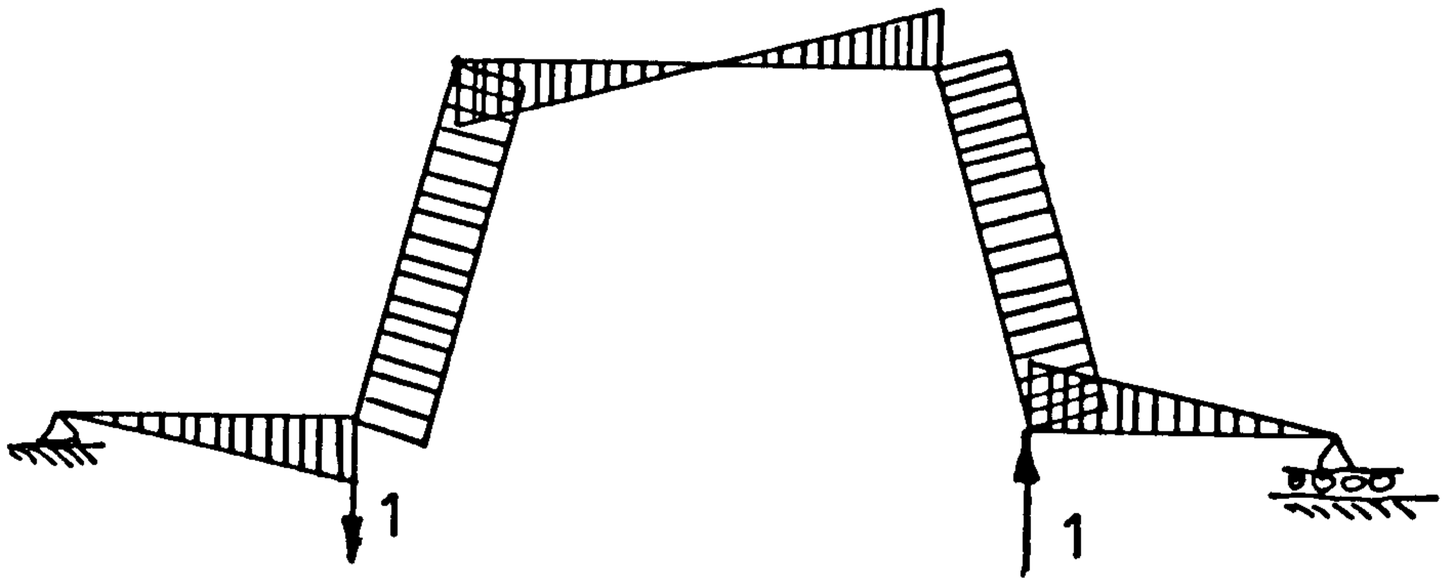

m_2

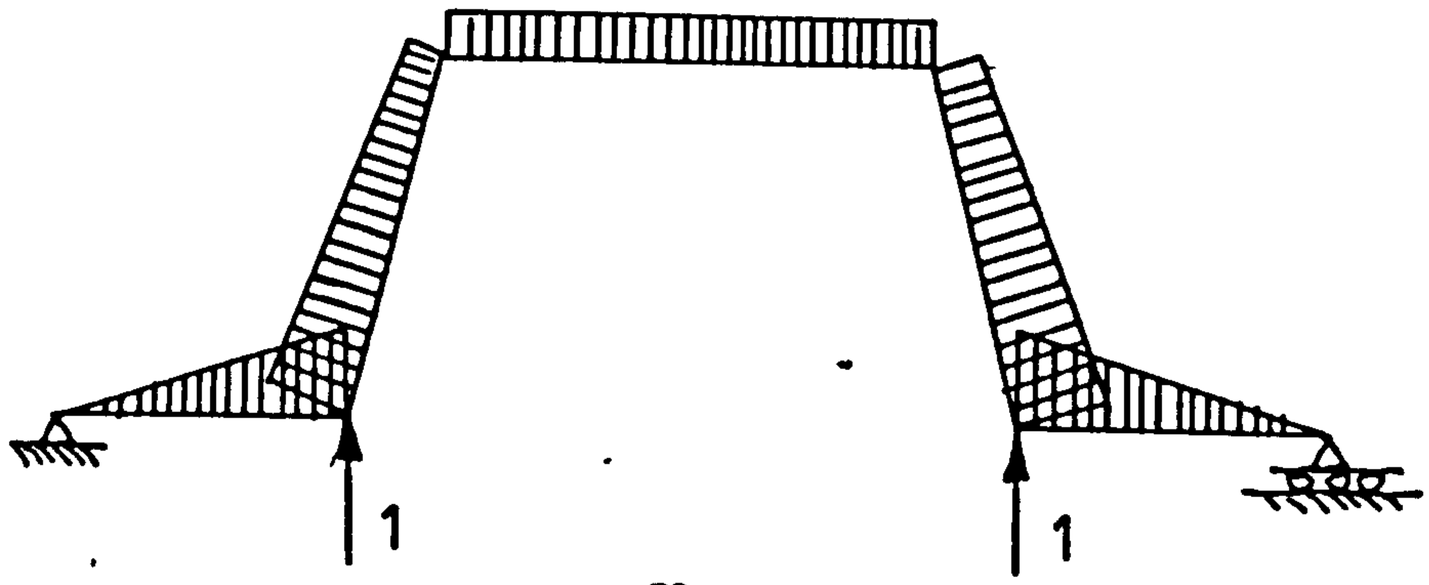

m_3

Fig. A 4.2 Moment Diagrams for every corrugation fastened

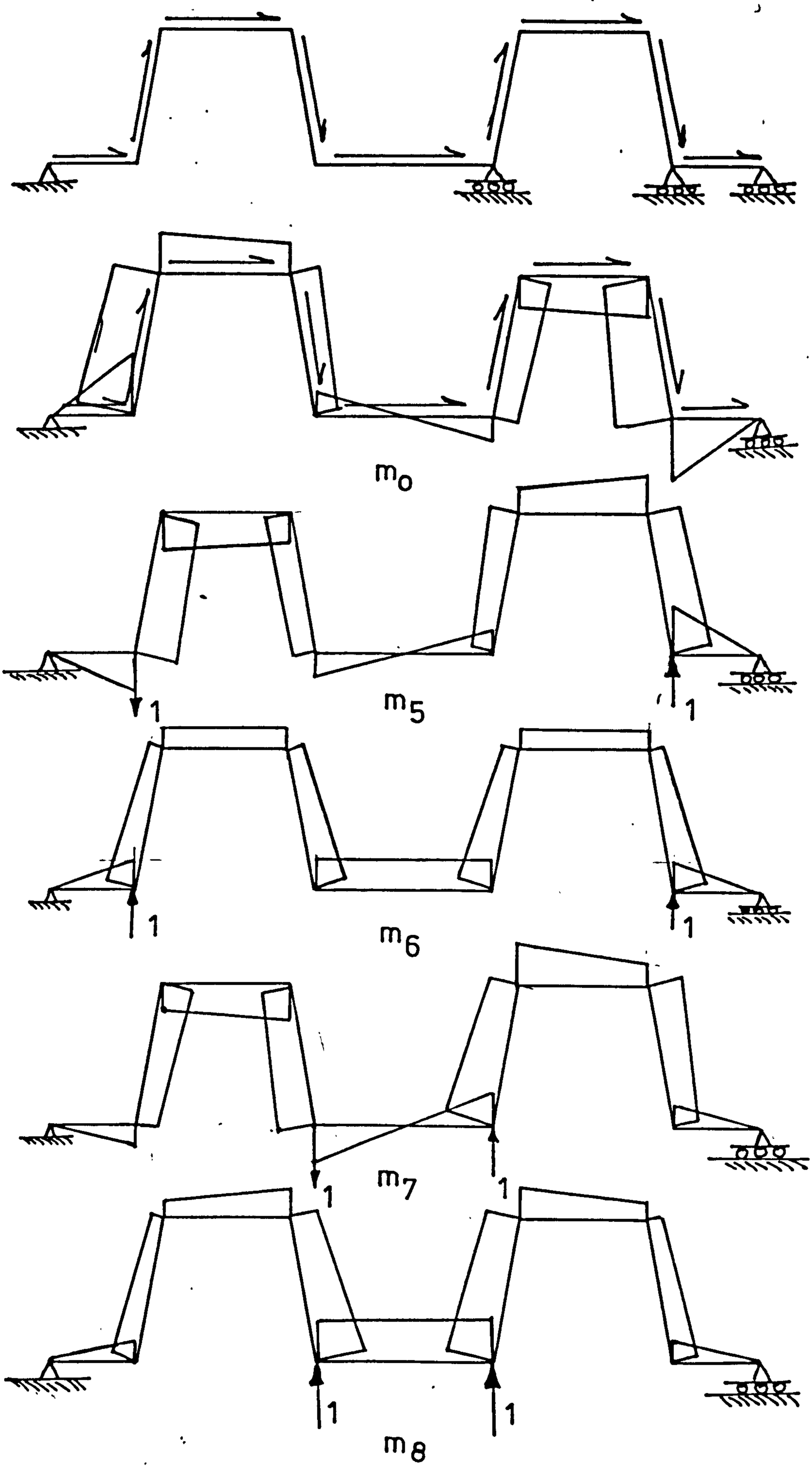

Fig A 4.3 Moment Diagrams for alt. corr. fastened

EVERY CORRUGATIONS (K)

	2BT/D	0.1	0.2	0.3	0.4	0.5	0.6	0.7	0.8
	H/D								
	0.1	0.0050	0.0196	0.0407	0.0602	0.0731	0.0584	-	-
	0.2	0.0115	0.0436	0.0885	0.1318	0.1540	0.1281	0.0074	-
	0.3	0.0189	0.0706	0.1406	0.2063	0.2390	0.2028	0.0350	-
θ=0	0.4	0.0270	0.0996	0.1959	0.2828	0.3269	0.2804	0.0675	-
	0.5	0.0356	0.1303	0.2534	0.3637	0.4167	0.3599	0.1027	-
	0.6	0.0446	0.1621	0.3125	0.4453	0.5080	0.4408	0.1398	-
	0.7	0.0540	0.1948	0.3730	0.5282	0.6005	0.5228	0.1781	-
	0.8	0.0636	0.2283	0.4345	0.6122	0.6939	0.6056	0.2713	-

EVERY CORRUGATIONS (K)

	2BT/D								
		0.1	0.2	0.3	0.4	0.5	0.6	0.7	0.8
	H/D								
	0.1	0.0062	0.0217	0.0433	0.0644	0.0742	0.0562	-	-
	0.2	0.0167	0.0523	0.0988	0.1409	0.1578	0.1193	-	-
	0.3	0.0316	0.0911	0.1640	0.2259	0.2465	0.1821	-	-
θ=5	0.4	0.0513	0.1374	0.2374	0.3176	0.3381	0.2408	-	-
	0.5	0.0759	0.1909	0.3181	0.4146	0.4310	0.2927	-	-
	0.6	0.1057	0.2511	0.4054	0.5160	0.5238	0.3349	-	-
	0.7	0.1409	0.3180	0.4986	0.6210	0.6155	0.3642	-	-
	0.8	0.1816	0.3913	0.5973	0.7288	0.7047	0.3771	-	-

EVERY CORRUGATIONS (K)

	2BT/D								
		0.1	0.2	0.3	0.4	0.5	0.6	0.7	0.8
	H/D								
	0.1	0.0075	0.0239	0.0459	0.0668	0.0572	0.0534	-	-
	0.2	0.0229	0.0618	0.1094	0.1497	0.1603	0.1060	-	-
	0.3	0.0475	0.1137	0.1877	0.2440	0.2486	0.1448	-	-
θ=10	0.4	0.0827	0.1791	0.2789	0.3465	0.3349	0.1570	-	-
	0.5	0.1292	0.2575	0.3812	0.4543	0.4138	0.1244	-	-
	0.6	0.1874	0.3485	0.4930	0.5645	0.4782	0.0172	-	-
	0.7	0.2586	0.4511	0.6128	0.6739	0.5180	-	-	-
	0.8	0.3418	0.5647	0.7386	0.7785	0.5174	-	-	-

EVERY CORRUGATION (K)

	2BT/D								
		0.1	0.2	0.3	0.4	0.5	0.6	0.7	0.8
	H/D								
	0.1	0.0090	0.0262	0.0487	0.0692	0.0760	0.0500	-	-
	0.2	0.0302	0.0722	0.1204	0.1581	0.1609	0.0862	-	-
	0.3	0.0667	0.1382	0.2117	0.2597	0.2425	0.0786	-	-
θ=15	0.4	0.1207	0.2238	0.3192	0.2676	0.3067	-	-	-
	0.5	0.1934	0.3276	0.4392	0.4743	0.3306	-	-	-
	0.6	0.2850	0.4478	0.5676	0.5691	0.2669	-	-	-
	0.7	0.3948	0.5819	0.6991	0.6335	-	-	-	-
	0.8	0.5217	0.7272	0.8260	0.6287	-	-	-	-

EVERY CORRUGATION (K)

	2BT/D								
		0.1	0.2	0.3	0.4	0.5	0.6	0.7	0.8
	H/D								
	0.1	0.0107	0.0288	0.0516	0.0716	0.0766	0.0456	-	-
	0.2	0.0387	0.0835	0.1319	0.1660	0.1587	0.0559	-	-
	0.3	0.0892	0.1646	0.2356	0.2718	0.2225	-	-	-
θ=20	0.4	0.1649	0.2707	0.3566	0.3752	0.2247	-	-	-
	0.5	0.2660	0.3982	0.4867	0.4525	0.0409	-	-	-
	0.6	0.3911	0.5423	0.6133	0.4459	-	-	-	-
	0.7	0.5373	0.6966	0.7111	0.1231	-	-	-	-
	0.8	0.7009	0.8504	0.7008	-	-	-	-	-

EVERY CORRUGATION (K)

	2BT/D							
	0.1	0.2	0.3	0.4	0.5	0.6	0.7	0.8
H/D								
0.1	0.0126	0.0316	0.0548	0.0742	0.0770	0.0400	-	-
0.2	0.0488	0.0959	0.1438	0.1732	0.1523	0.0075	-	-
0.3	0.1153	0.1930	0.2589	0.2776	0.1715	-	-	-
θ=25 0.4	0.2145	0.3187	0.3879	0.3533	-	-	-	-
0.5	0.3444	0.4655	0.5094	0.2924	-	-	-	-
0.6	0.5000	0.6210	0.5625	-	-	-	-	-
0.7	0.6745	0.7567	0.0483	-	-	-	-	-
0.8	0.8573	0.6839	-	-	-	-	-	-

EVERY CORRUGATION (K)

	2BT/D								
		0.1	0.2	0.3	0.4	0.5	0.6	0.7	0.8
	H/D								
	0.1	0.0149	0.0345	0.0583	0.0769	0.0770	0.0324	-	-
	0.2	0.0606	0.1097	0.1562	0.1790	0.1386	-	-	-
	0.3	0.1453	0.2231	0.2802	0.2705	0.0587	-	-	-
θ=30	0.4	0.2691	0.3661	0.4042	0.2401	-	-	-	-
	0.5	0.4256	0.5210	0.4399	-	-	-	-	-
	0.6	0.6042	0.6305	-	-	-	-	-	-
	0.7	0.7797	-	-	-	-	-	-	-

EVERY CORRUGATION (K)

	2BT/D						
	0.1	0.2	0.3	0.4	0.5	0.6	0.7
H/D							
0.1	0.0176	0.0385	0.0621	0.0797	0.0764	0.0219	-
0.2	0.0745	0.1250	0.1690	0.1820	0.1106	-	-
0.3	0.1893	0.2545	0.2966	0.2310	-	-	-
Φ=35 0.4	0.3275	0.4081	0.3696	-	-	-	-
0.5	0.5051	0.5176	-	-	-	-	-
0.6	0.6659	-	-	-	-	-	-

EVERY CORRUGATION (K)

	2BT/D						
	0.1	0.2	0.3	0.4	0.5	0.6	0.7
H/D							
0.1	0.0208	0.0427	0.0664	0.0825	0.0748	0.0064	-
0.2	0.0911	0.1421	0.1817	0.1793	0.0488	-	-
0.3	0.2176	0.2860	0.2979	0.0603	-	-	-
θ=40 0.4	0.3875	0.4241	-	-			
0.5	0.5538						

EVERY CORRUGATION (K)

	2BT/D					
	0.1	0.2	0.3	0.4	0.5	0.6
H/D						
0.1	0.0249	0.0478	0.0713	0.0854	0.0714	-
0.2	0.1109	0.1611	0.1930	0.1619	-	-
0.3	0.2599	0.3126	0.2285	-	-	-
0.4	0.4397	-	-	-	-	-

$\theta = 45$

EVERY CORRUGATION (K)

	2BT/D					
	0.1	0.2	0.3	0.4	0.5	0.6
H/D						
0.1	0.0300	0.0539	0.0769	0.0879	0.0644	-
0.2	0.1347	0.1819	0.1985	0.0926	-	-
0.3	0.3046	0.2980	-	-	-	-
0.4	-	-	-	-	-	-

$\theta = 50$

ALTERNATE CORRUGATIONS (K1)

	2BT/D	0.1	0.2	0.3	0.4	0.5	0.6	0.7	0.8	0.9
	H/D									
	0.1	0.0016	0.0022	0.0035	0.0056	0.0082	0.0106	0.0121	0.0120	0.0088
	0.2	0.0052	0.0050	0.0070	0.0104	0.0148	0.0190	0.0218	0.0210	0.0148
	0.3	0.0100	0.0082	0.0100	0.0146	0.0206	0.0266	0.0300	0.0286	0.0196
0=0	0.4	0.0156	0.0112	0.0126	0.0182	0.0258	0.0332	0.0376	0.0354	0.0238
	0.5	0.0218	0.0144	0.0150	0.0212	0.0306	0.0396	0.0446	0.0418	0.0280
	0.6	0.0284	0.0176	0.0172	0.0240	0.0348	0.0454	0.0514	0.0480	0.0318
	0.7	0.0352	0.0206	0.0190	0.0266	0.0390	0.0512	0.0578	0.0540	0.0354
	0.8	0.0424	0.0236	0.0206	0.0288	0.0428	0.0566	0.0642	0.0598	0.0392

ALTERNATE CORRUGATIONS (K2)

	2BT/D	0.1	0.2	0.3	0.4	0.5	0.6	0.7	0.8	0.9
	H/D									
	0.1	0.0122	0.0212	0.0312	0.0432	0.0576	0.0758	0.1004	0.1372	0.2086
	0.2	0.0326	0.0510	0.0716	0.0940	0.1206	0.1424	0.1918	0.2436	0.3242
	0.3	0.0594	0.0876	0.1176	0.1508	0.1880	0.2302	0.2788	0.3362	0.4082
0=0	0.4	0.0912	0.1294	0.1694	0.2120	0.2586	0.3094	0.3640	0.4212	0.4782
	0.5	0.1270	0.1758	0.2252	0.2772	0.3320	0.3896	0.4480	0.5020	0.5406
	0.6	0.1660	0.2256	0.2846	0.3452	0.4080	0.4712	0.5316	0.5802	0.5984
	0.7	0.2078	0.2782	0.3470	0.4158	0.4854	0.5538	0.6150	0.6566	0.6534
	0.8	0.2520	0.3336	0.4116	0.4886	0.5648	0.6354	0.6982	0.7320	0.7066

ALTERNATE CORRUGATIONS (K1)

0=5 H/D \ 2BT/D	0.1	0.2	0.3	0.4	0.5	0.6	0.7	0.8	0.9
0.1	0.0018	0.0024	0.0038	0.0060	0.0084	0.0106	0.0120	0.0116	0.0078
0.2	0.0064	0.0062	0.0082	0.0118	0.0158	0.0196	0.0214	0.0192	0.0106
0.3	0.0132	0.0114	0.0132	0.0176	0.0232	0.0276	0.0290	0.0244	0.0106
0.4	0.0224	0.0178	0.0192	0.0242	0.0304	0.0352	0.0354	0.0276	0.0084
0.5	0.0332	0.0256	0.0260	0.0312	0.0380	0.0426	0.0410	0.0294	0.0042
0.6	0.0458	0.0346	0.0338	0.0388	0.0456	0.0494	0.0254	0.0294	--
0.7	0.0596	0.0448	0.0424	0.0472	0.0534	0.0558	0.0490	0.0280	--
0.8	0.0748	0.0560	0.0518	0.0560	0.0614	0.0620	0.0514	0.0248	

ALTERNATE CORRUGATIONS (K2)

0=5 H/D \ 2BT/D	0.1	0.2	0.3	0.4	0.5	0.6	0.7	0.8	0.9
0.1	0.0124	0.0216	0.0318	0.0442	0.0592	0.0782	0.1044	0.1454	0.2312
0.2	0.0334	0.0526	0.0736	0.0978	0.1262	0.1608	0.2050	0.2668	0.3656
0.3	0.0610	0.0910	0.1232	0.1590	0.1998	0.2472	0.3038	0.3752	0.4804
0.4	0.0940	0.1360	0.1794	0.2266	0.2786	0.3366	0.4016	0.4748	0.5624
0.5	0.1362	0.1862	0.2412	0.3000	0.3620	0.4290	0.4986	0.5674	0.6266
0.6	0.1744	0.2414	0.3080	0.3772	0.4494	0.5234	0.5948	0.6536	--
0.7	0.2210	0.3008	0.3792	0.4590	0.5402	0.6196	0.6898	0.7336	--
0.8	0.2712	0.3640	0.4544	0.5446	0.6338	0.7174	0.7834	0.8072	--

ALTERNATE CORRUGATION (K1)

θ=15	2BT/D	0.1	0.2	0.3	0.4	0.5	0.6	0.7	0.8
	H/D								
	0.1	0.0020	0.0028	0.0044	0.0064	0.0088	0.0108	0.0118	0.0104
	0.2	0.0076	0.0082	0.0104	0.0138	0.0154	0.0198	0.0192	0.0134
	0.3	0.0164	0.0162	0.0186	0.0224	0.0260	0.0268	0.0224	0.0088
	0.4	0.0280	0.0264	0.0284	0.0318	0.0338	0.0310	0.0198	
	0.5	0.0416	0.0386	0.0396	0.0412	0.0396	0.0308	0.0100	
	0.6	0.0568	0.0518	0.0508	0.0490	0.0418	0.0244		
	0.7	0.0726	0.0654	0.0608	0.0540	0.0398	0.0100		
	0.8	0.0884	0.0778	0.0684	0.0542	0.0284			

ALTERNATE CORRUGATIONS (K2)

θ=15	2BT/D	0.1	0.2	0.3	0.4	0.5	0.6	0.7	0.8	0.9
	H/D									
	0.1	0.0132	0.0226	0.0334	0.0464	0.0626	0.0838	0.1142	0.1658	0.2986
	0.2	0.0366	0.0572	0.0802	0.1072	0.1402	0.1822	0.2404	0.3364	--
	0.3	0.0702	0.1030	0.1396	0.1816	0.2318	0.2942	0.3780	0.5128	
	0.4	0.1138	0.1602	0.2112	0.2692	0.3368	0.4186	0.5250	--	
	0.5	0.1680	0.2286	0.2950	0.3694	0.4544	0.5540	0.6792	--	
	0.6	0.2332	0.3090	0.3914	0.4826	0.5840	0.7990	--	--	
	0.7	0.3098	0.4016	0.5006	0.6082	0.7246	0.8504	--	--	
	0.8	0.3984	0.5068	0.6226	0.7458	0.8744	--	--	--	

ALTERNATE CORRUGATION (K1)

	2BT/D								
	0.1	0.2	0.3	0.4	0.5	0.6	0.7	0.8	0.9
H/D									
0.1	0.0022	0.0031	0.0045	0.0067	0.0089	0.0108	0.0115	0.0096	0.0032
0.2	0.0082	0.0090	0.0114	0.0147	0.0179	0.0194	0.0173	0.0088	
0.3	0.0179	0.0181	0.0207	0.0240	0.0260	0.0243	0.0154		
0=20 0.4	0.0302	0.0257	0.0315	0.0330	0.0313	0.0226	0.0025		
0.5	0.0443	0.0425	0.0420	0.0394	0.0307	0.0108			
0.6	0.0596	0.0548	0.0498	0.0401	0.0203				
0.7	0.0735	0.0640	0.0518	0.0311					
0.8	0.0838	0.0671	0.0441	0.0081					

ALTERNATE CORRUGATIONS (K2)

	2BT/D								
	0.1	0.2	0.3	0.4	0.5	0.6	0.7	0.8	0.9
H/D									
0.1	0.0136	0.0232	0.0344	0.0478	0.0646	0.0870	0.1200	0.1794	0.3544
0.2	0.0390	0.0602	0.0844	0.1134	0.1492	0.1964	0.2658	0.3944	--
0.3	0.0790	0.1114	0.1508	0.1972	0.2544	0.3290	0.4396	--	
0=20 0.4	0.1284	0.1778	0.2342	0.3002	0.3808	0.4860	0.6460	--	
0.5	0.1944	0.2608	0.3360	0.4236	0.5300	0.6698	-	-	
0.6	0.2790	0.3618	0.4578	0.5690	0.7034	--	--	--	
0.7	0.3774	0.4826	0.6010	0.7374	--	--	--	--	
0.8	0.4976	0.6246	0.7668	0.9300	--	--	--	--	

ALTERNATE CORRUGATIONS (K1)

	2BT/D	0.1	0.2	0.3	0.4	0.5	0.6	0.7	0.8	0.9
	H/D									
	0.1	0.0023	0.0032	0.0048	0.0075	0.0091	0.0108	0.0111	0.0087	0.0008
	0.2	0.0089	0.0100	0.0125	0.0156	0.0181	0.0183	0.0144	0.0025	
	0.3	0.0193	0.0202	0.0226	0.0248	0.0247	0.0193	0.0046		
0=25	0.4	0.0325	0.0323	0.0330	0.0314	0.0243	0.0071			
	0.5	0.0467	0.0436	0.0395	0.0301	0.0101				
	0.6	0.0690	0.0505	0.0373	0.0139					
	0.7	0.0650	0.0467	0.0185						
	0.8	0.0591	0.0246							

ALTERNATE CORRUGATIONS (K2)

	2BT/D	0.1	0.2	0.3	0.4	0.5	0.6	0.7	0.8	0.9
	H/D									
	0.1	0.0141	0.0239	0.0353	0.0492	0.0669	0.0908	0.1271	0.1960	0.4138
	0.2	0.0420	0.0640	0.0896	0.1208	0.1603	0.2144	0.3001	0.4889	
	0.3	0.0853	0.1220	0.1649	0.2171	0.2839	0.3781	0.5409		
0=25	0.4	0.1465	0.2007	0.2645	0.3425	0.4443	0.5962			
	0.5	0.2289	0.3038	0.3926	0.5028	0.6523				
	0.6	0.3358	0.4354	0.5348	0.7068					
	0.7	0.4716	0.6007	0.7584						
	0.8	0.6412	0.8061							

ALTERNATE CORRUGATIONS (K1)

	2BT/D								
		0.1	0.2	0.3	0.4	0.5	0.6	0.7	0.8	0.9
	H/D									
	0.1	0.0026	0.0034	0.0052	0.0072	0.0092	0.0108	0.0106	0.0074	--
	0.2	0.0096	0.0110	0.0136	0.0162	0.0180	0.0168	0.0102	--	
	0.3	0.0214	0.0220	0.0238	0.0244	0.0212	0.0106			
0=30	0.4	0.0344	0.0336	0.0316	0.0250	0.0096				
	0.5	0.0464	0.0400	0.0286	0.0070					
	0.6	0.0500	0.0320	0.0028						
	0.7	0.0350								

ALTERNATE CORRUGATIONS (K2)

	2BT/D								
		0.1	0.2	0.3	0.4	0.5	0.6	0.7	0.8	0.9
	H/D									
	0.1	0.0148	0.0248	0.0366	0.0512	0.0698	0.0954	0.1356	0.2184	—
	0.2	0.0456	0.0688	0.0962	0.1300	0.1744	0.2384	0.3510	—	
	0.3	0.0958	0.1356	0.1834	0.2438	0.3258	0.4556	—	—	
0=30	0.4	0.1704	0.2316	0.3066	0.4046	0.5480				
	0.5	0.2758	0.3650	0.4780	0.6358					
	0.6	0.4206	0.5482	0.7200						
	0.7	0.6172								

ALTERNATE CORRUGATIONS (K1)

	2BT/D							
	0.1	0.2	0.3	0.4	0.5	0.6	0.7	0.8
H/D								
0.1	0.0027	0.0037	0.0054	0.0074	0.0094	0.0106	0.0099	0.0059
0.2	0.0105	0.0121	0.0142	0.0166	0.0171	0.0139	0.0034	
0=35 0.3	0.0226	0.0235	0.0240	0.0219	0.0139			
0.4	0.0350	0.0319	0.0249	0.0097				
0.5	0.0396	0.0253						

ALTERNATE CORRUGATIONS (K2)

	2BT/D								
	0.1	0.2	0.3	0.4	0.5	0.6	0.7	0.8	0.9
H/D									
0.1	0.0156	0.0260	0.0382	0.0534	0.0734	0.1010	0.1466	0.2504	--
0.2	0.0502	0.0746	0.1042	0.1420	0.1932	0.2728	0.4306	--	
0=35 0.3	0.1096	0.1538	0.2086	0.2818	0.3914	--	--	--	
0.4	0.2032	0.2756	0.3702	0.5090	--	--	--	--	
0.5	0.3450	0.4616	--	--	--	--	--	--	

ALTERNATE CORRUGATIONS (K1)

	2BT/D							
	0.1	0.2	0.3	0.4	0.5	0.6	0.7	0.8
H/D								
0.1	0.0030	0.0040	0.0058	0.0078	0.0094	0.0104	0.0090	0.0034
0.2	0.0116	0.0132	0.0152	0.0166	0.0154	0.0090		
0=40 0.3	0.0240	0.0240	0.0220	0.0154				
0.4	0.0322	0.0238	0.0072					
0.5	0.0176							

ALTERNATE CORRUGATIONS (K2)

θ=40 H/D \ 2BT/D	0.1	0.2	0.3	0.4	0.5	0.6	0.7	0.8	0.9
0.1	0.0166	0.0272	0.0400	0.0560	0.0772	0.1080	0.1612	0.3010	--
0.2	0.0560	0.0824	0.1150	0.1580	0.2198	0.3272	--	--	
0.3	0.1284	0.1790	0.2456	0.3422	--	--	--	--	
0.4	0.2516	0.3446	0.4826	--	--	--	--	--	
0.5	0.4624	--	--	--	--	--	--	--	

ALTERNATE CORRUGATIONS (K1)

θ=45 H/D \ 2BT/D	0.1	0.2	0.3	0.4	0.5	0.6	0.7	0.8	0.9
0.1	0.0032	0.0044	0.0062	0.0080	0.0094	0.0098	0.0076	--	--
0.2	0.0128	0.0144	0.0156	0.0154	0.0116	--	--		
0.3	0.0244	0.0218	0.0152						
0.4	0.0204								

ALTERNATE CORRUGATIONS (K2)

θ=45 H/D \ 2BT/D	0.1	0.2	0.3	0.4	0.5	0.6	0.7	0.8	0.9
0.1	0.0180	0.0290	0.0424	0.0594	0.0824	0.1172	0.1824	--	--
0.2	0.0640	0.0930	0.1300	0.1814	0.2620	--	--	--	
0.3	0.1556	0.2176	0.3064	--	--	--	--	--	
0.4	0.3334	--	--	--	--	--	--	--	

Appendix 5

Proc. Instn Civ. Engrs, Part 2, 1979, 67, Dec., 891–906

8271

The diaphragm action of composite slabs

J. M. DAVIES, DSc, PhD, FICE, FIStructE*

J. FISHER, BSc*

Composite floor slabs consisting of profiled steel sheeting and in situ concrete topping act as horizontal diaphragms and attract significant in-plane loads. In this Paper, the diaphragm action of composite slabs fastened to the primary structure with mechanical fasteners such as self-drilling, self-tapping screws is considered. Four full-scale tests on cantilever diaphragms are described and three failure modes identified. A theory is then developed whereby the strength and flexibility may be predicted. The prediction of strength shows adequate accuracy but the prediction of flexibility is found to be applicable only when a diaphragm is reloaded. The calculation of the initial flexibility is shown to be difficult because there is a relatively large initial movement before full composite action is developed.

Notation

a width of diaphragm
b depth of diaphragm
F ultimate strength of a single fastener in shear
n_a number of fasteners to edge member, a/p_a
n_b number of fasteners to main beam, b/p_b
p_a pitch of fasteners to edge member
p_b pitch of fasteners to main beam

Introduction

Composite floors, consisting of profiled steel sheeting acting in conjunction with in situ concrete topping have been popular in the USA for many years. They are also becoming more widely used in Europe and design procedures have recently been developed for European use.[1]

2. Composite floors are efficient for their primary purpose of spanning between supporting beams under the action of vertical load. They have a very high in-plane stiffness and strength and it is apparent that they also serve to distribute lateral load between the frames of the primary structure. When acting in this way, the composite deck is behaving rather like a deep beam or diaphragm and as a consequence of the proportions of this diaphragm the influence of shear is more important than that of bending. Scant attention has been paid to the performance of composite decks acting as diaphragms and this is the subject of this Paper.

Written discussion closes 15 February, 1980, for publication in *Proceedings*, Part 2.
* Department of Civil Engineering, University of Salford.

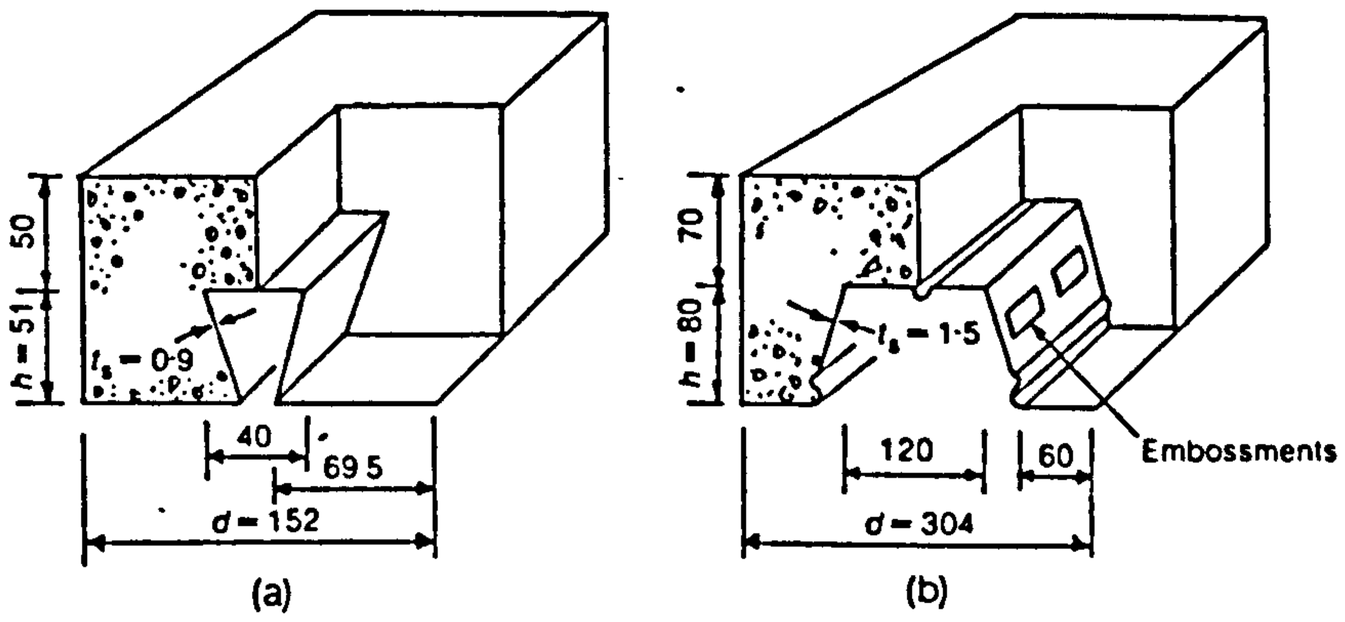

Fig. 1. Decking profile types ; (a) re-entrant profile, (b) trapezoidal profile

3. There are two distinct types of composite diaphragm

(*a*) diaphragms in which the profiled steel sheet is fastened to the supporting structure by mechanical fasteners or welds in such a way that there is no direct attachment of the concrete to the supporting structure

(*b*) diaphragms incorporating shear connectors which typically take the form of studs welded through the sheeting to the supporting steelwork thereby fastening the sheeting to this steelwork and, at the same time, providing a direct shear connection to the concrete.

Diaphragms of the second type are likely to be significantly more efficient in resisting shear loads than those without direct shear connection.

4. There are also two distinct types of profile used in composite floor construction as shown in Fig. 1: re-entrant profiles and trapezoidal profiles.

5. In this Paper, both types of profile are considered but attention is confined to diaphragms with no direct attachment of the concrete to the supporting structure. The Authors are not aware of any work on the diaphragm action of composite decks with shear connectors.

Previous tests on composite diaphragms

6. The first reported shear tests on composite diaphragms were carried out by S. B. Barnes and Associates.[2] They were only three in number and, of these, one used lightweight vermiculite fill and one was fabricated using a two-skin, box section, steel deck so that only one is directly relevant to the present study. In each case the decks were directly welded to the supporting structure using puddle welds; this is typical practice in the USA.

7. Each of the three diphragms tested appears to have failed by cracking of the concrete topping. The directly relevant test was carried out on a trapezoidally profiled steel deck 76·2 mm deep with a concrete topping 63·5 mm deep and a strength at the time of testing of 16·1 N/mm². Tension cracking started at a shear load of 31·0 kN/m and continued to increase until failure took place at a shear load of 86·4 kN/m due to direct shear of the concrete over the crests of the profiles. There was no indication of any slippage in the button-punched seams between adjacent sheets despite the fact that such seams are considerably

more flexible than those made with mechanical fasteners such as blind rivets or self-tapping screws.

8. The only other known tests on composite diaphragms were carried out by Luttrell[3] who tested nine diaphragms consisting of trapezoidally profiled steel sheets 9·5–34·9 mm deep with a topping of lightweight vermiculite concrete 63·5–76·2 mm deep and an average strength of 1·01 N/mm². He compared the stiffness and ultimate loads of composite diaphragms with those of similar diaphragms without topping and found a considerable increase in both strength and ultimate load. The failure modes obtained are not reported and, as the concrete topping was very weak, these tests are not of direct help in the present study.

Analysis of composite diaphragms

9. The analysis of light gauge steel diaphragms has now reached a high degree of refinement[4] and this work is relevant to an understanding of composite diaphragms which may be seen to be light gauge steel diaphragms with the addition of concrete topping. However, much of the theoretical work is of recent origin and was not available to influence previous research workers in the field of composite diaphragms. Luttrell[3] offers only a simple empirical treatment of diaphragm strength applicable to the particular arrangement that he tested. Barnes and Associates[2] give a more comprehensive theoretical treatment which is an extension of work on light gauge steel diaphragms. However, their expressions are complex and include a number of empirical constants which were derived for welded diaphragms only.

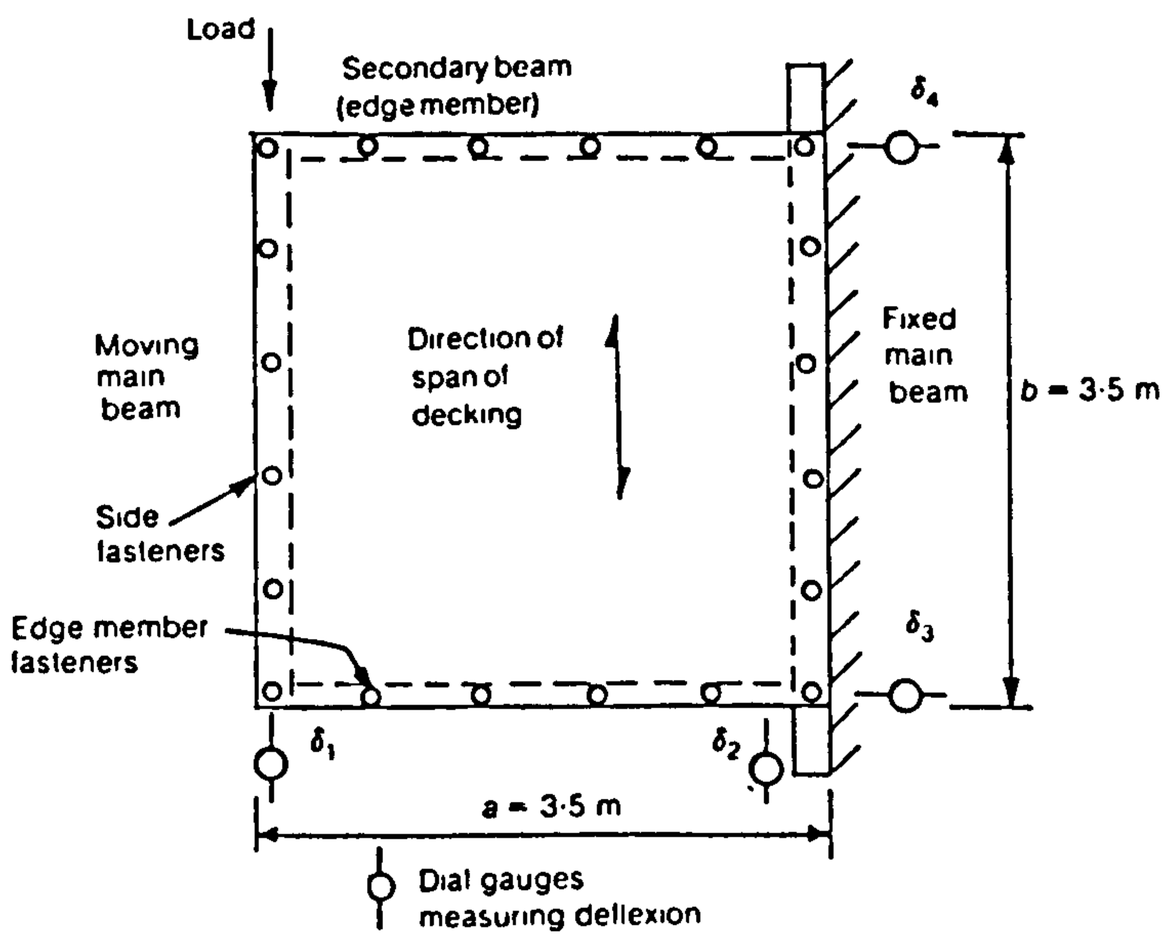

Fig. 2. General arrangement for cantilever diaphragm tests

Table 1. Details of tests

Test	Sheeting type	Slab thickness, mm	Topping thickness, mm	Nominal pitch of fasteners, mm	
				Main beam	Secondary beam
1	Re-entrant	100	50	300	304
2	Trapezoidal	150	70	585	608
3	Re-entrant	100	50	500	304
4	Re-entrant	100	50	700	456

Test programme

10. For the tests described in this Paper a rig was constructed so that cantilever diaphragms 3·5 m × 3·5 m could be subjected to loads of up to 150 kN. The general arrangement is shown in Fig. 2. The connections between the edge members and rafters were pinned so that the stiffness of the test frame itself was negligible.

11. The steel deck profile was either re-entrant or trapezoidal as shown in Fig. 1 and was fastened to the supporting structure on four sides using 6 mm dia. Teks self-drilling, self-tapping screws. Seams were fastened with 4·8 mm dia. monel pop rivets at 152 mm centres. Four tests were carried out as detailed in Table 1. With the exception of test 4, the procedure for each test was first to fix the steel deck to the supporting frame and then to apply load within the elastic range in order to determine the stiffness of the diaphragm without concrete topping.

12. Concrete topping was then placed and cured until cube tests indicated that the required 28 day strength had been obtained. This usually took between two and three weeks. The concrete used 9·5 mm aggregate and was designed to have a strength of 25 N/mm² at 28 days. A typical diaphragm ready for testing is shown in Fig. 3.

13. The composite slab was then tested by loading in increments up to failure. In the case of three of the four diaphragms tested, at a load of between a half and three quarters of the expected failure load, the diaphragm was unloaded and subsequently reloaded before continuing the test to failure. The load–deflexion curves are shown in Figs 4–7.

14. The shear deflexion Δ plotted was in each case obtained from the readings of the four dial gauges shown in Fig. 2 as

$$\Delta = \delta_1 - \delta_2 - \frac{a}{b}(\delta_3 - \delta_4)$$

15. For test 1, concrete strains were measured using Demec gauges and dial gauges were fixed to measure any slip between the steel and the concrete. At no time during the tests did the measured strain approach the tensile strain capacity of the concrete, nor was there any measurable slip between the steel deck and the concrete topping, and so these measurements were discontinued for subsequent tests.

16. For test 4, the composite diaphragm used in test 3 was reinstated by carefully breaking away the perimeter concrete to a width of about 150 mm in order to expose the failed fasteners which were removed. The diaphragm was

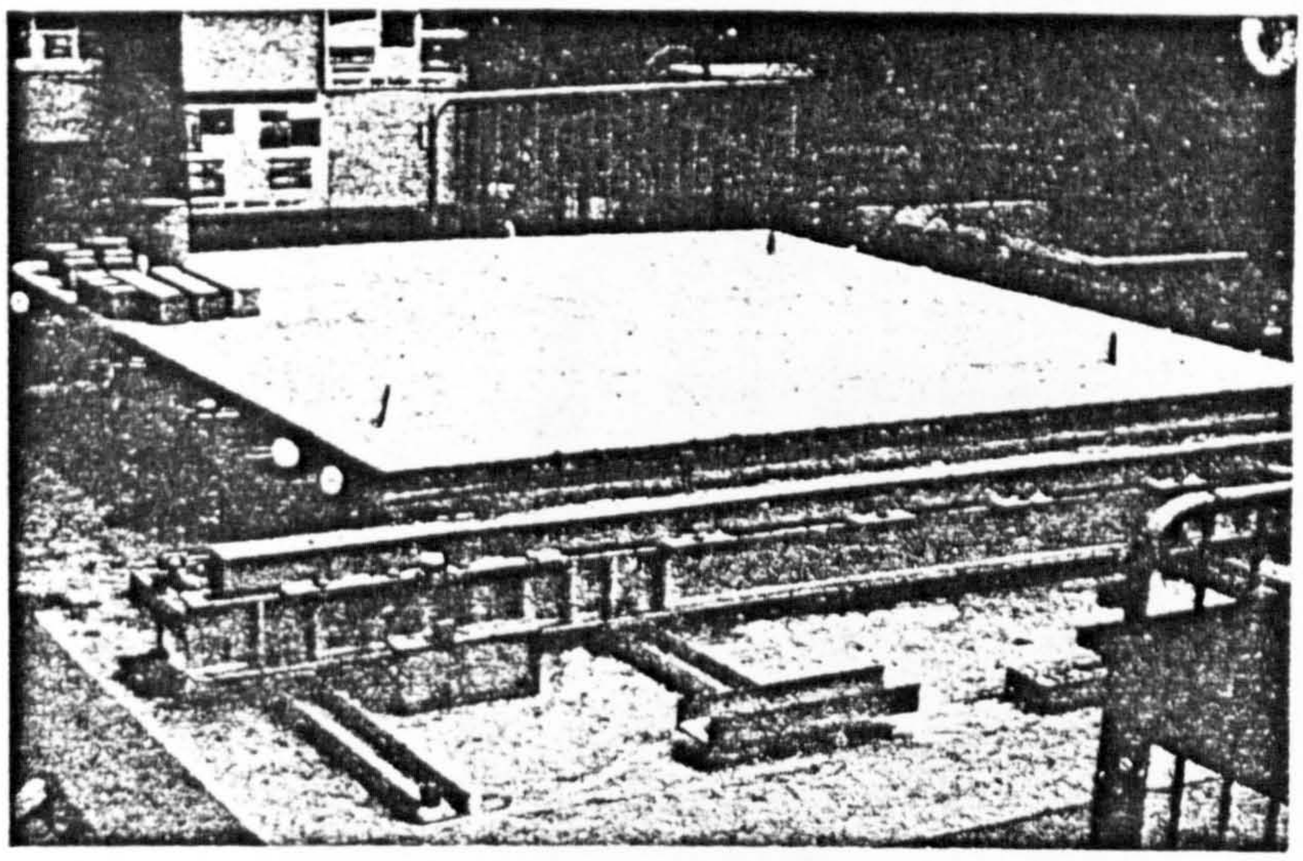

Fig. 3. Diaphragm prepared for test

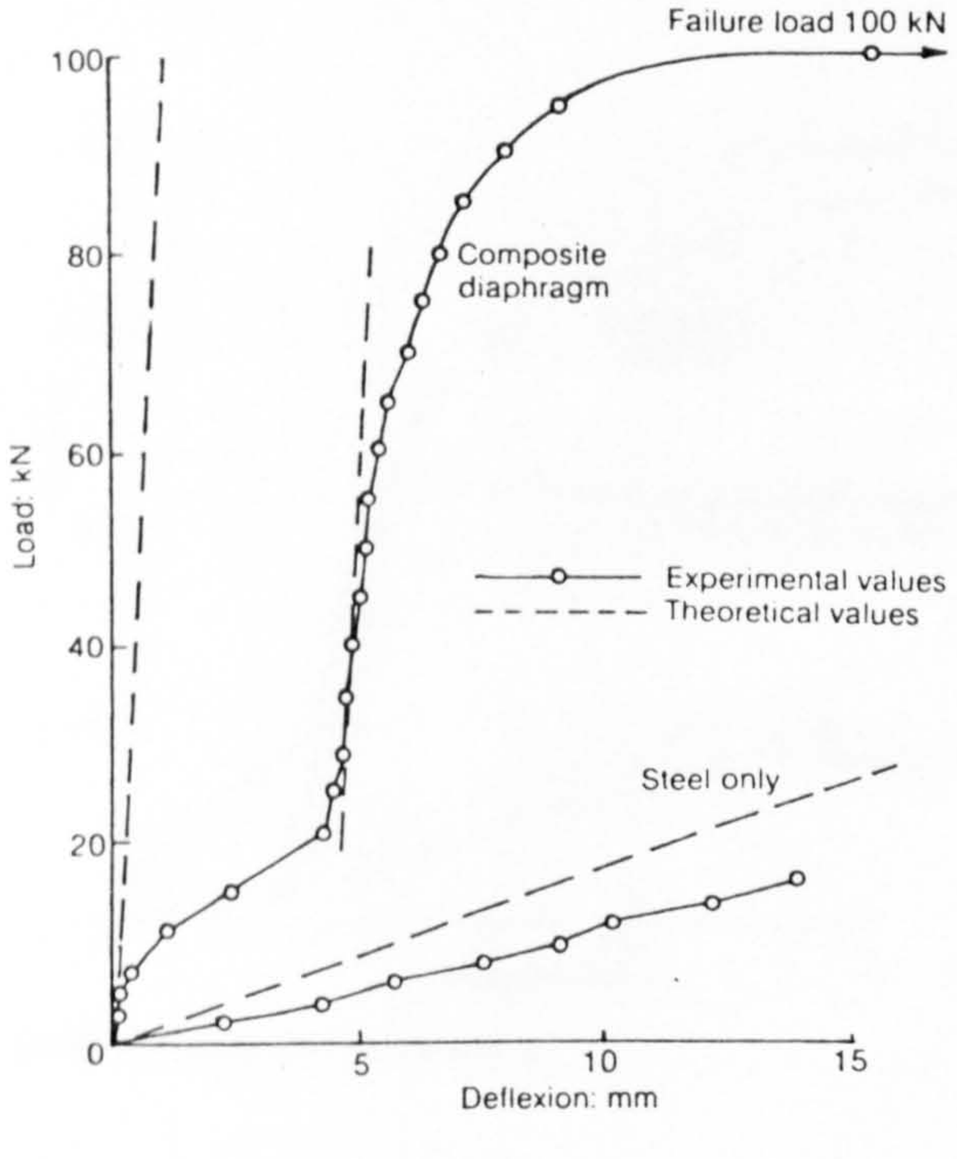

Fig. 4. Load–deflexion curves for test 1

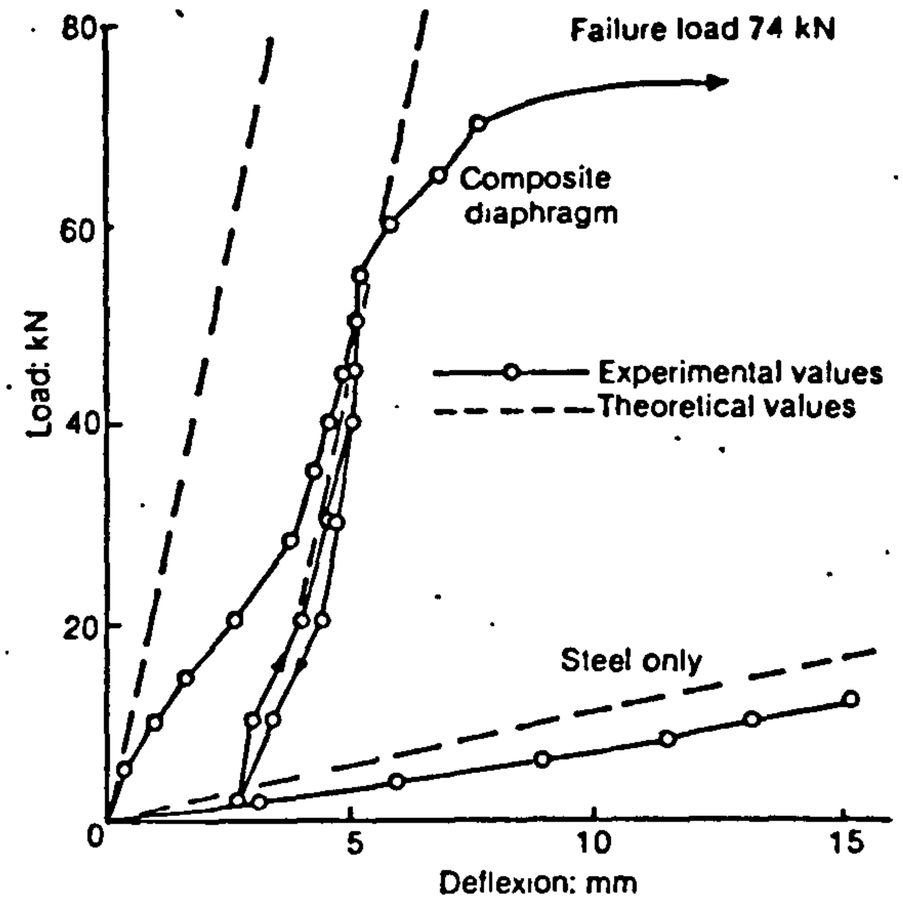

Fig. 5. Load–deflexion curves for test 2

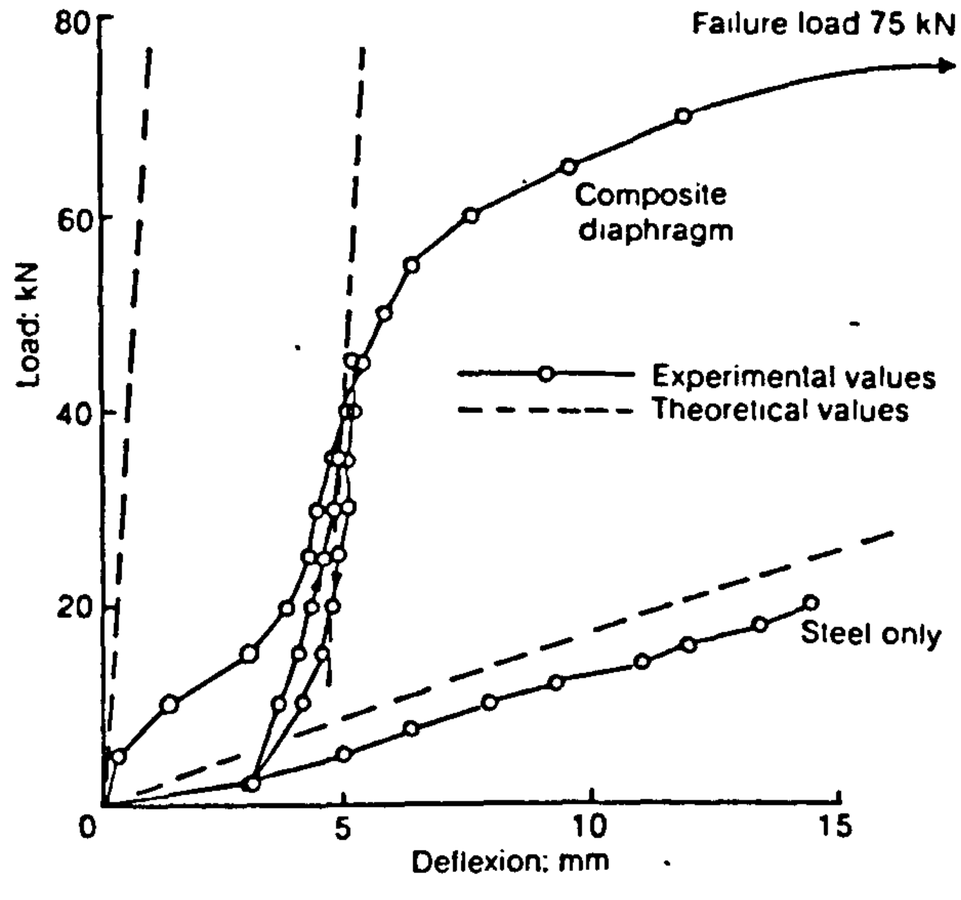

Fig. 6. Load–deflexion curves for test 3

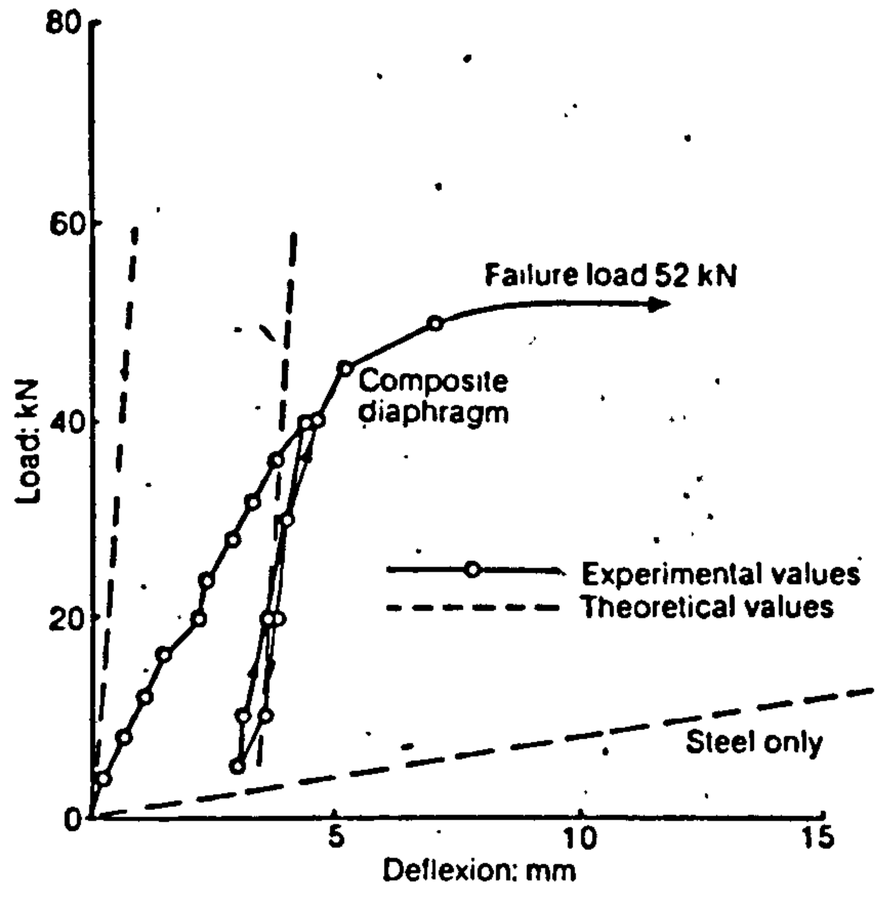

Fig. 7. Load–deflexion curves for test 4

then refixed with fresh fasteners at the required pitches given in Table 1 and the concrete slab made good by replacing the concrete which had been broken away. This procedure was adopted not only for reasons of economy but also to investigate the shape of the load–deflexion curve.

Failure modes and analysis

17. For tests 1, 3 and 4, which were carried out using the re-entrant profile, failure of the diaphragm was due to a failure of the fasteners between the profiled sheet and the supporting members (Fig. 8). The profiled sheet and its topping remained effectively rigid as the members of the supporting structure deformed in a parallelogram fashion below.

18. Figure 9 shows the basic mode of failure. This mode, which does not involve any rotation of the composite slab, is called mode 1. Considering the mechanism of failure as a rigid body failure mechanism and equating internal and external work, if there is a fastener on the centre line, the deflexion Δ_i at the ith fastener from the centre line is given by

$$\Delta_i = \Delta i/n_a \quad . \quad . \quad . \quad . \quad . \quad . \quad . \quad . \quad (1)$$

and, including the corner fasteners with those to the edge members

$$P\Delta = 2(n_b-1)F\frac{\Delta}{2}+4\sum_{i=1}^{n_a/2}\left(\frac{i}{n_a}\right)F\Delta \quad . \quad . \quad . \quad . \quad . \quad (2)$$

Therefore

$$P = (n_b-1)F+\frac{(n_a+2)F}{2} = \left(n_b+\frac{n_a}{2}\right)F \quad . \quad . \quad . \quad . \quad (3)$$

Similarly, it may be shown that if the total number of fasteners to the edge

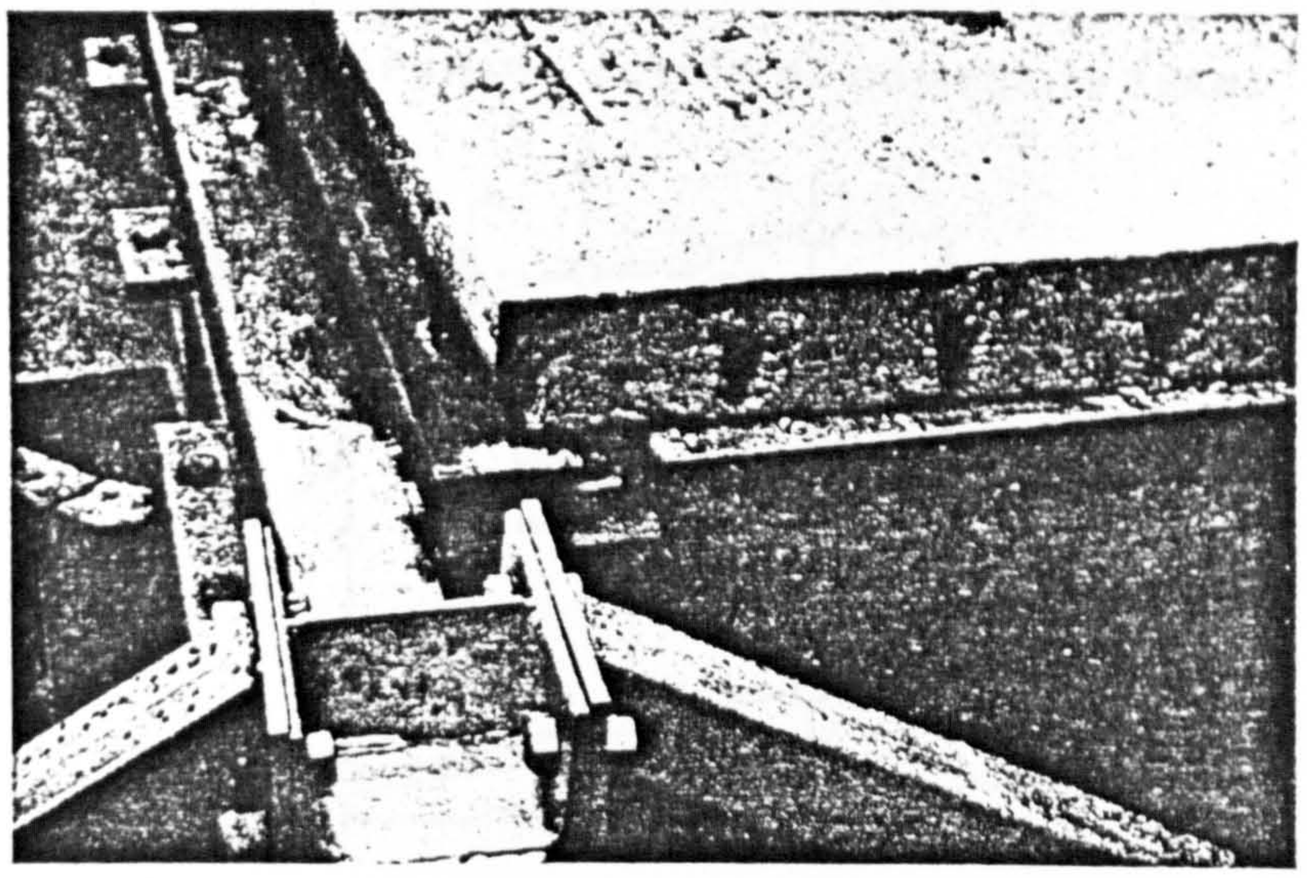

Fig. 8. Diaphragm used in test 1 after failure

member is an even number so that there is no fastener on the centre line

$$P = \left(n_b + \frac{n_a}{2} + \frac{1}{2n_a}\right) F \quad . \quad . \quad . \quad . \quad . \quad . \quad . \quad . \quad (4)$$

which gives similar numerical values unless n_a is small.

19. Obviously this analysis assumes that all fasteners reach failure simultaneously and this implies large deformations before failure which may not be achieved in practice. A more conservative approach is to assume that the forces in the fasteners to the edge members may vary linearly with distance from the centre line, so that if F_i is the force in the ith fastener

$$F_i = 2iF/n_a \quad . \quad . \quad . \quad . \quad . \quad . \quad . \quad . \quad . \quad (5)$$

$$P\Delta = 2(n_b - 1)F\frac{\Delta}{2} + 4\sum_{i=1}^{n_a/2}\left(\frac{i}{n_a}\right)2\left(\frac{i}{n_a}\right)F\Delta \quad . \quad . \quad . \quad . \quad (6)$$

Therefore

$$P = \left[n_b - 1 + 8\sum_{i=1}^{n_a/2}\left(\frac{i}{n_a}\right)^2\right]F = (n_b + \beta)F \quad . \quad . \quad . \quad . \quad (7)$$

where

$$\beta = 8\sum_{i=1}^{n_a/2}\left(\frac{i}{n_a}\right)^2 - 1 \quad . \quad . \quad . \quad . \quad . \quad . \quad . \quad . \quad (8)$$

20. A similar analysis for the case when the total number of fasteners to the edge member is an even number leads to an identical expression for the failure load P but with

$$\beta = 8\sum_{i=1}^{(n_a+1)/2}\left(\frac{i-\frac{1}{2}}{n_a}\right)^2 - 1 \quad . \quad . \quad . \quad . \quad . \quad . \quad . \quad (9)$$

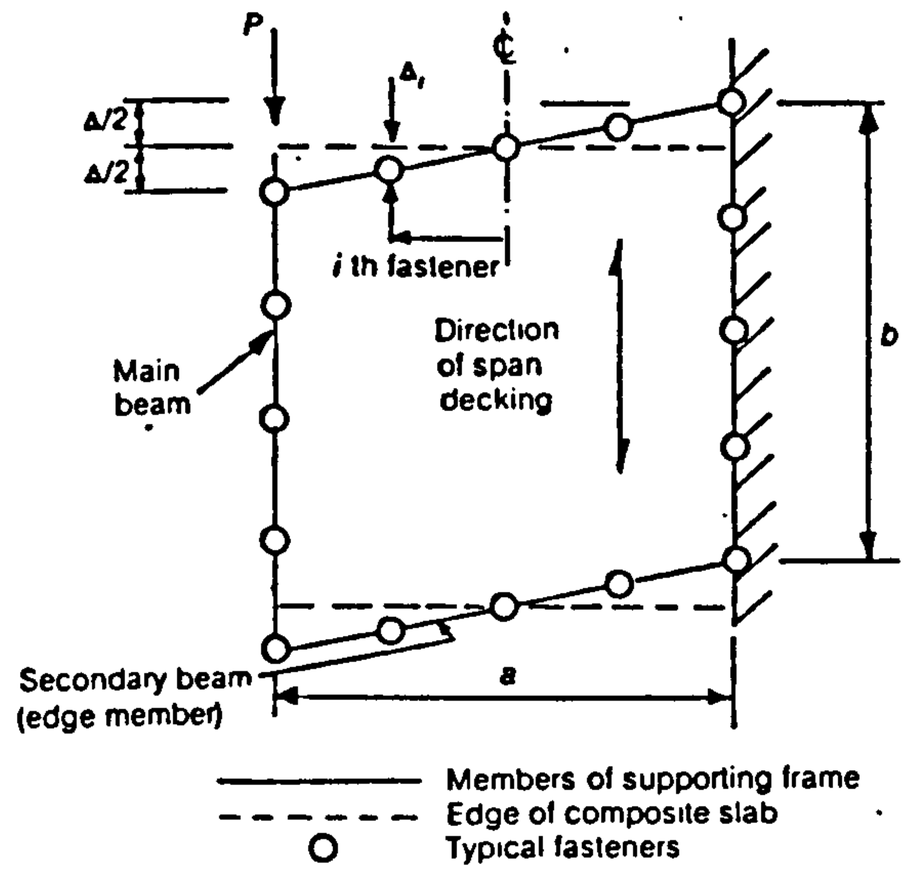

Fig. 9. Basic fastener failure mode—mode 1

21. There are many other assumptions regarding fastener force which might be made and the most suitable will be shown by comparison of the results of tests. However, in each case, the expression for the failure load will have the general form

$$P = (n_b + \beta)F \quad . \quad . \quad . \quad . \quad . \quad . \quad . \quad (10)$$

and alternative assumptions will merely vary the value of β. The two assumptions analysed in §§ 18–20 may be called plastic and linear respectively. The values of β for these assumptions are shown in Table 2 in terms of the

n	β	
	Plastic	Linear
2	1·0	1·0
3	1·67	1·22
4	2·0	1·5
5	2·6	1·8
6	3·0	2·11
7	3·57	2·43
8	4·0	2·75
9	4·56	3·07
10	5·0	3·4
11	5·55	3·73
12	6·0	4·06
13	6·54	4·38
14	7·0	4·71
15	7·53	5·04

Table 2. Values of β in expressions for failure load

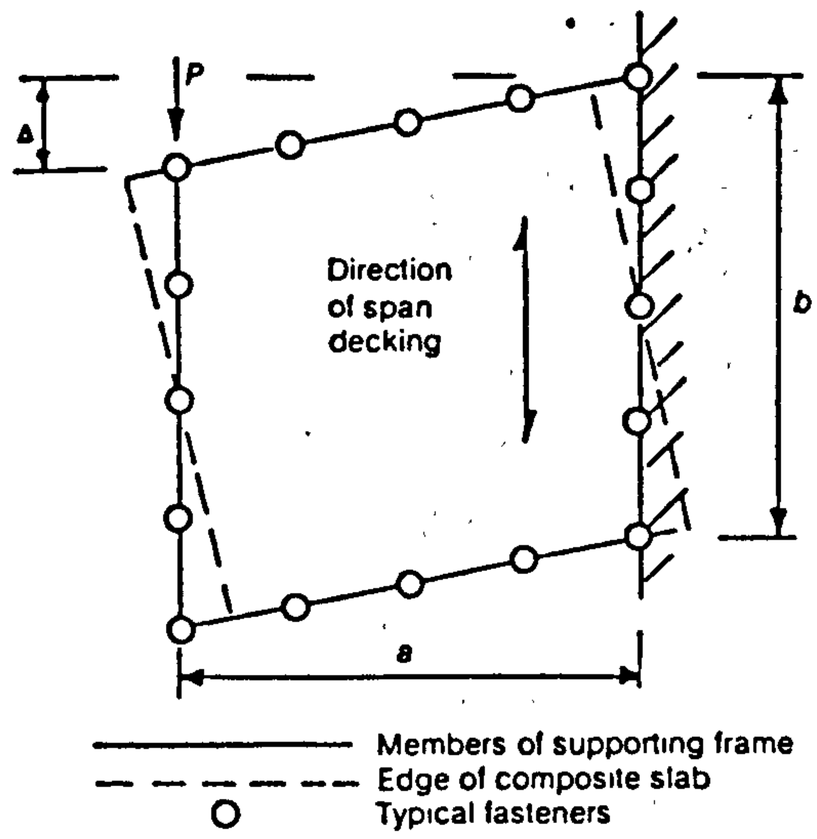

Fig. 10. Alternative fastener failure mode—mode 2

number of fasteners n equal to the length/pitch in the appropriate sides of the diaphragm, which in this analysis are the upper and lower sides of length a.

22. For isolated cantilever diaphragms, as tested, there is an alternative failure mode (Fig. 10) called mode 2. This involves bodily rotation of the composite slabs as well as parallelogram-like deformation of the supporting structure leading to fastener failure on all four sides of the diaphragm as before. For this mode of failure, the failure load is

$$P = \frac{b}{a}(n_a+\beta)F \quad . \quad . \quad . \quad . \quad . \quad . \quad . \quad (11)$$

where β is dependent on the number of fasteners n_b to the main beam.

23. For test 2 failure again took place with relative movement between the composite slab and the supporting frame with no noticeable deformation of the concrete. However, in this case, the relative movement took place partly in failure of the fasteners, as before, and partly in collapse of the profile adjacent to the fixed rafter as shown in Fig. 11. For this mode of failure, the entire slab rotated about a point near the top right-hand corner leading to the relative displacement between the slab and the supporting frame (Fig. 12). For fastener failure, this pattern of relative movements gives higher ultimate load than that given for the deformations shown in Fig. 9. This failure mode involving profile collapse is called mode 3.

24. At a distance x along the collapsing profile, the local deformations are as shown in Fig. 13. Assuming that these arise as a result of plastic hinges at B and C and, neglecting the small amount of twisting implied, the work done in a short length δ_x is $t^2\sigma_y\theta x\delta_x/2h$ and the total work done in collapsing the complete corrugation is $t^2b^2\sigma_y\theta/4h$. It can then be shown that the expression for the failure load is given by

$$P = \frac{b}{a}(n_a+\beta-\tfrac{1}{2})F+\frac{t^2b^2\sigma_y}{4ah} \quad . \quad . \quad . \quad . \quad . \quad (12)$$

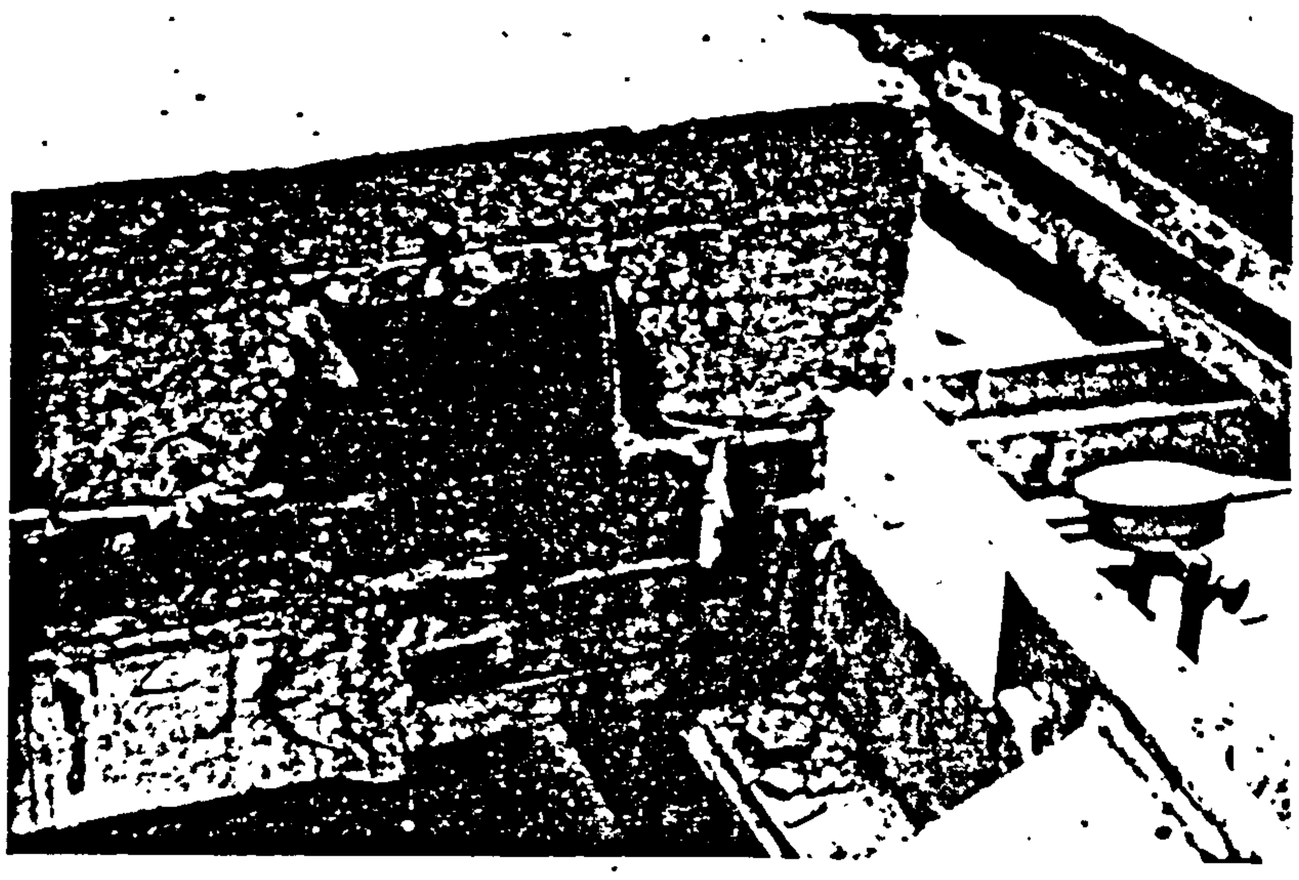

Fig. 11. Failure mode for test 2—mode 3

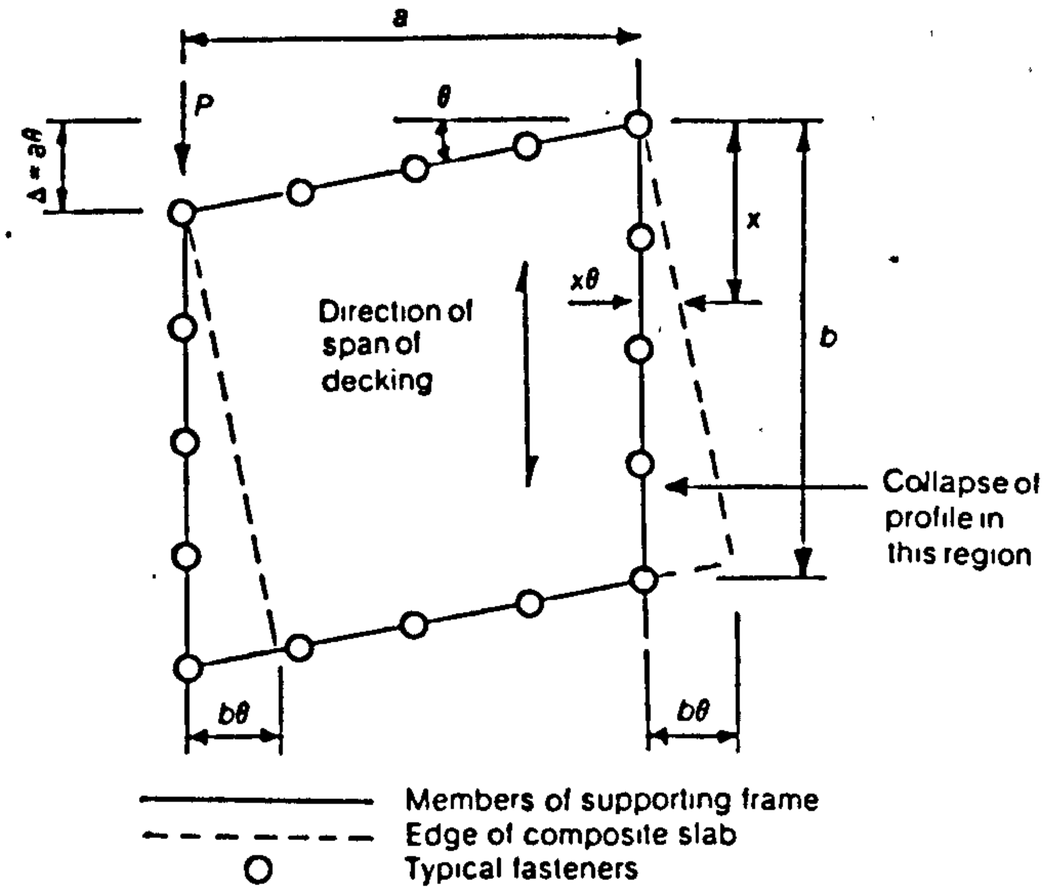

Fig. 12. Relative movements of slab and frame in failure mode 3

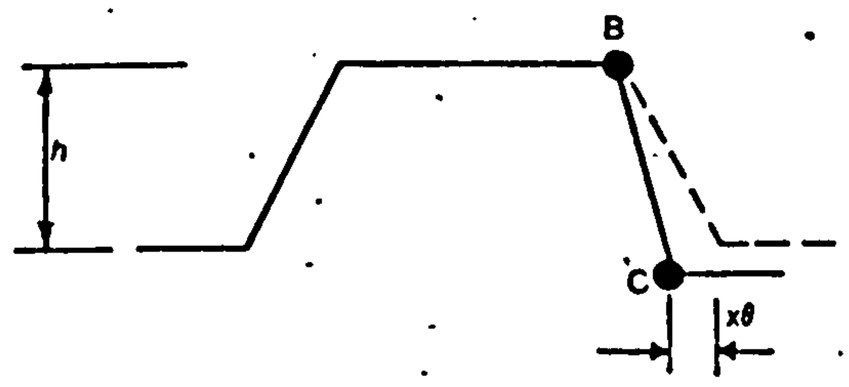

Fig. 13. Movements at section X in collapsing profile

which is exact for fully plastic fastener forces and very nearly so for linearly varying forces along the main beam. This failure may be expected to occur if the value of P given by equation (12) is less than that calculated for either of the two fastener failure modes considered previously.

25. The calculation in § 24 is conservative in that, in addition to the internal work considered, the deformations shown in Fig. 13 require the weight of concrete topping to be lifted a small distance and the resistance due to the head of the fasteners being embedded in the concrete to be overcome.

26. This mode is applicable only to trapezoidal profiles of the type shown in Fig. 1(b) and then only on the side of the diaphragm where the outermost profile closes as bodily rotation of the composite slab takes place over the supporting structure. When trapezoidal profiles tend to open and for both cases of re-entrant profile this type of failure mode is prevented by jamming against the concrete.

27. Barnes and Associates[2] reported failure in the concrete topping whereas in the present tests no distress in the topping was observed. However, the highest shear per unit length in the present tests was 28·6 kN/m, whereas in the test of Barnes and Associates cracking did not start until a load of 31·0 kN/m had been reached and failure was delayed until the load carried was 86·4 kN/m. The difference in behaviour is clearly a consequence of the relatively high strength of welded connections to the perimeter structure. If such fastening systems are to be used in the UK, there is a need for more tests but the present tests demonstrate the behaviour and design procedure for mechanically fastened diaphragms. In this respect Barnes and Associates reported that their diaphragm did not develop the full strength of the 63·5 mm thick concrete fill but the failure load was rather the shear strength of a net section across the flutes starting some distance back from the tension edge beam. There was negligible shear strength in the button-punched seam connections.

Flexibility of composite diaphragms

28. It was first shown by Bryan[5] that the flexibility of a light gauge steel diaphragm could be obtained by summing the component flexibilities

- $c_{1\cdot1}$ flexibility due to distortion of profiled steel sheeting
- $c_{1\cdot2}$ flexibility due to shear strain in the sheeting
- $c_{2\cdot1}$ flexibility due to slip in sheet to purlin fasteners
- $c_{2\cdot2}$ flexibility due to slip in seam fasteners
- $c_{2\cdot3}$ flexibility due to slip in connections to rafters
- c_3 flexibility due to axial strain in purlins

Some of the expressions used in the evaluation of these components have been modified[6,7] but the basic principle remains valid.

29. This approach may readily be extended to composite diaphragms if the following reasonable assumptions are made.

(*a*) The confining effect of the concrete eliminates distortion of the steel profile so that $c_{1\cdot1}$ may be ignored.
(*b*) At seams between adjacent steel sheets, the concrete carries almost all of the shear force and $c_{2\cdot2}$ may be ignored.
(*c*) The expressions for $c_{2\cdot1}$, $c_{2\cdot3}$ and c_3 are unchanged.
(*d*) The shear force is shared between the steel and the concrete according to the requirements for strain compatibility and $c_{1\cdot2}$ requires modification.

30. In order to derive the modified expression for $c_{1\cdot2}$, the notation in Fig. 14 is used. Considering a single corrugation subject to a unit shear load and with a shear deflexion $c_{1\cdot2}$, let the load carried by the steel be P_s and the load carried by the concrete be P_c. Then

$$P_s + P_c = 1 \quad \ldots\ldots\ldots (13)$$

31. From the accepted expression[4] for shear strain in the steel

$$c_{1\cdot2} = \frac{2(1+\gamma_s)(d+2h)P_s}{E_s t_s b} \quad \ldots\ldots\ldots (14)$$

where γ_s and E_s are respectively Poisson's ratio and Young's modulus for steel. For shear strain in the concrete, it may be shown that

$$c_{1\cdot2} = \frac{2(1+\gamma_c)dP_c}{E_c t_c b} \quad \ldots\ldots\ldots (15)$$

where γ_c and E_c are respectively Poisson's ratio and Young's modulus for concrete. Equating equations (14) and (15) gives

$$P_s = \frac{(1+\gamma_c)dE_s t_s}{(1+\gamma_c)dE_s t_s + (1+\gamma_s)(d+2h)E_c t_c} \quad \ldots\ldots\ldots (16)$$

and hence the modified expression for $c_{1\cdot2}$ is

$$c_{1\cdot2} = \frac{2(1+\gamma_c)(1+\gamma_s)(d+2h)a}{[(1+\gamma_c)dE_s t_s + (1+\gamma_s)(d+2h)E_c t_c]b} \quad \ldots\ldots\ldots (17)$$

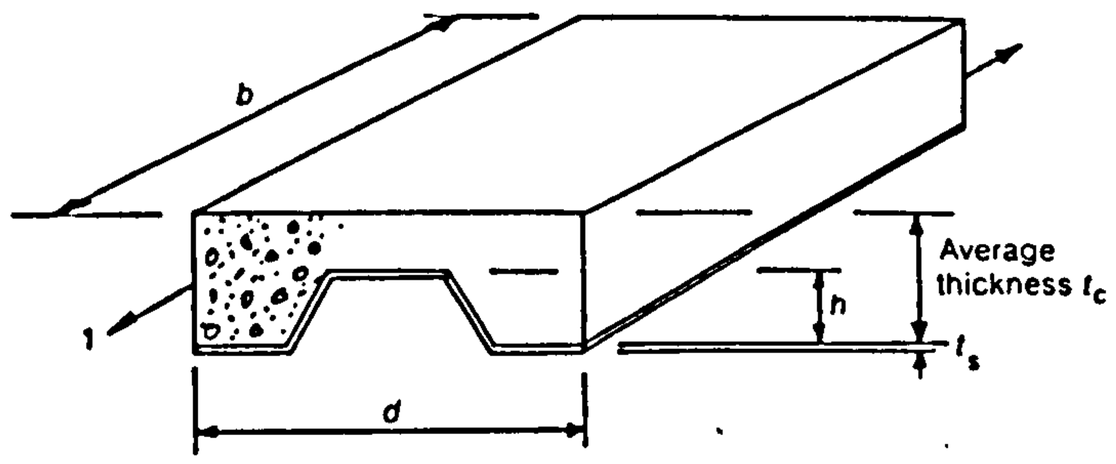

Fig. 14. Notation for flexibility calculation

32. In the theoretical comparisons which follow, the flexibility c of a composite diaphragm is calculated as

$$c = c_{1\cdot2} + c_{2\cdot1} + c_{2\cdot3} + c_3 \quad \ldots\ldots\ldots \quad (18)$$

where $c_{1\cdot2}$ is as given in equation (17) and the expressions for the remaining components are taken direct from reference 4. Where theoretical comparisons for diaphragms without concrete topping are given these are also taken from reference 4.

Comparison of theory and tests

33. As a preliminary to the interpretation of the test results, shear tests on the actual fasteners and sheeting used were carried out and gave the average values shown in Table 3. These values were used in the failure expressions (equations (10)–(12)) to give the comparison between experimental and theoretical ultimate loads (Table 4).

34. For the fastener failure in tests 1, 3 and 4, the plastic calculation is unsafe and must be rejected. However, the theory based on a linear distribution of fastener forces gives an adequate design approach, being conservative for tests 1 and 3 and only slightly unconservative for test 4.

35. For test 2, which failed in a mode including profile collapse, even the linear theory is unconservative. The reason for this probably lies in the assumptions inherent in Fig. 12. In theory, because of potential jamming between the steel profile and the surrounding concrete, relative movement is possible only in the manner shown in Fig. 13, and this means that the composite slab must rotate about the top right-hand corner of Fig. 12. In practice, because other small relative movements are possible, the composite slab probably rotates about some other point lower in Fig. 12, resulting in a smaller failure load. Detailed investigation reveals that the failure load is sensitive to the assumed

Table 3. Experimental fastener characteristics

Fasteners	Sheeting	Number of tests	Average ultimate load	Average flexibility
6 mm Tek	Holorib 0·9 mm	3	6·15 kN	0·017 mm/kN
6 mm Tek	Robertson 1·5 mm	4	10·38 kN	0·058 mm/kN

Table 4. Comparison of experimental and theoretical failure loads

Test	n_a	n_b	Experimental failure load, kN	Predicted failure load, kN		Predicted failure mode	Failure load per unit length, kN/m
				Plastic	Linear		
1	11	12	100	104·6	92·6	2	28·6
2	6	6	74	93·4	84·2	1, 2 or 3	21·1
3	11	7	75	77·2	66·0	1	21·4
4	8	6	52	61·5	53·8	2	15·0

centre of rotation and that the experimental failure load can be explained on this basis.

36. This mode of failure may be worth further investigation, although it must be admitted that both failure modes 2 and 3, which require rotation of the composite slab, are of limited practical importance because, in most applications, assemblies of composite panels will act more in the nature of simply supported beams than as cantilevers. In such circumstances, rotation of the composite slab is prevented by the adjacent slabs and, of the modes investigated, only mode 1 is possible.

37. The behaviour before failure is shown in the load-deflexion curves in Figs 4–7. In each case the predicted stiffness is shown both through the origin and alongside the relevant part of the load–deflexion curve.

38. In the initial stages of loading in tests 1, 2 and 3 the response is dominated by a large initial movement which does not reappear on unloading and reloading. This is probably due to there being some initial freedom of movement between the steel and the concrete before full composite action takes place. That test 4, which was constructed rather differently to minimize this initial movement, shows a response of a different shape would seem to confirm this assumption. There was probably also some additional flexibility in the test rig as evidenced by the bare steel diaphragms also being more flexible than predicted. It is obviously extremely difficult to predict the stiffness of a composite diaphragm on first loading and no further analytical treatment is offered.

39. On reloading, the diaphragms all exhibited a considerable increase in stiffness and the reloading stiffness agreed well with the predicted stiffness. A similar although smaller increase in stiffness on reloading was also observed in tests on light gauge steel diaphragms and it may be due in part to the characteristics of the fasteners as well as the relative movement already discussed. There is no difficulty in predicting the reloading stiffness of composite diaphragms.

Conclusions

40. Four tests on composite diaphragms have been described and a theory has been developed which makes it possible to assess accurately the ultimate load due to fastener failure. An alternative failure mode due to profile collapse has also been described, but this failure mode may prove to be of limited practical importance as it would appear to be possible only in cantilever diaphragms.

41. Shear at the seams between adjacent steel sheets is taken largely by the concrete and tests of Barnes and Associates[2] indicate that for diaphragms with strong perimeter fasteners and weak seams there is an additional mode of failure involving cracking of the concrete over the seams.

42. Composite diaphragms are considerably stiffer than their light gauge steel counterparts because of the absence of profile distortion and seam slip. The stiffness on first loading is dominated by a large initial movement and so it is extremely difficult to predict this stiffness.

43. Composite diaphragms show a considerable increase in stiffness on reloading; the reloading stiffness may be predicted using a suitable modification of established procedures for light gauge steel diaphragms.

44. As a consequence of the possibility of rotation of the composite slab over the supporting frame, cantilever composite diaphragms behave differently from simply supported diaphragms. It is recommended that in further experi-

mental studies simply supported diaphragms should be used despite the great increase in cost.

References

1. EUROPEAN CONVENTION FOR CONSTRUCTIONAL STEELWORK. *European recommendations for the design of composite floors with profiled steel sheeting.* Constrado, London, 1975.
2. S. B. BARNES and ASSOCIATES. *Report on the use of H. H. Robertson steel roof and floor decks as horizontal diaphragms.* Barnes and Associates, California, 1963.
3. LUTTRELL L. D. Shear diaphragms with lightweight concrete fill. *Proceedings of the 1st speciality conference on cold-formed steel structures.* University of Missouri-Rolla, 1971, 111–117.
4. EUROPEAN CONVENTION FOR CONSTRUCTIONAL STEELWORK. *European recommendations for the stressed skin design of steel structures.* Constrado, London, 1977.
5. BRYAN E. R. *The stressed skin design of steel buildings.* Crosby Lockwood Staples, London, 1973.
6. DAVIES J. M. Calculation of steel diaphragm behaviour. *J. Struct. Div. Am. Soc. Civ. Engrs*, 1976, 102, ST 7, July, 1411–1430.
7. DAVIES J. M. and LAWSON R. M. The shear deformation of profiled metal sheeting. *Int. J. Numer. Meth. Engng*, 1978, 12, No. 10, 1507–1541.

Appendix 6

A - series

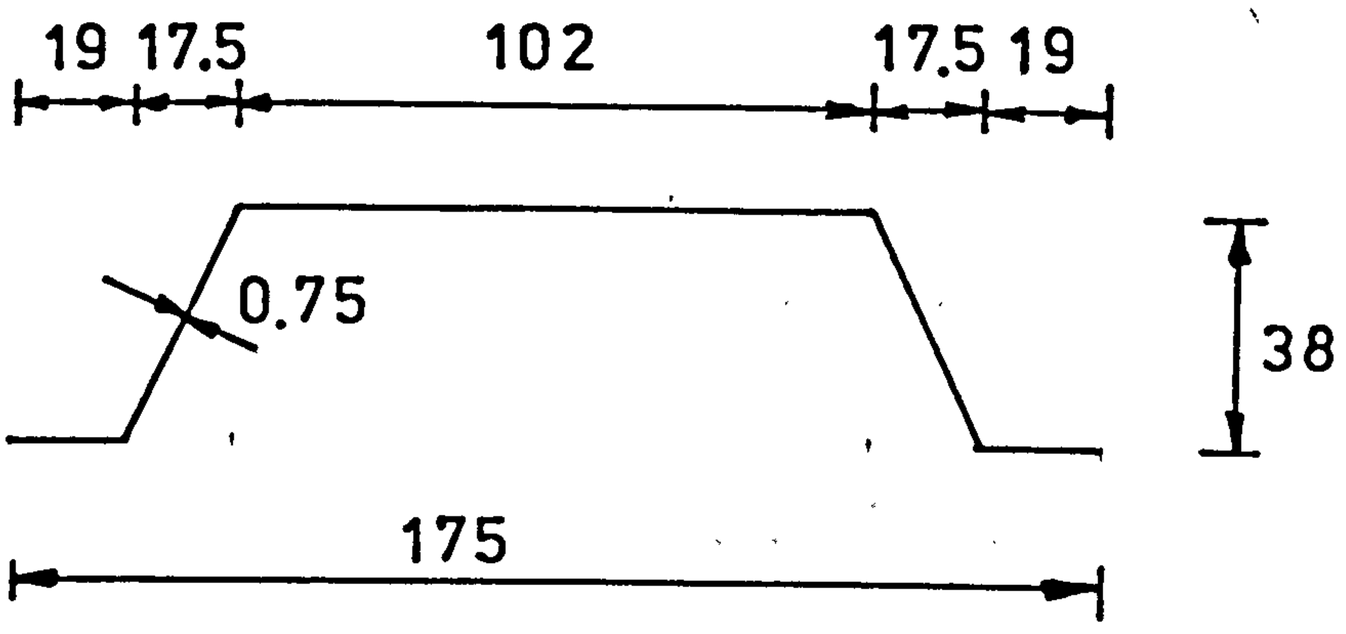

B - series

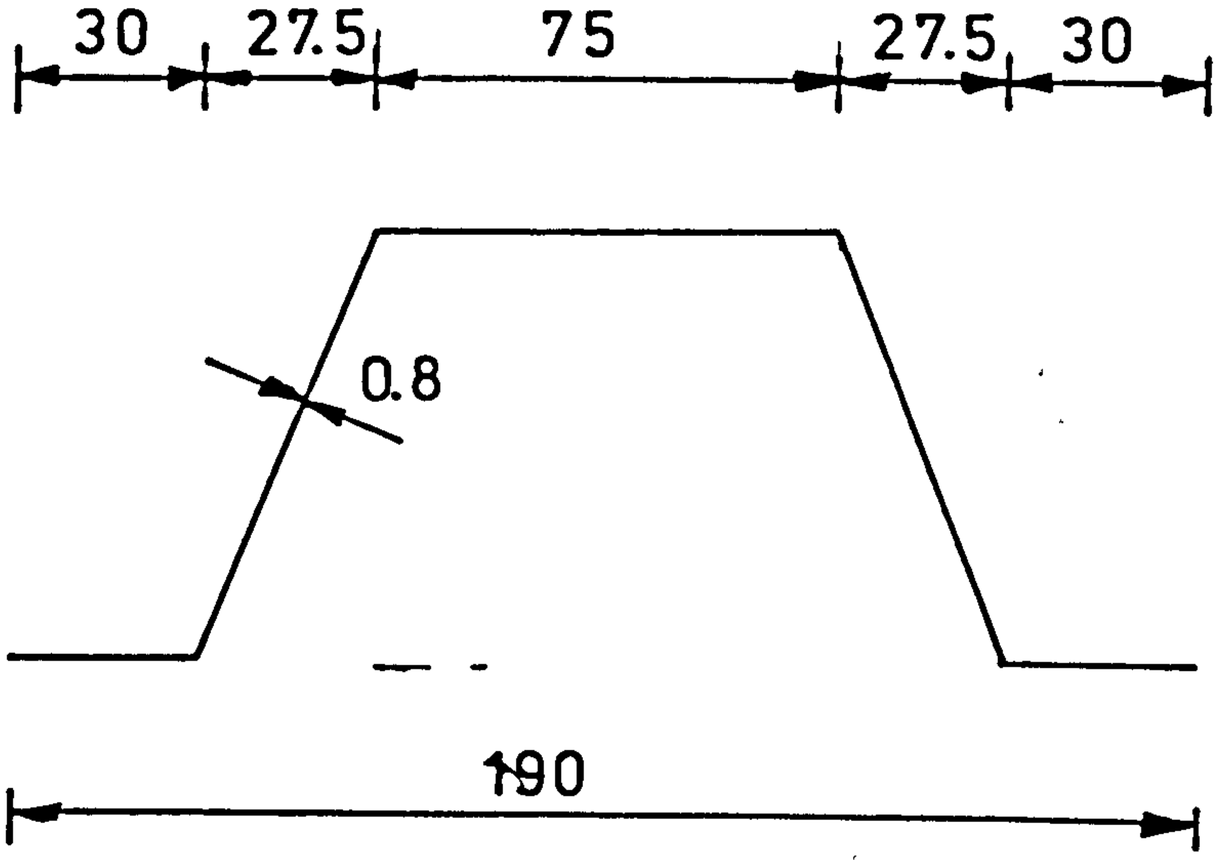

C.- series

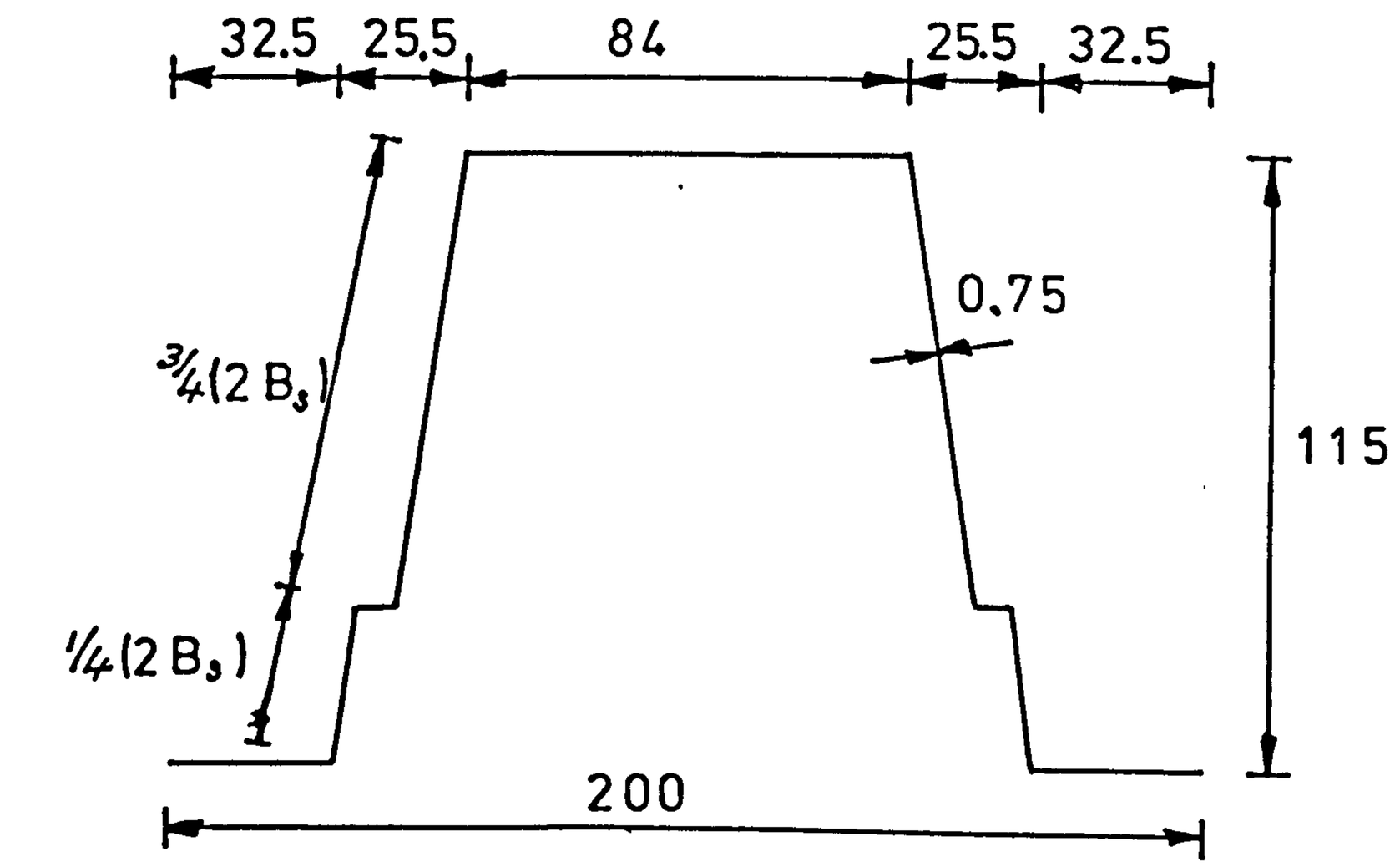

D-series

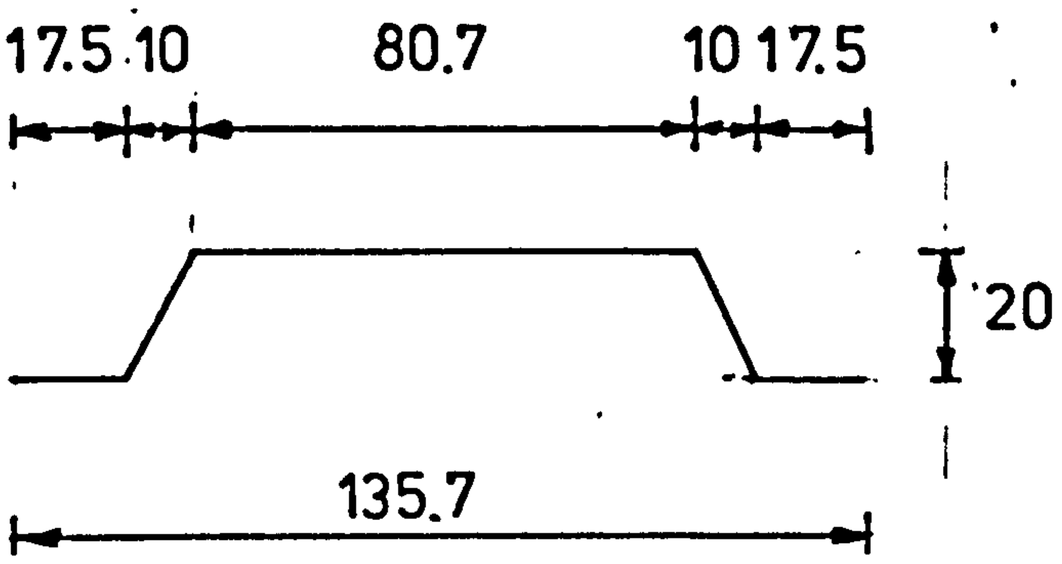

E-series

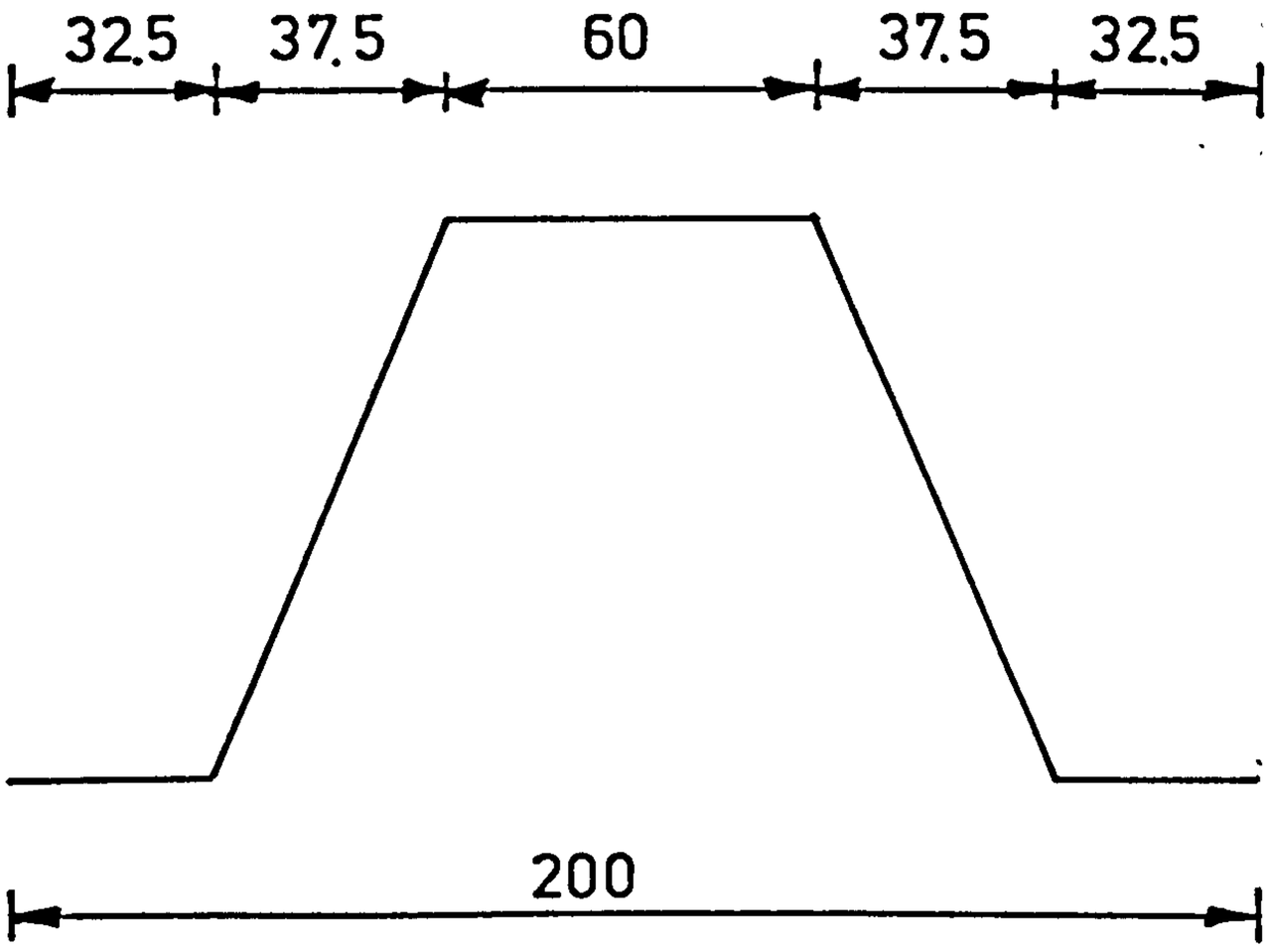

F-series

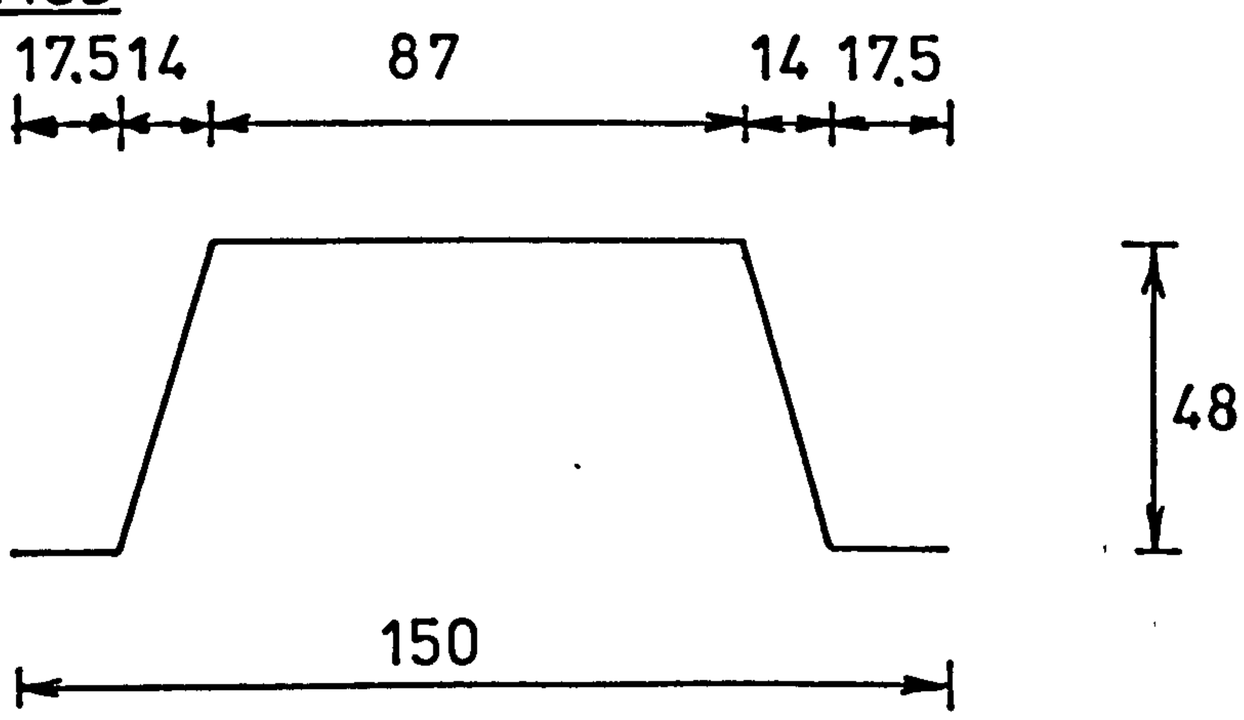

G-series

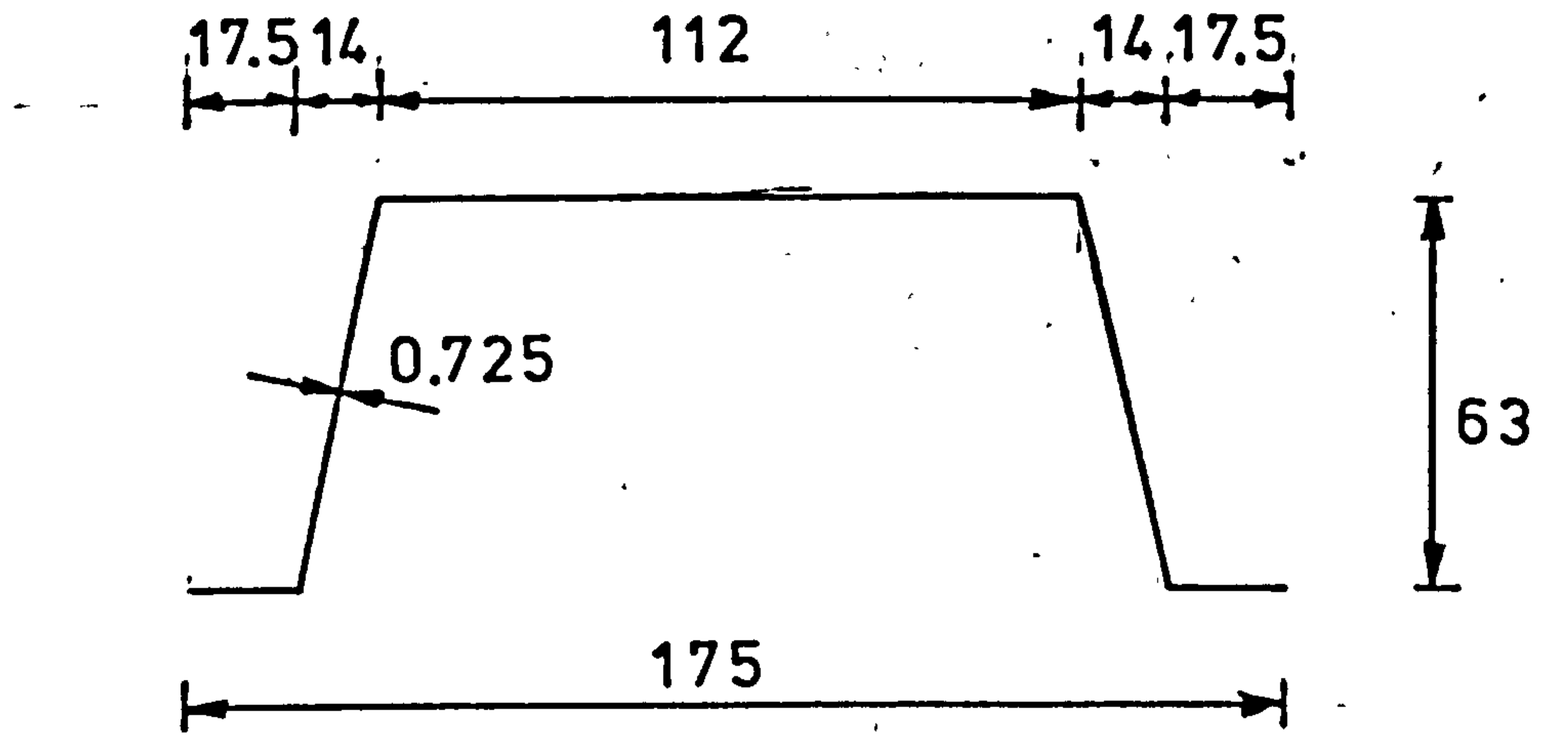

REFERENCES

1. LITTLE, D. H. and SMITH, A. A. — "Some Steel Structural Frames Designed by Plastic Theory", Proc. Inst. Civ. Eng. December 1955.

2. JOHNSON, C. B. — "Light Gauge Steel Diaphragms in Building Construction", ASCE meeting, February 1950.

3. NILSON, A. H. — "Shear Diaphragms in Light Gauge Steel" Proc. American Soc. of Civil Engineers, J, Struct. Div., November 1960

4. BRYAN, E. R. — "Stressed Skin Roof Decks for SEAC and CLASP Building Systems", Constrado, March 1973.

5. BRYAN, E. R. and JACKSON, P. — "The Shear Behaviour of Corrugated Steel Sheeting", Symposium on Thin Walled Structures, Univ. College of Swansea, September 1967.

6. DAVIES, J. M. — "Calculation of Steel Diaphragm behaviour" Proc. American Soc. of Civil Engineers, J. Struct. Div., July 1976.

7. DAVIES, J. M. and LAWSON, R. M. — "The Shear Flexibility of Corrugated Metal Sheeting" Proc. 3rd Spec. Conf. on Cold-Formed Steel Structures, University of Missouri-Rolla. November 1975.

8. DAVIES, J. M and LAWSON, R. M. — "Shear Deformation of Profiled Metal Sheeting", Int. Journal for Num. Methods in Engineering 12. 1978, No. 10.

9. LAWRENCE, S. J. and SVED, G. "A Finite Element Analysis of Clad Structures", Conf. on Metal Structures Research and its Applications, Sydney November 1972.

10. NILSON, A. H. "Analysis of Light Gauge Steel Shear Diaphragms" Proc. 2nd Spec. Conf. on Cold-Formed Steel Structures, University of Missouri-Rolla, November 1975.

11. DAVIES, J. M. "The Design of Multi-Storey Building Stiffened by Diaphragm Action", University of Salford, Report 77/95 August 1978.

12. DAVIES, J. M. and FISHER, J. "The Diaphragm Action of Composite Slabs", Proc. of Inst. Civ. Eng. Part 2. December 1979.

13. LIBOVE, C. "Survey of Recent Work on the Analysis of Discretely Attached Corrugated Shear Webs", American Institute of Aeronautics and Astronautics, April 1972.

14. "European Recommendations for the Design of Composite Floors with Profiled Steel Sheeting", Committe 11, Constrado May 1975.

15. "Tentative Recommendations for the Design of Composite Steel Deck Slabs" American Iron and Steel Institute, Washington 1976.

16. FULOP, A. and MOUM, C. "Proposed Method for the Design of Profiled Sheet Steel / Concrete Composite Floors under Positive Moment", C.T.U.C.M. 1976.

17. SCHUSTER, R. M. "Composite Steel Deck Reinforced Concrete Systems Failing in Shear Bond", Int. Ass. for Bridge and Structural Engineering, Amsterdam 1972.

18. ROBERTS, P. "Profiled Steel Sheet and Concrete Composite Floors", M.Sc. Thesis, University of Salford 1977.

19. BARNES, S. B. and ASSOCIATES "Report on the Use of H. H. Robertson Steel Roof and Floor Decks as Horizontal Diaphragms, July 1963.

20. LUTTRELL, L. D. "Shear Diaphragms with Light-weight Concrete Fill", Proc. 1st Spec. Conf. on Cold-Formed Steel Structures, University of Missouri-Rolla, August 1971.

21. EASLEY, J. T. "Buckling Formulas for Corrugated Metal Shear Diaphragm", ASCE J. Struct. Div. July 1975.

22. BRYAN, E. R. "Stressed Skin Design in Buldings" Constrado Monograph, Crosby Lockwood Staples, London 1973.

23. "European Recommendations for the Testing of Connections in Profiled Sheeting", Committee 17, Constrado 1977.

24. STAMATO, M. C, and STAFFORD-SMITH, B. "An Approximate Method for the Three Dimensional Analysis of Tall Buildings", Proc. Inst. Civ. Eng., July 1969.

25. MAJID, K. I. and CROXTON, P. C. L. "Wind Analysis of Complete Building Structures by Influence Coefficients", Proc. Inst. Civ. Eng. 1970.

26. DAVIES, J. M. "The Computer Anaalysis of Stressed Skin Buildings", Civil Eng. and Public Works Review Vol. 67, November 1972.

27. BATES, W. "Modern Design of Steel Frames for Multi-Storey Buldings", BCSA Publication, No. 20, 1963.

28. ZIENKIEWICZ, O. C. "The Finite Element Method", McGraw-Hill, London.

29. CHEUNG, Y. K. "Finite Strip Method in the Analysis of Elastic Plates with Two Opposite Ends", Proc. Inst. Civ. Engs. May 1968.

30. LOO, Y, C. "Development and Application of the Finite Strip Method in the Analysis of Right Bridge Decks", P.hD. Thesis, University of Dundee, 1972.

31. CHEUNG, Y. K. "Finite Strip Method in Structural Analysis", Pergamon Press, Oxford.

32. VLAZOV, V. "General Theory of Shells and its Applications in Engineering", NASA TT F-99, April 1964.

33. CHEUNG, Y. K. and CHEUNG, M. S. "Flexural Vibrations of Rectangular and other Polyonal Plates", ASCE April 1971.

34. SIDDIQI, G. H. and GIRIJA-VALLABHAM, C. V. "Extended Finite Strip Method for prismatic plate and shell structures" I.A.S.S. Pacific Symposium on Hydromechonically Loaded Shells, University of Hawaii, October 1971.

35. SIDDIQI, G. H. and GIRIJA-VALLABHAM, C. V. "Orthotropic Folded Plate Structures by Extended Finite Strip Method", 1st Spec. Conf. on Cold-Formed Steel Structures August 1971.

36. SIDDIQI, G. H. "Extended Finite Strip Method for Prismatic Plate and Shell Structures", P.hD. Thesis, Texas Tech. University 1971.

37. SABIR, A. B. "The Nodal Solution Routine for the Large Number of Linear Simultaneous Equations in the Finite Element Analysis of Plates and Shells", Finite Elements for Thin Shells and Curved Members, ed. Ashwell and Gallagher.

38. TIMOSHENKI and GOODIER "Theory of Elasticity", McGraw-Hill.

39. YOUNG, J "Analysis of Corrugated Cylindrical Shell Roofs", PhD Thesis, University of Salford, September 1976.

40. SCORDELIS, A. C. and LO, K. S. "Computer Analysis of Cylindrical Shells" ACI, May 1964.

41. HORNE, M. R. and RASLAN, R.A.S. "An Energy Solution to the Shear Deformation of Corrugated Plates", Int. Ass. for Bridge and Structural Engineers, 31-I / 1971.

42. HORNE, M.R. and RASLAN, R.A.S. "A Finite Difference Approach to Corrugated Shear Panels", Int. Ass. for Bridge and Structural Engineers, 31-I /1971.

43. LAWSON, R. M. "The Flexibility and Strength of Corrugated Diaphragms and Folded Plates", PhD Thesis, University of Salford, 1976.

44. LOO, Y. C. "Development and Applications of the Finite Strip Method in the Analysis of Right Bridge Decks", PhD Thesis, University of Dundee, 1972.

45. "European Recommendation on Stressed Skin Design of Steel Structures", Constrado 1977

46. FALKENBERG, J.C. "Shell and Folded Plate Roofs of Corrugated Sheet Steel Panels", Norwegian Building Research Institute.

47. SCHARDT, R. and STREHL, C. "Theoretische Grundlagen fur die Bestimmung der Schebsteifigkeit von Trapezblechscheiben - Vergleich mit anderen Berechnungsansatzen und Versuchsergebnissen", Der Stahlbau, April 1976

48. B.S. 449 : 1969 "The Use of Structural Steel in Buildings", British Standards Institution

49. HORNE, M.R. "Plastic Theory of Structures", Pergamon Press, 1979

50. DAVIES, J.M. - Private Communication